

# Engineering Lymphangiogenesis: Implications for Cancer Immunotherapy and Beyond

THÈSE N° 7047 (2016)

PRÉSENTÉE LE 23 SEPTEMBRE 2016

À LA FACULTÉ DES SCIENCES DE LA VIE

LABORATOIRE DE RECHERCHE INTÉGRATIVE DU SYSTÈME LYMPHATIQUE ET DU CANCER  
PROGRAMME DOCTORAL EN BIOTECHNOLOGIE ET GÉNIE BIOLOGIQUE

ÉCOLE POLYTECHNIQUE FÉDÉRALE DE LAUSANNE

POUR L'OBTENTION DU GRADE DE DOCTEUR ÈS SCIENCES

PAR

Manuel Andreas FANKHAUSER

acceptée sur proposition du jury:

Prof. M. Dal Peraro, président du jury

Prof. M. Swartz, directrice de thèse

Prof. B. Ludewig, rapporteur

Prof. T. Padera, rapporteur

Prof. D. Hanahan, rapporteur



ÉCOLE POLYTECHNIQUE  
FÉDÉRALE DE LAUSANNE

Suisse  
2016





## Acknowledgments

Research is a team effort. It is based on the exchange of hypothesis, arguments, questions, visions, ideas, and often, crazy ideas. It is based on mentorship, receiving and giving practical advice, sharing skills and experimental hints, and simply offering hands when most needed. It is a never-ending exploration of the unknown that leads to breakthrough discoveries only when the crew holds together. In that sense, I would like to express my gratitude towards each and everyone who has been part of shaping my path as a PhD student, everyone who has been part of my exploration.

Melody Swartz. Melody. Your creativity and vision is the reason that together with your lab, you will always keep on steering towards new, unexplored areas of fascinating science. Thank you for giving me guidance, and yet unlimited freedom during my thesis research. Thank you being so generous, for sending me to conferences, for letting me do whatever crazy experiment I wanted to do. Thank you for sharing great moments during lab retreat, in Lucca, in Chicago, and elsewhere. I would not have developed to who I am today without having worked with you.

Douglas Hanahan, Ludewig Burkhard, Timothy Padera, and Matteo Dal Peraro. Thank you for critically reviewing my work, and for taking your valuable time for being on my thesis defense committee.

John McKinney. Thank you for being a very thoughtful thesis mentor. Thank you for devoting some of your time and sharing your interesting approaches to science and life.

Amanda Lund. Amanda. Thank you for being my first great mentor in the lab. Thank you for getting me more and more excited about the world of *in vivo* tumor immunology. Thank you for showing me that great science can be done while enjoying life.

Witold Kilarski. Witusch. Thank you for being my second great mentor in the lab. I will never forget the hours and hours we spent together in the imaging room. It was always like an exhilarating lecture about history, biology, conspiracy theories, politics, philosophy, poetry, and more... I loved it! Thank you for sharing the nitty-gritty experimental details, you truly are a walking encyclopedia.

Laura Jeanbart. Laura. Thank you for being my third great mentor in the lab. Thank you for making sure I did things properly. Thank you for sharing almost everything with me: your skills in the lab, some runs along the lake, political discussions, Boston, and lots of amazing bakeries.

Maria Broggi. Broggin. Thank you for being my fourth great mentor in the lab. Thank you for truly having been on my side for the past few years, going through all ups and downs that science has to offer together with me. Thank you for spreading an atmosphere of enthusiasm and curiosity every single day. Your energy has been contagious and it has been a pleasure working with you.

Shann Yu. Shanno. Thank you for being my fifth great mentor, or rather, partner. Thank you for coming with an unbreakable “we can do it” mentality, and rescuing a project that would have died away without you. Thank you for always offering a helping hand, whether it was for thesis writing, moving an apartment, or finishing a bottle of wine.

Marco Pisano. Marcone. Pijamo. What can I say. It's hard to imagine a world where I can't have coffee without you twice a day. Thank you for being a partner in crime for literally anything during the past years. Thank you for always being supportive, for all the great nights out, the awesome dinners at the collocation. Thank you for being a great friend.

Esra Guc. Esrusch. Thank you for being a great mentor in the imaging room. Thank you for always taking your time to explain and show things. Thank you for buffering Witusch. Thank you for the great times outside of the lab! Thank you for all the interesting conversations and being a joyful spirit!

Sachiko Hirose. Sach. Thank you for being my quiet, yet energetic office neighbor in all these years. Thank you for sharing other perspective on science and the world. Thank you for being my mentor for life any beyond. Thank you for making sure the lab runs smoothly behind the scenes.

Efthymia Vokalis. Effie. Kollite. Thank you for always listening, always helping, always lending a hand when needed. Thank you having been the calm, rational spirit in the lab. Thank you for showing me that a PhD can eventually be finished!

Marcela Rincon. Matschuppita. Thank you for always helping around the lab. Thank you for always smiling. Thank you for brining some Latin vibes to the lab. Like Effie, thank you for showing me that a PhD can eventually be finished!

Valentina Triacca. Vale. Thank you for being one of the few “normal ones” around. Thank you for always being kind and helpful. Thank you for always giving rational suggestions. Thank you for sharing great moments outside of the lab, on Aare, on the slopes, during beers! Thank you for making sure Pijamo stayed healthy.

Lambert Potin. Poppotino. Don L. Thank you for “going hard or going home”. Thank you for closing Jagger’s with me. Thank you for working on our project so hard. Thank you for asking the critical questions. Thank you for hosting and feeding me whenever needed. Thank you for Ubering with me.

Alexandre De Titta. Alehandros. Thank you for all the great times. Thank you for organizing some of the best parties in town. Thank you for being an awesome office neighbor. Thank you for immersing me in the local Vaudoise culture. Thank you for all the fun Jass evenings.

Marie Ballester. Mariiii. Thank you for having been as you are. Thank you for having shared lots of great moments. Thank you for having brought the sunshine even on the rainiest day. Thank you for having showed up at lab every now and sharing some laughs even if you were busy studying for your exams.

Cara Buchanan. Cara. Thank you for having joined “the other office side”. Thank you for always being kind, patient, and up for a chat. Thank you for enjoying live music and partying hard when needed. Thank you for bringing me closer to healthy food.

Christopher Tremblay. Chris. Thank you for having been my first amazing student. Thank you for having stayed motivated even if the project was painful at times. Thank you for helping us with all other experiments during that summer.

Elodie Da Costa. Elodia. Thank you for having been my second amazing student. Thanks for having spent all your energy and time on our project. Thank you for being a careful, independent and reliable. Thank you for showing me how I can improve myself.

Gabriele Galliverti. GG. Thank you GG for all the Espresso. Thank you for all the great scientific conversations. Thank you for all the insights from the Milanese lifestyle. Thank you for being a considerate office neighbor.

Ingrid Van Mier. Ingrido. Thank you for bringing some Züridütsch combined with some hoe gaat het met jou to the lab. Thank you for always being in for a little chitchat, for always having a story to tell.

Sylvie Hauert. Sylvie. Thank you for being the unpredictable. Thank you for all the shots at Jagger's. Thank you for running the lab meeting smoothly and having skipped me whenever needed.

Léa Maillat. Léa. Thank you for having been a great lab mate during the short time we overlapped. Thank you for having kept me safe and sound during my time in Chicago.

Patricia Cortes. Patricia. Thank you for being the "lab mother". Thank you for making sure this place kept running. Thank you for always being nice even if you had reason enough to be super mad. Thank you for all your experimental help. Thank you for sharing some Vaudoise culture.

Yassin Ben Saida. Yassino. Thank you for being the fittest and coolest lab tech around. Thank you for all your help with experiments. Thank you for having tried to make me a machine in the gym. And sorry it didn't quite work out.

Ingrid Margot. Ingrid. Thank you for making sure the administration was running so smoothly. Thank you for making even the most impossible thing possible. Vielen herzlichen Dank für alles!

Natacha Bordry. Tuscha. Thank you for bringing in the crazy MD spirit every now and then. Thank you for all the great times inside and outside the lab. Thank you for all your help on our joint project.

Stephan Wullschleger. Thank you for all your support and time on our joint project. Thank you for all the fruitful discussions.

Jenny Shu. Jenny. Thank you for having been a great role model. Thank you for having made sure that I will not only do science. Thank you for having opened me the doors to the exciting visions and opportunities that brought me here.

Ton Schumacher. Ton. Thank you for having accepted me to your lab as a master student without any skills. Thank you for having immersed me in the exciting world of tumor immunology. Thank you for having given me the opportunity to go see how things are done in Boston.

Paul König, Paule. Thank you for being a mentor and companion in my early lab days. Thank you for having taught me the basics of biology. Thank you for having shown me that making mistakes is human.

My friends in Bern and elsewhere. Thank you for always being there, no matter how long I disappear. Thank you for reminding me that there is another life besides work.

Florian Aeschmann. Flo. Thank you for sharing the thesis writing time with me. Thank you for all the coffees, lunches, dinners, and scientific discussion. Suffering together was mutually supportive.

Marianna, Andreas, Simi, Hu Yi Schmid. Thank you for always taking me as I am. Thank you for all the great moments we have shared and will share.

Barbara and Christoph Fankhauser. Ma und Peppel. Thank you for your unconditional support. Thank you for never asking why, what and where. Thank you for trusting me in taking the right decisions. Thank you for having been so generous and caring all along this time.

Anna Schmid. Mini Anna. Where would I be without you? Certainly not as safe and sound as I am today. Thank you for always having offered a safe haven, even during the stormiest times. Thank you for taking me as I am. This thesis is dedicated to you and our future together ☺

## Abstract

Skin cancer is the most commonly diagnosed human malignancy. Even though melanoma only accounts for 1% of all skin cancer cases, it causes the vast majority of skin cancer deaths. There is currently no conventional treatment available that is able to cure metastatic melanoma patients. However, recent advances in the understanding of immunology have led to the development of an entirely novel treatment modality: cancer immunotherapy. Cancer immunotherapy approaches are designed to raise potent, tumor-specific T cell responses that are able to recognize and eliminate cancerous cells. Despite the fact that for the first time in history some metastatic melanoma patients can be cured, it is currently unclear why a large fraction of patients does not respond to immunotherapy. Thus, the overarching goal of this thesis was to gain a better understanding of the molecular mechanisms dictating the outcome to immunotherapy.

Pre-existing inflammation within the tumor microenvironment is associated with good clinical prognosis following immunotherapy. Because our lab has previously shown that tumor associated lymphatic vessels can modulate tumor inflammation, we hypothesized that the lymphatic system might be involved in modulating the outcome of cancer immunotherapy. To explore this hypothesis, we characterized two mouse models that recapitulate primary human lymphangiogenic melanoma. Using these models, we found that the secretion of CCL21 chemokine is a novel mechanism by which tumor associated lymphatics can actively attract naïve T cells into the tumor microenvironment. Interestingly, we found that immunogenic cell death following tumor antigen-specific immunotherapy induced activation of these naïve T cell infiltrates, which not only resulted in eradication of the primary melanoma tumors, but also conferred the mice with long-term protection against tumor re-challenge. We thus demonstrate that lymphatics actively increase the quantity and quality of tumor inflammation, thereby establishing a microenvironment that is able to potentiate antigen-specific immunotherapy.

We then engineered an injectable hydrogel system based on fibrin and functionalized polyethylene glycol, and show that controlled release of VEGFC from these hydrogels leads to lymphangiogenesis in the mouse dermis. Similar to what we found in lymphangiogenic tumors, engineered lymphangiogenic skin sites displayed increased expression of CCL21, and increased infiltrations of CD4<sup>+</sup> and CD8<sup>+</sup> T cells. Delivery of the model antigen ovalbumin into lymphangiogenic sites led to enhanced release of the effector cytokine interferon- $\gamma$  upon antigen-restimulation, suggesting that engineered lymphangiogenic sites could be exploited for therapeutic immunomodulation.

Finally, to better understand mechanisms underlying successful cancer immunotherapy, we established a tool for the observation of anti-tumor immune responses in the context of the native tumor microenvironment. By combining existing methods in a novel way, we developed an intravital microscopy method based on immunofluorescence that allows simultaneous, high resolution and dynamic visualization of the tumor microenvironment including immune cells and extracellular matrix proteins.

In conclusion, this thesis demonstrates that lymphatic endothelial cells orchestrate immune cell recruitment into peripheral tissues by secretion of CCL21 chemokine, both in steady-state and

disease. Our findings add more evidence to the hypothesis that LECs might play an underappreciated role in driving the formation of peripheral sites of immunomodulation. Our findings have translational potential, as immune cell infiltrates attracted by local lymphangiogenesis can be exploited for therapeutic immune regulation, such as to improving the efficacy of cancer immunotherapy.

Keywords: cancer, melanoma, immunotherapy, lymphangiogenesis, VEGFC, tumor infiltrating lymphocytes, tumor microenvironment, bioengineering, hydrogels, intravital microscopy

## Sommario

Il cancro della pelle è il tumore maligno più comunemente diagnosticato umana. Anche se il melanoma rappresenta solo l' 1% di tutti i casi di cancro della pelle, che provoca la stragrande maggioranza dei decessi per cancro della pelle. Non vi è attualmente alcun trattamento convenzionale disponibile che è in grado di curare pazienti con melanoma metastatico. Tuttavia, recenti progressi nella comprensione dell'immunologia hanno portato allo sviluppo di una completamente nuova modalità di trattamento: immunoterapia del cancro. Questi approcci, cosiddetti metodi immunoterapici per il cancro, sono progettati per sollevare una potente risposta immunitaria da parte delle cellule T specifiche per il tumore, le quali sono in grado di riconoscere ed eliminare le cellule cancerogene. Utilizzando gli approcci immunoterapici, alcuni pazienti con melanoma metastatico sono stati completamente curati, per la prima volta nella storia. Ad oggi, la terapia cellulare adottiva con cellule T (ACT) e il blocco dei checkpoint rappresentano le immunoterapie più efficaci nel trattamento del melanoma metastatico. La terapia ACT, l'infusione di cellule T che sono istruite e/o attrezzate a riconoscere e uccidere le cellule tumorali, di solito guarisce circa il 20% dei pazienti. Il blocco dei checkpoint, consistente nell'uso di anticorpi per bloccare le vie molecolari essenziali per la soppressione delle cellule T, ha dimostrato di avere un potenziale terapeutico simile. Nonostante questi risultati incoraggianti, non è ancora chiaro il motivo per cui una larga parte di pazienti non risponde alle immunoterapie. Pertanto, l'obiettivo di questa tesi è lo studio e l'analisi dei meccanismi molecolari che dettano il risultato di immunoterapia.

Uno stato infiammatorio preesistente all'interno del microambiente tumorale è associato ad un buon risultato clinico dopo l'immunoterapia. Poiché il nostro laboratorio ha già dimostrato che i vasi linfatici presenti nella massa tumorale possono modulare tale infiammazione, abbiamo ipotizzato che il sistema linfatico possa avere un ruolo importante nel modulare l'immunoterapia del cancro. Per esplorare questa ipotesi, abbiamo caratterizzato due modelli murini che ricapitolano il melanoma primario linfangiogenico umano: il B16 con sovraespressione di VEGFC (B16-OVA/VC) e il melanoma mutante iBIP2 guidato dal BRAF. Usando questi modelli, abbiamo evidenziato per la prima volta come la secrezione della chemochina CCL21 sia un meccanismo attraverso il quale i linfatici associati al tumore possono aumentare attivamente la presenza di cellule T naive nel tumore primario. Abbiamo scoperto che la morte cellulare immunogenica seguente all'immunoterapia induce l'attivazione di tali cellule immunitarie, le quali non solo provocano l'eliminazione del melanoma primario, ma conferisce ai topi anche una protezione a lungo termine contro la ricrescita tumorale. In conclusione, abbiamo dimostrato che i vasi linfatici aumentano la quantità e la qualità di infiammazione tumorale, promuovendo così un microambiente che favorisce e intensifica l'effetto dell'immunoterapia antigene-specifica.

Per decifrare ulteriormente il ruolo delle cellule endoteliali linfatiche nello sviluppo della risposta immunitaria nei tessuti periferici, abbiamo voluto creare una piattaforma che consente l'induzione di linfangiogenesi in un ambiente più controllato rispetto al tumore. Abbiamo quindi ingegnerizzato un sistema basato su un idrogel iniettabile, composto da fibrina e poly(ethylene glycol) (PEG), mostrando che il rilascio controllato del fattore di crescita linfatica VEGFC a partire da questo

idrogelo induce linfangiogenesi nei tessuti periferici. Analogamente a quanto abbiamo trovato nei tumori linfangiogenici, i tratti di pelle ingegnerizzati per indurre linfangiogenesi presentano un incremento nell'espressione di CCL21, e una maggiore infiltrazione di cellule CD4<sup>+</sup> e CD8<sup>+</sup>. La presentazione simultanea del modello di antigene ovoalbumina nei siti linfangiogenici ha comportato un aumento del rilascio della citochina interferone- $\gamma$  a seguito della ri-stimolazione con lo stesso antigene, suggerendo che i siti con linfangiogenesi ingegnerizzata possono essere sfruttati per l'immunomodulazione terapeutica.

Infine, per meglio comprendere il meccanismo alla base dell'immunoterapia del cancro, abbiamo voluto sviluppare uno strumento che consenta l'osservazione di risposte antitumorali immunitarie nel contesto del microambiente tumorale nativo. Combinando metodi esistenti in un modo nuovo, abbiamo sviluppato un nuovo metodo di microscopia intravitale basato sull'immunofluorescenza, la quale permette allo stesso tempo una alta risoluzione ed una visualizzazione dinamica delle diverse componenti del microambiente tumorale. Utilizzando questa modalità di imaging, siamo stati in grado di osservare i processi dinamici nel microambiente tumorale, come l'uccisione delle cellule tumorali mediata dai linfociti.

Nel suo insieme, questa tesi di ricerca dimostra che le cellule endoteliali linfatiche orchestrano il reclutamento delle cellule immunitarie nei tessuti periferici attraverso la secrezione della chemochina CCL21, sia in omeostasi che in condizioni patologiche. I nostri risultati aggiungono ulteriori elementi di prova a sostegno dell'ipotesi formulata in precedenza, secondo la quale le LECs potrebbero avere un ruolo, finora sottovalutato, nel guidare la formazione di siti periferici di immunomodulazione, i cosiddetti organi linfoidi terziari. Infine, abbiamo dimostrato come sia possibile ingegnerizzare uno stato immunitario localizzato basato sulla linfangiogenesi, e susseguentemente sfruttarlo per regolazione terapeutica della risposta immunitaria, in modo da migliorare l'efficacia dell'immunoterapia del cancro.

Parole chiave: cancro, melanoma, immunoterapia, linfangiogenesi, VEGFC, linfociti infiltranti il tumore, microambiente tumorale, idrogeli, rilascio controllato, microscopia intravitale.

## Résumé

Cancer de la peau est le cancer le plus fréquemment diagnostiqué humaine. Même si le mélanome ne représente que 1 % de tous les cas de cancer de la peau, il provoque la grande majorité des décès dus au cancer de la peau. Il n'y a actuellement aucun traitement conventionnel disponible qui est capable de guérir les patients atteints de mélanome métastatique. Cependant, les avancées récentes dans la compréhension de l'immunologie ont conduit à l'élaboration d'un mode de traitement entièrement nouvelle : immunothérapie du cancer. Les immunothérapies contre le cancer servent à induire une réponse de type lymphocyte T, puissante et spécifique à la tumeur, qui est capable de reconnaître et éliminer les cellules cancéreuses. Grâce aux immunothérapies, certains patients atteints de mélanomes avancés ont été entièrement guéris. A ce jour, le transfert adoptif de cellules (ACT) et le "blocage de checkpoints" sont les thérapies les plus efficaces dans le traitement du mélanome. L'infusion de lymphocytes T manipulés afin de reconnaître et de tuer la tumeur (aussi appelé ACT) peut soigner jusqu'à 20% des patients. Le blocage de molécules inhibitrices de lymphocytes T par des anticorps monoclonaux (blocage de checkpoints) est aussi efficace que l'ACT. En dépit de ces résultats encourageants, on ne comprend pas encore pourquoi la plupart des patients de répondent pas à ces modalités immunothérapeutiques. Par conséquent, le but principal de cette thèse était de comprendre et décrire certains des mécanismes moléculaires impliqués dans la réponse aux immunothérapies.

L'inflammation pré-existante dans le microenvironnement de la tumeur est associé à des résultats positifs d'immunothérapie. Comme notre laboratoire a auparavant montré que les vaisseaux lymphatiques associés aux tumeurs peuvent moduler l'inflammation tumorale, nous avons émis l'hypothèse que le système lymphatique pourrait jouer un rôle encore méconnu dans la modulation de l'immunothérapie du cancer. Afin d'explorer cette hypothèse, nous avons étudié deux modèles murins qui récapitulent le mélanome lymphangiogénique humain, notamment le mélanome B16 qui surexprime VEGFC (B16-OVA/VC) et le mélanome iBIP2 dû à une mutation de BRAF. Grâce à ces modèles, nous avons trouvé que la sécrétion de la chimiokine CCL21 est un nouveau mécanisme par lequel les vaisseaux lymphatiques associés à la tumeur peuvent attirer des lymphocytes T naïfs dans la tumeur. Nous avons trouvé que la mort immunogénique des cellules tumorales suite à une immunothérapie spécifique aux antigènes de la tumeur induit l'activation des lymphocytes infiltrés dans la tumeur, ce qui non seulement mène à l'éradication des tumeurs, mais aussi confère une protection à long terme contre un re-challenge avec des cellules tumorales. En conclusion, nous démontrons que les vaisseaux lymphatiques augmentent la quantité et la qualité de l'inflammation tumorale et ainsi établissent un microenvironnement favorable aux immunothérapies spécifiques aux antigènes de la tumeur. Contre toute attente, même si la densité des vaisseaux lymphatiques et CCL21 constituent tous deux un pronostic négatif, les deux pourraient servir de biomarqueurs pour des résultats positifs suite à une immunothérapie spécifique à la tumeur.

Afin d'étudier plus en profondeur le rôle des cellules endothéliales lymphatiques (LECs) dans la modulation des réponses immunitaires dans les organes lymphoïdes périphériques, nous avons généré une plateforme qui permet l'induction de lymphangiogénèse d'une manière plus contrôlée que



dans une tumeur. Nous avons mis au point un système d'hydrogel injectable composé de fibrine et de poly(éthylène glycol) fonctionnalisé et avons montré que la libération contrôlée du facteur de croissance lymphatique VEGFC de ces gels mène à la lymphangiogénèse dans les tissus lymphatiques périphériques. Comme dans les tumeurs lymphangiogéniques, les sites cutanés injectés de gels lymphangiogéniques affichaient une expression élevée de CCL21 et une infiltration importante de lymphocytes T CD4<sup>+</sup> et CD8<sup>+</sup>. La livraison simultanée de l'antigène type ovalbumine dans les sites lymphangiogéniques mena à une sécrétion plus forte de la cytokine IFN- $\gamma$  après restimulation avec l'antigène, suggérant ainsi que les sites lymphangiogéniques mis au point pourraient être utilisés à des fins d'immunomodulation thérapeutique.

Finalement, afin de mieux comprendre les mécanismes régulant les immunothérapies fructueuses contre le cancer, nous avons essayé d'établir un outil qui permettrait d'observer les réponses immunitaires anti-tumorales dans le contexte du microenvironnement natif de la tumeur. En combinant des méthodes existantes d'une manière innovante, nous avons développé une nouvelle méthode de microscopie intravitale basée sur l'immunofluorescence qui permet une visualisation simultanée, dynamique et à haute résolution des différents composants du microenvironnement de la tumeur, notamment des cellules immunitaires et des protéines de la matrice extracellulaire. Grâce à cette méthode d'imagerie, nous avons pu observer des procédés dynamiques dans la tumeur tels que l'attaque des lymphocytes sur les cellules cancéreuses et leur mort ensuivante.

Dans l'ensemble, cette thèse démontre que les cellules endothéliales lymphatiques orchestrent le recrutement des cellules immunitaires dans les organes lymphoïdes périphériques en sécrétant la chimiokine CCL21, dans l'homéostasie et dans la maladie. Nos découvertes s'ajoutent à l'hypothèse que les LECs peuvent jouer un rôle encore sous-estimé dans la formation de sites lymphoïdes périphériques d'immunomodulation, aussi appelés organes tertiaires lymphoïdes. Finalement, nous montrons que le milieu local immunitaire formé par lymphangiogénèse peut être manipulé et exploité à des fins de régulations immunitaires thérapeutiques, comme pour améliorer l'efficacité des immunothérapies contre le cancer.

Mots-clefs: cancer, mélanome, immunothérapie, lymphangiogénèse, VEGF-C, lymphocytes infiltrant la tumeur, microenvironnement tumoral, hydrogels, libération contrôlée, microscopie intravitale.

# Table of Contents

<b>CHAPTER 1: OVERVIEW OF THE THESIS</b>	<b>1</b>
1.1 MOTIVATION	2
1.2 AIMS	4
1.3 THESIS OVERVIEW AND ACCOMPLISHMENTS	5
1.4 REFERENCES	7
 <b>CHAPTER 2: BACKGROUND AND STATE-OF-THE-ART</b>	 <b>9</b>
2.1 CANCER IMMUNOTHERAPY	10
2.1.1 THE TUMOR MICROENVIRONMENT SUPPRESSES THE CANCER-IMMUNITY CYCLE	10
2.1.2 IMMUNOTHERAPY AIMS AT BOOSTING THE CANCER-IMMUNITY CYCLE	12
2.1.3 BIOMARKERS IN CANCER IMMUNOTHERAPY	13
2.2 THE LYMPHATIC SYSTEM	14
2.2.1 THE LYMPHATIC SYSTEM AS A TRANSPORT ROUTE	14
2.2.2 LYMPHANGIOGENESIS	15
2.2.3 THE LYMPHATIC SYSTEM AS AN ACTIVE IMMUNOMODULATOR	18
2.3 REFERENCES	21
 <b>CHAPTER 3: NAÏVE T CELLS RECRUITED TO LYMPHANGIOGENIC MELANOMA VIA CCL21 POTENTIATE ANTIGEN-SPECIFIC IMMUNOTHERAPY</b>	 <b>29</b>
3.1 ABSTRACT	30
3.2 INTRODUCTION	31
3.3 MATERIALS AND METHODS	33
3.3.1 MICE	33
3.3.2 TUMOR CELL LINES	33
3.3.3 B16 TUMOR INOCULATION, IBIP2 TUMOR INDUCTION, AND MEASUREMENTS	33
3.3.4 ANTIBODY INJECTIONS	33
3.3.5 THERAPEUTIC VACCINATION	34
3.3.6 OT-I <i>EX VIVO</i> ACTIVATION AND THERAPEUTIC ADOPTIVE TRANSFER	34
3.3.7 THERAPEUTIC DENDRITIC CELL VACCINATION	34
3.3.8 LYMPH NODE AND TUMOR CELL ISOLATION	34
3.3.9 IMMUNOHISTOCHEMISTRY	35
3.3.10 FLOW CYTOMETRY	36
3.3.11 ANALYSIS OF TCGA DATA SET CONTAINING 469 SKIN CUTANEOUS MELANOMA PATIENTS	36

3.3.12	STATISTICAL ANALYSIS	36
<b>3.4</b>	<b>RESULTS</b>	<b>37</b>
3.4.1	LYMPHANGIOGENIC B16 MELANOMAS ARE HIGHLY SENSITIVE TO ANTIGEN-SPECIFIC IMMUNOTHERAPY.	37
3.4.2	LYMPHANGIOGENIC B16 MELANOMAS SHOW INCREASED TILS OF REGULATORY AND NAÏVE PHENOTYPE.	39
3.4.3	CCL21 SECRETION IS UPREGULATED IN LYMPHANGIOGENIC B16 AND IBIP2 MELANOMAS.	42
3.4.4	VEGFC EXPRESSION CORRELATES WITH CCL21 AND CCR7 IN HUMAN PRIMARY AND METASTATIC MELANOMA.	45
3.4.5	LYMPHANGIOGENIC POTENTIATION OF ANTIGEN-SPECIFIC IMMUNOTHERAPY DEPENDS ON INTRATUMORAL ACTIVATION OF NAÏVE TILS.	47
3.4.6	MICE THAT REJECTED LYMPHANGIOGENIC B16 MELANOMAS AFTER ANTIGEN-SPECIFIC IMMUNOTHERAPY SHOW ANTIGEN SPREADING AND PROTECTION TO RE-CHALLENGE.	48
<b>3.5</b>	<b>DISCUSSION</b>	<b>52</b>
<b>3.6</b>	<b>REFERENCES</b>	<b>56</b>

## **CHAPTER 4: ENGINEERED LYMPHANGIOGENESIS PROMOTES LOCAL EXPRESSION OF CCL21 AND ACCUMULATION OF T CELL INFILTRATES**

<b>4.1</b>	<b>ABSTRACT</b>	<b>64</b>
<b>4.2</b>	<b>INTRODUCTION</b>	<b>65</b>
<b>4.3</b>	<b>MATERIALS AND METHODS</b>	<b>67</b>
4.3.1	HYDROGEL-BINDING PROTEIN VARIANTS	67
4.3.2	HYDROGEL SYNTHESIS, PREPARATION, AND INJECTION	67
4.3.3	VEGFR3 PHOSPHORYLATION ASSAY	68
4.3.4	PLASMIN INHIBITION ASSAY	68
4.3.5	OT-I PROLIFERATION ASSAY	68
4.3.6	<i>IN VITRO</i> VEGFC-TG RELEASE ASSAY	68
4.3.7	MICE	69
4.3.8	INTRAVITAL IMAGING AND ANALYSIS	69
4.3.9	LYMPH NODE AND GEL SITE CELL ISOLATION	69
4.3.10	FLOW CYTOMETRY	70
4.3.11	ELISA AND LUMINEX	70
4.3.12	ELISPOT ASSAY	71
<b>4.4</b>	<b>RESULTS</b>	<b>72</b>
4.4.1	PURIFICATION AND CHARACTERIZATION OF RECOMBINANT VEGFC-TG, APROTININ-TG, AND OVA-TG.	72
4.4.2	FIBRIN HYDROGELS CONTAINING APROTININ-TG CAN BE INJECTED INTRADERMALLY TO POLYMERIZE <i>IN SITU</i> AND PERSIST OVER EXTENDED PERIODS OF TIME <i>IN VIVO</i> .	75
4.4.3	EMPTY FIBRIN HYDROGELS INDUCE INFLAMMATION IN THE DRAINING LNs.	75

4.4.4	PEG GELS INDUCE INFLAMMATION AT THE INJECTION SITE BUT NOT IN THE DRAINING LNS.	78
4.4.5	THE RELEASE RATE OF VEGFC FROM PEG HYDROGELS DICTATES THE SITE OF LYMPHANGIOGENESIS.	79
4.4.6	VEGFC-TG INDUCED LYMPHANGIOGENESIS INCREASES LOCAL CCL21 EXPRESSION.	79
4.4.7	LYMPHANGIOGENESIS INCREASES LOCAL INFILTRATION OF CD4 <sup>+</sup> AND CD8 <sup>+</sup> T CELLS.	82
4.4.8	ENGINEERED LYMPHANGIOGENIC SITES MODULATE LOCAL IMMUNE RESPONSES.	83
<b>4.5</b>	<b>DISCUSSION</b>	<b>85</b>
<b>4.6</b>	<b>REFERENCES</b>	<b>89</b>

## **CHAPTER 5: INTRAVITAL IMMUNOFLUORESCENCE IMAGING OF THE DYNAMIC TUMOR MICROENVIRONMENT**

<b>5.1</b>	<b>ABSTRACT</b>	<b>96</b>
<b>5.2</b>	<b>INTRODUCTION</b>	<b>97</b>
<b>5.3</b>	<b>PROTOCOL</b>	<b>99</b>
5.3.1	TUMOR INOCULATION OF THE EAR	99
5.3.2	INTERACTIONS OF ACTIVATED SPLENOCYTES WITH TUMOR CELLS <i>IN SITU</i>	99
5.3.3	EAR SURGERY	101
5.3.4	IMMUNOFLUORESCENCE STAINING	101
5.3.5	INTRAVITAL IMAGING USING FLUORESCENCE STEREOMICROSCOPE	102
5.3.6	INTRAVITAL IMAGING USING TWO-PHOTON MICROSCOPY	102
5.3.7	REAGENTS	103
<b>5.4</b>	<b>RESULTS</b>	<b>104</b>
5.4.1	IMMERSION OF THE EXPOSED EAR TISSUE IN A LARGE VOLUME OF ASCORBATE BUFFER INHIBITS PHOTOBLEACHING DURING IMAGE ACQUISITION.	104
5.4.2	INTRAVITAL IMMUNOFLUORESCENCE CAN BE USED TO VISUALIZE ECM COMPONENTS SUCH AS PERLECAN AND CCL21 IN THE NORMAL MOUSE EAR.	104
5.4.3	INTRAVITAL IMMUNOFLUORESCENCE IS SUITABLE FOR THE LONG-TERM VISUALIZATION OF INTERACTIONS BETWEEN TUMOR CELLS AND THEIR MICROENVIRONMENT INCLUDING ANTI-TUMOR IMMUNE RESPONSES.	106
5.4.4	INTRAVITAL TWO-PHOTON MICROSCOPY CAN BE USED TO VISUALIZE B16F10 MELANOMA CELLS IN THE CONTEXT OF FIBRILLAR AND NON-FIBRILLAR EXTRACELLULAR MATRIX PROTEINS.	108
<b>5.5</b>	<b>DISCUSSION</b>	<b>111</b>
<b>5.6</b>	<b>REFERENCES</b>	<b>113</b>

<b>CHAPTER 6: CONCLUSIONS, IMPLICATIONS AND FUTURE DIRECTIONS</b>	<b>117</b>
6.1 LEC-MEDIATED CHEMOKINE SECRETION AS A DRIVING FORCE OF IMMUNE CELL TRAFFICKING INTO PERIPHERAL TISSUES	118
6.2 EXPLOITING LYMPHANGIOGENIC SITES TO INDUCE TOLERANCE OR IMMUNITY: A QUESTION OF CONTEXT?	121
6.3 IMPLICATIONS FOR THE TRANSLATION INTO CLINICS	121
6.4 FUTURE DIRECTIONS	122
6.4.1 THE ROLE OF LYMPHANGIOGENESIS IN CANCER IMMUNOTHERAPY	122
6.4.2 ENGINEERING LYMPHANGIOGENIC SITES FOR THERAPEUTIC IMMUNOMODULATION	123
6.4.3 INTRAVITAL IMMUOFLUORESCENCE TO OBSERVE ANTI-TUMOR IMMUNE RESPONSES	123
6.5 REFERENCES	124
 7 CURRICULUM VITAE	 127

## Table of Figures

Figure 2.1 The Hallmarks of Cancer.....	10
Figure 2.2 The Cancer-Immunity Cycle.....	11
Figure 2.3 The targets of cancer immunotherapy.....	12
Figure 2.4 Mutational load across cancer types.....	14
Figure 2.5 The structure of the lymphatic network.....	16
Figure 2.6 Molecular pathways of lymphangiogenesis.....	17
Figure 2.7 Mechanisms of immunoregulation by lymphatic endothelial cells.....	19
Figure 3.1 Lymphangiogenic B16 melanomas respond to antigen-specific immunotherapy with increased growth in the short-term, but with profound regression in the long-term.....	38
Figure 3.2 (Supplementary Figure 3.1). Increased efficacy of immunotherapy in B16-OVA/VC tumor-bearing mice depends on host lymphangiogenesis.....	39
Figure 3.3 Lymphangiogenic B16 melanomas contain increased regulatory and naïve TILs.....	40
Figure 3.4 (Supplementary Figure 3.3). VEGFR3 blocking specifically abrogates intratumoral lymphatic endothelial cells within VEGFC overexpressing B16 melanomas.....	41
Figure 3.5 CCL21 secretion is upregulated in lymphangiogenic B16 melanomas and CCR7 signaling is essential to increased naïve T cell tumor infiltration.....	42
Figure 3.6 (Supplementary Figure 3.5).....	44
Figure 3.7 VEGFC expression correlates with CCL21 and CCR7 in human primary and metastatic melanoma.....	46
Figure 3.8 Intratumoral activation of CCR7 <sup>+</sup> immune cells following antigen-specific immunotherapy is responsible for increased efficacy in lymphangiogenic B16 melanomas.....	47
Figure 3.9 Mice that rejected primary lymphangiogenic B16 tumors in response to antigen-specific immunotherapy show antigen spreading and protection to re-challenge in a model of lung metastasis.....	49
Figure 3.10 (Supplementary Figure 3.9). Antigen-specific immunotherapy in lymphangiogenic B16 tumor bearing mice induces high levels of circulating SIINFEKL <sup>+</sup> and rare populations of gp100 <sup>+</sup> and Trp2 <sup>+</sup> CD8 <sup>+</sup> T cells, while primary tdLNs show melanin depositions.....	50
Figure 4.1 Purification and characterization of recombinant TG-proteins.....	73
Figure 4.2 Fibrin hydrogels containing aprotinin-TG can be injected intradermally to polymerize <i>in situ</i> and persist over extended periods of time <i>in vivo</i> .....	74
Figure 4.3 Empty fibrin hydrogels induce inflammation in the draining lymph node.....	76
Figure 4.4 PEG gels induce inflammation at the injection site but not in the dLNs.....	77
Figure 4.5 The release rate of VEGFC from PEG hydrogels dictates the site of lymphangiogenesis.....	78
Figure 4.6 VEGFC-TG induced lymphangiogenesis increases local CCL21 expression.....	80
Figure 4.7 Lymphangiogenesis increases the local infiltration of CD4 <sup>+</sup> and CD8 <sup>+</sup> T cells.....	81
Figure 4.8 Engineered lymphangiogenic sites modulate local immune responses.....	83
Figure 5.1 Schematic of the intravital immunofluorescence imaging method.....	100

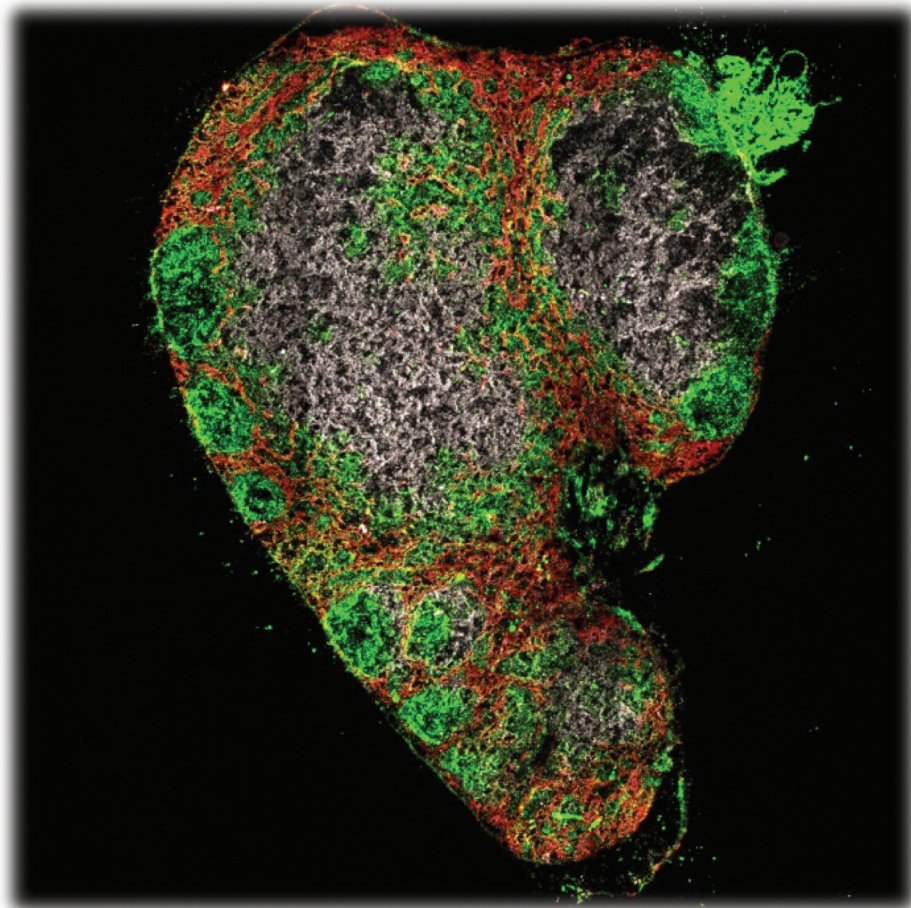
Figure 5.2 Placing the exposed ear tissue in a large volume of ascorbate buffer inhibits photobleaching during image acquisition. ....	105
Figure 5.3 Intravital immunofluorescence can be used to visualize ECM components such as perlecan and CCL21 in the normal mouse ear.....	106
Figure 5.4 Intravital immunofluorescence is suitable for the long-term visualization of interactions between tumor cells and their microenvironment including anti-tumor immune responses. ....	107
Figure 5.5 Intravital two-photon microscopy can be used to visualize B16F10 melanoma cells in the context of fibrillar and non-fibrillar extracellular matrix proteins.....	109
Figure 6.1 Lymphangiogenic potentiation of antigen-specific cancer immunotherapy. ....	120





## Chapter 1

### Overview of the thesis



Lymph node of a mouse with lymphatic vessels (red), B cell follicles (green), and T cell zones (gray).  
Confocal microscopy.

## 1.1 Motivation

Cancer is one of the major global health threats. It represents a collection of hundreds of types of diseases that all have one characteristic in common: the uncontrolled proliferation of cells that can eventually lead to organ failure and death. Facing the devastating consequences that these diseases have already had on our societies, former US president Richard Nixon even declared a “war on cancer” in 1971. This doctoral thesis can be considered as a small contribution to the global efforts that have ever since been devoted to winning this war.

A battle can be won in three steps: 1) Identify the most dangerous opponent, 2) try to understand how he operates, and 3) focus all the efforts on targeting his weaknesses. In case of this thesis, the opponent of choice was melanoma, a rare but deadly form of skin cancer. Even though melanoma only accounts for 1% of all skin cancer cases, it causes the vast majority of skin cancer deaths (Simões et al., 2015). Patients can only be cured by surgical resection of the tumor mass if they are diagnosed before the cancer was able to spread to distant organs. However, once melanoma cells colonize other organs such as lymph nodes, the lung, liver, or brain, the survival rate drops dramatically. Radio- and chemotherapy, the conventional approaches for cancer therapy, are unfortunately not able to cure metastatic patients. The quest for alternative therapeutic approaches led to the development of targeted therapies, small molecular drugs that inhibit proteins of cellular pathways essential for tumor growth (Flaherty, 2012). Introducing these drugs into clinics has doubled the 12-month overall survival of metastatic melanoma patients from about 36% using conventional therapy to about 72% (Eroglu and Ribas, 2016). However, because melanoma cells constantly mutate their genome, they evolve to survive in an ever-changing environment. This constant evolution ensures that the cells find alternative growth pathways that are not inhibited by targeted therapies, allowing them to develop so called resistance. Essentially all metastatic melanoma patients eventually develop resistance to targeted therapy and succumb to disease (Fedorenko et al., 2015; Holohan et al., 2013).

The recent introduction of a novel treatment modality, immunotherapy, has led to a paradigm shift in the fight against metastatic melanoma. Immunotherapy approaches are designed to raise a potent, tumor-specific immune response that is able to recognize and eliminate cancerous cells (Drake et al., 2013). Using immunotherapy, metastatic melanoma patients have been completely cured for the first time in the history. There are three main reasons why the immune system seems to be so efficient for anti-tumor therapy: Firstly, immune cells have evolved to specifically recognize their target cells, allowing them to kill cancer cells without damaging any normal tissues. Secondly, immune responses tackle cancer cells from multiple sides at the same time, thus making it more difficult for them to evolve resistance mechanism and escape therapy. Thirdly, the immune system develops memory, allowing it to recognize and eliminate cancer cells even more efficiently in case the tumor recurs at a later stage of life. Amongst the different immunotherapy approaches, adoptive T cell therapy (ACT) and checkpoint blockade have proven especially promising in human clinical trials. ACT, the infusion of autologous, *ex vivo* stimulated lymphocytes, has shown clinical response rates of up to 50%, with around 20% of patients being cured (Hinrichs and Rosenberg, 2014; Restifo et al.,

2012). Similarly, antibody-mediated blocking of pathways essential to T cell suppression, called checkpoint blockade, has resulted in complete response rates of up to 22% in human clinical trials (Larkin et al., 2015; Postow et al., 2015). Despite these encouraging results, about 80% of patients do not respond to immunotherapy. It is currently unclear, why only certain patient populations can benefit from immunotherapy. A better understanding of the molecular mechanisms dictating the clinical response to immunotherapy will allow the development of rational approaches to increase the number of metastatic melanoma patients who can be cured.

Until today, no clear-cut biomarkers have been described that are able to distinguish whether metastatic melanoma patients will or will not respond to immunotherapy (Patel and Kurzrock, 2015; Schumacher et al., 2015). However, recent research has highlighted that pre-existing inflammation within the tumor microenvironment is associated with good clinical outcome following these types of therapies (Ji et al., 2011; Spranger et al., 2015; Tumei et al., 2014). Interestingly, our lab has established several connections between the lymphatic system and tumor-associated inflammation over the past few years. For example, we have shown that CCL21, a chemokine that can be secreted by lymphatic endothelial cells (LECs), can promote inflammation in the tumor microenvironment (Shields et al., 2010). Furthermore, we found that lymphatic endothelial cells in the draining lymph node can actively regulate anti-tumor immune responses (Lund et al., 2012), and that the presence of tumor draining lymphatics is essential for the generation of a T cell inflamed microenvironment in mouse and human melanoma (Lund et al., under review). These findings have been strengthening the broader notion that the lymphatic system is not only a passive transport system, but actively involved in immune cell education and trafficking both in steady-state and disease (Card et al., 2014; Hirose and Dubrot, 2015; Hirose et al., 2014; Lund et al., 2016; Tewalt et al., 2012). However, it has never been explored whether and how peri- and intratumoral lymphatic vessels actively participate in the regulation of tumor inflammation. Because intratumoral lymphatic vessels (LVs) have previously been shown to be non-functional in terms of drainage (Padera et al., 2002), their relevance in tumor progression has always been questioned. Nevertheless, considering that secretion of bioactive factors and engagement in cell-cell interactions by LECs does not specifically require LVs to have a lumen, we hypothesized that both peri- and intratumoral LECs might be actively involved in the regulation of tumor inflammation. Furthermore, we speculated that if indeed this was the case, tumor-associated lymphatics might be critical in guiding the outcome of cancer immunotherapy. Not only could LECs be a biomarker to stratify patients eligible for immunotherapy, but inducing them locally might also improve response rates of patients with non-inflamed primary melanomas. The overall motivation behind this thesis research was thus to create knowledge and tools that could potentially have a translational impact on improving immunotherapy in metastatic melanoma patients.

## 1.2 Aims

The overall aim of this thesis was to determine whether and how peri- and intratumoral LECs are actively involved in the regulation of tumor inflammation, and if so, whether this could be therapeutically exploited. We wanted to approach our overall hypothesis from three different angles. First, we utilized two lymphangiogenic mouse melanoma models to study how peri- and intratumoral LEC density regulates the presence and/or phenotype of tumor infiltrating lymphocytes. Once characterized, we used these models to assess whether the extent of primary tumor lymphangiogenesis affects the outcome of different immunotherapy approaches. Second, we wanted to determine whether mechanistic findings from the tumor studies could be recapitulated and/or expanded by studying the same biology in a more controlled setting. We thus aimed at creating non-inflammatory lymphangiogenesis by engineering controlled release of VEGFC from intradermally injectable hydrogels. Third, we wanted to develop a novel intravital imaging method to study how anti-tumor immune responses unfold in the native tumor microenvironment.

The specific aims addressed in this thesis are:

- 1) Identify and characterize two mouse melanoma models that show similar peri- and intratumoral lymphatic density as human melanomas.
- 2) Using antibody-mediated anti-VEGFR3 blocking, determine whether peri- and intratumoral lymphatic density influences intratumoral cytokine levels in these models *in vivo*.
- 3) Similarly to 2), determine whether peri- and intratumoral lymphatic density influences the number and phenotype of tumor infiltrating lymphocytes *in vivo*.
- 4) Based on the insights gathered in 2) and 3), determine the mechanism of LEC-mediated immunoregulation in primary melanomas *in vivo*.
- 5) Assess whether and how the presence of peri- and intratumoral lymphatics influences the outcome of cancer immunotherapy *in vivo*.
- 6) Engineer a hydrogel-based system for controlled *in vivo* release of VEGFC to induce non-inflammatory lymphangiogenesis in mouse dermis.
- 7) Similarly to 2) and 3), assess whether engineered lymphangiogenesis induces changes in the local chemokine and/or immune cell milieu.
- 8) Determine whether engineered lymphangiogenic sites can be exploited for therapeutic immunoregulation.
- 9) Establish an intravital imaging method based on immunofluorescence that is suitable for the visualization with two-photon microscopy.
- 10) Using the intravital imaging method established in 9), study how anti-tumor immune responses unfold in the native tumor microenvironment, especially in the context of fibrillar and non-fibrillar extracellular matrix.

### 1.3 Thesis overview and accomplishments

The chapters of this thesis are summarized below to put their content in the context of the motivation and the overall goals.

Chapter 2 provides a general overview of relevant literature, focusing on the state-of-the-art in cancer immunotherapy and lymphatic immunomodulation.

Chapter 3 presents our studies on lymphangiogenic melanoma. Specifically, the aim of this chapter was to determine whether chemokine-mediated recruitment of tumor infiltrating lymphocytes (TILs) is dependent on lymphatic density within primary melanoma tumors, and if so, whether this could be therapeutically exploited. Using two lymphangiogenic mouse models, we found that the secretion of CCL21 chemokine is a novel mechanism by which tumor associated lymphatics can actively increase the recruitment of naïve CCR7<sup>+</sup> T cells into the primary tumor. To evaluate whether these findings are relevant in human, we mined a gene expression data set and show that the expression of VEGFC, CCL21 and CCR7 indeed correlate in human melanoma. Finally, we establish that naïve T cell infiltrates in lymphangiogenic tumors can be locally activated in response to immunotherapy, leading to antigen spreading and long lasting protection from tumor re-challenge. We conclude that peri- and intratumoral LECs secrete CCL21 to actively increase tumor inflammation, thereby establishing a microenvironment that is more sensitive to antigen-specific immunotherapy.

Chapter 4 builds upon the insights gained in chapter 3, and asks whether the observed mechanisms of LEC-mediated immunoregulation are specific to the tumor environment, or whether they are more broadly valid in settings of lymphangiogenesis. Specifically, we asked whether engineered lymphangiogenesis induces chemokine mediated immune cell recruitment into the steady-state dermis and if so, whether this could be therapeutically exploited. We first establish an injectable hydrogel system for the sustained and localized delivery of the lymphatic growth factor VEGFC, and show that this system is able to induce dermal lymphangiogenesis with minimal bystander inflammation. These lymphangiogenic sites resemble tertiary lymphoid organs (TLOs) as they present an altered immune milieu with high levels of CCL21 and T cells infiltrates, similar to what we observed in the lymphangiogenic melanomas in chapter 3. Delivering the model antigen ovalbumin (OVA) into engineered lymphangiogenic sites increased the numbers of IFN $\gamma$  secreting cells upon *ex vivo* antigen re-stimulation, indicating that engineered lymphangiogenic sites can potentially be exploited to steer therapeutic immune responses.

Chapter 5 describes a novel intravital imaging method that we established to study anti-tumor immune responses in the context of the native tumor microenvironment. The aim was to overcome certain shortcomings of existing intravital imaging methods, such as a limited variety of structures and cells that can be visualized, and photobleaching of fluorescent probes. We thus further optimized an existing protocol that is based on staining the exposed mouse ear dermis with primary and secondary

antibodies, so called intravital immunofluorescence (IF). Intravital IF allows simultaneous, high resolution and dynamic visualization of different components of the tumor microenvironment, including immune cells and fibrillar as well as mesh-like matrix proteins. The protocol includes all the procedures from tumor inoculation in the thin dorsal ear skin, to immunolabeling components of the tumor microenvironment with primary and secondary antibodies, to live imaging of the exposed tissue using fluorescence stereomicroscopy and two-photon microscopy. We show that intravital IF is suitable for the prolonged observation of interactions between tumor cells and their microenvironment, without inducing noticeable immunotoxicity or photobleaching. We thus propose that this novel method allows investigating dynamic processes within the tumor microenvironment, and might as such be used to better understand LEC-mediated immune regulation during cancer immunotherapy.

Chapter 6 summarizes the major conclusions that came out of this thesis research and proposes a novel model by which lymphatic vessels influence immunity by regulating immune cell trafficking into peripheral tissues. We discuss the implications that our results might have for the clinics, especially considering cancer immunotherapy, and suggest some of the most exciting directions that future research in this field could take.



## 1.4 References

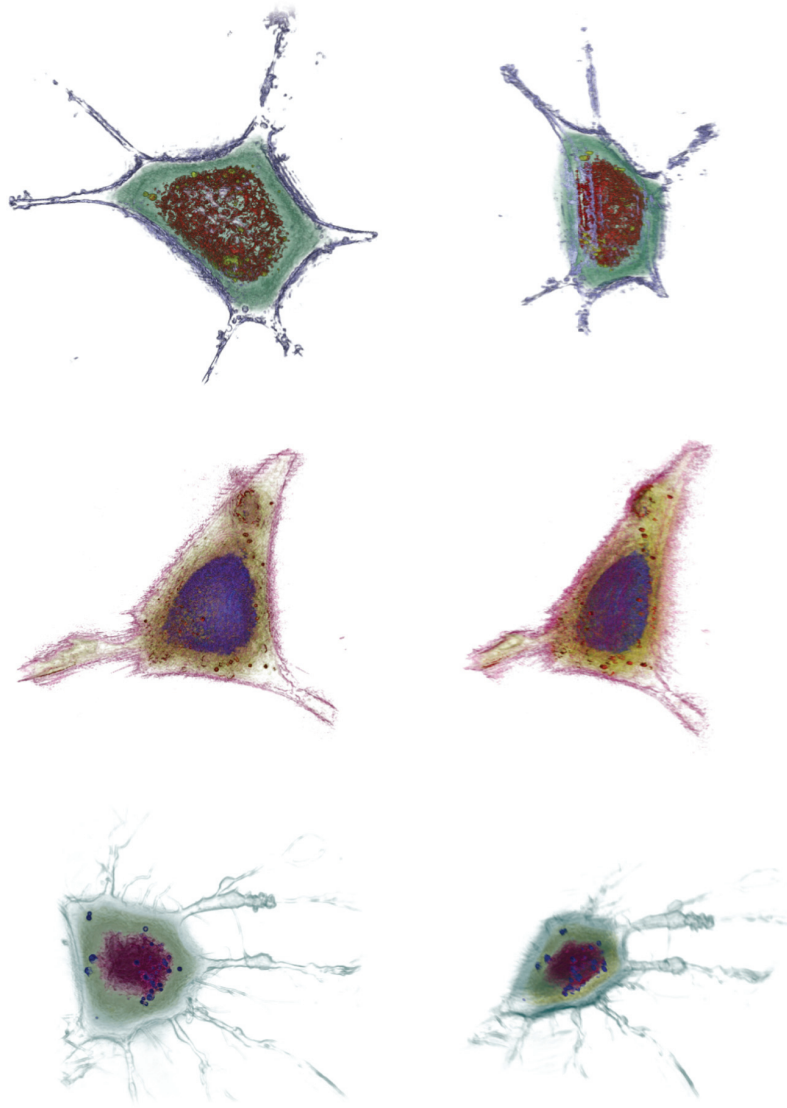
- Card, C.M., Yu, S.S., Swartz, M.A., 2014. Emerging roles of lymphatic endothelium in regulating adaptive immunity. *J. Clin. Invest.* 124, 943–952. doi:10.1172/JCI73316
- Drake, C.G., Lipson, E.J., Brahmer, J.R., 2013. Breathing new life into immunotherapy: review of melanoma, lung and kidney cancer. *Nat Rev Clin Oncol.* doi:10.1038/nrclinonc.2013.208
- Eroglu, Z., Ribas, A., 2016. Combination therapy with BRAF and MEK inhibitors for melanoma: latest evidence and place in therapy. *Ther Adv Med Oncol* 8, 48–56. doi:10.1177/1758834015616934
- Fedorenko, I.V., Gibney, G.T., Sondak, V.K., Smalley, K.S.M., 2015. Beyond BRAF: where next for melanoma therapy? *Br J Cancer* 112, 217–226. doi:10.1038/bjc.2014.476
- Flaherty, K.T., 2012. Targeting Metastatic Melanoma. *Annu. Rev. Med.* 63, 171–183. doi:10.1146/annurev-med-050410-105655
- Hinrichs, C.S., Rosenberg, S.A., 2014. Exploiting the curative potential of adoptive T-cell therapy for cancer. *Immunol. Rev.* 257, 56–71. doi:10.1111/imr.12132
- Hirosue, S., Dubrot, J., 2015. Modes of Antigen Presentation by Lymph Node Stromal Cells and Their Immunological Implications. *Front Immunol* 6, 446. doi:10.3389/fimmu.2015.00446
- Hirosue, S., Vokali, E., Raghavan, V.R., Rincon-Restrepo, M., Lund, A.W., Corthésy-Henrioud, P., Capotosti, F., Halin Winter, C., Hugues, S., Swartz, M.A., 2014. Steady-state antigen scavenging, cross-presentation, and CD8<sup>+</sup> T cell priming: a new role for lymphatic endothelial cells. *The Journal of Immunology* 192, 5002–5011. doi:10.4049/jimmunol.1302492
- Holohan, C., Van Schaeybroeck, S., Longley, D.B., 2013. Cancer drug resistance: an evolving paradigm. *Nature Reviews* doi:10.1038/nrc3599
- Ji, R.-R., Chasalow, S.D., Wang, L., Hamid, O., Schmidt, H., Cogswell, J., Alaparthi, S., Berman, D., Jure-Kunkel, M., Siemers, N.O., Jackson, J.R., Shahabi, V., 2011. An immune-active tumor microenvironment favors clinical response to ipilimumab. *Cancer Immunol Immunother* 61, 1019–1031. doi:10.1007/s00262-011-1172-6
- Larkin, J., Chiarion-Sileni, V., Gonzalez, R., Grob, J.J., Cowey, C.L., Lao, C.D., Schadendorf, D., Dummer, R., Smylie, M., Rutkowski, P., Ferrucci, P.F., Hill, A., Wagstaff, J., Carlino, M.S., Haanen, J.B., Maio, M., Marquez-Rodas, I., McArthur, G.A., Ascierto, P.A., Long, G.V., Callahan, M.K., Postow, M.A., Grossmann, K., Sznol, M., Dreno, B., Bastholt, L., Yang, A., Rollin, L.M., Horak, C., Hodi, F.S., Wolchok, J.D., 2015. Combined Nivolumab and Ipilimumab or Monotherapy in Untreated Melanoma. *N Engl J Med* 373, 23–34. doi:10.1056/NEJMoa1504030
- Lund, A.W., Duraes, F.V., Hirosue, S., Raghavan, V.R., Nembrini, C., Thomas, S.N., Issa, A., Hugues, S., Swartz, M.A., 2012. VEGF-C promotes immune tolerance in B16 melanomas and cross-presentation of tumor antigen by lymph node lymphatics. *Cell Rep* 1, 191–199. doi:10.1016/j.celrep.2012.01.005
- Lund, A.W., Medler, T.R., Leachman, S.A., Coussens, L.M., 2016. Lymphatic Vessels, Inflammation, and Immunity in Skin Cancer. *Cancer Discovery* 6, 22–35. doi:10.1158/2159-8290.CD-15-0023

- Patel, S.P., Kurzrock, R., 2015. PD-L1 Expression as a Predictive Biomarker in Cancer Immunotherapy. *Molecular Cancer Therapeutics* 14, 847–856. doi:10.1158/1535-7163.MCT-14-0983
- Postow, M.A., Chesney, J., Pavlick, A.C., Robert, C., Grossmann, K., McDermott, D., Linette, G.P., Meyer, N., Giguere, J.K., Agarwala, S.S., Shaheen, M., Ernstoff, M.S., Minor, D., Salama, A.K., Taylor, M., Ott, P.A., Rollin, L.M., Horak, C., Gagnier, P., Wolchok, J.D., Hodi, F.S., 2015. Nivolumab and Ipilimumab versus Ipilimumab in Untreated Melanoma. *N Engl J Med* 372, 2006–2017. doi:10.1056/NEJMoa1414428
- Restifo, N.P., Dudley, M.E., Rosenberg, S.A., 2012. Adoptive immunotherapy for cancer: harnessing the T cell response. *Nat. Rev. Immunol.* 12, 269–281. doi:10.1038/nri3191
- Schumacher, T.N., Kesmir, C., van Buuren, M.M., 2015. Biomarkers in Cancer Immunotherapy. *Cancer Cell* 27, 12–14. doi:10.1016/j.ccell.2014.12.004
- Shields, J.D., Kourtis, I.C., Tomei, A.A., Roberts, J.M., Swartz, M.A., 2010. Induction of lymphoidlike stroma and immune escape by tumors that express the chemokine CCL21. *Science* 328, 749–752. doi:10.1126/science.1185837
- Simões, M.C.F., Sousa, J.J.S., Pais, A.A.C.C., 2015. Skin cancer and new treatment perspectives: a review. *Cancer Lett.* 357, 8–42. doi:10.1016/j.canlet.2014.11.001
- Spranger, S., Bao, R., Gajewski, T.F., 2015. Melanoma-intrinsic  $\beta$ -catenin signalling prevents anti-tumour immunity. *Nature* 523, 231–235. doi:10.1038/nature14404
- Tewalt, E.F., Cohen, J.N., Rouhani, S.J., Engelhard, V.H., 2012. Lymphatic endothelial cells—key players in regulation of tolerance and immunity. *Front Immunol.* doi:10.3389/fimmu.2012.00305/abstract
- Tumeh, P.C., Harview, C.L., Yearley, J.H., Shintaku, I.P., Taylor, E.J.M., Robert, L., Chmielowski, B., Spasic, M., Henry, G., Ciobanu, V., West, A.N., Carmona, M., Kivork, C., Seja, E., Cherry, G., Gutierrez, A.J., Grogan, T.R., Mateus, C., Tomasic, G., Glaspy, J.A., Emerson, R.O., Robins, H., Pierce, R.H., Elashoff, D.A., Robert, C., Ribas, A., 2014. PD-1 blockade induces responses by inhibiting adaptive immune resistance. *Nature* 515, 568–571. doi:10.1038/nature13954



## Chapter 2

### Background and state-of-the-art



Lymph node stromal cells acquired with the Nanolive 3D CellExplorer.  
Courtesy of Christopher Tremblay.

## 2.1 Cancer immunotherapy

### 2.1.1 The tumor microenvironment suppresses the Cancer-Immunity Cycle

Genomic instability is the most prominent characteristic shared amongst cancer cells. Together with tumor-promoting inflammation, genetic alterations represent the so-called enabling characteristics that drive the eight hallmarks of cancer: sustained proliferative signaling, evading growth suppressors, enabling replicative immortality, activating invasion and metastasis, inducing angiogenesis, resisting cell death, avoiding immune destruction, and deregulating cellular energetics (Figure 2.1) (Hanahan and Weinberg, 2011). Even though random mutations are essential for tumor initiation and progression, they also render cancer cells vulnerable to immune cell destruction. This is because mutations can lead to the aberrant expression of tumor antigens including neoantigens, differentiation antigens, and cancer testis antigens, which are then presented by cancer cells on major histocompatibility class I and II (MHC I and MHC II) molecules (Chen and Mellman, 2013). Recognition of these cancer-specific peptide-MHC complexes by cognate T cells can initiate spontaneous anti-tumor immune responses, occasionally leading to tumor regression (Halliday et al., 1995; Heemskerk

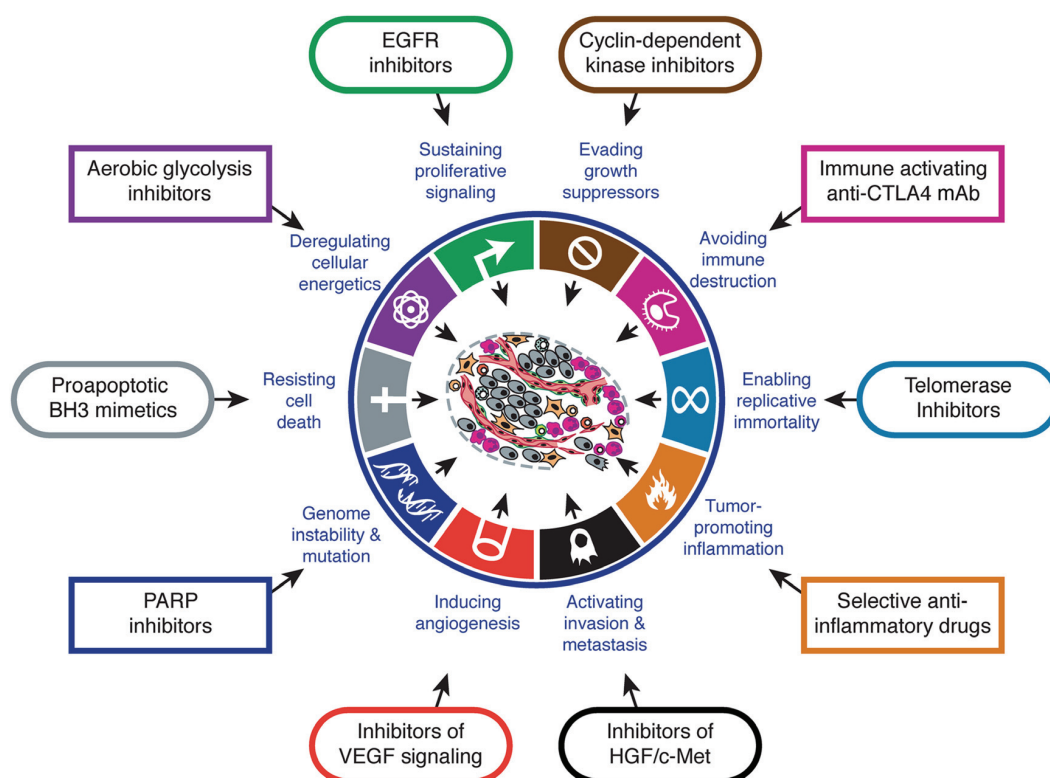


**Figure 2.1 The Hallmarks of Cancer.** There are ten capabilities necessary for tumor growth and progression. Genome instability and tumor promoting inflammation are the enabling characteristics that drive the eight hallmarks of cancer: sustained proliferative signaling, evading growth suppressors, enabling replicative immortality, activating invasion and metastasis, inducing angiogenesis, resisting cell death, avoiding immune destruction, and deregulating cellular energetics. The two latter ones have only recently been added to this list, and are thus called emerging hallmarks. Drugs targeting each one of these characteristic have been developed (shown in the most outer circle), some of which are used in clinics today. Illustration taken from Hanahan and Weinberg, 2011.

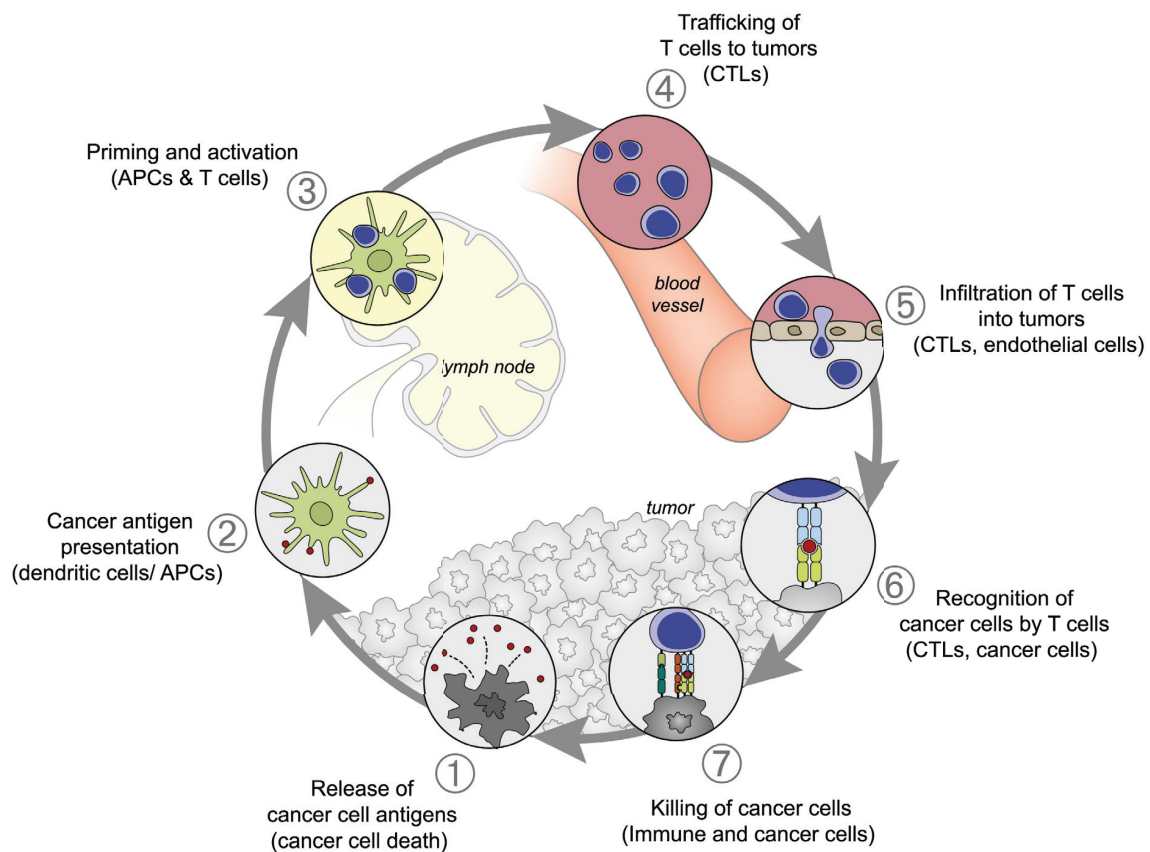


**Figure 2.2 The Cancer-Immunity Cycle.** The immune system is highly efficient in recognizing and killing tumor cells. However, the induction of anti-tumor immune responses requires a series of stepwise events to take place. (1) Tumor-associated antigens are released by dying cancer cells and captured by dendritic cells (DCs). (2) DCs process the antigens, migrate to the draining lymph node, and present them on MHC class I and II molecules to the naïve T cell repertoire. (3) If a T cell recognizes its cognate antigen, priming and activation ensues, leading to an effector T cell response against the tumor antigen. (4) Effector T cells egress into the circulation to home to and (5) extravasate into the tumor tissue. (6) In the tumor tissue, the interaction between the T cell receptor (TCR) and its cognate antigen presented by MHC-I on the cancer cell surface leads to the release of mediators such as IFN $\gamma$  and perforins that (7) induce tumor cell death. The Cancer-Immunity Cycle represents a positive feedback loop that is able to increase the breadth and depth of an ongoing anti-tumor immune response. However, in order to escape immune-mediated destruction, tumors evolve immunosuppressive mechanisms to inhibit one or multiple steps of the Cancer-Immunity Cycle. Illustration taken from Chen and Mellman, 2013.

et al., 2013). However, tumors have several strategies to escape immune-mediated destruction. One such strategy, immunoediting, has been described by Dunn and colleagues (Dunn et al., 2002; 2004). During immunoediting, cancer cells that express T cell targets are eliminated, while cells that have evolved genetic and epigenetic changes conferring them with resistance to immune detection and/or elimination will be selected for. Another set of evasion strategies, collectively called immunosuppressive mechanisms of the tumor microenvironment, actively dampen anti-tumor immune responses in lymphoid organs and in the tumor microenvironment itself (Rabinovich et al., 2007). These mechanisms can interfere at any step of the Cancer-Immunity Cycle, a stepwise process needed to initiate effective anti-tumor immune responses (Figure 2.2) (Chen and Mellman, 2013).

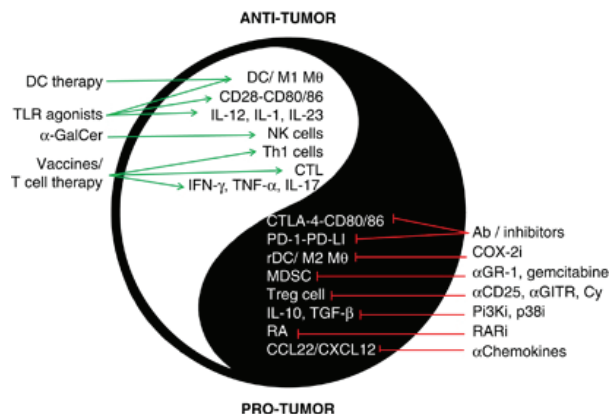


**Figure 2.3 The targets of cancer immunotherapy.** Cancer immunotherapy aims at initiating or potentiating the Cancer-Immunity Cycle. Many different approaches have been evaluated, and they can be divided on whether they potentiate anti-tumor or inhibit pro-tumor mechanisms of immunoregulation. In all cases, the ultimate goal is to induce a potent anti-tumor immune response that kills cancer cells. So far, adoptive T cell therapy and checkpoint blockade (antibodies against CTLA-4, PD-1, PDL-1) have shown most efficacy in clinics. DC, dendritic cell; TLR, Toll-like receptor; αGalCer, alpha-galactosylceramide; M1 M0, type I macrophage; NK, Natural killer; Th1, IFN $\gamma$ -secreting CD4 T cell; CTL, cytotoxic T lymphocyte; MDSC, myeloid-derived suppressor cell; Treg cell, regulatory T cell; RA, retinoic acid; Ab, antibody; i, inhibitor; Cy, cyclophosphamide; PI3Ki, Phosphatidylinositol 3-kinase inhibitor; p38i, p38 MAP kinase inhibitor; RARi, retinoic acid receptor-alpha inhibitor. Illustration taken from Butt and Mills, 2014.

Briefly, the cycle is divided into seven major steps, starting with the release of antigens from dying cancer cells, to antigen-presentation by dendritic cells in the draining lymph node, to trafficking of tumor-specific effector T cells into the tumor and the killing of individual cancer cells. Interestingly, once the Cancer-Immunity Cycle is underway, it represents a self-propelling machinery that increases the breadth and depth of an ongoing anti-tumor immune response. However, in most patients, one or multiple immunosuppressive mechanisms are active to inhibit the optimal performance of the Cancer-Immunity Cycle (Motz and Coukos, 2013).

### 2.1.2 Immunotherapy aims at boosting the Cancer-Immunity Cycle

Cancer immunotherapy aims at initiating and reinforcing the Cancer-Immunity Cycle, thereby creating an environment that enables a potent anti-tumor immune response to develop. Many different approaches of cancer immunotherapy have been evaluated, either potentiating anti-tumor, or inhibiting pro-tumor immunity (Figure 2.3) (Butt and Mills, 2014). Even though a major part of pre-clinical research has focused on designing therapeutic cancer vaccines, unfortunately no clinical success stories have come out from these efforts (Melief et al., 2015). In contrast, adoptive T cell therapy (ACT) and checkpoint blockade have recently introduced a paradigm shift in the fight against cancer, curing patients for which there was no therapy available before (Restifo et al., 2016). During ACT, either autologous, *ex vivo* stimulated tumor-reactive T cells, or host cells that have been genetically engineered are infused into patients (Rosenberg and Restifo, 2015). ACT using autologous T cells has shown clinical response rates of up to 50%, with around 20% of patients having complete and long-lasting regression in solid tumors, including metastatic melanoma (Hinrichs and Rosenberg, 2014; Restifo et al., 2012). Alternatively to using autologous T cells, host cells can be

genetically engineered to carry either tumor-specific T cell receptors (TCRs) or chimeric antigen receptors (CARs) that are designed to target a tumor-specific antigen (Gill and June, 2015). CAR modified T cells targeting CD19 have been especially successful in the treatment of leukemia patients, with complete response rates of up to 60% depending on the exact patient population (Lee et al., 2015; Porter et al., 2015). The main hurdle to broadly implement these promising therapies in clinics might be the fact that performing ACT is expensive, resource intensive, and require specialized GMP facilities (Tey et al., 2006). Checkpoint therapy, antibody-mediated blocking of pathways essential to T cell suppression, would certainly be easier to implement in clinics. Similarly to ACT, combined checkpoint therapy of the immunosuppressive molecules CTLA-4 and PD-1 has resulted in complete response rates of up to 22% in human clinical trials (Larkin et al., 2015; Postow et al., 2015). Because every tumor may rely on different immunosuppressive mechanisms to interfere with the Cancer-Immunity Cycle, personalized immunotherapy combining multiple approaches are believed to lead to even better response rates in the future (Mahoney et al., 2015; Rosenberg and Restifo, 2015).

### **2.1.3 Biomarkers in cancer immunotherapy**

Despite the encouraging results from clinics, it is currently unclear why only a fraction of patients responds to immunotherapy (Sharma and Allison, 2015). Thus, the identification of biomarkers that allow patient stratification based upon whether they can benefit from immunotherapy or not is urgently needed (Patel and Kurzrock, 2015; Schumacher et al., 2015). Intuitively, tumor cell expression of the PD-1 ligand PD-L1 should be a positive prognostic marker for checkpoint inhibition using antibodies targeting the PD-1/PDL-1 pathway. However, while some studies found a correlation between tumor PDL-1 expression and patient outcome (Topalian et al., 2012), others did not (Hamid et al., 2013). Citing James Allison, one of the founding fathers of checkpoint inhibition: *“Because of the very nature of immune checkpoint therapy, the development of pharmacodynamics, predictive, or prognostic biomarkers faces unique challenges”* (Sharma and Allison, 2015). Interfering with tumor immunity creates dynamic and complex changes in the microenvironment, and it is unlikely that a single parameter will be able to serve as a biomarker. For example, the secretion of the effector cytokine interferon- $\gamma$  by tumor infiltrating CD8<sup>+</sup> T cells induces adaptive resistance mechanisms of the tumor microenvironment, including the upregulation of IDO, PD-L1 and the influx of regulatory T cells (Spranger et al., 2013). However, recent research has highlighted two readouts that might serve as predictive biomarkers for checkpoint therapy. First, pre-existing inflammation within the tumor microenvironment has been shown to correlate with good clinical outcome following immunotherapy (Ji et al., 2011; Spranger et al., 2015; Tumeh et al., 2014). It has been suggested that means to inducing T cell infiltration into “cold tumors”, tumors that do not present pre-existing T cell inflammation, prior to immunotherapy might therefore improve therapy outcome (Gajewski, 2015). Second, it has been shown that the mutational load of the tumor and the number of generated neoantigens correlate with immunotherapy outcome (Snyder et al., 2014; Van Allen et al., 2015). It has been proposed that due to the lack of central tolerance, much more potent immune responses can be raised against neoantigens as compared to self-antigens (Gilboa, 1999). Because different tumor types have very different mutational loads (Figure 2.4), this indicates that immunotherapy might

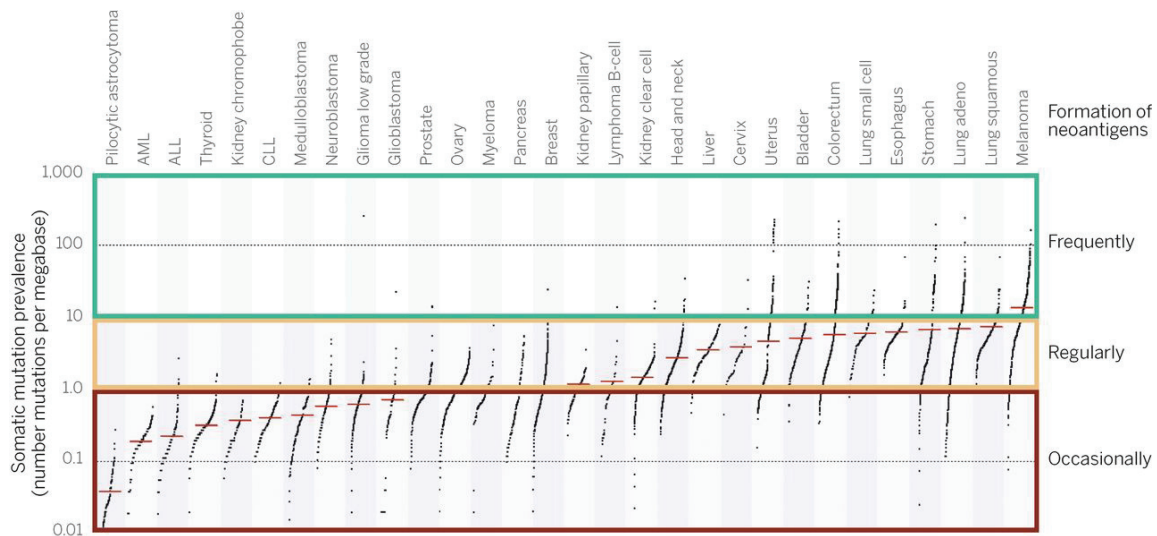


**Figure 2.4 Mutational load across cancer types.** The number of antigens that are created correlates with the mutational load of cancer cells. Neoantigens are critical for the induction of potent anti-tumor immunotherapy. The graph shows individual tumor samples (dots) and the median number of mutation per cancer type (red bars). The y-axis indicates the number of mutations per megabase (log scale). Most melanomas have more than 10 somatic mutations per megabase of coding DNA, which corresponds to roughly 150 nonsynonymous mutations within expressed genes. All of these can potentially lead to the generation of neoantigens. The tumor types are categorized according to the likelihood of neoantigen formation. Illustration taken from Schumacher et al., 2015.

not be equally suitable for all indications. Patients with tumors at the high end of the mutational spectrum, such as metastatic melanoma patients, are more likely to benefit from immunotherapy (Alexandrov et al., 2013; Schumacher et al., 2015). Taken together, even though cancer immunotherapy is revolutionizing the way cancer patients can be treated, the field is still in its infancy. A better understanding of the molecular mechanisms dictating the clinical response to immunotherapy is needed and will increase the number of cancer patients who can be cured.

## 2.2 The lymphatic system

### 2.2.1 The lymphatic system as a transport route

Hippocrates has observed components of what today are considered the blood and lymphatic networks, the two major circulatory systems of the human body, more than two thousand years ago. Even though the two systems have a lot in common in terms of function (transport of liquid, cells, and solutes), structure (networks of vessels), and anatomic distribution (they mostly run in parallel), the extent to which they have been studied has varied greatly. While the blood vascular system has been object to vast investigation ever since, the lymphatic system has largely been neglected by the scientific community (Choi et al., 2012; Swartz, 2001). It was a series of landmark discoveries in the late 1990s, which sparked a new area of lymphatic research. First, the major signaling pathways for lymphatic vessel growth, VEGFC and VEGFD mediated stimulation of the VEGFR2 and VEGFR3 tyrosine kinases, were described (Achen et al., 1998; Jeltsch et al., 1997; Joukov et al., 1996;



Kaipainen et al., 1995; Kukk et al., 1996; Lee et al., 1996; Oh et al., 1997). A few years later, the lymphatic markers Lyve1, podoplanin, and Prox1 were discovered almost simultaneously (Banerji et al., 1999; Breiteneder-Geleff et al., 1999; Wigle and Oliver, 1999).

The high pressure in the blood circulation forces plasma fluid and proteins continuously out of the capillaries into the interstitial space. About 90% of this filtrate gets reabsorbed at the venous side. However, because of osmotic forces resulting from extravasated protein, there is a net fluid flux of about 10% out of the vasculature into the interstitium. One of the main functions of the lymphatic system is to return this excess fluid back into the blood circulation (Tammela and Alitalo, 2010). By forming a one-way drainage system consisting of a hierarchical network of open-ended initial lymphatics that lead into pre-collecting, then collecting vessels and finally empty into the subclavian veins, the lymphatic network is perfectly built to perform this function. Initial lymphatics are blind-ended sacs that have minimal basement membrane coverage and are attached to the extracellular matrix (ECM) with anchoring filaments. This allows them to adapt their permeability to the interstitial fluid pressure (IFP), such that when the ECM is stretched under elevated IFP, the initial capillaries are dilated to allow enhanced fluid flows and cellular trafficking. In contrast, collecting vessels are equipped to ensure optimal downstream drainage of the lymph fluid. They are characterized by a continuous basement membrane, pericyte coverage that allows active pumping of lymph fluid, and a system of valves that prevents retrograde fluid flow (Figure 2.5) (Kerjaschki, 2014; Stacker et al., 2014).

### **2.2.2 Lymphangiogenesis**

Remodeling of the lymphatic vessel structure and morphology can be achieved either by lymphatic vessel enlargement or lymphangiogenesis (Stacker et al., 2014). Lymphangiogenesis is the process of new lymphatic vessel formation by sprouting from pre-existing vessels, even though some studies suggest that macrophages may also contribute to lymphangiogenesis by transdifferentiating into lymphatic endothelium (Kerjaschki, 2014). Physiologic lymphangiogenesis in the adult only occurs during the development of the corpus luteum and wound healing (Tammela and Alitalo, 2010). However, lymphangiogenesis is also induced in a variety of pathological conditions, including cancer, inflammation, and transplant rejection. In most cases, it remains unclear whether lymphangiogenesis is contributing to pathology by driving inflammation or whether it is an active attempt to resolve inflammation. Recent research suggests that there might indeed not be a black and white answer that is valid for all situations, but rather, that the consequences of lymphangiogenesis on the host might be highly context dependent (Lund et al., 2016). However, in the context of tumors, it is well established that tumor-associated lymphangiogenesis correlates with poor prognosis (Dadras et al., 2010; Pasquali et al., 2013; Shayan et al., 2012). The main hypothesis has been that newly generated lymphatic vessels offer routes for metastatic spread to the draining lymph nodes and distant organs (Karaman and Detmar, 2014; Stacker et al., 2014; Tammela and Alitalo, 2010). More recently, it has been appreciated that tumor-associated lymphatic vessels might also influence tumor progression by actively shaping anti-tumor immunity, a concept which we will further introduce in chapter 2 of this thesis (Lund et al., 2016; Swartz, 2014).

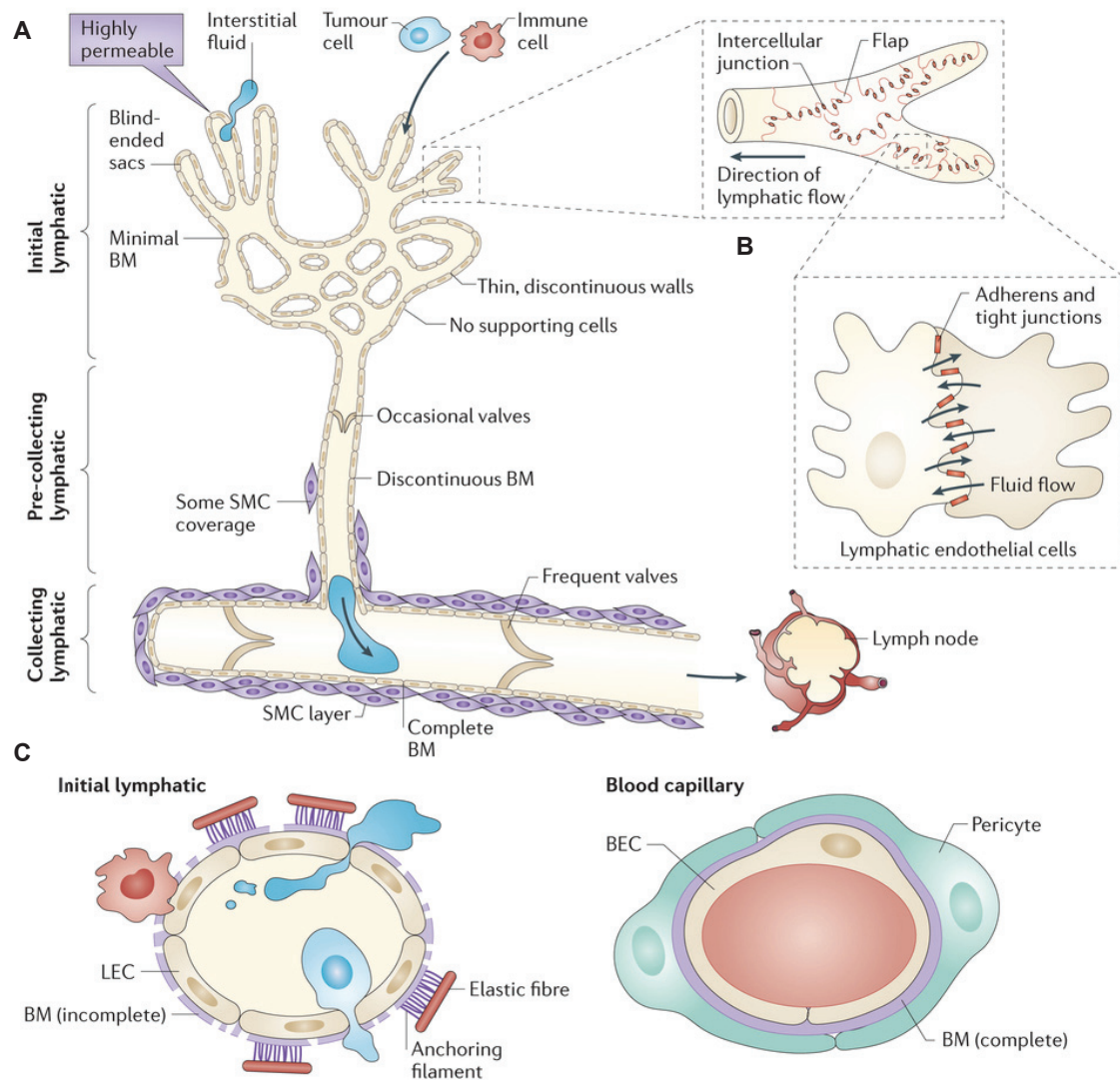


**Figure 2.5 The structure of the lymphatic network.** (A) The illustration shows the structural differences between initial (open-ended, minimal basal membrane (BM), no pericyte coverage), pre-collecting (occasional valves and discontinuous BM), and collecting (frequent valves, active pumping thanks to pericyte coverage) lymphatic vessels. (B) Lymphatic endothelial cells connect with each other via button-like tight junctions. Fluid and cells can easily traffic across the vessel wall by crossing the interendothelial gaps between the tight junctions. (C) Cross-section of an initial lymphatic and a blood capillary. While blood capillaries are covered by pericytes, initial lymphatics are not. In addition, LECs are anchored to the extracellular matrix via elastic fibers. This ensured that under conditions when the interstitial pressure increases, the gaps between the vessels are enlarged to allow increased fluid drainage. Illustration adapted from Stacker et al., 2014

Lymphangiogenesis is mediated by a variety of growth factors and receptors (Figure 2.6). However, as mentioned previously, the receptor tyrosine kinase VEGFR3 seems to be the major receptor mediating lymphangiogenesis and was one of the first LEC markers to be described (Kaipainen et al., 1995). VEGFR3 has two known ligands, VEGFC and VEGFD, both from the VEGF family of growth factors. VEGFC and VEGFD are matured by proteolytic processing, allowing them to



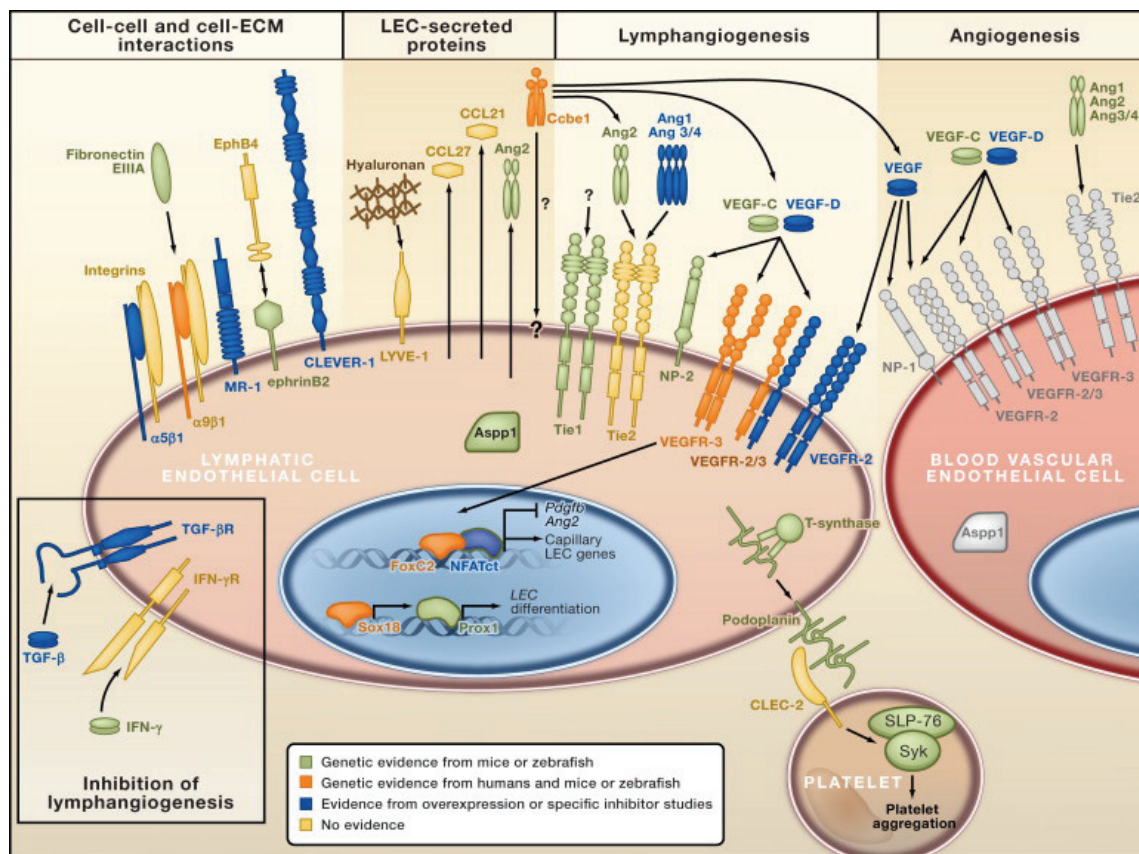


**Figure 2.6 Molecular pathways of lymphangiogenesis.** A multitude of signaling pathways exist that can induce or influence lymphangiogenesis. Most prominently are the growth factors VEGFC and VEGFD, which mainly signal through VEGFR3 homo- or VEGFR2/VEGFR3 heterodimers. Neuropilin-2 (NP-2) can acts as co-receptor to increase signaling sensitivity. Lymphangiogenic signaling pathways converge on the regulation of Prox1 and FoxC2/NFATct, transcription factors that regulate genes essential to the lymphatic endothelial cell phenotype. It is interesting to note that there is considerable overlap in angiogenic and lymphangiogenic signaling, mainly via involvement of VEGFR2. The cytokines TGF- $\beta$  and IFN $\gamma$  both inhibit lymphangiogenesis. Illustration taken from Tammela et al., 2010

bind to VEGFR3 homo- and VEGFR3/VEGFR2 heterodimers (Joukov et al., 1997; Olsson et al., 2006; Tammela and Alitalo, 2010). Both VEGFC and VEGFR3 can interact with the co-receptor neuropilin-2, which increases VEGFR3 downstream signaling (Karpanen, 2006). Other growth factors that stimulate lymphangiogenesis in various contexts have been described, including fibroblast growth factor 2 (FGF-2) (Chang et al., 2004), insulin-like growth factor 1 (IGF-1) and IGF-2 (Björndahl et al., 2005), hepatocyte growth factor (HGF) (Cao et al., 2006; Kajiya et al., 2005), endothelin-1 (ET-1) (Spinella et al., 2009), and platelet-derived growth factor B (PDGF-B) (Cao et al., 2004). However, it is unclear what the direct contribution of these factors to lymphangiogenesis is, as some of them might induce VEGFC and VEGFD secretion by immune cells and fibroblasts (Tammela and Alitalo, 2010). Lymphangiogenic signaling pathways converge on the induction of the transcription factors Prox1 and FoxC2/NFATct, both of which regulate genes essential that induce proliferation, migration, and survival of lymphatic endothelial cells (Tammela and Alitalo, 2010). Finally, it is worth noting that there is considerable overlap in angiogenic and lymphangiogenic signaling, mainly via VEGFR2 signaling

(Olsson et al., 2006), and that the cytokines TGF $\beta$ , IFN $\gamma$ , IL4 and IL13 have been suggested to act as inhibitors of lymphangiogenesis (Oka et al., 2008; Savetsky et al., 2015; Shao and Liu, 2006).

### 2.2.3 The lymphatic system as an active immunomodulator

The lymphatic network acts as a messenger for the immune system. While draining cells, macromolecules, ions, and interstitial fluid from peripheral tissues back to the blood circulation, lymph passes through to secondary lymphoid organs (SLOs), the control centers of adaptive immune responses (Ruddle and Akirav, 2009). The information that lymphatics deliver to SLOs contains important cues essential to regulating adaptive immunity including soluble antigens (Clement et al., 2011), antigen-loaded dendritic cells (Randolph et al., 2005), danger signals and cytokines (Card et al., 2014). Depending on the tissue context such as homeostasis, inflammation, cancer, or infection, these cues lead to either tolerogenic adaptive immune mechanisms that maintain tolerance to self-antigens, or to the induction or resolution of effector mechanisms that try to battle tumor cells and invading pathogens (Lund et al., 2016). The role of lymphatic vessels in shaping immunity as passive conduits, or simple messengers, has been well established. However, more recently, it has become appreciated that LVs are also actively involved in regulating immunity, both by taking an active role in immune cell education as well as trafficking (Card et al., 2014).

Antigen-presenting cells (APCs) are key mediators of adaptive immune responses. The function of APCs is to present “self” and “foreign” antigens loaded on major histocompatibility complex (MHC) class I and II molecules to CD4<sup>+</sup> and CD8<sup>+</sup> T cells. If a T cell recognizes a cognate peptide-MHC complex to its T cell receptor (TCR), an immune response is elicited. In case of “self” antigen, this classically leads to a tolerogenic, or non-productive immune response to protect the host tissue, while “foreign” antigen such as from a virus or bacteria will induce an effector T cell response against the invading pathogen. Professional antigen-presenting cells include B cells, macrophages and dendritic cells (DCs). Because they possess many unique features of antigen processing and presentation, such as cross-presentation of exogenous antigen on MHC class I, DCs are often considered to be the most critical induced of adaptive immunity (Vyas et al., 2008). However, recent research suggests that lymph node stromal cells (LNSCs), namely fibroblastic reticular cells (FRCs), lymphatic endothelial cells (LECs) and extrathymic *Aire*-expressing cells (eTACs), can act as antigen presenting cells in SLOs (Fletcher et al., 2011; Hirose and Dubrot, 2015; Link et al., 2007). While the rare eTAC subpopulation expresses peripheral tissue antigens (PTAs) dependent on the autoimmune regulator *Aire* gene (similar to mTECs in the thymus), FRCs and LECs do so partially independent of *Aire* (Cohen et al., 2010). Presentation of PTAs on MHC class I molecules on the surface of stromal cells leads to deletional CD8<sup>+</sup> T cell tolerance (Cohen et al., 2010; Fletcher et al., 2010; Gardner et al., 2008). Indeed, LECs do not express costimulatory molecules needed to induce effector immune responses, and instead express the T cell inhibitory ligand of PD-1, PDL-1 (Tewalt et al., 2012). Interestingly, data from the same study suggests that blocking of inhibitory signals or enhancing of costimulatory signals bypasses LEC-mediated tolerance. In these settings, LECs have the potential to induce fully differentiated effector CD8<sup>+</sup> T cells capable of causing autoimmune disease. Besides presenting endogenous PTAs, our lab has demonstrated that LECs are capable of up taking, process-

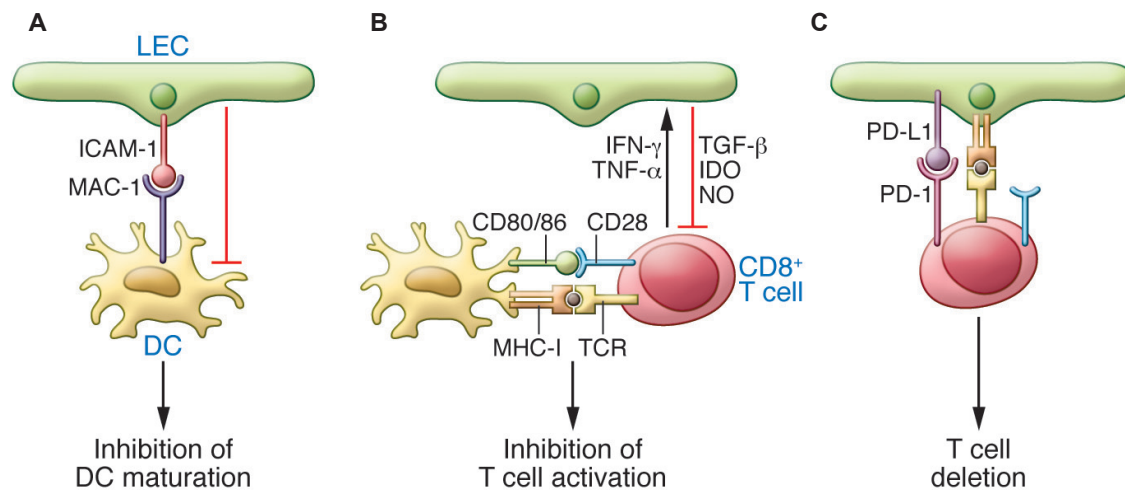


**Figure 2.7 Mechanisms of immunoregulation by lymphatic endothelial cells.** (A) LECs can inhibit dendritic cell maturation by binding ICAM-1 to MAC-1, thereby dampening the ability of DCs to activate T cells. (B) When stimulated with pro-inflammatory cytokines such as IFN $\gamma$  and TNF $\alpha$ , LECs can secrete immunosuppressive mediators including nitric oxide (NO), indoleamine 2,3-dioxygenase (IDO), and TGF $\beta$ . (C) LECs can present endogenous and exogenous antigen on MHC-I and MHC-II complexes to guide T cell activation. However, because LECs lack co-stimulatory molecules such as CD80 and CD86 but express the T cell inhibitor PDL-1, these interactions lead to tolerogenic rather than effector immune responses. Illustration adapted from Card et al., 2014.

ing, and cross-presenting exogenous antigen on MHC-I in a transport associated with antigen processing 1 (TAP1)-dependent manner (Hirosue et al., 2014; Lund et al., 2012). CD8<sup>+</sup> T cell responses elicited this way are characterized by hallmarks of immune tolerance, including reduced IFN $\gamma$  secretion, high levels of PD-1 expression, and increased apoptosis (Hirosue et al., 2014; Lund et al., 2012). A novel role of LEC-mediated immunoregulation via capturing and archiving of viral antigens has recently been introduced (Tamburini et al., 2014). Archiving of antigen over prolonged periods of time increased the protective immunity provided by circulating antigen-specific CD8<sup>+</sup> memory T cells. Because LECs can only induce tolerogenic responses, the authors speculated that LECs might transfer antigen to dendritic cells, which are then able to induce productive antigen-specific immune responses (Tamburini et al., 2014).

The role of LNSCs in presenting antigen in the context of MHC class II complexes has remained more elusive. LECs express low levels of MHC-II in steady-state, and upregulate its expression upon exposure to the pro-inflammatory cytokine IFN $\gamma$  (Dubrot et al., 2014; Nörder et al., 2012). Even though LECs do express the non-conventional T cell co-stimulatory molecules CD54 and CD58, they failed to induce effector CD4<sup>+</sup> T cell responses *in vitro* (Nörder et al., 2012). Interestingly, peptide-MHC-II complexes can be transferred from DCs to LECs via exosomes, explaining the low basal presence of MHC-II on LECs under non-inflammatory conditions (Dubrot et al., 2014). Similarly to archiving viral antigens, it has been suggested that LECs act as antigen reservoirs for CD4<sup>+</sup> tolerance by transferring PTAs to dendritic cells, which subsequently present it on MHC-II to induce CD4 T-cell anergy (Rouhani et al., 2015).

Apart from shaping T cell activation, FRCs and LECs can have a suppressive influence on already activated T cells (Lukacs-Kornek et al., 2011). These LNSC subsets can upregulate nitric oxide synthase 2 (NOS2) in response to three synergistic signals  $\text{IFN}\gamma$ ,  $\text{TNF}\alpha$ , and direct contact with activated T cells. Expression of NOS2 leads to inhibition of activated T cell proliferation, suggesting that FRCs and LECs could be important not only in controlling the naïve T cell pool, but also in fine-tuning the magnitude of ongoing T cell responses. Finally, apart from directly interacting with T cells, LNSCs inhibit immune responses indirectly by manipulating DCs in their proximity. It has been shown that inflamed  $\text{TNF}\alpha$  activated dermal LECs suppress the maturation of DCs via cell-cell signaling (Podgrabinska et al., 2009). Interaction of ICAM-1 expressed on LECs and Mac-1 on DCs resulted in decreased expression of the costimulatory molecule CD86 on DCs, leading to decreased T cell activation. In summary, it is now evident that lymph node stromal cells actively participate in educating immune responses towards both exogenous and endogenous antigens in steady-state and disease. To influence immunity, they employ mechanisms both mediated by engaging in cell-cell contacts, as well as through secretion of soluble mediators influencing neighboring cells (Figure 2.7).

## 2.3 References

- Achen, M.G., Jeltsch, M., Kukk, E., Makinen, T., Vitali, A., Wilks, A.F., Alitalo, K., Stacker, S.A., 1998. Vascular endothelial growth factor D (VEGF-D) is a ligand for the tyrosine kinases VEGF receptor 2 (Flk1) and VEGF receptor 3 (Flt4). *Proc. Natl. Acad. Sci. U.S.A.* 95, 548–553.
- Alexandrov, L.B., Nik-Zainal, S., Wedge, D.C., Aparicio, S.A.J.R., Behjati, S., Biankin, A.V., Bignell, G.R., Bolli, N., Borg, A., Børresen-Dale, A.-L., Boyault, S., Burkhardt, B., Butler, A.P., Caldas, C., Davies, H.R., Desmedt, C., Eils, R., Eyfjörd, J.E., Foekens, J.A., Greaves, M., Hosoda, F., Hutter, B., Ilcic, T., Imbeaud, S., Imielinski, M., Jäger, N., Jones, D.T.W., Jones, D., Knappskog, S., Kool, M., Lakhani, S.R., López-Otín, C., Martin, S., Munshi, N.C., Nakamura, H., Northcott, P.A., Pajic, M., Papaemmanuil, E., Paradiso, A., Pearson, J.V., Puente, X.S., Raine, K., Ramakrishna, M., Richardson, A.L., Richter, J., Rosenstiel, P., Schlesner, M., Schumacher, T.N., Span, P.N., Teague, J.W., Totoki, Y., Tutt, A.N.J., Valdés-Mas, R., van Buuren, M.M., van t Veer, L., Vincent-Salomon, A., Waddell, N., Yates, L.R., Zucman-Rossi, J., Andrew Futreal, P., McDermott, U., Lichter, P., Meyerson, M., Grimmond, S.M., Siebert, R., Campo, E., Shibata, T., Pfister, S.M., Campbell, P.J., Stratton, M.R., 2013. Signatures of mutational processes in human cancer. *Nature* 500, 415–421. doi:10.1038/nature12477
- Banerji, S., Ni, J., Wang, S.X., Clasper, S., Su, J., Tammi, R., Jones, M., Jackson, D.G., 1999. LYVE-1, a new homologue of the CD44 glycoprotein, is a lymph-specific receptor for hyaluronan. *J Cell Biol* 144, 789–801.
- Björndahl, M., Cao, R., Nissen, L.J., Clasper, S., Johnson, L.A., Xue, Y., Zhou, Z., Jackson, D., Hansen, A.J., Cao, Y., 2005. Insulin-like growth factors 1 and 2 induce lymphangiogenesis in vivo. *Proc. Natl. Acad. Sci. U.S.A.* 102, 15593–15598. doi:10.1073/pnas.0507865102
- Breiteneder-Geleff, S., Soleiman, A., Kowalski, H., Horvat, R., Amann, G., Kriehuber, E., Diem, K., Weninger, W., Tschachler, E., Alitalo, K., Kerjaschki, D., 1999. Angiosarcomas express mixed endothelial phenotypes of blood and lymphatic capillaries - Podoplanin as a specific marker for lymphatic endothelium. *The American Journal of Pathology* 154, 385–394. doi:10.1016/S0002-9440(10)65285-6
- Butt, A.Q., Mills, K.H.G., 2014. Immunosuppressive networks and checkpoints controlling antitumor immunity and their blockade in the development of cancer immunotherapeutics and vaccines. *Oncogene* 33, 4623–4631. doi:10.1038/onc.2013.432
- Cao, R., Björndahl, M.A., Gallego, M.I., Chen, S., Religa, P., 2006. Hepatocyte growth factor is a lymphangiogenic factor with an indirect mechanism of action. *Blood*. doi:10.1182/blood-2005-06
- Cao, R., Björndahl, M.A., Religa, P., Clasper, S., Garvin, S., Galter, D., Meister, B., Ikomi, F., Tritsaris, K., Dissing, S., Ohhashi, T., Jackson, D.G., Cao, Y., 2004. PDGF-BB induces intratumoral lymphangiogenesis and promotes lymphatic metastasis. *Cancer Cell* 6, 333–345. doi:10.1016/j.ccr.2004.08.034
- Card, C.M., Yu, S.S., Swartz, M.A., 2014. Emerging roles of lymphatic endothelium in regulating adaptive immunity. *J. Clin. Invest.* 124, 943–952. doi:10.1172/JCI73316



- Chang, L.K., Garcia-Cardena, G., Farnebo, F., Fannon, M., Chen, E.J., Butterfield, C., Moses, M.A., Mulligan, R.C., Folkman, J., Kaipainen, A., 2004. Dose-dependent response of FGF-2 for lymphangiogenesis. *Proc. Natl. Acad. Sci. U.S.A.* 101, 11658–11663. doi:10.1073/pnas.0404272101
- Chen, D.S., Mellman, I., 2013. Oncology Meets Immunology: The Cancer-Immunity Cycle. *Immunity* 39, 1–10. doi:10.1016/j.immuni.2013.07.012
- Choi, I., Lee, S., Hong, Y.-K., 2012. The new era of the lymphatic system: no longer secondary to the blood vascular system. *Cold Spring Harbor Perspectives in Medicine* 2, a006445. doi:10.1101/cshperspect.a006445
- Clement, C.C., Rotzschke, O., Santambrogio, L., 2011. The lymph as a pool of self-antigens. *Trends in Immunology* 32, 6–11. doi:10.1016/j.it.2010.10.004
- Cohen, J.N., Guidi, C.J., Tewalt, E.F., Qiao, H., Rouhani, S.J., Ruddell, A., Farr, A.G., Tung, K.S., Engelhard, V.H., 2010. Lymph node-resident lymphatic endothelial cells mediate peripheral tolerance via Aire-independent direct antigen presentation. *Journal of Experimental Medicine* 207, 681–688. doi:10.1084/jem.20092465
- Dadras, S.S., Paul, T., Bertocini, J., Brown, L.F., Muzikansky, A., Jackson, D.G., Ellwanger, U., Garbe, C., Mihm, M.C., Detmar, M., 2010. Tumor Lymphangiogenesis. *The American Journal of Pathology* 162, 1951–1960. doi:10.1016/S0002-9440(10)64328-3
- Dubrot, J., Duraes, F.V., Potin, L., Capotosti, F., Brighouse, D., Suter, T., LeibundGut-Landmann, S., Garbi, N., Reith, W., Swartz, M.A., Hugues, S., 2014. Lymph node stromal cells acquire peptide-MHCII complexes from dendritic cells and induce antigen-specific CD4<sup>+</sup> T cell tolerance. *Journal of Experimental Medicine* 211, 1153–1166. doi:10.1084/jem.20132000
- Dunn, G.P., Bruce, A.T., Ikeda, H., Old, L.J., Schreiber, R.D., 2002. Cancer immunoediting: from immunosurveillance to tumor escape. *Nat Immunol* 3, 991–998. doi:10.1038/ni1102-991
- Dunn, G.P., Old, L.J., Schreiber, R.D., 2004. The three Es of cancer immunoediting. *Annu. Rev. Immunol.* 22, 329–360. doi:10.1146/annurev.immunol.22.012703.104803
- Fletcher, A.L., Lukacs-Kornek, V., Reynoso, E.D., Pinner, S.E., Bellemare-Pelletier, A., Curry, M.S., Collier, A.-R., Boyd, R.L., Turley, S.J., 2010. Lymph node fibroblastic reticular cells directly present peripheral tissue antigen under steady-state and inflammatory conditions. *Journal of Experimental Medicine* 207, 689–697. doi:10.1084/jem.20092642
- Fletcher, A.L., Malhotra, D., Turley, S.J., 2011. Lymph node stroma broaden the peripheral tolerance paradigm. *Trends in Immunology* 32, 12–18. doi:10.1016/j.it.2010.11.002
- Gajewski, T.F., 2015. The Next Hurdle in Cancer Immunotherapy: Overcoming the Non-T-Cell-Inflamed Tumor Microenvironment. *Seminars in Oncology* 42, 663–671. doi:10.1053/j.seminoncol.2015.05.011
- Gardner, J.M., DeVoss, J.J., Friedman, R.S., Wong, D.J., Tan, Y.X., Zhou, X., Johannes, K.P., Su, M.A., Chang, H.Y., Krummel, M.F., 2008. Deletional tolerance mediated by extrathymic Aire-expressing cells. *Science* 321, 843–847. doi:10.1126/science.1156121
- Gilboa, E., 1999. The makings of a tumor rejection antigen. *Immunity* 11, 263–270. doi:10.1016/S1074-7613(00)80101-6

- Gill, S., June, C.H., 2015. Going viral: chimeric antigen receptor T-cell therapy for hematological malignancies. *Immunol. Rev.* 263, 68–89. doi:10.1111/imr.12243
- Halliday, G.M., Patel, A., Hunt, M.J., Tefany, F.J., Barnetson, R.S.C., 1995. Spontaneous regression of human melanoma/nonmelanoma skin cancer: Association with infiltrating CD4+ T cells. *World J Surg* 19, 352–358. doi:10.1007/BF00299157
- Hamid, O., Robert, C., Daud, A., Hodi, F.S., Hwu, W.-J., Kefford, R., Wolchok, J.D., Hersey, P., Joseph, R.W., Weber, J.S., Dronca, R., Gangadhar, T.C., Patnaik, A., Zarour, H., Joshua, A.M., Gergich, K., Ellassaiss-Schaap, J., Algazi, A., Mateus, C., Boasberg, P., Tumei, P.C., Chmielowski, B., Ebbinghaus, S.W., Li, X.N., Kang, S.P., Ribas, A., 2013. Safety and Tumor Responses with Lmbrolizumab (Anti-PD-1) in Melanoma. *N Engl J Med* 369, 134–144. doi:10.1056/NEJMoa1305133
- Hanahan, D., Weinberg, R.A., 2011. Hallmarks of cancer: the next generation. *Cell* 144, 646–674. doi:10.1016/j.cell.2011.02.013
- Heemskerk, B., Kvistborg, P., Schumacher, T.N.M., 2013. The cancer antigenome. *The EMBO Journal* 32, 194–203. doi:10.1038/emboj.2012.333
- Hinrichs, C.S., Rosenberg, S.A., 2014. Exploiting the curative potential of adoptive T-cell therapy for cancer. *Immunol. Rev.* 257, 56–71. doi:10.1111/imr.12132
- Hirosue, S., Dubrot, J., 2015. Modes of Antigen Presentation by Lymph Node Stromal Cells and Their Immunological Implications. *Front Immunol* 6, 446. doi:10.3389/fimmu.2015.00446
- Hirosue, S., Vokali, E., Raghavan, V.R., Rincon-Restrepo, M., Lund, A.W., Corthésy-Henrioud, P., Capotosti, F., Halin Winter, C., Hugues, S., Swartz, M.A., 2014. Steady-state antigen scavenging, cross-presentation, and CD8+ T cell priming: a new role for lymphatic endothelial cells. *The Journal of Immunology* 192, 5002–5011. doi:10.4049/jimmunol.1302492
- Jeltsch, M., Kaipainen, A., Joukov, V., Meng, X., Lakso, M., Rauvala, H., Swartz, M., Fukumura, D., Jain, R.K., Alitalo, K., 1997. Hyperplasia of lymphatic vessels in VEGF-C transgenic mice. *Science* 276, 1423–1425.
- Joukov, V., Pajusola, K., Kaipainen, A., Chilov, D., Lahtinen, I., Kukk, E., Saksela, O., Kalkkinen, N., Alitalo, K., 1996. A novel vascular endothelial growth factor, VEGF-C, is a ligand for the Flt4 (VEGFR-3) and KDR (VEGFR-2) receptor tyrosine kinases. *The EMBO Journal* 15, 290–298.
- Joukov, V., Sorsa, T., Kumar, V., Jeltsch, M., Claesson-Welsh, L., Cao, Y., Saksela, O., Kalkkinen, N., Alitalo, K., 1997. Proteolytic processing regulates receptor specificity and activity of VEGF-C. *The EMBO Journal* 16, 3898–3911.
- Kaipainen, A., Korhonen, J., Mustonen, T., van Hinsbergh, V.W., Fang, G.H., Dumont, D., Breitman, M., Alitalo, K., 1995. Expression of the fms-like tyrosine kinase 4 gene becomes restricted to lymphatic endothelium during development. *Proc. Natl. Acad. Sci. U.S.A.* 92, 3566–3570.
- Kajiyama, K., Hirakawa, S., Ma, B., Drinnenberg, I., Detmar, M., 2005. Hepatocyte growth factor promotes lymphatic vessel formation and function. *EMBO J.* 24, 2885–2895. doi:10.1038/sj.emboj.7600763
- Karaman, S., Detmar, M., 2014. Mechanisms of lymphatic metastasis. *J. Clin. Invest.* 124, 922–928. doi:10.1172/JCI71606

- Karpanen, T., 2006. Functional interaction of VEGF-C and VEGF-D with neuropilin receptors. *The FASEB Journal* 20, 1462–1472. doi:10.1096/fj.05-5646com
- Kerjaschki, D., 2014. The lymphatic vasculature revisited. *J. Clin. Invest.* 124, 874–877. doi:10.1172/JCI74854
- Kukk, E., Lymboussaki, A., Taira, S., Kaipainen, A., Jeltsch, M., Joukov, V., Alitalo, K., 1996. VEGF-C receptor binding and pattern of expression with VEGFR-3 suggests a role in lymphatic vascular development. *Development* 122, 3829–3837.
- Larkin, J., Chiarion-Sileni, V., Gonzalez, R., Grob, J.J., Cowey, C.L., Lao, C.D., Schadendorf, D., Dummer, R., Smylie, M., Rutkowski, P., Ferrucci, P.F., Hill, A., Wagstaff, J., Carlino, M.S., Haanen, J.B., Maio, M., Marquez-Rodas, I., McArthur, G.A., Ascierto, P.A., Long, G.V., Callahan, M.K., Postow, M.A., Grossmann, K., Sznol, M., Dreno, B., Bastholt, L., Yang, A., Rollin, L.M., Horak, C., Hodi, F.S., Wolchok, J.D., 2015. Combined Nivolumab and Ipilimumab or Monotherapy in Untreated Melanoma. *N Engl J Med* 373, 23–34. doi:10.1056/NEJMoa1504030
- Lee, D.W., Kochenderfer, J.N., Stetler-Stevenson, M., Cui, Y.K., Delbrook, C., Feldman, S.A., Fry, T.J., Orentas, R., Sabatino, M., Shah, N.N., Steinberg, S.M., Stroncek, D., Tschernia, N., Yuan, C., Zhang, H., Zhang, L., Rosenberg, S.A., Wayne, A.S., Mackall, C.L., 2015. T cells expressing CD19 chimeric antigen receptors for acute lymphoblastic leukaemia in children and young adults: a phase 1 dose-escalation trial. *The Lancet* 385, 517–528. doi:10.1016/S0140-6736(14)61403-3.
- Lee, J., Gray, A., Yuan, J., Luoh, S.M., Avraham, H., Wood, W.I., 1996. Vascular endothelial growth factor-related protein: a ligand and specific activator of the tyrosine kinase receptor Flt4. *Proc. Natl. Acad. Sci. U.S.A.* 93, 1988–1992.
- Link, A., Vogt, T.K., Favre, S., Britschgi, M.R., Acha-Orbea, H., Hinz, B., Cyster, J.G., Luther, S.A., 2007. Fibroblastic reticular cells in lymph nodes regulate the homeostasis of naive T cells. *Nat Immunol* 8, 1255–1265. doi:10.1038/ni1513
- Lukacs-Kornek, V., Malhotra, D., Fletcher, A.L., Acton, S.E., Elpek, K.G., Tayalia, P., Collier, A.-R., Turley, S.J., 2011. Regulated release of nitric oxide by nonhematopoietic stroma controls expansion of the activated T cell pool in lymph nodes. *Nat Immunol* 12, 1096–1104. doi:10.1038/ni.2112
- Lund, A.W., Duraes, F.V., Hirosue, S., Raghavan, V.R., Nembrini, C., Thomas, S.N., Issa, A., Hugues, S., Swartz, M.A., 2012. VEGF-C promotes immune tolerance in B16 melanomas and cross-presentation of tumor antigen by lymph node lymphatics. *Cell Rep* 1, 191–199. doi:10.1016/j.celrep.2012.01.005
- Lund, A.W., Medler, T.R., Leachman, S.A., Coussens, L.M., 2016. Lymphatic Vessels, Inflammation, and Immunity in Skin Cancer. *Cancer Discovery* 6, 22–35. doi:10.1158/2159-8290.CD-15-0023
- Mahoney, K.M., Rennert, P.D., Freeman, G.J., 2015. Combination cancer immunotherapy and new immunomodulatory targets. *Nat Rev Drug Discov* 14, 561–584. doi:10.1038/nrd4591
- Melief, C.J.M., van Hall, T., Arens, R., Ossendorp, F., van der Burg, S.H., 2015. Therapeutic cancer vaccines. *Journal of Clinical Investigation* 125, 3401–3412. doi:10.1172/JCI80009
- Motz, G.T., Coukos, G., 2013. Deciphering and Reversing Tumor Immune Suppression. *Immunity* 39, 61–73. doi:10.1016/j.immuni.2013.07.005



- Nörder, M., Gutierrez, M.G., Zicari, S., Cervi, E., Caruso, A., Guzmán, C.A., 2012. Lymph node-derived lymphatic endothelial cells express functional costimulatory molecules and impair dendritic cell-induced allogenic T-cell proliferation. *FASEB J.* 26, 2835–2846. doi:10.1096/fj.12-205278
- Oh, S.J., Jeltsch, M.M., Birkenhager, R., McCarthy, J., Weich, H.A., Christ, B., Alitalo, K., Wilting, J., 1997. VEGF and VEGF-C: Specific induction of angiogenesis and lymphangiogenesis in the differentiated avian chorioallantoic membrane. *Dev. Biol.* 188, 96–109. doi:10.1006/dbio.1997.8639
- Oka, M., Iwata, C., Suzuki, H.I., Kiyono, K., Morishita, Y., Watabe, T., Komuro, A., Kano, M.R., Miyazono, K., 2008. Inhibition of endogenous TGF-beta signaling enhances lymphangiogenesis. *Blood* 111, 4571–4579. doi:10.1182/blood-2007-10-120337
- Olsson, A.-K., Dimberg, A., Kreuger, J., Claesson-Welsh, L., 2006. VEGF receptor signalling — in control of vascular function. *Nat Rev Mol Cell Biol* 7, 359–371. doi:10.1038/nrm1911
- Pasquali, S., van der Ploeg, A.P.T., Mocellin, S., Stretch, J.R., Thompson, J.F., Scolyer, R.A., 2013. Lymphatic biomarkers in primary melanomas as predictors of regional lymph node metastasis and patient outcomes. *Pigment Cell Melanoma Res* 26, 326–337. doi:10.1111/pcmr.12064
- Patel, S.P., Kurzrock, R., 2015. PD-L1 Expression as a Predictive Biomarker in Cancer Immunotherapy. *Molecular Cancer Therapeutics* 14, 847–856. doi:10.1158/1535-7163.MCT-14-0983
- Podgrabinska, S., Kamalu, O., Mayer, L., Shimaoka, M., Snoeck, H., Randolph, G.J., Skobe, M., 2009. Inflamed lymphatic endothelium suppresses dendritic cell maturation and function via Mac-1/ICAM-1-dependent mechanism. *The Journal of Immunology* 183, 1767–1779. doi:10.4049/jimmunol.0802167
- Porter, D.L., Hwang, W.-T., Frey, N.V., Lacey, S.F., Shaw, P.A., Loren, A.W., Bagg, A., Marcucci, K.T., Shen, A., Gonzalez, V., Ambrose, D., Grupp, S.A., Chew, A., Zheng, Z., Milone, M.C., Levine, B.L., Melenhorst, J.J., June, C.H., 2015. Chimeric antigen receptor T cells persist and induce sustained remissions in relapsed refractory chronic lymphocytic leukemia. *Sci Transl Med* 7, –303ra139. doi:10.1126/scitranslmed.aac5415
- Postow, M.A., Chesney, J., Pavlick, A.C., Robert, C., Grossmann, K., McDermott, D., Linette, G.P., Meyer, N., Giguere, J.K., Agarwala, S.S., Shaheen, M., Ernstoff, M.S., Minor, D., Salama, A.K., Taylor, M., Ott, P.A., Rollin, L.M., Horak, C., Gagnier, P., Wolchok, J.D., Hodi, F.S., 2015. Nivolumab and Ipilimumab versus Ipilimumab in Untreated Melanoma. *N Engl J Med* 372, 2006–2017. doi:10.1056/NEJMoa1414428
- Rabinovich, G.A., Gabrilovich, D., Sotomayor, E.M., 2007. Immunosuppressive Strategies that are Mediated by Tumor Cells. *Annu. Rev. Immunol.* 25, 267–296. doi:10.1146/annurev.immunol.25.022106.141609
- Randolph, G.J., Angeli, V., Swartz, M.A., 2005. Dendritic-cell trafficking to lymph nodes through lymphatic vessels. *Nat. Rev. Immunol.* 5, 617–628. doi:10.1038/nri1670
- Restifo, N.P., Dudley, M.E., Rosenberg, S.A., 2012. Adoptive immunotherapy for cancer: harnessing the T cell response. *Nat. Rev. Immunol.* 12, 269–281. doi:10.1038/nri3191

- Restifo, N.P., Smyth, M.J., Snyder, A., 2016. Acquired resistance to immunotherapy and future challenges. *Nature Reviews Cancer*. doi:10.1038/nrc.2016.2
- Rosenberg, S.A., Restifo, N.P., 2015. Adoptive cell transfer as personalized immunotherapy for human cancer. *Science* 348, 62–68. doi:10.1126/science.aaa4967
- Rouhani, S.J., Eccles, J.D., Riccardi, P., Peske, J.D., Tewalt, E.F., Cohen, J.N., Liblau, R., Kinen, T.M.A., Engelhard, V.H., 2015. Roles of lymphatic endothelial cells expressing peripheral tissue antigens in CD4 T-cell tolerance induction. *Nature Communications* 6, 1–13. doi:10.1038/ncomms7771
- Ruddle, N.H., Akirav, E.M., 2009. Secondary lymphoid organs: responding to genetic and environmental cues in ontogeny and the immune response. *The Journal of Immunology* 183, 2205–2212. doi:10.4049/jimmunol.0804324
- Savetsky, I.L., Ghanta, S., Gardenier, J.C., Torrisi, J.S., García Nores, G.D., Hespe, G.E., Nitti, M.D., Kataru, R.P., Mehrara, B.J., 2015. Th2 Cytokines Inhibit Lymphangiogenesis. *PLoS ONE* 10, e0126908–14. doi:10.1371/journal.pone.0126908
- Schumacher, T.N., Kesmir, C., van Buuren, M.M., 2015. Biomarkers in Cancer Immunotherapy. *Cancer Cell* 27, 12–14. doi:10.1016/j.ccell.2014.12.004
- Shao, X., Liu, C., 2006. Influence of IFN- $\alpha$  and IFN- $\gamma$  on Lymphangiogenesis. *Journal of Interferon & Cytokine Research* 26, 568–574. doi:10.1089/jir.2006.26.568
- Sharma, P., Allison, J.P., 2015. The future of immune checkpoint therapy. *Science* 348, 56–61. doi:10.1126/science.aaa8172
- Shayan, R., Karnezis, T., Murali, R., Wilmott, J.S., Ashton, M.W., Taylor, G.I., Thompson, J.F., Hersey, P., Achen, M.G., Scolyer, R.A., Stacker, S.A., 2012. Lymphatic vessel density in primary melanomas predicts sentinel lymph node status and risk of metastasis. *Histopathology* 61, no–no. doi:10.1111/j.1365-2559.2012.04310.x
- Snyder, A., Makarov, V., Merghoub, T., Yuan, J., Zaretsky, J.M., Desrichard, A., Walsh, L.A., Postow, M.A., Wong, P., Ho, T.S., Hollmann, T.J., Bruggeman, C., Kannan, K., Li, Y., Elipenahli, C., Liu, C., Harbison, C.T., Wang, L., Ribas, A., Wolchok, J.D., Chan, T.A., 2014. Genetic Basis for Clinical Response to CTLA-4 Blockade in Melanoma. *N Engl J Med* 371, 2189–2199. doi:10.1056/NEJMoa1406498
- Spinella, F., Garrafa, E., Di Castro, V., Rosanò, L., Nicotra, M.R., Caruso, A., Natali, P.G., Bagnato, A., 2009. Endothelin-1 stimulates lymphatic endothelial cells and lymphatic vessels to grow and invade. *Cancer Res.* 69, 2669–2676. doi:10.1158/0008-5472.CAN-08-1879
- Spranger, S., Spaapen, R.M., Zha, Y., Williams, J., Meng, Y., Ha, T.T., Gajewski, T.F., 2013. Up-Regulation of PD-L1, IDO, and T-regs in the Melanoma Tumor Microenvironment Is Driven by CD8(+) T Cells. *Sci Transl Med* 5, –200ra116. doi:10.1126/scitranslmed.3006504
- Stacker, S.A., Williams, S.P., Karnezis, T., Shayan, R., Fox, S.B., Achen, M.G., 2014. Lymphangiogenesis and lymphatic vessel remodelling in cancer. *Nature Publishing Group* 14, 159–172. doi:10.1038/nrc3677
- Swartz, M.A., 2014. Immunomodulatory roles of lymphatic vessels in cancer progression. *Cancer Immunology Research* 2, 701–707. doi:10.1158/2326-6066.CIR-14-0115

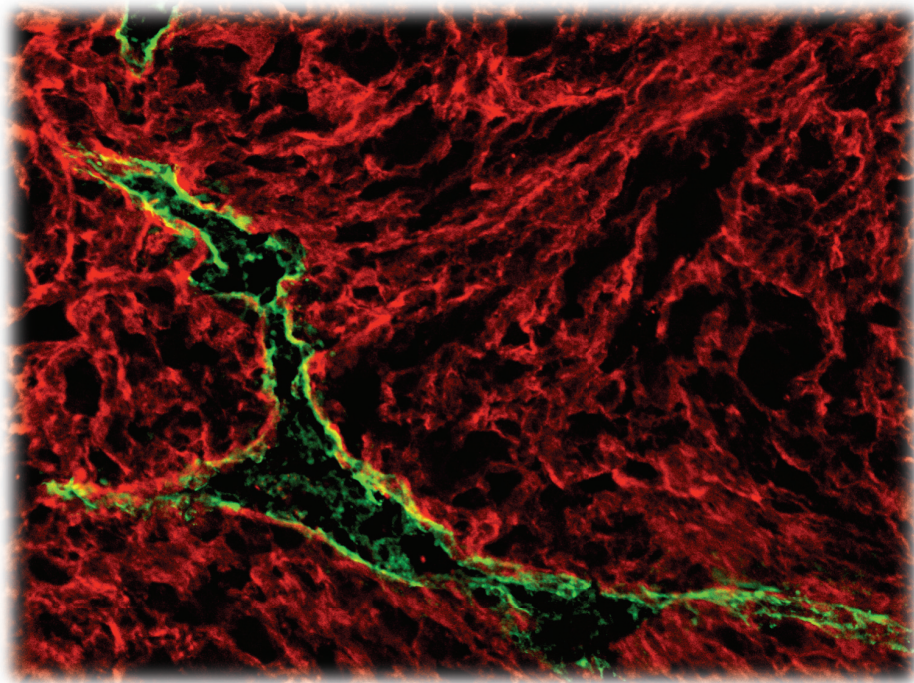
- Swartz, M.A., 2001. The physiology of the lymphatic system. *Adv. Drug Deliv. Rev.* 50, 3–20.
- Tamburini, B.A., Burchill, M.A., Kedl, R.M., 2014. Antigen capture and archiving by lymphatic endothelial cells following vaccination or viral infection. *Nature Communications* 5, 3989. doi:10.1038/ncomms4989
- Tammela, T., Alitalo, K., 2010. Lymphangiogenesis: Molecular Mechanisms and Future Promise. *Cell* 140, 460–476. doi:10.1016/j.cell.2010.01.045
- Tewalt, E.F., Cohen, J.N., Rouhani, S.J., Guidi, C.J., Qiao, H., Fahl, S.P., Conaway, M.R., Bender, T.P., Tung, K.S., Vella, A.T., Adler, A.J., Chen, L., Engelhard, V.H., 2012. Lymphatic endothelial cells induce tolerance via PD-L1 and lack of costimulation leading to high-level PD-1 expression on CD8 T cells. *Blood*. doi:10.1182/blood-2012-04-427013
- Tey, S.K., Bollard, C.M., Heslop, H.E., 2006. Adoptive T-cell transfer in cancer immunotherapy. *Immunology and cell biology*. doi:10.1111/j.1440-1711.2006.01441.x
- Topalian, S.L., Hodi, F.S., Brahmer, J.R., Gettinger, S.N., Smith, D.C., McDermott, D.F., Powderly, J.D., Carvajal, R.D., Sosman, J.A., Atkins, M.B., Leming, P.D., Spigel, D.R., Antonia, S.J., Horn, L., Drake, C.G., Pardoll, D.M., Chen, L., Sharfman, W.H., Anders, R.A., Taube, J.M., McMiller, T.L., Xu, H., Korman, A.J., Jure-Kunkel, M., Agrawal, S., McDonald, D., Kollia, G.D., Gupta, A., Wigginton, J.M., Sznol, M., 2012. Safety, Activity, and Immune Correlates of Anti-PD-1 Antibody in Cancer. *N Engl J Med* 366, 2443–2454. doi:10.1056/NEJMoa1200690
- Van Allen, E.M., Miao, D., Schilling, B., Shukla, S.A., Blank, C., Zimmer, L., Sucker, A., Hillen, U., Foppen, M.H.G., Goldinger, S.M., Utikal, J., Hassel, J.C., Weide, B., Kaehler, K.C., Loquai, C., Mohr, P., Gutzmer, R., Dummer, R., Gabriel, S., Wu, C.J., Schadendorf, D., Garraway, L.A., 2015. Genomic correlates of response to CTLA-4 blockade in metastatic melanoma. *Science* 350, 207–211. doi:10.1126/science.aad0095
- Vyas, J.M., Van der Veen, A.G., Ploegh, H.L., 2008. The known unknowns of antigen processing and presentation. *Nat. Rev. Immunol.* 8, 607–618. doi:10.1038/nri2368
- Wigle, J.T., Oliver, G., 1999. Prox1 function is required for the development of the murine lymphatic system. *Cell* 98, 769–778. doi:10.1016/S0092-8674(00)81511-1



## Chapter 3

# Naïve T cells recruited to lymphangiogenic melanoma via CCL21 potentiate antigen-specific immunotherapy

Manuel Fankhauser\*, Maria AS Broggi\*, Lambert Potin, Elodie Da Costa, Natacha Bordry, Laura Jeanbart, Amanda W Lund, Christopher Tremblay, Stephan Wullschleger, Krisztian Homicsko, Douglas Hanahan, Daniel E Speiser, and Melody A Swartz (to be submitted.)



Lymphatic vessel (green) within the tumor extracellular matrix (red) of an iBIP2 mouse melanoma. Confocal microscopy.

### 3.1 Abstract

Tumor-associated lymphangiogenesis, the formation of new lymphatic vessels, correlates with poor prognosis in melanoma patients. However, while lymphatic vessels might offer a physical escape route for metastatic cells, it has been elusive whether this is the predominant reason for the observed correlation in clinics. Recent research has highlighted that the cells lining lymphatic vessels, lymphatic endothelial cells (LECs), can actively and passively modulate immune responses. This has raised the possibility that tumor-associated lymphangiogenesis might influence tumor progression by regulating anti-tumor immune responses. In the context of melanoma, we have previously shown that lymphangiogenic B16 melanomas establish an immunosuppressive microenvironment in the draining lymph nodes, inhibiting the activation of tumor-specific CD8<sup>+</sup> T cells. We thus hypothesized that blocking the formation of intra- and peritumoral lymphatic vessels might similarly decrease immunosuppression in the primary tumor microenvironment itself, thereby increasing the efficacy of therapeutic immunotherapy. Strikingly, we found that the opposite was the case. Mice inoculated with B16 melanomas overexpressing the lymphatic growth factor VEGFC and the model antigen ovalbumin (B16-OVA/VC) were more sensitive to systemic antigen-specific immunotherapy approaches as compared to mice with non-lymphangiogenic B16 melanomas. Intriguingly, both B16-OVA/VC as well as naturally lymphangiogenic, mutant BRAF-driven iBIP2 melanomas recruited CCR7<sup>+</sup> tumor infiltrating lymphocytes (TILs) by VEGFR3-dependent secretion of CCL21 chemokine. Accordingly, VEGFC correlated with CCL21 and CCR7 in a human melanoma gene expression data set, and CCL21 co-localized with LECs in sections of primary human melanoma. We further demonstrate that naïve TILs enhanced the efficacy of antigen-specific immunotherapy against B16-OVA/VC tumors, as they were locally activated in response to tumor cell death, leading to antigen spreading and long lasting protection to re-challenge with lung metastasis. We conclude that secretion of CCL21 is a novel pathway by which tumor-associated LECs actively increase tumor inflammation, thereby establishing a microenvironment that is able to potentiate antigen-specific immunotherapy. We propose that lymphangiogenesis and CCL21, both biomarkers indicative of poor primary disease outcome, might serve as biomarkers predicting favorable response to antigen-specific immunotherapy.

### 3.2 Introduction

De novo formation of lymphatic vessels during tumor progression, so called lymphangiogenesis, correlates with poor prognosis in melanoma patients (Dadras et al., 2010; Pasquali et al., 2013; Shayan et al., 2012). Apart from offering physical routes for metastatic spread (Karaman and Detmar, 2014; Stacker et al., 2014; Tammela and Alitalo, 2010), tumor-associated lymphatic vessels (LVs) are passively and actively involved in shaping anti-tumor immunity (Lund et al., 2016; Swartz, 2014). They passively drain antigens, cytokines, and danger signal from the tumor to the sentinel lymph nodes (LNs), which is essential for the generation of a T cell-inflamed microenvironment in mouse and human melanoma (Lund et al., under review). Moreover, lymphatic endothelial cells (LECs) actively impact immune cell function by releasing immunomodulatory cytokines and by presenting endogenous and exogenous antigens on MHC I and MHC II molecules (Card et al., 2014). In this context, we have previously shown that LECs in the draining LNs of lymphangiogenic B16 melanoma tumors can directly suppress the activation of tumor-specific CD8<sup>+</sup> T cell responses by tolerogenic cross-presentation of tumor-derived antigen (Lund et al., 2012). Considering that secretion of bioactive factors and engagement in cell-cell interactions by LECs does not specifically require LVs to have a lumen, we anticipated that both peri- and intratumoral LVs might be actively involved in the regulation of anti-tumor immunity. Thus, while intratumoral lymphatic vessels have previously been reported to be non-functional in terms of drainage (Padera et al., 2002), we here wanted to determine the role of tumor-associated lymphangiogenesis in regulating immune responses within the primary tumor itself. A better understanding of LEC-mediated immunoregulation within primary melanomas would inform rational approaches to modify this aspect of the tumor microenvironment, with the ultimate goal of increasing the number of metastatic melanoma patients who can benefit from immunotherapy.

Tumor-associated CCL21, a chemokine classically expressed by lymph node stromal cells to guide immune cell subsets into the lymph node parenchyma (Förster et al., 2008), recruits CCR7<sup>+</sup> immune cells into primary mouse melanomas and induces the formation of a lymphoid-like stroma with hallmarks of immunosuppression (Peske et al., 2015; Shields et al., 2010). Even though CCL21 can be expressed by lymphatic endothelial cells (Förster et al., 2008; Gunn et al., 1998; Kuroshima et al., 2004; Shields et al., 2007), it is not known whether there is a link between the presence of intra- and peritumoral LECs, local CCL21 levels, and CCL21 mediated immunoregulation in primary melanomas. Thus, the purpose of this study was to determine whether CCL21 induced chemoattraction of tumor infiltrating lymphocytes (TILs) depends on lymphatic density within primary melanoma tumors, and if so, whether this can be exploited to increase the efficacy of therapeutic immunotherapy. Given the previous associations of both draining lymph node lymphangiogenesis and CCL21 with immunosuppression, we hypothesized that blocking the formation of intra- and peritumoral LVs might decrease CCL21-induced immunosuppression in the tumor microenvironment, and thus increase the efficacy of systemic immunotherapies.

We characterized the injectable B16F10 and the inducible BRAF<sup>V600E</sup>-driven iBIP2 mouse models of melanoma in terms of their lymphatic density, CCL21 expression, immune infiltrates, and



response to various antigen-specific and antigen-non-specific immunotherapy approaches. Tumor-associated lymphangiogenesis was manipulated through overexpression of the lymphatic growth factor VEGFC and/or through antibody mediated blocking of the VEGFC receptor VEGFR3. To assess how lymphangiogenesis would affect cancer immunotherapy, we inoculated mice with B16F10 cell lines that express VEGFC as well as chicken ovalbumin (B16-OVA/VC), a model antigen for which multiple antigen-specific immunotherapy approaches exist. Opposite to what we hypothesized, we found that lymphangiogenic B16-OVA/VC melanomas respond much more profoundly to systemic antigen-specific immunotherapy including adoptive T cell transfer, dendritic cell vaccination and protein vaccination as compared to control tumors, a phenomenon we call lymphangiogenic potentiation. In contrast, the lymphangiogenic status of neither B16 nor iBIP2 tumors influenced the outcome of non-antigen-specific immunotherapy, such as checkpoint inhibition using anti-PD1 and anti-CTLA4 antibodies. To understand why lymphangiogenic melanomas are more permissive to antigen-specific immunotherapy, we analyzed the immune cell and cytokine environment of primary tumors prior to immunotherapy. In agreement with our previous publications, lymphangiogenic melanomas had increased levels of regulatory CD4<sup>+</sup> T cells, a hallmark of an immunosuppressed microenvironment. In addition, however, we found that VEGFR3 signaling was also driving increased infiltration of naïve T cells into lymphangiogenic B16 and central memory T cells into iBIP2 melanomas. Considering that regulatory, naïve, and central memory T cells are known to rely on CCL21 chemokine gradients for CCR7 chemokine receptor mediated tissue homing, we analyzed this signaling axis within lymphangiogenic melanomas. Indeed, we found that lymphangiogenic mouse melanomas express high levels of CCL21, and that B16-OVA/VC tumors contained higher densities of T cells expressing CCR7. Furthermore, VEGFC but not VEGFA and VEGFD correlated with CCL21 and CCR7 in a gene expression data set from 469 melanoma patients retrieved from The Cancer Genome Atlas (TCGA), suggesting that our findings could be relevant for human pathology. Finally, by blocking lymphocyte egress from secondary lymphoid organs using the small molecule FTY720, we demonstrate that local activation and expansion of naïve T cell infiltrates was responsible for lymphangiogenic potentiation of antigen-specific immunotherapy in B16-OVA/VC tumors. The locally activated T cells with specificities for endogenous antigens ensured antigen-spreading of the anti-tumor immune response, protecting mice from re-challenge with non-ovalbumin expressing wildtype B16 melanoma in a model of lung metastasis. Taken together, our findings reveal that naïve endogenous T cells recruited into lymphangiogenic tumors via the CCL21/CCR7 axis are locally primed and activated following antigen-specific immunotherapy-induced tumor cell death, leading to antigen-spreading and long lasting protection against tumor re-challenge. These results attribute a completely novel role to tumor-associated lymphangiogenesis. While they have been indicative of poor prognosis because it supports metastatic spread (Karaman and Detmar, 2014; Stacker et al., 2014) and inhibits anti-tumor immune responses in the draining lymph node (Lund et al., 2012), it might serve as a biomarker to stratify metastatic melanoma patients that can benefit from systemic, antigen-specific immunotherapies.



### 3.3 Materials and methods

#### 3.3.1 Mice

Female wild-type mice (Harlan), OT-I RAG-1<sup>-/-</sup> (Jackson Labs), and CD45.1 (Harlan), all on the C57BL/6 background, were used between 8-12 weeks of age. iBIP2 mice were on the FVB/N background and bred in house. iBIP2 mice were generated by crossing the previously published iBIP mice (Kwong et al., 2015) into a FVB/N line with floxed Cdkn2a alleles. iBIP2 mice have a Tet-inducible human BRAF<sup>V600E</sup> transgene, floxed alleles of Cdkn2a and Pten, and inducible Cre expression under melanocyte-specific control. All experiments were performed with approval from the Veterinary Authority of the Canton de Vaud, Switzerland, and IACUC of University of Chicago, #72414.

#### 3.3.2 Tumor cell lines

B16-F10 melanoma cells (ATCC) were maintained in high glucose DMEM (E15-843; GE Healthcare) supplemented with 10% heat-inactivated fetal bovine serum (FBS) (GIBCO Invitrogen). B16-F10 ovalbumin (OVA) expressing cells (gift of B. Huard) were engineered to overexpress VEGFC as described previously (Lund et al., 2012). All cell lines were split 1:20 or 1:40 every 3-4 days.

#### 3.3.3 B16 tumor inoculation, iBIP2 tumor induction, and measurements

For B16 tumor inoculation, mice were anesthetized with isoflurane and their backs were shaved.  $2.5 \times 10^5$  cells were resuspended in 30  $\mu$ l PBS and then injected intradermally on the front, dorsolateral side. To induce iBIP2 tumors, mice received one microliter of 5mM 4-hydroxy-tamoxifen (70% Z-isomer, 30% E-isomer, H6278; Sigma-Aldrich) dissolved in 70% EtOH topically applied on the ventral side of the ear. Upon topical application of tamoxifen, Cdkn2a and Pten were specifically deleted only in the treated melanocytes, and rtTA was activated. Subsequent continuous administration of doxycycline in the drinking water (1mg/ml) (D43020; Research Products International) activated the BRAF<sup>V600E</sup> transgene only in the cells in which the LSL-Stop-rtTA cassette as well as Cdkn2a and Pten were codeleted. Both B16 and iBIP2 tumors were measured with a caliper, and volumes (V) were calculated as ellipsoids ( $V = 4/3 \cdot \pi \cdot \text{length} \cdot \text{width} \cdot \text{height} / 8$ ). Mice were sacrificed when mice reached a humane end-point according to an animal well-being score sheet or when tumor volumes reached  $> 500 \text{ mm}^3$  (before reaching the legal limit of  $1 \text{ cm}^3$ ). For long-term studies, they were then accounted dead the next day. In immunotherapy studies, mice that succumbed for unknown reasons prior to the regression phase were excluded.

#### 3.3.4 Antibody injections

For VEGFR3 blocking studies, mice received i.p. injections of 500 $\mu$ g anti-VEGFR3 antibody (mF4-31C1; ImClone/Eli Lilly) or isotype rat IgG (I4131; Sigma) every 3-4 days starting the day of B16 inoculation. For CCR7 blocking studies, mice received i.p. injections of 25 $\mu$ g anti-CCR7 antibody (16-1971; eBioscience) or isotype rat IgG on day 0, 3, and 6 after tumor inoculation. For combination therapy of PD1 and CTLA4 checkpoint blockade, mice were treated with 250 $\mu$ g anti-CTLA4 antibody (BE0164; BioXCell) every 3 days and 100 $\mu$ g anti-PD1 antibody (BE0146; BioXCell) every 2 days both

starting on day 4. For combination therapy of PD1 checkpoint blockade and ACT, mice were treated with 250µg anti-PD1 antibody every 3-4 days starting on the day of ACT.

### **3.3.5 Therapeutic vaccination**

Mice received 50µg CpG-B (5'-TCCATGACGTTCTGACGTT-3'; Microsynth) + 10µg OVA grade V (A5503; Sigma) in two i.d. doses 25µl per hind footpad (targeting tumor non-draining lymph nodes) on day 4, 7, and 10 after tumor inoculation.

### **3.3.6 OT-I *ex vivo* activation and therapeutic adoptive transfer**

Spleens and lymph nodes were recovered from OT-I mice. Spleens were placed in a petri dish containing 10ml basal IMDM medium (31980-022; Gibco) and disrupted with a scalpel before being transferred through a 70µm filter (22363548; Fisher Scientific) into a 50ml conical tube. Cells were then spun down at 2000rpm for 5' and resuspended in 1ml ACK red blood cells lysis buffer (150mM NH<sub>4</sub>Cl + 10mM KHCO<sub>3</sub> + 0.1mM Na<sub>2</sub>EDTA dissolved in H<sub>2</sub>O, pH 7.2). After 5' incubation, 10ml basal IMDM was added, and the cells spun down at 2000rpm for 5'. Lymph nodes were placed in a well of a twelve well plate containing 2ml digestion medium (IMDM + 1mg/ml Collagenase D (1108886600; Roche)). The lymph node capsules were gently opened with two syringe needles (26G) to allow better digestion, and then incubated for 15' at 37°C. Lymph node cells were then spun down at 2000rpm for 5' and pooled in 10ml basal IMDM with the splenocytes for further processing. CD11c<sup>+</sup> dendritic cells (DCs) were first isolated by positive magnetic cell sorting (130-052-001; Milteny Biotec) before CD8<sup>+</sup> T cells were isolated from the remaining cells by negative magnetic cell sorting (130-095-236; Milteny Biotec) according to the manufacturer's protocol. Next, isolated CD11c<sup>+</sup> DCs and CD8<sup>+</sup> T cells were plated 1:10 on a 96 well plate (10'000 CD11c<sup>+</sup> DCs and 100'000 CD8<sup>+</sup> T cells per well) in stimulation medium (IMDM + 10%FBS + Pen/Strep + 1nM SIINFEKL peptide + 10U/ml mIL-2 (212-12; PreproTech)). Cells were collected after 4 days and injected i.v. into tumor-bearing mice (1x10<sup>6</sup> cells in 200µl in basal IMDM).

### **3.3.7 Therapeutic dendritic cell vaccination**

BMDCs were generated from the bone marrow of C57BL/6 mice as previously described (Lutz et al., 1999). At day 8 of BMDC culture, 10ng/ml LPS was added for 12h. The activated BMDCs were then washed 1x with 20ml full medium (IMDM + 10% FBS) and plated at 2-5x10<sup>6</sup> cells/ml in 10cm petri dishes. The cells were then pulsed with 1µM of SIINFEKL for 1h. Cells were then collected and washed 3x with 20ml PBS. Finally, cells were resuspended in PBS at 10x10<sup>6</sup> cells/ml, and 100µl injected intraperitoneally per mouse.

### **3.3.8 Lymph node and tumor cell isolation**

Stromal cells (CD45<sup>-</sup>) and CD45<sup>+</sup> immune cells were recovered from tumors, and tumor draining and non-draining lymph nodes (LNs) according to the "Broggi Style" protocol (Broggi, Schmalzer, Lagarde, & Rossi, 2014). Lymph nodes were placed in a well of a 24 well plate containing 500µl digestion medium consisting of DMEM (41965-062; GIBCO, no pyruvate) + 1% Pen/Strep + 1.2mM CaCl<sub>2</sub> + 2% FBS. The lymph node capsules were then gently opened with two syringe needles (26G) to allow

better digestion. The opened LNs were then transferred into a 5ml round-bottom tube (Falcon-BD Bioscience) containing 750 $\mu$ l digestion buffer I, which consisted of digestion medium + 1mg/ml Collagenase IV (CLS4 LS004188; Worthington) + 40 $\mu$ g/ml DNase I (11284932001; Roche). Digestion was done for 30' at 37°C in a beaker with water on a heating plate with magnetic stirring (~1turn/sec). The supernatant was then carefully collected into a 5ml round-bottom filter tube (Falcon-BD Bioscience), and 750 $\mu$ l digestion buffer II, which consisted of digestion medium + 3.3mg/ml Collagenase D (1108886600; Roche) + 40 $\mu$ g/ml DNase I, was added to the 5ml tube with the remaining tissue pieces. Digestion was then continued for 5', before pipetting 10 times using an electronic pipette. Digestion was then continued for 10', before pipetting 100 times. 7.5 $\mu$ l EDTA (500mM) was added to each tube to reach a final concentration of 5mM (pH 7.2), before pipetting again 100 times. The entire cell suspension was then collected into a 5ml round-bottom filter tube (Falcon-BD Bioscience), and spun down at 2000rpm for 5'. Cells were then resuspended in an appropriate volume of FACS buffer (PBS + 2% FBS) to proceed for FACS staining. For the tumors, the Broggi Style protocol was slightly adapted. Approximately 100mg of tumor tissue was placed in a 5ml round-bottom tube containing 750 $\mu$ l digestion buffer I. The tumor piece was then cut into small pieces using scissors, before being digested for 30' at 37°C in a beaker with water on a heating plate with magnetic stirring (~1turn/sec). The supernatant was then carefully collected through a 70 $\mu$ m nylon filter into a 50ml conical tube and 750 $\mu$ l digestion buffer II was added to the 5ml tube with the remaining tissue pieces. Three cycles of 15' digestion, followed by 100 times pipetting were then done. After the last cycle, 7.5 $\mu$ l EDTA (500mM) was added to each tube to reach a final concentration of 5mM (pH 7.2), before pipetting again 100 times. The entire cell suspension was then collected through the 70 $\mu$ m into the 50ml conical tube. Remaining tissue pieces were smashed through the filter using the plunger of a 3ml syringe, and the filter subsequently washed with 10ml HBSS. The cell suspension was then spun down at 2000rpm for 5' and resuspended in an appropriate amount of FACS buffer to proceed for FACS staining.

### **3.3.9 Immunohistochemistry**

Mouse tumor samples were fixed in Zinc fixation buffer (4.5mM CaCl<sub>2</sub> + 51.5mM ZnCl<sub>2</sub> + 32mM Zn(CF<sub>3</sub>CO<sub>2</sub>)<sub>2</sub> + 38.5mM glycine in H<sub>2</sub>O, pH 6.5) (Kilarski et al., 2012), paraffin-embedded and cut into 8 $\mu$ m sections. Formalin-fixed human tumors were, paraffin-embedded and cut into 4-5 $\mu$ m sections. For immunolabeling, paraffin-embedded tissue sections were deparaffinized and rehydrated. Antigen retrieval was done on PFA-fixed samples at 98°C for 15min in TRIS/EDTA buffer (pH 9.0). Sections were then stained according to standard immunohistochemistry protocols. Primary antibodies used were: rabbit anti-msLyve1 (103-PA50; RELIAtech, 1:200), biotinylated rat anti-msCD45 (13-0451-85; eBioscience, 1:100), anti-huD2-40 (SIG-3739; Covance), anti-huCCL21 (HPA051210; Sigma.), anti-huCD8 (M7103; DakoCytomation), anti-huProx1 (AF2727, RnD System). Quantification of lymphatic vessels was done manually on entire tumor tile images using Fiji. Single positive Lyve1 nuclei were excluded as macrophages. The iBIP2 peritumoral space was defined as 250 $\mu$ m inwards from the tumor border, corresponding to approximately half the thickness of the ear skin adjacent to the tumors. A trained medical doctor defined the tumor areas in primary human melanoma.

### **3.3.10 Flow cytometry**

Antibody stainings for surface targets were done in FACS buffer (PBS + 2% FCS), and intracellular stainings were done after fixation and permeabilization according to the manufacturers protocol. The following anti-mouse antibodies were used for flow cytometry: CD45-APC (17-0451-82; eBioscience) or biotinylated CD45 (13-0451-85; eBioscience), CD4-PacBlue (100531; Biolegend) or CD4-PE-Cy7 (100528; Biolegend), CD8 $\alpha$ -PacOrange (MCD0830; Invitrogen), F4/80-PerCPCy5.5 (123128; Biolegend), CD25-FITC (101908; Biolegend), FoxP3-PerCPCy5.5 (45-5773-82; eBioscience), CD62L-PE (12-0621-82; eBioscience), CD44-APCeF780 (47-0441-82; eBioscience), CCR7-PE-Cy7 (25-1971-82; eBioscience) or CCR7-PerCPCy5.5 (45-1971-82; eBioscience), biotinylated CD11b (13-0112-82; eBioscience). Pentamer staining for H-2kb-Trp2-PE (SVYDFFVWL; TC Metrix), H-2Db-gp100-PE (KVPRNQDWL; TC Metrix) and H-2kb-SIINFEKL-PE (F093-2B; ProImmune) was performed according to manufacturers guidelines. Cell viability was determined using live/dead aqua (L34957; Invitrogen) or red (L23102; Invitrogen) dyes. Flow cytometry acquisition was performed on a Cyan flow cytometer (Beckman Coulter) and data analysis was performed with FlowJo (Version 9.7.7.).

### **3.3.11 Analysis of TCGA data set containing 469 skin cutaneous melanoma patients**

TCGA level 3 gene expression data were downloaded for skin cutaneous melanoma (SKCM) from the Broad GDAC Firehose database (<http://gdac.broadinstitute.org/>). The RNAseq data set called "illuminahisec\_rnaseqv2-RSEM\_genes\_normalized (MD5)" with release date 20151101 contained upper quartile normalized RSEM values summarized at the gene level (Li and Dewey, 2011). The data was log2 transformed after the addition of one pseudoread. The total of 469 SKCM samples were split into two groups according to whether the tissue biopsy was retrieved from the primary melanoma site (103 samples) or a metastatic site (369 samples) including sentinel lymph nodes and distant organ metastasis.

### **3.3.12 Statistical analysis**

Statistical analysis was done using Prism (v5.0d, GraphPad). Except mentioned differently, statistically significant differences between two experimental groups were determined by an unpaired student's t-test, and by one-way ANOVA followed by Tukey's post-test when more than two groups were compared. \*  $p < 0.05$ , \*\*  $p < 0.01$ , \*\*\*  $p < 0.001$ , ns: not significant.

### 3.4 Results

#### 3.4.1 Lymphangiogenic B16 melanomas are highly sensitive to antigen-specific immunotherapy.

Tumor lymphangiogenesis correlates with poor prognosis in human cancer patients (Dadras et al., 2010; Pasquali et al., 2013; Shayan et al., 2012). Apart from offering routes for metastatic spread (Karaman and Detmar, 2014; Stacker et al., 2014; Tammela and Alitalo, 2010), tumor-associated lymphangiogenesis has been shown to suppress the activation of anti-tumor immunity in the tumor draining lymph node (Lund et al., 2012). We thus hypothesized that blocking lymphangiogenesis using anti-VEGFR3 antibodies might reverse the immunosuppressive microenvironment, thereby increasing the efficacy of cancer immunotherapy. To test this, we adoptively transferred *ex vivo* activated OVA-specific CD8<sup>+</sup> OT-I cells into tumor bearing mice and assessed tumor growth over time (Figure 3.1A-B). In line with our previous findings (Lund et al., under review), non-lymphangiogenic B16 tumors were more sensitive to adoptive T cell therapy (ACT) in the short-term, leading to an almost 2 fold decreased tumor size on day 12 (Figure 3.1B). However, to our surprise, B16-OVA tumors and anti-VEGFR3 treated B16-OVA/VC tumors started progressing shortly after peak regression on day 16, while IgG treated B16-OVA/VC tumors showed a profound and long lasting response to ACT. This translated into significantly decreased tumor volume in the progression phase and into increased survival of control treated B16-OVA/VC tumor bearing mice. To control for potential intrinsic differences of the tumor cell lines in terms of their susceptibility to immunotherapy, we performed the same ACT experiment in mice that lack dermal lymphatic vessels (K14 mice). There was no difference between B16-OVA and B16-OVA/VC tumor growth or host survival in K14 mice (Figure 3.2A-B), confirming that the observed therapeutic benefit after ACT in B16-OVA/VC tumors was dependent on host lymphangiogenesis. We next asked whether the lymphangiogenic status of B16 melanomas also modulates the response towards an antigen-specific immunotherapy approach that relies on raising an endogenous anti-tumor response. We thus performed a therapeutic dendritic cell vaccination (DC vax) protocol, in which dendritic cells are activated with LPS and then pulsed with the immunodominant OVA peptide SIINFEKL *ex vivo*, before being intraperitoneally injected into recipient mice on day four and ten after tumor inoculation (Figure 3.1C). As for ACT, lymphangiogenic tumors grew significantly larger in the short-term response to DC vax, but then underwent profound regression (Figure 3.1D). Accordingly, the median survival increased from 21.5 days for anti-VEGFR3 treated to 72 days for control treated B16-OVA/VC tumors bearing mice. Based on the observations in the models of antigen-specific immunotherapy, we wanted to determine whether the lymphangiogenic status of B16 tumors modulates non-antigen-specific immunotherapy approaches. We performed a therapeutic checkpoint inhibition protocol that has been described to induce delayed tumor outgrowth, but not regression, in the B16 model of melanoma (Figure 3.1E) (Spranger et al., 2014). We found that while combinatorial treatment of tumor bearing mice with anti-PD1 and anti-CTLA4 antibodies did lead to delayed tumor outgrowth, the lymphangiogenic status of B16 tumors did not influence the magnitude of response (Figure 3.1F). However, when PD1 inhibition was performed in combination with ACT, the therapeutic benefit of lymphangiogenic tumors could be

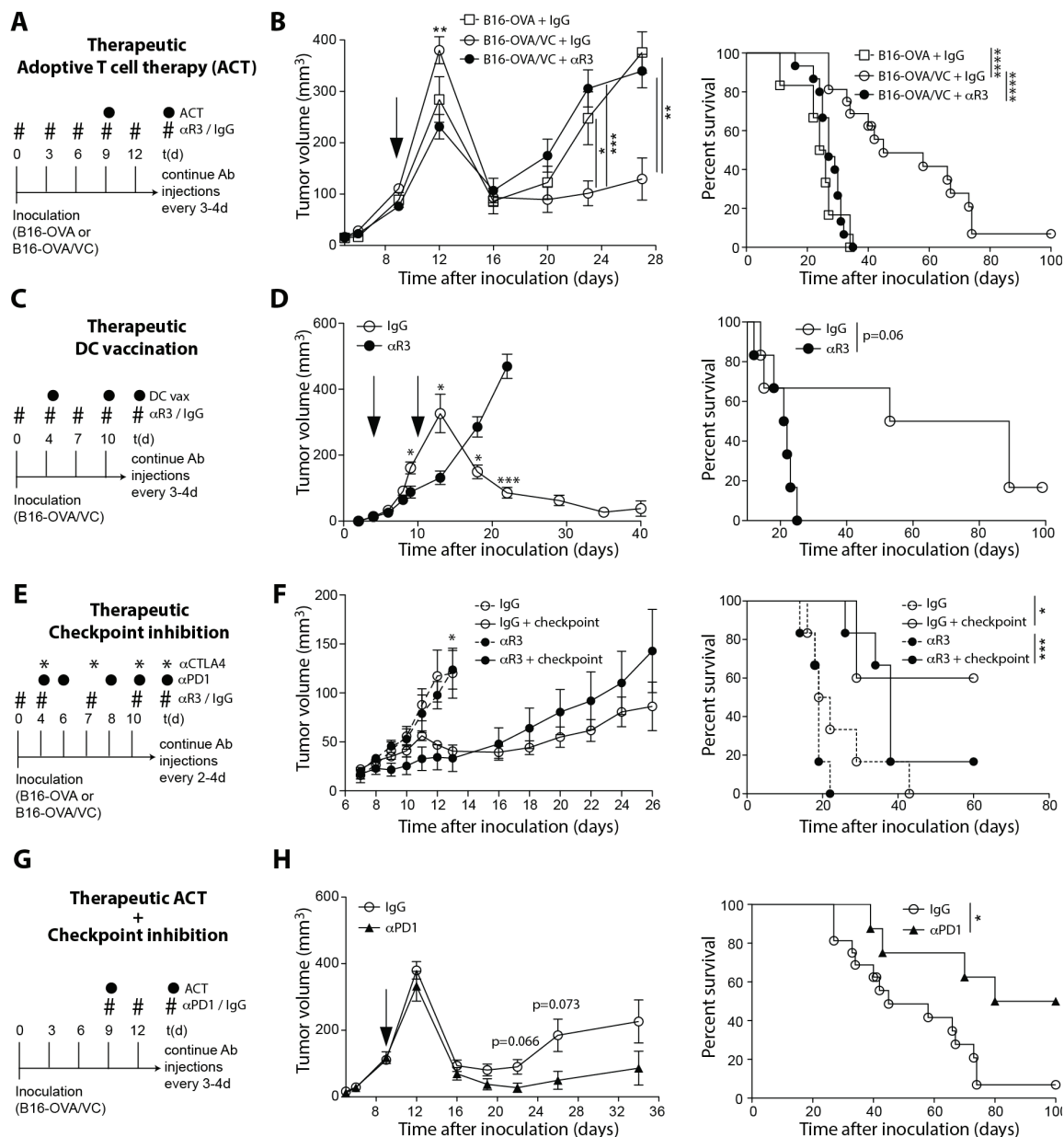


**Figure 3.1 Lymphangiogenic B16 melanomas respond to antigen-specific immunotherapy with increased growth in the short-term, but with profound regression in the long-term.** (A-B) Antigen-specific adoptive T cell therapy (ACT) in B16 tumor-bearing wildtype C57BL/6 mice. (A) Mice received transfer of  $1 \times 10^6$  ex vivo activated effector OT-I cells injected intravenously on day nine after tumor cell inoculation. (B) Tumor growth profiles and survival curves for B16-OVA and B16-OVA/VC tumor-bearing mice treated with ACT in combination with isotype (IgG) or anti-VEGFR3 ( $\alpha$ VR3) antibodies. Data pooled from 3 independent experiments,  $n \geq 20$ . (C-D) Antigen-specific dendritic cell vaccination (DC vax) in B16 tumor-bearing wildtype C57BL/6 mice. (C) Mice received i.p. injections of  $1 \times 10^6$  ex vivo SIINFEKL peptide pulsed dendritic cells on day four and ten after tumor cell inoculation. (D) Tumor growth profiles and survival curves for B16-OVA/VC tumor-bearing mice treated with DC vax in combination with isotype (IgG) or anti-VEGFR3 ( $\alpha$ VR3) antibodies.  $n = 6$ . (E-F) Non antigen-specific immunotherapy by combined checkpoint inhibition of PD1 and CTLA4 in B16 tumor-bearing wildtype C57BL/6 mice. (E) Mice received i.p. injections of anti-PD1 and anti-CTLA4 antibodies every 2-3 days starting on day four after tumor cell inoculation. (F) Tumor growth profiles and survival curves for B16-OVA/VC tumor-bearing mice treated with checkpoint inhibition in combination with isotype (IgG) or anti-VEGFR3 ( $\alpha$ VR3) antibodies. Data representative of 2 independent experiments,  $n \geq 5$ . (G-H)



Combinatorial immunotherapy with ACT and checkpoint inhibition in B16 tumor-bearing wildtype C57BL/6 mice. (G) Mice received i.p. injections of anti-PD1 starting at the same time as ACT was performed, nine days after tumor cell inoculation. (H) Tumor growth profiles and survival curves for B16-OVA/VC tumor-bearing mice treated with ACT only (IgG) or ACT + checkpoint inhibition ( $\alpha$ PD1, data pooled from 2 independent experiments,  $n=8$ ). Growth curves shown as mean  $\pm$  SEM over time (\*  $p \leq 0.05$ , \*\*  $p \leq 0.01$ , \*\*\*  $p \leq 0.001$ , \*\*\*\*  $p \leq 0.0001$ ).

even further increased (Figure 3.1G-H), suggesting that checkpoint inhibition has most impact in combination with potent tumor antigen-specific immunity. Even though there was no significant difference in tumor size on day 40, 4 out of 8 (50%) mice that received ACT together with checkpoint inhibition were tumor free as compared to 1 out of 9 (11.1%) mice that received ACT only (Figure 3.1H). This translated into significantly increased survival, with 50% of mice receiving combinatorial treatment still alive 100 days after inoculation. Altogether, these data demonstrate that mice with lymphangiogenic B16 melanoma benefit significantly more from antigen-specific immunotherapy as compared to mice with non-lymphangiogenic B16 tumors.

### 3.4.2 Lymphangiogenic B16 melanomas show increased TILs of regulatory and naïve phenotype.

Having found that lymphangiogenic B16 melanomas are more sensitive towards antigen-specific immunotherapy, we wondered whether there are any changes to the local tumor microenvironment that could render them more permissive to therapy. We first assessed whether anti-VEGFR3 treatment had a specific effect on peri- and intratumoral lymphatics. Consistent with previous reports (Lund et al., 2012), primary tumor growth of isotype treated B16-OVA and B16-OVA/VC tumors was unaffected, while treatment of B16-OVA/VC tumors with VEGFR3 antibodies led to a slight decrease in tumor size on day 9 (Figure 3.4A). Intratumoral VEGFC expression was confirmed in B16-OVA/VC tumors (Figure 3.4B). Interestingly, blocking VEGFR3 signaling in these tumors lead to increased VEGFC levels, suggesting that the growth factor might accumulate because of decreased receptor-ligand internalization (Karpanen, 2006). As expected, VEGFC expression increased the density of

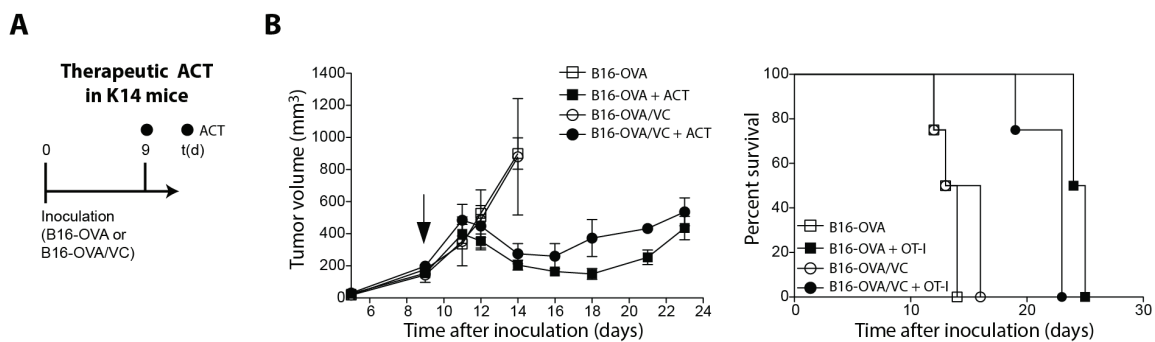


**Figure 3.2 (Supplementary Figure 3.1). Increased efficacy of immunotherapy in B16-OVA/VC tumor-bearing mice depends on host lymphangiogenesis.** (A-B) Antigen-specific adoptive T cell therapy (ACT) in B16 tumor-bearing mice lacking dermal lymphatics (K14 mice). (A) Mice received transfer of  $1 \times 10^6$  ex vivo activated effector OT-I cells injected intravenously on day nine after tumor cell inoculation. (B) Tumor growth profiles and survival curves for B16-OVA and B16-OVA/VC tumor-bearing K14 mice that did or did not receive ACT (OT-I).  $n=4$ .

intratumoral Lyve-1 positive lymphatic vessels, while anti-VEGFR3 treated tumors were devoid of them (Figure 3.4C). This was confirmed by flow cytometry, where gp38<sup>+</sup>CD31<sup>+</sup> lymphatic endothelial cells (LECs) (Figure 3.4D and 3.4E) but not gp38<sup>+</sup>CD31<sup>+</sup> blood endothelial cells (BECs) were enriched only in lymphangiogenic tumors. Even though subpopulations of monocytes and macrophages can express VEGFR3 (Schoppmann et al., 2002), we could not detect a significant change in the abundance of intratumoral F4/80<sup>+</sup> macrophages in the different treatment groups (Figure 3.4E). We next analyzed tumor infiltrating lymphocytes (TILs) (Figure 3.3A). In line with previous reports, we found a trend towards increased CD45<sup>+</sup> immune cell density in B16-OVA/VC tumors, including CD4<sup>+</sup>FoxP3<sup>+</sup> regulatory T cells (Figure 3.3B). This shifted the balance of regulatory versus effector T cells in favor of the former ones, indicating that the environment is immunosuppressed (Figure 3.4F). Interestingly, there was also a significant increase (~2.5 fold) of conventional CD4<sup>+</sup>FoxP3<sup>-</sup> T cell density as well as a trend of increased CD8<sup>+</sup> T cell density in lymphangiogenic as compared to non-

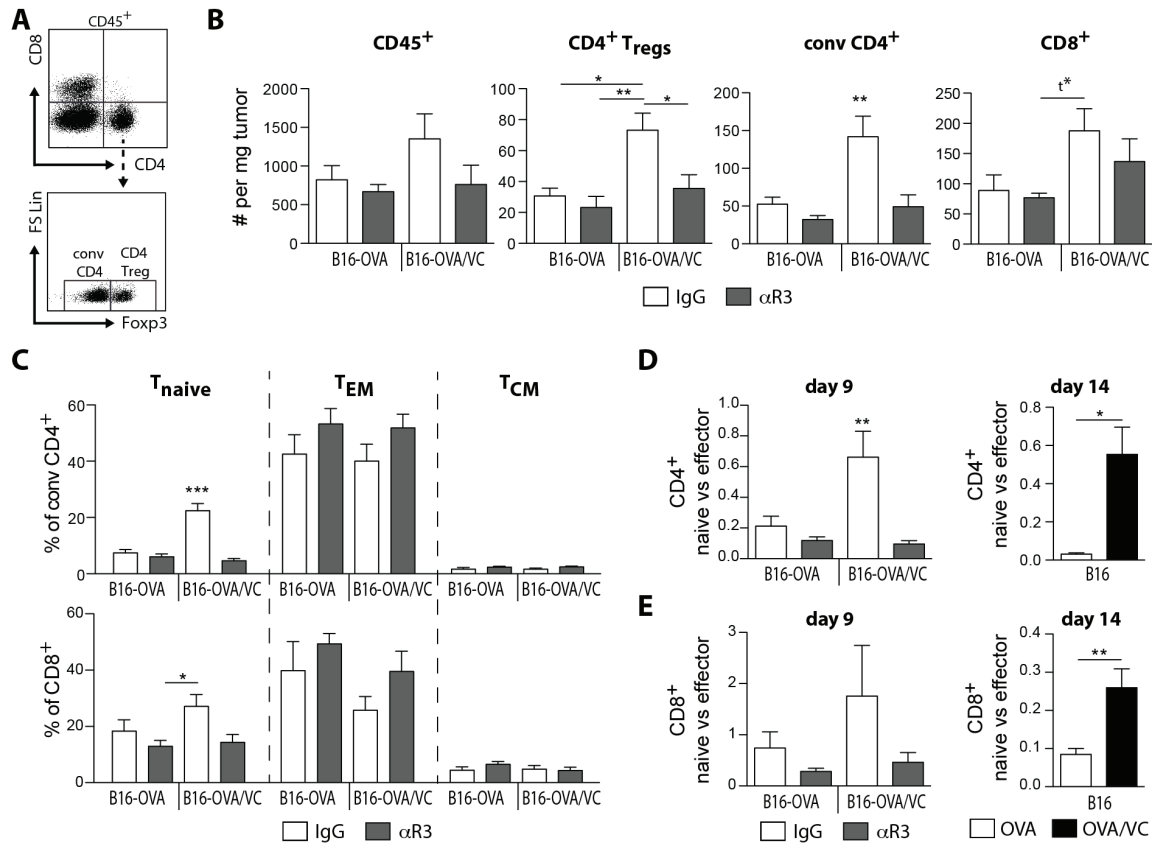


**Figure 3.3 Lymphangiogenic B16 melanomas contain increased regulatory and naïve TILs.** B16-OVA and B16-OVA/VC tumor bearing mice treated with isotype (IgG) or anti-VEGFR3 (αVR3) antibodies were euthanized 9 days (A-E) or 14 days (D-E, right graphs) after inoculation, and tumor single cell suspensions analyzed by flow cytometry. Representative flow cytometry plots (A) and quantification (B) of overall CD45<sup>+</sup> immune cells (gated on live), regulatory CD4<sup>+</sup> T cells (CD45<sup>+</sup>CD4<sup>+</sup>FoxP3<sup>+</sup>), conventional CD4<sup>+</sup> T cells (CD45<sup>+</sup>CD4<sup>+</sup>FoxP3<sup>-</sup>) and CD8<sup>+</sup> T cells (CD45<sup>+</sup>CD8<sup>+</sup>). (C) Phenotype of TILs according to CD44 and CD62L expression status. Naïve (T<sub>naïve</sub>): CD44<sup>+</sup>CD62L<sup>+</sup>, effector/effector memory (T<sub>EM</sub>): CD44<sup>+</sup>CD62L<sup>-</sup>, central memory (T<sub>CM</sub>): CD44<sup>+</sup>CD62L<sup>+</sup>T. (D-E) Ratio of naïve versus effector CD4<sup>+</sup> (D) or CD8<sup>+</sup> (E) T cells on day 9 and 14 after tumor inoculation. Bar graphs shown as mean ± SEM (representative of 2 independent experiments, n=5 for day 9, n≥4 for day 14).



lymphangiogenic tumors. TILs infiltrating lymphangiogenic B16 melanomas were mostly of a naïve ( $CD62L^+CD44^-$ ) phenotype (Figure 3.3C), shifting the balance between naïve and effector

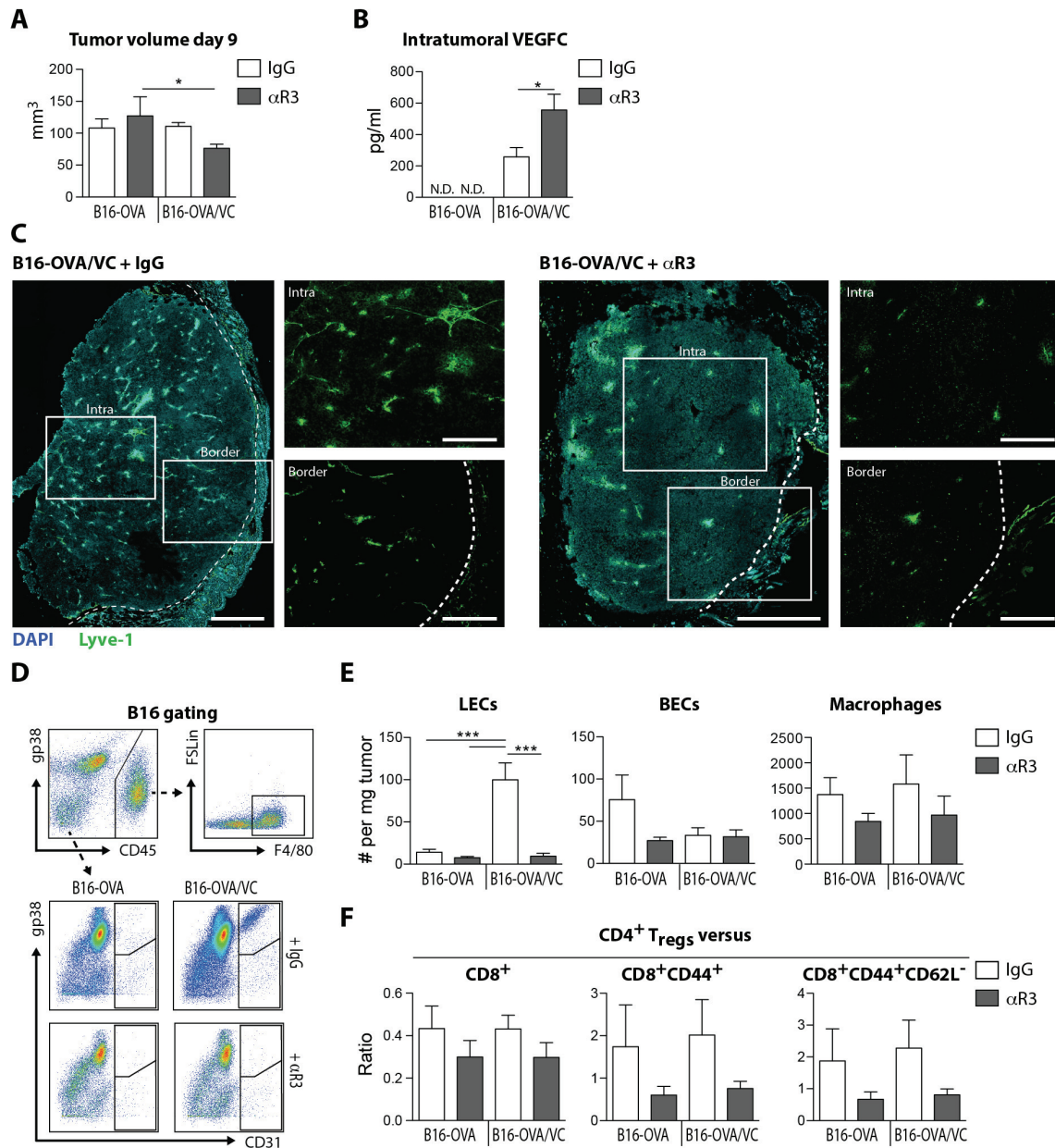


**Figure 3.4 (Supplementary Figure 3.3). VEGFR3 blocking specifically abrogates intratumoral lymphatic endothelial cells within VEGFC overexpressing B16 melanomas.** (A-F) B16-OVA and B16-OVA/VC tumor bearing mice treated with isotype (IgG) or anti-VEGFR3 ( $\alpha R3$ ) antibodies were euthanized nine days after inoculation. (A) Tumor size on day 9 (data pooled from  $\geq 2$  independent experiments,  $n \geq 10$ ). (B) Intratumoral VEGFC concentration as assessed by ELISA (normalized to 1mg/ml total protein,  $n=5$ ). (C) Representative immunofluorescence images of whole tumor sections (10X tiles, scale bar = 500 $\mu$ m and 200 $\mu$ m in zoom-in images) showing nuclei (DAPI, cyan) and LECs (Lyve-1, green). (D-F) Tumor single cell suspensions were analyzed by flow cytometry (representative of 2 independent experiments,  $n=5$ ). Representative flow cytometry plots (D) and quantification (E) of LECs ( $CD45^-gp38^+CD31^+$ ), BECs ( $CD45^-gp38^+CD31^+$ ), and macrophages ( $CD45^+F4/80^+$ ). (F) Ratio of regulatory  $CD4^+$  T cells versus effector T cells. Bar graphs shown as mean  $\pm$  SEM.

(CD62L<sup>+</sup>CD44<sup>+</sup>) T cells in favor of naïve ones (Figure 3.3D-E). This trend was even more pronounced when TILs were analyzed at a later stage of tumor development (day 14 after inoculation), suggesting that naïve immune cell infiltration might be proportional to tumor size and thus to the total amount of released VEGFC and CCL21. Taken together, these data demonstrate that apart from increased regulatory CD4<sup>+</sup> T cells, there is an accumulation of naïve TILs within lymphangiogenic tumors.

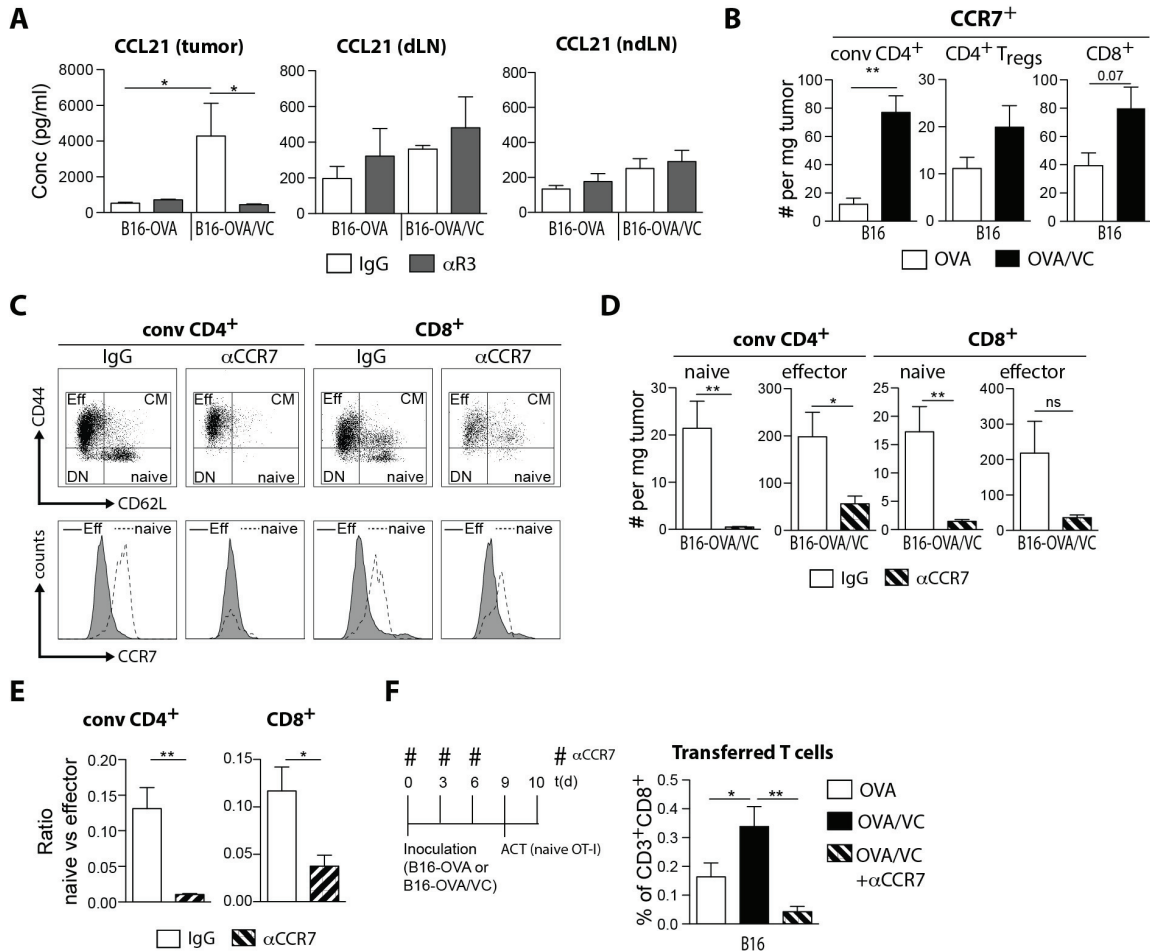


**Figure 3.5 CCL21 secretion is upregulated in lymphangiogenic B16 melanomas and CCR7 signaling is essential to increased naïve T cell tumor infiltration.** (A) B16-OVA and B16-OVA/VC tumor bearing mice treated with isotype (IgG) or anti-VEGFR3 ( $\alpha$ VR3) antibodies were euthanized nine days after inoculation, and tumor tissue as well as draining (dLN) and non-draining (ndLN) lymph nodes snap frozen for subsequent protein extraction. CCL21 concentration as assessed by ELISA in the tumor (normalized to 1mg/ml total protein), dLNs, and ndLNs (normalized to 0.025mg/ml total protein) (n=5). (B) B16-OVA and B16-OVA/VC tumor bearing mice were euthanized 14 days after inoculation, and tumor single cell suspensions analyzed by flow cytometry. Quantification of CCR7<sup>+</sup> conventional CD4<sup>+</sup>, regulatory CD4<sup>+</sup>, and CD8<sup>+</sup> T cells (n≥4). (C-E) B16-OVA and B16-OVA/VC tumor bearing mice treated with isotype (IgG) or anti-CCR7 ( $\alpha$ CCR7) antibodies were euthanized 9 days after inoculation, and tumor single cell suspensions analyzed by flow cytometry (n=6). (C) Representative flow cytometry plots of TIL naïve and effector phenotype based on CD62L and CD44 expression, and (D) quantification thereof. (E) Ratio of naïve versus effector T cells. (F) Control B16-OVA and control or anti-CCR7 ( $\alpha$ CCR7) treated B16-OVA/VC tumor bearing mice (CD45.1) received adoptive transfer of  $1 \times 10^6$  naïve CD45.2<sup>+</sup> OT-I T cells on day nine after inoculation and were euthanized 24h later. Tumor single cell suspensions were analyzed by flow cytometry and intratumoral OT-I (CD45<sup>+</sup>CD3<sup>+</sup>CD8<sup>+</sup>CD45.2<sup>+</sup>) cells plotted as percentage of overall CD8<sup>+</sup> T cells (n≥6). Bar graphs shown as mean  $\pm$  SEM.

### 3.4.3 CCL21 secretion is upregulated in lymphangiogenic B16 and iBIP2 melanomas.

Naïve, regulatory and central memory T cells as well as dendritic cells express the chemokine receptor CCR7 to home towards gradients of CCL21 chemokine. CCL21 is classically expressed by lymph node stromal cells to guide these immune cell subsets into the lymph node parenchyma, either from the blood stream (T cells) or from peripheral tissues (DCs) (Cyster, 1999; Förster et al., 2008). However, CCL21 has previously also been implicated in the regulation of anti tumor immunity (Peske et al., 2015; Shields et al., 2010). Because CCL21 can be expressed by lymphatic endothelial cells (Förster et al., 2008; Gunn et al., 1998; Kriehuber et al., 2001; Kuroshima et al., 2004; Shields et al., 2007), we asked whether changing the extent of tumor-associated lymphangiogenesis in B16 melanomas would lead to altered CCL21 levels. Indeed, CCL21 protein concentrations within tissue lysates of isotype treated B16-OVA/VC tumors were significantly increased as compared to isotype B16-OVA or anti-VEGFR3 treated B16-OVA/VC tumors (Figure 3.5A). This effect was restricted to the local tumor microenvironment as no change in CCL21 levels could be detected in the tumor draining (dLN) or non-draining (ndLN) lymph nodes. Accordingly, there were higher numbers of CCR7<sup>+</sup> conventional CD4<sup>+</sup> and CD8<sup>+</sup> T cells in B16-OVA/VC as compared to B16-OVA tumors (Figure 3.5B). To test whether CCL21/CCR7 signaling was indeed a mechanism underlying increased recruitment of naïve T cells into lymphangiogenic tumors, B16-OVA/VC tumor bearing mice were treated with CCR7 blocking antibodies (Figure 3.5C-E). As expected, naïve tumor infiltrating CD4<sup>+</sup> and CD8<sup>+</sup> T cells had higher surface levels of CCR7 as compared to effector ones (Figure 3.5C), and CCR7 blockade significantly decreased naïve T cell infiltration (CD4<sup>+</sup>: 40.7 fold, CD8<sup>+</sup>: 11.9 fold) while affecting effector T cell infiltration to a lesser extent (CD4<sup>+</sup>: 3.5 fold, CD8<sup>+</sup>: ns) (Figure 3.5D-E). To further strengthen the role of CCL21/CCR7 dependent recruitment of naïve T cells into lymphangiogenic tumors, we adoptively transferred allogeneic (CD45.2), naïve CD8<sup>+</sup> T cells into wildtype B16-OVA or B16-OVA/VC tumor bearing CD45.1 mice. 24h later, tumors were harvested and TILs analyzed by FACS. Consistent with the previous results, significantly higher numbers of transferred cells were detected in B16-OVA/VC as compared to B16-OVA or anti-CCR7 treated B16-OVA/VC tumors (Figure 3.5F), suggesting that CCL21/CCR7 signaling is indeed a mechanism of naïve T cell recruitment into lymphangiogenic tumors. To investigate the broader relevance of CCL21-mediated chemoattraction of immune cells into lymphangiogenic melanomas, we investigated the same parameters in the genetically engineered mouse model iBIP2 (inducible BRAF INK/ARK PTEN 2). We found that iBIP2 tumors are intrinsically lymphangiogenic, and that VEGFR3 blockade induced a 2.4 fold reduction in the overall lymphatic vessels coverage as compared to isotype treated mice (18.5 $\pm$ 6.3 versus 7.7 $\pm$ 3.4 LVs per mm<sup>2</sup>) (Figure 3.6A-B). While blocking VEGFR3 did not have any effect on primary iBIP2 tumor growth (Figure 3.6C), it did reduce the levels of intratumoral CCL21 (Figure 3.6D), similarly to our findings in VEGFR3 blocked B16-OVA/VC tumors. Flow cytometry analysis confirmed these findings, showing that anti-VEGFR3 treatment decreased the intratumoral LEC density, while BECs and CD11b<sup>+</sup> macrophages were not significantly affected (Figure 3.6E-F). We found that control iBIP2 tumors are highly infiltrated by CD45<sup>+</sup> immune cells (Figure 3.6E and 3.6G), and that VEGFR3 blockade decreased the infiltration of CD4<sup>+</sup>Foxp3<sup>+</sup> regulatory T cells (Figure 3.6G), and central memory but not naïve CD4<sup>+</sup> T cells (Figure 3.6H). As iBIP2 mice are on the FVB/n

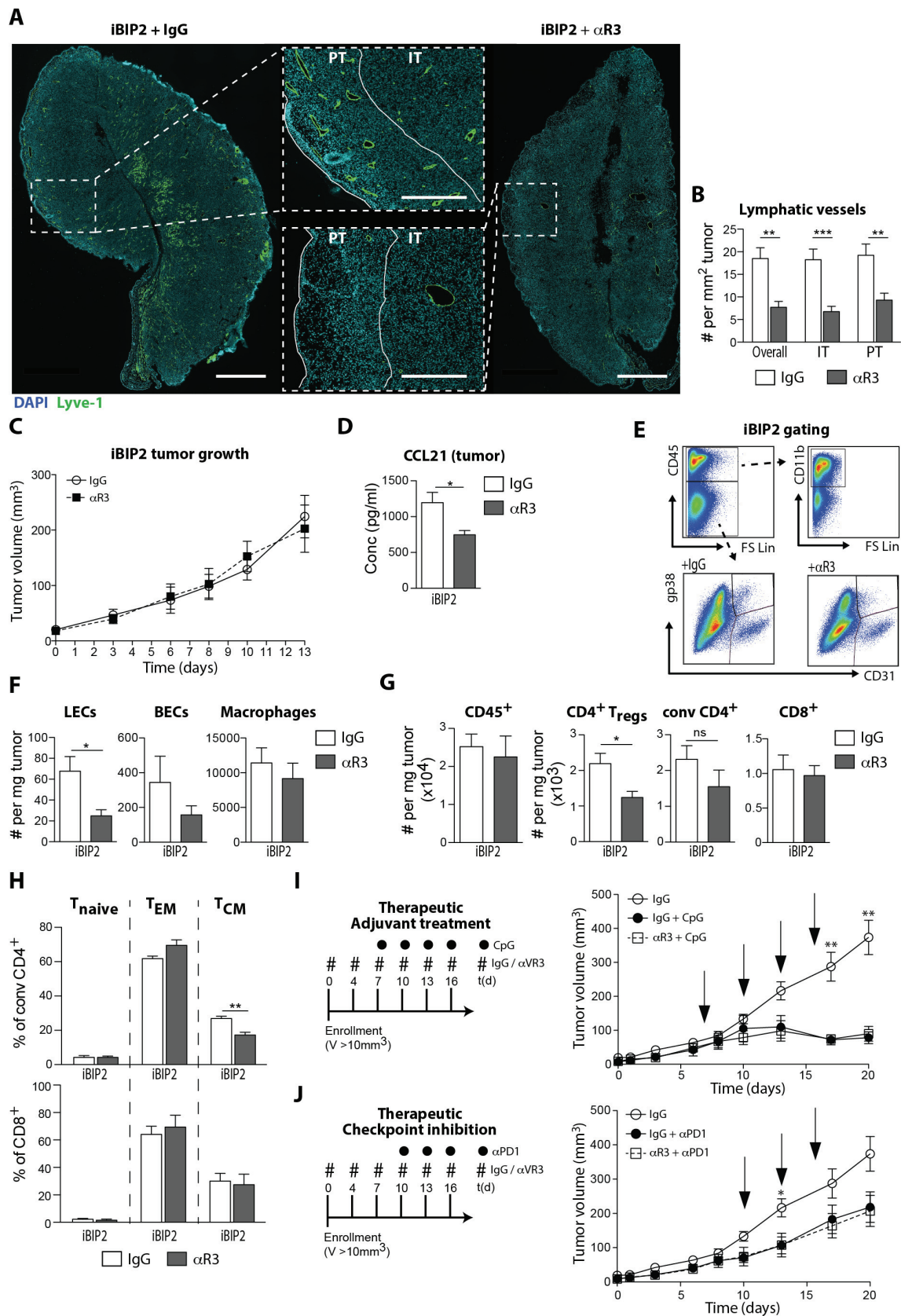


Figure 3.6 (Supplementary Figure 3.5). VEGFR3 blocking in the iBIP2 mouse model of melanoma decreased intratumoral CCL21 expression and infiltration of central memory CD4<sup>+</sup>



**T cells.** (A-H) Isotype (IgG) or anti-VEGFR3 ( $\alpha$ R3) antibody treated iBIP2 mice were euthanized 12-14 days after enrollment (enrollment criteria: tumor  $\geq 7\text{mm}^3$ ). (A) Representative immunofluorescence images of whole tumor sections (10X tiles, scale bar =  $500\mu\text{m}$  and  $200\mu\text{m}$  in zoom-in images) showing nuclei (DAPI, cyan) and LECs (Lyve-1, green). (B) Quantification of lymphatic vessel density based on peritumoral (PT) and intratumoral (IT) location ( $n=7$ ). (C) Tumor volume over time (mean  $\pm$  SEM, data pooled from  $\geq 2$  independent experiments,  $n\geq 17$ ). (D) Intratumoral CCL21 concentration as assessed by ELISA (normalized to  $1\text{mg/ml}$  total protein, data pooled from  $\geq 2$  independent experiments,  $n\geq 11$ ). (E-H) Tumor single cell suspensions were analyzed by flow cytometry ( $n=6$ ). (E) Representative flow cytometry plots, and (F) quantification of LECs ( $\text{CD45}^+\text{gp38}^+\text{CD31}^+$ ), BECs ( $\text{CD45}^+\text{gp38}^+\text{CD31}^+$ ) and macrophages ( $\text{CD45}^+\text{CD11b}^+$ ). (G) quantification of overall  $\text{CD45}^+$  immune cells (gated on live), conventional  $\text{CD4}^+$  ( $\text{CD45}^+\text{CD4}^+\text{FoxP3}^-$ ), regulatory  $\text{CD4}^+$  ( $\text{CD45}^+\text{CD4}^+\text{FoxP3}^+$ ), and  $\text{CD8}^+$  ( $\text{CD45}^+\text{CD8}^+$ ) T cells. (H) Phenotype of  $\text{CD4}^+$  ( $\text{CD45}^+\text{CD3}^+\text{CD8}^-$ ) and  $\text{CD8}^+$  ( $\text{CD45}^+\text{CD3}^+\text{CD8}^+$ ) TILs according to CD44 and CD62L expression status. Naïve ( $T_{\text{naïve}}$ ):  $\text{CD44}^-\text{CD62L}^+$ , effector/effector memory ( $T_{\text{EM}}$ ):  $\text{CD44}^+\text{CD62L}^+$ , central memory ( $T_{\text{CM}}$ ):  $\text{CD44}^+\text{CD62L}^+\text{T}$ . (I-J) Non antigen-specific immunotherapy in iBIP2 mice treated with isotype (IgG) or anti-VEGFR3 ( $\alpha$ R3) antibodies. (I) Mice received i.d. injections of CpG into all four footpads ( $40\mu\text{g}$  in total) every 3 days, starting on day 7. Shown is the tumor volume over time (mean  $\pm$  SEM, CpG groups:  $n \geq 4$ ). (J) Mice received i.p. injections of anti-PD1 ( $\alpha$ PD1) antibodies ( $250\mu\text{g}$  per injection) every 3 days, starting on day 10. Shown is the tumor volume over time (mean  $\pm$  SEM,  $\alpha$ PD1 groups: data pooled from 2 independent experiments,  $n \geq 11$ ). Bar graphs shown as mean  $\pm$  SEM.

background and do not express any common tumor antigens (data not shown), we were limited to non-antigen specific immunotherapy approaches. Both therapeutic adjuvant therapy using CpG oligonucleotides (Figure 3.6I) and checkpoint inhibition using anti-PD1 antibodies (Figures 3.6J) delayed iBIP2 tumor growth. However, similarly to non-antigen-specific approaches in the B16-OVA/VC model, the efficacy did not depend on the lymphangiogenic status of iBIP2 tumors. Collectively, these data demonstrate that tumor VEGFC/VEGFR3 signaling influences the quantity and quality of TILs both in B16 and iBIP2 melanomas, and that lymphangiogenic B16 melanomas are specifically infiltrated by naïve T cells in a CCR7 dependent manner.

#### **3.4.4 VEGFC expression correlates with CCL21 and CCR7 in human primary and metastatic melanoma.**

Because we demonstrated that lymphangiogenesis drives CCL21 dependent chemoattraction in two mouse models of melanoma, we next wanted to determine whether similar mechanisms might be relevant for disease progression in human melanoma. We first analyzed the expression of the lymphatic marker podoplanin in tissue sections of 14 primary human melanomas (Figure 3.7A). The lymphatic density was significantly higher in peritumoral areas and the invasive margin and compared to healthy skin in a subset of patients, confirming that human primary melanomas have lymphangiogenic potential (Figure 3.7B). Strikingly, the average overall density of lymphatic vessels within human primary melanoma ( $20.9\pm 8.3$  LVs per  $\text{mm}^2$ ) closely resembled the one of iBIP2 mouse melanoma ( $18.5\pm 6.3$  LVs per  $\text{mm}^2$ ). To investigate whether CCL21 could be driven by VEGFR3 signaling in human melanoma, we analyzed a dataset from The Cancer Genome Atlas (TCGA) containing expression data from skin cutaneous melanoma (SKCM) patients. In line with our findings in mice, expression of VEGFC correlated with CCL21 in human primary melanoma, while expression of the alternative VEGFR3 ligands VEGFA and VEGFD did not (Figure 3.7C). Interestingly, we observed the same trends in metastatic sites, suggesting that VEGFC driven CCL21 expression might also be relevant for metastatic disease. Furthermore, we co-stained sections of human primary

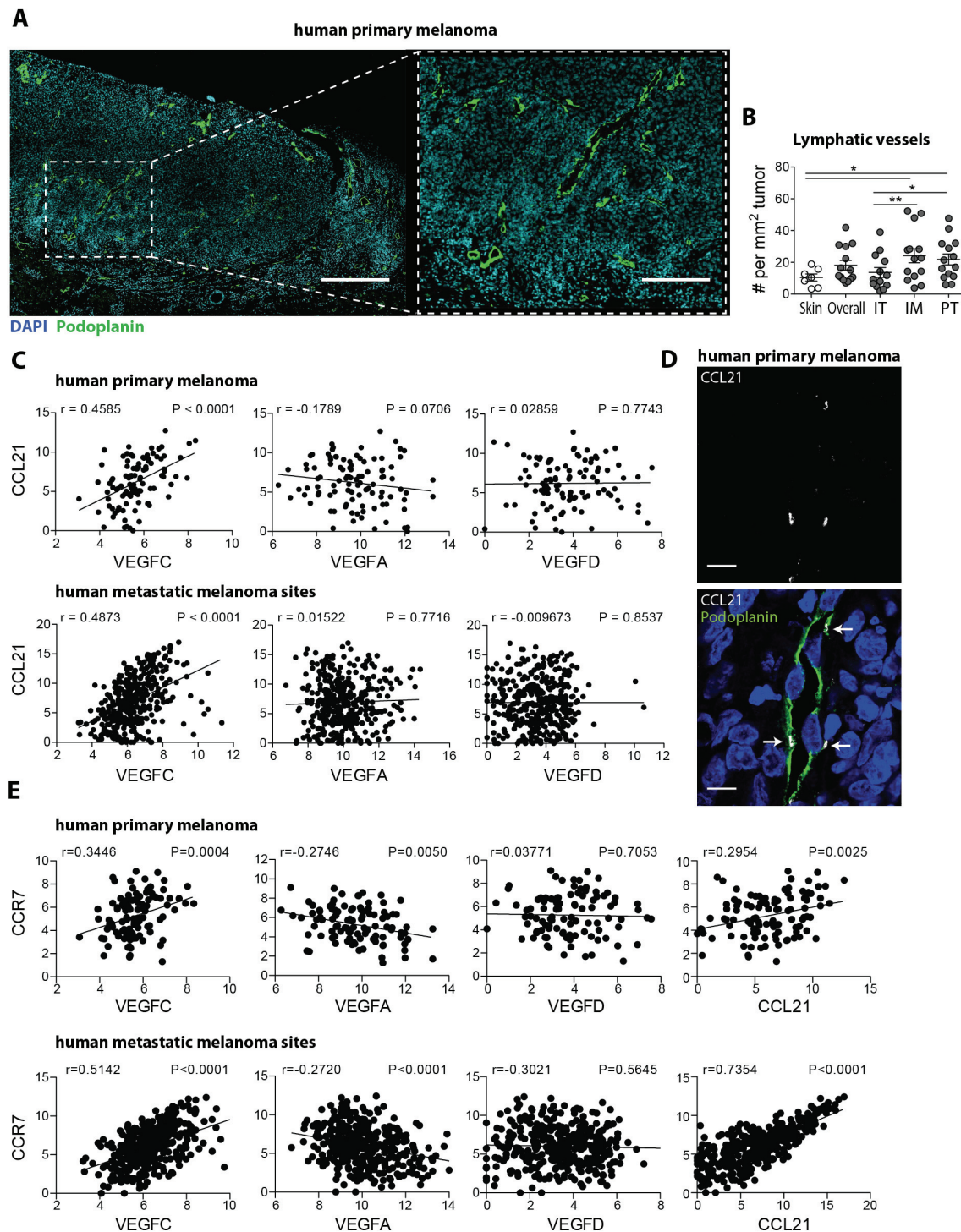


**Figure 3.7 VEGFC expression correlates with CCL21 and CCR7 in human primary and metastatic melanoma.** (A) Representative immunofluorescence images of whole tumor sections (10X tiles, scale bar = 500 $\mu$ m and 200 $\mu$ m in zoom-in images) showing nuclei (DAPI, cyan) and LECs (podoplanin, green). (B) Quantification of lymphatic vessel density based on peritumoral (PT), invasive margin (IV) and intratumoral (IT) location. Normal skin was analyzed on the same section if available. Scatter dot plots shown with mean  $\pm$  SEM (n=7 for normal skin, n=14 for tumors, \*p<0.05, \*\*p<0.01 with Student's t-test). (C) Gene expression data of human primary metastatic melanoma samples from the cancer genome atlas (TCGA) correlating VEGFA, VEGFC, and VEGFD with CCL21 expression. (D) Representative immunofluorescence image of an intratumoral lymphatic vessel

(podoplanin, green) expressing CCL21 (gray) in a section of human primary melanoma (63X, scale bar = 10µm). (E) Data from (C) was used to correlate VEGFA, VEGFC, and VEGFD with CCR7 expression. Dot plots shown with linear regression curve (n=103 for primary melanoma, n=369 for metastatic melanoma sites, correlation was tested using non-parametric Spearman's test).

melanoma with fluorescent antibodies specific for podoplanin and CCL21, and found that intratumoral lymphatic endothelial cells (LECs) can be a source of CCL21 in human melanoma (Figure 3.7D). Finally, expression of VEGFC, but not VEGFA or VEGFD positively correlated with CCR7 both in human primary melanoma as well as in metastatic sites (Figure 3.7E). Taken together, these data suggest that VEGFC driven upregulation of CCL21 and subsequent infiltration of CCR7<sup>+</sup> immune cells might be relevant for shaping the tumor microenvironment in human melanoma.

### 3.4.5 Lymphangiogenic potentiation of antigen-specific immunotherapy depends on intratumoral activation of naïve TILs.

It has been previously been shown that naïve T cells can be recruited and primed within primary tumors (Schrama et al., 2007; Thompson et al., 2010; Yu et al., 2004), and that adoptive transfer of naïve OT-I cells into B16-OVA tumors can delay primary tumor growth (Peske et al., 2015). We thus wanted to assess whether there was a mechanistic link between the increased susceptibility to

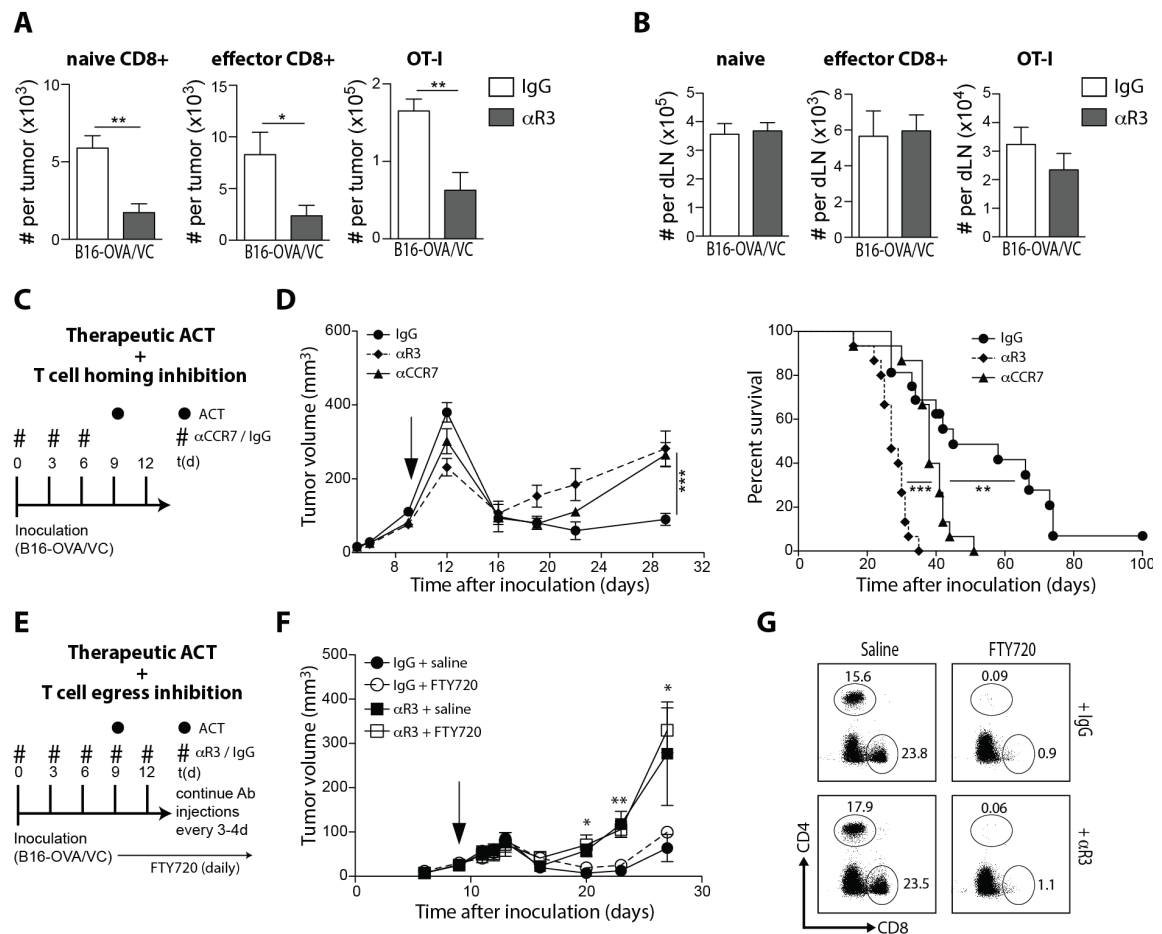


**Figure 3.8** Intratumoral activation of CCR7<sup>+</sup> immune cells following antigen-specific immunotherapy is responsible for increased efficacy in lymphangiogenic B16 melanomas.

(A-B) B16-OVA and B16-OVA/VC tumor-bearing mice treated with isotype (IgG) or anti-VEGFR3 ( $\alpha$ VR3) antibodies were euthanized three days after ACT, and tumor single cell suspensions analyzed by flow cytometry (n=5). (A-B) Quantification of overall OT-I ( $CD45^+CD8^+CD45.1^+$ ), naïve  $CD8^+$  ( $CD45^+CD8^+CD44^-CD62L^+$ ) and effector  $CD8^+$  ( $CD45^+CD8^+CD44^+CD62L^-$ ) T cells in the tumor (A) and draining lymph node (B). (C-D) Role of CCR7 dependent T cell homing prior to immunotherapy. (C) B16-OVA/VC tumor-bearing mice were treated with anti-CCR7 ( $\alpha$ CCR7) antibodies on day 0, 3, and 6 prior to receiving adoptive T cell transfer on day 9. (D) Tumor growth profiles and survival curve for isotype (IgG), anti-CCR7 ( $\alpha$ CCR7) or anti-VEGFR3 ( $\alpha$ VR3) treated B16-OVA/VC tumor-bearing mice ( $\alpha$ CCR7 group: data pooled from 2 independent experiments, n=15). (E-G) Role of lymphocyte egress from secondary lymphoid organs post immunotherapy. (E) B16-OVA/VC tumor-bearing mice treated with isotype (IgG) or anti-VEGFR3 ( $\alpha$ VR3) antibodies received injections of the small molecular S1P inhibitor FTY720 daily (1mg/kg i.p.), starting on the same day as ACT was performed (day 9) (n≥5). (F) Tumor growth profiles. (G) Representative flow cytometry plots of a  $CD4^+$  and  $CD8^+$  cell staining of blood taken on day 26. Cells were gated on  $CD45^+B220^-$ . Statistics represent differences between IgG and  $\alpha$ VR3 groups.

---

antigen-specific immunotherapy and the increased accumulation of naïve TILs within lymphangiogenic B16 tumors. We hypothesized that naïve  $CCR7^+$  cells within lymphangiogenic tumors might be locally activated following immunotherapy-induced release of tumor antigen and innate immune activation (“danger signals”). In line with this, we found that three days after ACT, lymphangiogenic tumors but not their draining lymph nodes contained significantly higher numbers of endogenous naïve and effector  $CD8^+$  T cells as well as OT-I cells (Figure 3.8A-B), suggesting that local activation and expansion of naïve T cells may potentiate both the endogenous and exogenous anti-tumor immune response. To test whether the efficacy of ACT in B16 melanoma indeed relied on VEGFC-induced recruitment of naïve immune cells, B16-OVA/VC tumor-bearing mice were treated with CCR7 blocking antibodies during tumor development prior to therapy (Figure 3.8C). We found that after the initial response to ACT, B16-OVA/VC tumors of CCR7 blocked mice progressed similar to B16-OVA tumors, both in terms of tumor growth and survival (Figure 3.8D). To exclude that increased T cell activation in and egress from secondary lymphoid organs (SLOs) was responsible for the enhanced sensitivity of lymphangiogenic tumors, we next performed ACT while blocking lymphocyte egress from SLOs using the small molecular inhibitor FTY720 (Figure 3.8E). Indeed, tumor growth in the progression phase after ACT was only dependent on VEGFR3 signaling, but independent of lymphocyte egress (Figure 3.8F). Accordingly, the blood of FTY720 treated mice was essentially devoid of lymphocytes (Figure 3.8G), further indicating that in this phase of disease progression, anti-tumor immunity did not rely on circulating lymphocytes but on intratumoral activation and expansion of TILs.

#### **3.4.6 Mice that rejected lymphangiogenic B16 melanomas after antigen-specific immunotherapy show antigen spreading and protection to re-challenge.**

Immunotherapy has previously shown to broaden the endogenous anti-tumor immune response to tumor epitopes that were previously not or not sufficiently visible, a process called antigen spreading (Corbière et al., 2011; GuhaThakurta et al., 2015; Kreiter et al., 2015). Because we found that naïve endogenous T cells are activated and expanded within lymphangiogenic B16 melanomas in response to antigen-specific immunotherapy, we hypothesized that spreading of the anti-tumor immune response to antigens other than ovalbumin could occur in these settings. To determine whether this



was the case, we performed a therapeutic vaccination protocol using OVA protein in combination with CpG adjuvant (Figure 3.9A). The vaccines were injected on days four, seven, and ten after inoculation intradermally into the hind footpads, deliberately avoiding the suppressive microenvironment present in the brachial tumor draining lymph nodes (Lund et al., 2012). We found that while B16-OVA and anti-VEGFR3 treated B16-OVA/VC tumors only showed a short-term response to vaccination, lymphangiogenic tumors underwent profound regression so that a majority of mice were tumor free 15 days after the last boost vaccination (Figure 3.9B). Intriguingly, we found that mice that rejected B16-OVA/VC tumors had increased numbers of overall effector CD4<sup>+</sup> and CD8<sup>+</sup> T cells as well as of SIINFEKL-specific CD8<sup>+</sup> T cells in blood as compared to mice that had progressing B16-OVA tumors

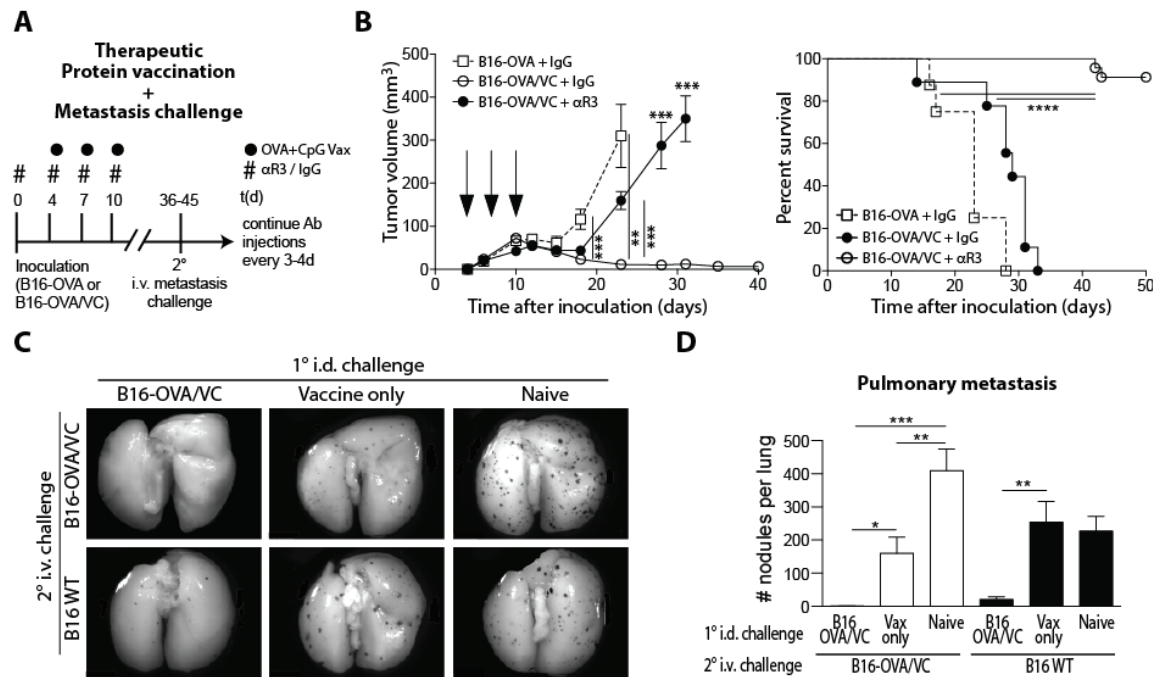


**Figure 3.9 Mice that rejected primary lymphangiogenic B16 tumors in response to antigen-specific immunotherapy show antigen spreading and protection to re-challenge in a model of lung metastasis.** (A-B) Antigen-specific protein vaccination in B16 tumor-bearing wildtype C57BL/6 mice. (A) Mice received CpG-B (50μg) + OVA (10μg) vaccinations i.d. into hind footpads on day four, seven and ten after tumor cell inoculation. (B) Tumor growth profiles and survival curves for isotype (IgG) treated B16-OVA and isotype (IgG) or anti-VEGFR3 (αVR3) treated B16-OVA/VC tumors. (C) Blood was drawn on day 23 after inoculation and lymphocytes analyzed by flow cytometry. Effector CD4<sup>+</sup> (CD45<sup>+</sup>B220<sup>-</sup>CD4<sup>+</sup>CD44<sup>+</sup>CD62L<sup>-</sup>), effector CD8<sup>+</sup> (CD45<sup>+</sup>B220<sup>-</sup>CD8<sup>+</sup>CD44<sup>+</sup>CD62L<sup>-</sup>), and SIINFEKL-specific CD8<sup>+</sup> (CD45<sup>+</sup>B220<sup>-</sup>CD8<sup>+</sup>SIINFEKL-pentamer<sup>+</sup>) T cells were quantified). (D-G) B16-OVA/VC tumor bearing mice that rejected the primary tumor following therapeutic vaccination were re-challenged with intravenous injections of 0.2x10<sup>6</sup> B16 WT or B16-OVA/VC cells (2° i.v. challenge) at least ten days after complete regression. Mice that either received no treatment (naïve) or vaccination only (Vax only) served as control for the first challenge (1° i.d. challenge). (D-E) Mice were euthanized 9 days after the 2° i.v. challenge and lung metastasis analyzed. (D) Representative images of lungs and (E) quantification of metastatic nodules per lung. (F-G) Flow cytometry analysis of circulating tumor antigen-specific CD8<sup>+</sup> T cell responses nine days after metastatic challenge. (F) Quantification of SIINFEKL-specific CD8<sup>+</sup> T cells (CD45<sup>+</sup>CD8<sup>+</sup>SIINFEKL-pentamer<sup>+</sup>) and (G) representative dot plots of Trp2 (CD45<sup>+</sup>B220<sup>-</sup>CD8<sup>+</sup>Trp2-pentamer<sup>+</sup>) and gp100 (CD45<sup>+</sup>B220<sup>-</sup>CD8<sup>+</sup>gp100-pentamer<sup>+</sup>) specific T cell responses. Bar graphs shown as mean ± SEM (data pooled from 2 independent experiments, n≥5).

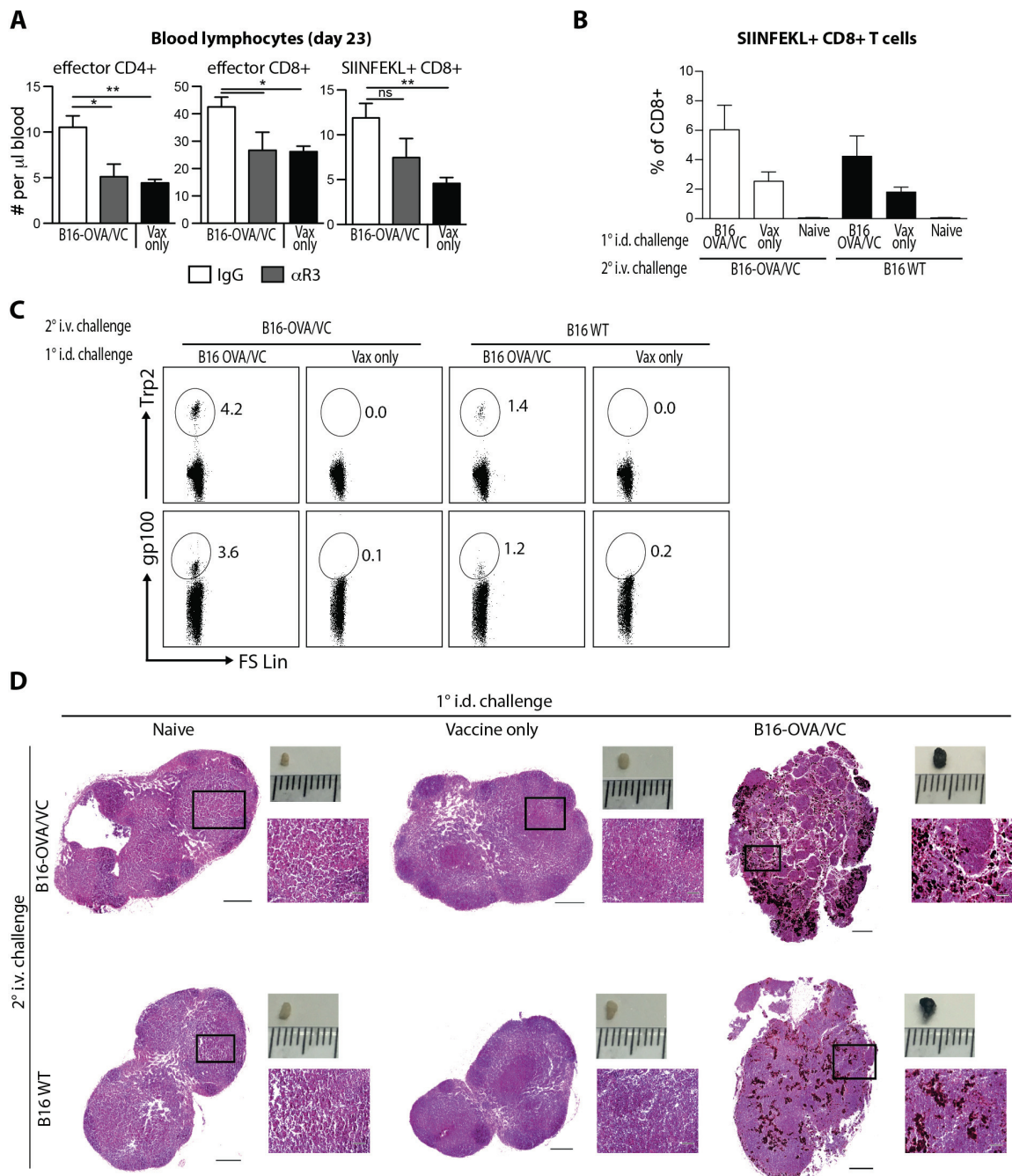


**Figure 3.10 (Supplementary Figure 3.9). Antigen-specific immunotherapy in B16-OVA/VC tumor bearing mice induces high levels of circulating SIINFEKL<sup>+</sup> and rare populations of gp100<sup>+</sup> and Trp2<sup>+</sup> CD8<sup>+</sup> T cells.** Experiment from Figure 3.9. (A) Blood was drawn 23 days after inoculation and effector CD4<sup>+</sup> (CD45<sup>+</sup>B220<sup>-</sup>CD4<sup>+</sup>CD44<sup>+</sup>CD62L<sup>-</sup>), effector CD8<sup>+</sup> (CD45<sup>+</sup>B220<sup>-</sup>CD8<sup>+</sup>CD44<sup>+</sup>CD62L<sup>-</sup>), and SIINFEKL-specific CD8<sup>+</sup> (CD45<sup>+</sup>B220<sup>-</sup>CD8<sup>+</sup>SIINFEKL-pentamer<sup>+</sup>) T cells quantified by flow cytometry. (B-C) Flow cytometry analysis of circulating tumor-specific CD8<sup>+</sup> T cell responses 9 days after metastatic challenge. (B) Quantification of SIINFEKL-specific (CD45<sup>+</sup>CD8<sup>+</sup>SIINFEKL-pentamer<sup>+</sup>) and (C) representative dot plots of rare Trp2 (CD45<sup>+</sup>B220<sup>-</sup>CD8<sup>+</sup>Trp2-pentamer<sup>+</sup>) and gp100 (CD45<sup>+</sup>B220<sup>-</sup>CD8<sup>+</sup>gp100-pentamer<sup>+</sup>) specific responses. Bar graphs shown as mean  $\pm$  SEM (data pooled from 2 independent experiments,  $n \geq 5$ ). (D) Representative H&E stainings of tumor draining lymph node sections (10X tiles, scale bar = 500 $\mu$ m and 200 $\mu$ m in zoom-in images).

(Figure 3.10A). To assess whether the increased numbers of effector T cells were the result of antigen spreading within the tumor microenvironment, we re-challenged mice that were tumor free for at least ten days with experimental pulmonary metastasis (2° i.v. challenge). To evaluate whether anti-tumor responses did spread to other antigens apart from OVA, one group of survivor mice was challenge with B16-OVA cells, while another group was challenged with B16 wildtype (WT) cells that only express endogenous tumor antigens. Strikingly, while control mice that only received OVA + CpG vaccinations were only partially protected against B16-OVA but not B16 wildtype metastasis, mice that previously rejected B16-OVA/VC tumors were completely protected against both B16-OVA and B16 wildtype metastasis (Figure 3.9C-D). The resistance to pulmonary metastasis was accompanied by increased levels of circulating SIINFEKL-specific CD8<sup>+</sup> T cells (Figure 3.10B), but also by the presence of novel CD8<sup>+</sup> T cell specificities against the endogenous B16 antigens Trp2 and gp100 in a subset of mice (Figure 3.10C). Mice that rejected both lymphangiogenic B16 melanomas as well as pulmonary metastasis challenge had black tumor draining lymph nodes, indicating enhanced drainage of melanin and/or B16 tumor cells from lymphangiogenic tumors (Figure 3.10D). However, nuclear stainings did not localize into these areas, suggesting that it was accumulation of melanin rather than live metastatic B16 cells. Taken together, these data suggest that antigen-specific immunotherapy of lymphangiogenic B16 tumors induces secondary immune responses against a variety of endogenous tumor antigens, conferring long-term memory and protection against pulmonary metastasis re-challenge.

### 3.5 Discussion

Even though tumor-associated lymphangiogenesis generally correlates with poor prognosis in melanoma patients, we here introduce an unexpected role of lymphangiogenesis in enhancing systemic antigen-specific immunotherapy. In contrast to our original hypothesis, lymphangiogenic B16-OVA/VC tumors are more sensitive to systemic antigen-specific immunotherapy as compared to non-lymphangiogenic ones (Figure 3.1, Figure 3.9A-B). We demonstrate that this lymphangiogenic potentiation of immunotherapy depends on CCL21-mediated recruitment of CCR7<sup>+</sup> immune cells into primary melanoma tumors (Figure 3.5, Figure 3.8C-D). Our results suggest that the naïve fraction of these cells can be locally activated by immunotherapy-induced release of antigens and danger signals, leading to a diversification of the endogenous anti-tumor response and long lasting immune memory against tumor re-challenge (Figure 3.9, Figure 3.10). Considering that immunotherapy has been revolutionizing the treatment of metastatic melanoma, our findings attribute a completely novel role to tumor-associated lymphangiogenesis that could potentially be therapeutically exploited.

Pre-existing immune infiltration within the tumor microenvironment is associated with clinical response to immunotherapies (Ji et al., 2011; Spranger et al., 2015; Tumei et al., 2014). Interestingly, T cell-inflamed tumor microenvironments usually express hallmarks of immunosuppression (Gajewski, 2015; Munn and Bronte, 2016). In response to sensing effector cytokines such as interferon- $\gamma$ , the tumor microenvironment upregulates immunosuppressive molecules such as IDO, PD-L1 and increases the influx of T<sub>reg</sub> cells, a process called adaptive resistance (Spranger et al., 2013). Thus, tumor microenvironments with pre-existing T cell infiltrates are more permissive to immunotherapy than non-T cell-inflamed ones, even if the former presents hallmarks of immunosuppression (Gajewski, 2015; Spranger et al., 2015). We have previously shown that primary lymphangiogenic B16-OVA/VC tumors contain high number of regulatory T cells, and that they establish an immunosuppressive microenvironment in the draining lymph node (Lund et al., 2012). Here, we found that in addition, they also contain high densities of naïve CD4<sup>+</sup> and CD8<sup>+</sup> T cells (Figure 3.3), a subset of immune cells that is not classically considered of directly contributing to anti-tumor immunity (Gajewski et al., 2013). However, naïve T cells in the tumor might indirectly alter the immune-microenvironment. For example, one might speculate that naïve T cells affect immune cell subsets by competing for (1) local nutrients (Chang et al., 2015; Delgoffe and Powell, 2015; Ho et al., 2015) or (2) homeostatic cytokines such as IL-7 (Schmaler et al., 2015). Moreover, it is known that naïve T cells can also be activated directly within primary tumors (Schrama et al., 2007; Thompson et al., 2010; Yu et al., 2004). Activation of naïve T cells in the LN depends on three signals: TCR engagement with cognate antigen presented by MHC molecules, costimulation, and stimulatory cytokines, provided by DCs upon innate immune stimulation (Sckisel et al., 2015). This led us to the hypothesis that release of antigen combined with innate immune stimulation following immunotherapy-induced tumor cell death might provide all three signals needed for naïve T cell activation within the primary tumor itself.

Because cancer immunotherapy seems to be most efficient when targeting neoantigens (Schumacher and Schreiber, 2015; Snyder et al., 2014; Van Allen et al., 2015), we mainly used immunotherapy approaches that target the model antigen ovalbumin, to which there is no central

tolerance similar as to neoantigens. In addition, by delivering immunotherapies systemically rather than to the tumor draining lymph nodes, we deliberately avoided the immunosuppressive microenvironment that is specifically present within these organs (Lund et al., 2012). Strikingly, lymphangiogenic B16-OVA/VC tumors were much more sensitive to ovalbumin-specific immunotherapy including ACT, dendritic cell and protein vaccination as compared to non-lymphangiogenic control tumors (Figure 3.1A-B, Figure 3.9A-B). The beneficial outcome was at least partially dependent on naïve T cell homing into the tumor prior to therapy, as CCR7 blocking prior to ACT almost completely reversed this effect (Figure 3.8C-D). In contrast, lymphangiogenic tumors did not show an increased benefit to non-antigen specific immunotherapy such as checkpoint inhibition (Figure 3.1E-F, 3.6I-J). In our models, these treatments induce tumor control rather than tumor cell death, thus supporting our hypothesis that release of antigen and danger signal is necessary to activate tumor resident naïve T cells. In line with this, we found that lymphangiogenic potentiation was independent from the ability to recruit lymphocytes from secondary lymphoid organs (Figure 3.8E-G). It has previously been shown that antigen-specific immunotherapy induces antigen spreading, thereby initiating secondary humoral and cellular tumor-specific immune responses that enhance therapy outcome (Corbière et al., 2011; GuhaThakurta et al., 2015; Kreiter et al., 2015). Our data add a novel mechanism by which immunotherapy-induced cell death leads to antigen spreading. Specifically, we found that antigen-specific immunotherapy induces secondary immune responses via the activation of tumor resident naïve CD4<sup>+</sup> and CD8<sup>+</sup> T cells, which conferred long-term memory and protection against tumor re-challenge with wildtype B16 tumor cells in a model of lung metastasis (Figure 3.9C-D, Figure 3.10).

Our data suggest that intra- and peritumoral lymphatics can actively influence primary tumor inflammation by secreting CCL21. The lymphocyte homing chemokine CCL21 is best known for its function within the lymph node where it attracts CCR7<sup>+</sup> cells including activated, antigen-loaded dendritic cells from the periphery as well as naïve T cells from circulating blood (Cyster, 1999; Förster et al., 2008). This allows these two cells types to co-localize within the T cell zone of lymph nodes, allowing TCR/MHC-peptide interactions necessary to raise immune responses (Andrian and Mempel, 2003). Interestingly, similar functions have been attributed to CCL21 within primary tumors. Intratumoral injection of exogenous CCL21 leads to increased recruitment of T cells and DCs into the primary tumor, resulting in better tumor control (Sharma et al., 2000; 2001). Our lab has previously published that endogenous expression of CCL21 by B16F10 melanoma cells leads to the development of an immunosuppressive lymph-node like tumor stroma characterized by the presence of high-endothelial venules (HEVs) and CCR7<sup>+</sup> immune cells such as T<sub>reg</sub> cells (Shields et al., 2010). Similarly, production of CCL21 by intratumoral blood endothelial cells and fibroblasts leads to naïve CCR7<sup>+</sup> T cell infiltration into non-lymphangiogenic tumors (Peske et al., 2015). While these studies have established CCL21 as a major factor for immune cell homing into primary tumors, it has been elusive what the endogenous source of this chemokine is within lymphangiogenic melanoma. Since CCL21 can be expressed by LECs (Förster et al., 2008; Gunn et al., 1998; Kuroshima et al., 2004; Shields et al., 2007), we wondered whether they contribute to CCL21 in the tumor microenvironment. Indeed, we observed that CCL21 expression within lymphangiogenic mouse melanomas depends on



VEGFR3 signaling (Figure 3.5A, 3.6B), and that VEGFC expression correlates with CCL21 expression within primary human melanomas (Figure 3.7C). However, extravasation of immune cells into the tumor depends not only on chemokine gradients but also on the phenotype of the tumor vasculature including the presence of adhesion molecules (Lanitis et al., 2015; Motz et al., 2014). This might explain why VEGFR3 signaling differentially affects tumor immune cell infiltration in iBIP2 and B16-OVA/VC melanomas (Figure 3.3, 3.63).

We found an unexpected discrepancy between the short-term and the long-term responses to antigen-specific immunotherapy in B16-OVA/VC tumors. While in the short-term, lymphangiogenic tumors grew significantly larger than anti-VEGFR3 blocked ones, they had the most durable responses in the long-term, many of which regressed completely. This was especially striking after adoptive T cell transfer (Figure 3.1A) and DC vaccination (Figure 3.1B). Interestingly, increased tumor growth before regression can be indicative of effective immunotherapy in clinics, indicating that effector immune cells might be infiltrating into and expanding within tumor lesions (Hoos et al., 2010). Our findings that more endogenous T cells and transferred OT-I cells infiltrated into lymphangiogenic tumors 3 days after ACT (Figure 3.8A) are in line with these observations. In the clinic, the immune-related response criteria (irRC) was developed to better predict patient outcome by taking into account the distinct tumor growth patterns specific to immunotherapy (Wolchok et al., 2009). However, in pre-clinical studies, researchers are often limited to the evaluation of short-term responses, mainly because the treatment window of many tumor models is only a few days to weeks before the animals need to be euthanized. Because adaptive immune responses take five to seven days to impact the host, and because tumor immune infiltration might initially lead to an increase instead of decrease in tumor growth, it is questionable whether short-term tumor growth is indeed a valid endpoint to measure the efficacy of immunotherapies in mice. Phenotypical and functional analysis of TILs might be more indicative of the quality of response to immunotherapy in such short trials.

Our study has limitations. First of all, even though VEGFC may be one of the major growth factor for lymphangiogenic signaling, it is not the only one. Other factors include VEGFA and VEGFD (Zheng et al., 2014), fibroblast growth factor (FGF) (Cao et al., 2004b), angiopoietins (Ang1/2) (Thurston, 2003), platelet-derived growth factors (PDGF) (Cao et al., 2004a), hepatocyte growth factor (HGF) (Kajiya et al., 2005), and insulin-growth factors (IGF1/2) (Björndahl et al., 2005). This might explain some of the differences between the B16 and iBIP2 model. While lymphangiogenesis in the B16-OVA/VC model is mainly VEGFC driven, it is most likely a combination of different factors in the iBIP2 model, offering an explanation why VEGFR3 blockade only led to a partial abrogation of intratumoral LECs (Figure 3.6F). Approaches that target multiple lymphangiogenic pathways should have a more profound effect on lymphatic density within primary iBIP2 tumors. Secondly, we did not assess gene expression of lymphangiogenic versus non-lymphangiogenic tumors in an unbiased manner. Even though we did an unbiased protein analysis of some of the most prominent chemokines and cytokines that would likely be involved in immune regulation, there is a multitude of other candidates that might be differentially expressed. Performing RNA sequencing experiments might offer a broader and more unbiased view in the future. Nevertheless, having shown that CCR7

blockade completely or at least partially inhibited the observed phenomena indicates that the CCL21/CCR7 axis is indeed one of the major drivers thereof. Thirdly, LECs might not be the only source of CCL21 as other cells including gp38<sup>+</sup> fibroblasts and CD31<sup>+</sup> endothelial cells have shown to express this chemokine within tumors (Peske et al., 2015). However, in both of our lymphangiogenic melanoma models, CCL21 expression decreased to a similar extent as VEGFR3 blocking decreased LEC density, suggesting that the main producer of CCL21 within this type of tumors might indeed be the lymphatic endothelium. It remains to be determined whether LECs are the main source of CCL21 within primary human lymphangiogenic melanoma, but our finding that VEGFC expression correlates with CCL21 (Figure 3.7C), and that LECs can express CCL21 (Figure 3.7D) establishes a strong link between the two.

We conclude that secretion of CCL21 is a novel mechanism by which tumor associated lymphatics actively increase naïve immune cell infiltration. Activation of naïve T cells can be induced by immunogenic cell death following antigen-specific immunotherapy, resulting in a broad and long lasting anti-tumor immune response. Considering our pre-clinical results, the immune microenvironment specific to lymphangiogenic melanoma might represent a window of opportunity to jumpstarting an immunosuppressed Cancer-Immunity Cycle in clinics (Chen and Mellman, 2013). We therefore propose lymphangiogenesis to be a biomarker to stratify patients eligible for antigen-specific immunotherapy and speculate that engineering lymphangiogenesis within primary melanoma might improve response rates of patients with non-T cell-inflamed primary melanomas.



### 3.6 References

- Alexandrov, L.B., Nik-Zainal, S., Wedge, D.C., Aparicio, S.A.J.R., Behjati, S., Biankin, A.V., Bignell, G.R., Bolli, N., Borg, A., Børresen-Dale, A.-L., Boyault, S., Burkhardt, B., Butler, A.P., Caldas, C., Davies, H.R., Desmedt, C., Eils, R., Eyfjörd, J.E., Foekens, J.A., Greaves, M., Hosoda, F., Hutter, B., Ilcic, T., Imbeaud, S., Imielinski, M., Jäger, N., Jones, D.T.W., Jones, D., Knappskog, S., Kool, M., Lakhani, S.R., López-Otín, C., Martin, S., Munshi, N.C., Nakamura, H., Northcott, P.A., Pajic, M., Papaemmanuil, E., Paradiso, A., Pearson, J.V., Puente, X.S., Raine, K., Ramakrishna, M., Richardson, A.L., Richter, J., Rosenstiel, P., Schlesner, M., Schumacher, T.N., Span, P.N., Teague, J.W., Totoki, Y., Tutt, A.N.J., Valdés-Mas, R., van Buuren, M.M., van t Veer, L., Vincent-Salomon, A., Waddell, N., Yates, L.R., Zucman-Rossi, J., Andrew Futreal, P., McDermott, U., Lichter, P., Meyerson, M., Grimmond, S.M., Siebert, R., Campo, E., Shibata, T., Pfister, S.M., Campbell, P.J., Stratton, M.R., 2013. Signatures of mutational processes in human cancer. *Nature* 500, 415–421. doi:10.1038/nature12477
- Andrian, von, U.H., Mempel, T.R., 2003. Homing and cellular traffic in lymph nodes. *Nat. Rev. Immunol.* 3, 867–878. doi:10.1038/nri1222
- Björndahl, M., Cao, R., Nissen, L.J., Clasper, S., Johnson, L.A., Xue, Y., Zhou, Z., Jackson, D., Hansen, A.J., Cao, Y., 2005. Insulin-like growth factors 1 and 2 induce lymphangiogenesis in vivo. *Proc. Natl. Acad. Sci. U.S.A.* 102, 15593–15598. doi:10.1073/pnas.0507865102
- Broggi, M.A.S., Schmalzer, M., Lagarde, N., Rossi, S.W., 2014. Isolation of Murine Lymph Node Stromal Cells. *JoVE* 1–6. doi:10.3791/51803
- Cao, R., Björndahl, M.A., Religa, P., Clasper, S., Garvin, S., Galter, D., Meister, B., Ikomi, F., Tritsarlis, K., Dissing, S., Ohhashi, T., Jackson, D.G., Cao, Y., 2004a. PDGF-BB induces intratumoral lymphangiogenesis and promotes lymphatic metastasis. *Cancer Cell* 6, 333–345. doi:10.1016/j.ccr.2004.08.034
- Cao, R., Eriksson, A., Kubo, H., Alitalo, K., Cao, Y., Thyberg, J., 2004b. Comparative evaluation of FGF-2-, VEGF-A-, and VEGF-C-induced angiogenesis, lymphangiogenesis, vascular fenestrations, and permeability. *Circ. Res.* 94, 664–670. doi:10.1161/01.RES.0000118600.91698.BB
- Card, C.M., Yu, S.S., Swartz, M.A., 2014. Emerging roles of lymphatic endothelium in regulating adaptive immunity. *J. Clin. Invest.* 124, 943–952. doi:10.1172/JCI73316
- Chang, C.-H., Qiu, J., O'Sullivan, D., Buck, M.D., Noguchi, T., Curtis, J.D., Chen, Q., Gindin, M., Gubin, M.M., van der Windt, G.J.W., Tonc, E., Schreiber, R.D., Pearce, E.J., Pearce, E.L., 2015. Metabolic Competition in the Tumor Microenvironment Is a Driver of Cancer Progression. *Cell* 162, 1229–1241. doi:10.1016/j.cell.2015.08.016
- Chen, D.S., Mellman, I., 2013. Oncology Meets Immunology: The Cancer-Immunity Cycle. *Immunity* 39, 1–10. doi:10.1016/j.immuni.2013.07.012

- Corbière, V., Chapiro, J., Stroobant, V., Ma, W., Lurquin, C., Lethé, B., van Baren, N., Van den Eynde, B.J., Boon, T., Coulie, P.G., 2011. Antigen spreading contributes to MAGE vaccination-induced regression of melanoma metastases. *Cancer Res.* 71, 1253–1262. doi:10.1158/0008-5472.CAN-10-2693
- Cyster, J.G., 1999. Chemokines and the homing of dendritic cells to the T cell areas of lymphoid organs. *J. Exp. Med.* 189, 447–450.
- Dadras, S.S., Paul, T., Bertoncini, J., Brown, L.F., Muzikansky, A., Jackson, D.G., Ellwanger, U., Garbe, C., Mihm, M.C., Detmar, M., 2010. Tumor Lymphangiogenesis. *The American Journal of Pathology* 162, 1951–1960. doi:10.1016/S0002-9440(10)64328-3
- Delgoffe, G.M., Powell, J.D., 2015. Sugar, fat, and protein: new insights into what T cells crave. *Curr. Opin. Immunol.* 33, 49–54. doi:10.1016/j.coi.2015.01.015
- Eroglu, Z., Ribas, A., 2016. Combination therapy with BRAF and MEK inhibitors for melanoma: latest evidence and place in therapy. *Ther Adv Med Oncol* 8, 48–56. doi:10.1177/1758834015616934
- Förster, R., Davalos-Misilitz, A.C., Rot, A., 2008. CCR7 and its ligands: balancing immunity and tolerance. *Nat. Rev. Immunol.* 8, 362–371. doi:10.1038/nri2297
- Gajewski, T.F., 2015. The Next Hurdle in Cancer Immunotherapy: Overcoming the Non-T-Cell-Inflamed Tumor Microenvironment. *Seminars in Oncology* 42, 663–671. doi:10.1053/j.seminoncol.2015.05.011
- Gajewski, T.F., Schreiber, H., Fu, Y.-X., 2013. Innate and adaptive immune cells in the tumor microenvironment. *Nat Immunol* 14, 1014–1022. doi:10.1038/ni.2703
- GuhaThakurta, D., Sheikh, N.A., Fan, L.-Q., Kandadi, H., Meagher, T.C., Hall, S.J., Kantoff, P.W., Higano, C.S., Small, E.J., Gardner, T.A., Bailey, K., Vu, T., DeVries, T., Whitmore, J.B., Frohlich, M.W., Trager, J.B., Drake, C.G., 2015. Humoral Immune Response against Nontargeted Tumor Antigens after Treatment with Sipuleucel-T and Its Association with Improved Clinical Outcome. *Clinical Cancer Research* 21, 3619–3630. doi:10.1158/1078-0432.CCR-14-2334
- Gunn, M.D., Tangemann, K., Tam, C., Cyster, J.G., Rosen, S.D., Williams, L.T., 1998. A chemokine expressed in lymphoid high endothelial venules promotes the adhesion and chemotaxis of naive T lymphocytes. *Proc. Natl. Acad. Sci. U.S.A.* 95, 258–263.
- Hinrichs, C.S., Rosenberg, S.A., 2014. Exploiting the curative potential of adoptive T-cell therapy for cancer. *Immunol. Rev.* 257, 56–71. doi:10.1111/imr.12132
- Ho, P.-C., Bihuniak, J.D., Macintyre, A.N., Staron, M., Liu, X., Amezcua, R., Tsui, Y.-C., Cui, G., Micevic, G., Perales, J.C., Kleinstein, S.H., Abel, E.D., Insogna, K.L., Feske, S., Locasale, J.W., Bosenberg, M.W., Rathmell, J.C., Kaech, S.M., 2015. Phosphoenolpyruvate Is a Metabolic Checkpoint of Anti-tumor T Cell Responses. *Cell* 162, 1217–1228. doi:10.1016/j.cell.2015.08.012
- Hoos, A., Eggermont, A.M.M., Janetzki, S., Hodi, F.S., Ibrahim, R., Anderson, A., Humphrey, R., Blumenstein, B., Old, L., Wolchok, J., 2010. Improved endpoints for cancer immunotherapy trials. *JNCI Journal of the National Cancer Institute* 102, 1388–1397. doi:10.1093/jnci/djq310

- Ji, R.-R., Chasalow, S.D., Wang, L., Hamid, O., Schmidt, H., Cogswell, J., Alaparthi, S., Berman, D., Jure-Kunkel, M., Siemers, N.O., Jackson, J.R., Shahabi, V., 2011. An immune-active tumor microenvironment favors clinical response to ipilimumab. *Cancer Immunol Immunother* 61, 1019–1031. doi:10.1007/s00262-011-1172-6
- Kajiya, K., Hirakawa, S., Ma, B., Drinnenberg, I., Detmar, M., 2005. Hepatocyte growth factor promotes lymphatic vessel formation and function. *EMBO J.* 24, 2885–2895. doi:10.1038/sj.emboj.7600763
- Karaman, S., Detmar, M., 2014. Mechanisms of lymphatic metastasis. *J. Clin. Invest.* 124, 922–928. doi:10.1172/JCI71606
- Karpanen, T., 2006. Functional interaction of VEGF-C and VEGF-D with neuropilin receptors. *The FASEB Journal* 20, 1462–1472. doi:10.1096/fj.05-5646com
- Kilarski, W.W., Petersson, L., Fuchs, P.F., Zielinski, M.S., Gerwins, P., 2012. An in vivo neovascularization assay for screening regulators of angiogenesis and assessing their effects on pre-existing vessels. *Angiogenesis* 15, 1–13. doi:10.1007/s10456-012-9287-8
- Kreiter, S., Vormehr, M., van de Roemer, N., Diken, M., Löwer, M., Diekmann, J., Boegel, S., Schrörs, B., Vascotto, F., Castle, J.C., Tadmor, A.D., Schoenberger, S.P., Huber, C., Türeci, Ö., Sahin, U., 2015. Mutant MHC class II epitopes drive therapeutic immune responses to cancer. *Nature* 520, 692–696. doi:10.1038/nature14426
- Kriehuber, E., Breiteneder-Geleff, S., Groeger, M., Soleiman, A., Schoppmann, S.F., Stingl, G., Kerjaschki, D., Maurer, D., 2001. Isolation and characterization of dermal lymphatic and blood endothelial cells reveal stable and functionally specialized cell lineages. *J. Exp. Med.* 194, 797–808.
- Kuroshima, S.-I., Sawa, Y., Yamaoka, Y., Notani, K., Yoshida, S., Inoue, N., 2004. Expression of cys–cys chemokine ligand 21 on human gingival lymphatic vessels. *Tissue and Cell* 36, 121–127. doi:10.1016/j.tice.2003.10.004
- Kwong, L.N., Boland, G.M., Frederick, D.T., Helms, T.L., Akid, A.T., Miller, J.P., Jiang, S., Cooper, Z.A., Song, X., Seth, S., Kamara, J., Protopopov, A., Mills, G.B., Flaherty, K.T., Wargo, J.A., Chin, L., 2015. Co-clinical assessment identifies patterns of BRAF inhibitor resistance in melanoma. *J. Clin. Invest.* 125, 1459–1470. doi:10.1172/JCI78954
- Lanitis, E., Irving, M., Coukos, G., 2015. Targeting the tumor vasculature to enhance T cell activity. *Curr. Opin. Immunol.* 33, 55–63. doi:10.1016/j.coi.2015.01.011
- Larkin, J., Chiarion-Sileni, V., Gonzalez, R., Grob, J.J., Cowey, C.L., Lao, C.D., Schadendorf, D., Dummer, R., Smylie, M., Rutkowski, P., Ferrucci, P.F., Hill, A., Wagstaff, J., Carlino, M.S., Haanen, J.B., Maio, M., Marquez-Rodas, I., McArthur, G.A., Ascierto, P.A., Long, G.V., Callahan, M.K., Postow, M.A., Grossmann, K., Sznol, M., Dreno, B., Bastholt, L., Yang, A., Rollin, L.M., Horak, C., Hodi, F.S., Wolchok, J.D., 2015. Combined Nivolumab and Ipilimumab or Monotherapy in Untreated Melanoma. *N Engl J Med* 373, 23–34. doi:10.1056/NEJMoa1504030

- Lee, D.W., Kochenderfer, J.N., Stetler-Stevenson, M., Cui, Y.K., Delbrook, C., Feldman, S.A., Fry, T.J., Orentas, R., Sabatino, M., Shah, N.N., Steinberg, S.M., Stronck, D., Tschernia, N., Yuan, C., Zhang, H., Zhang, L., Rosenberg, S.A., Wayne, A.S., Mackall, C.L., 2015. T cells expressing CD19 chimeric antigen receptors for acute lymphoblastic leukaemia in children and young adults: a phase 1 dose-escalation trial. *The Lancet* 385, 517–528. doi:10.1016/S0140-6736(14)61403-3
- Li, B., Dewey, C.N., 2011. RSEM: accurate transcript quantification from RNA-Seq data with or without a reference genome. *BMC Bioinformatics* 12, 323. doi:10.1186/1471-2105-12-323
- Lund, A.W., Duraes, F.V., Hirose, S., Raghavan, V.R., Nembrini, C., Thomas, S.N., Issa, A., Hugues, S., Swartz, M.A., 2012. VEGF-C promotes immune tolerance in B16 melanomas and cross-presentation of tumor antigen by lymph node lymphatics. *Cell Rep* 1, 191–199. doi:10.1016/j.celrep.2012.01.005
- Lund, A.W., Medler, T.R., Leachman, S.A., Coussens, L.M., 2016. Lymphatic Vessels, Inflammation, and Immunity in Skin Cancer. *Cancer Discovery* 6, 22–35. doi:10.1158/2159-8290.CD-15-0023
- Lutz, M.B., Kukutsch, N., Ogilvie, A., Rossner, S., Koch, F., Romani, N., Schuler, G., 1999. An advanced culture method for generating large quantities of highly pure dendritic cells from mouse bone marrow. *J. Immunol. Methods* 223, 77–92. doi:10.1016/S0022-1759(98)00204-X
- Motz, G.T., Santoro, S.P., Wang, L.-P., Garrabrant, T., Lastra, R.R., Hagemann, I.S., Lal, P., Feldman, M.D., Benencia, F., Coukos, G., 2014. Tumor endothelium FasL establishes a selective immune barrier promoting tolerance in tumors. *Nature Medicine* 20, 607–615. doi:10.1038/nm.3541
- Munn, D.H., Bronte, V., 2016. Immune suppressive mechanisms in the tumor microenvironment. *Current Opinion in Immunology*. doi:10.1016/j.coi.2015.10.009
- Munn, D.H., Mellor, A.L., 2006. The tumor-draining lymph node as an immune-privileged site. *Immunol. Rev.* 213, 146–158. doi:10.1111/j.1600-065X.2006.00444.x
- Padera, T.P., Kadambi, A., di Tomaso, E., Carreira, C.M., Brown, E.B., Boucher, Y., Choi, N.C., Mathisen, D., Wain, J., Mark, E.J., Munn, L.L., Jain, R.K., 2002. Lymphatic metastasis in the absence of functional intratumor lymphatics. *Science* 296, 1883–1886. doi:10.1126/science.1071420
- Pasquali, S., van der Ploeg, A.P.T., Mocellin, S., Stretch, J.R., Thompson, J.F., Scolyer, R.A., 2013. Lymphatic biomarkers in primary melanomas as predictors of regional lymph node metastasis and patient outcomes. *Pigment Cell Melanoma Res* 26, 326–337. doi:10.1111/pcmr.12064
- Patel, S.P., Kurzrock, R., 2015. PD-L1 Expression as a Predictive Biomarker in Cancer Immunotherapy. *Molecular Cancer Therapeutics* 14, 847–856. doi:10.1158/1535-7163.MCT-14-0983
- Peske, J.D., Thompson, E.D., Gemta, L., Baylis, R.A., Fu, Y.-X., Engelhard, V.H., 2015. Effector lymphocyte-induced lymph node-like vasculature enables naive T-cell entry into tumours and enhanced anti-tumour immunity. *Nature Communications* 6, 7114. doi:10.1038/ncomms8114

- Porter, D.L., Hwang, W.-T., Frey, N.V., Lacey, S.F., Shaw, P.A., Loren, A.W., Bagg, A., Marcucci, K.T., Shen, A., Gonzalez, V., Ambrose, D., Grupp, S.A., Chew, A., Zheng, Z., Milone, M.C., Levine, B.L., Melenhorst, J.J., June, C.H., 2015. Chimeric antigen receptor T cells persist and induce sustained remissions in relapsed refractory chronic lymphocytic leukemia. *Sci Transl Med* 7, –303ra139. doi:10.1126/scitranslmed.aac5415
- Postow, M.A., Chesney, J., Pavlick, A.C., Robert, C., Grossmann, K., McDermott, D., Linette, G.P., Meyer, N., Giguere, J.K., Agarwala, S.S., Shaheen, M., Ernstoff, M.S., Minor, D., Salama, A.K., Taylor, M., Ott, P.A., Rollin, L.M., Horak, C., Gagnier, P., Wolchok, J.D., Hodi, F.S., 2015. Nivolumab and Ipilimumab versus Ipilimumab in Untreated Melanoma. *N Engl J Med* 372, 2006–2017. doi:10.1056/NEJMoa1414428
- Restifo, N.P., Dudley, M.E., Rosenberg, S.A., 2012. Adoptive immunotherapy for cancer: harnessing the T cell response. *Nat. Rev. Immunol.* 12, 269–281. doi:10.1038/nri3191
- Robert, C., Karaszewska, B., Schachter, J., Rutkowski, P., Mackiewicz, A., Stroiakovski, D., Lichinitser, M., Dummer, R., Grange, F., Mortier, L., Chiarion-Sileni, V., Drucis, K., Krajsova, I., Hauschild, A., Lorigan, P., Wolter, P., Long, G.V., Flaherty, K., Nathan, P., Ribas, A., Martin, A.-M., Sun, P., Crist, W., Legos, J., Rubin, S.D., Little, S.M., Schadendorf, D., 2015. Improved Overall Survival in Melanoma with Combined Dabrafenib and Trametinib. *N Engl J Med* 372, 30–39. doi:10.1056/NEJMoa1412690
- Rosenberg, S.A., Restifo, N.P., 2015. Adoptive cell transfer as personalized immunotherapy for human cancer. *Science* 348, 62–68. doi:10.1126/science.aaa4967
- Schmalzer, M., Broggi, M.A.S., Lagarde, N., Stöcklin, B.F., King, C.G., Finke, D., Rossi, S.W., 2015. IL-7R signaling in regulatory T cells maintains peripheral and allograft tolerance in mice. *Proc. Natl. Acad. Sci. U.S.A.* 112, 13330–13335. doi:10.1073/pnas.1510045112
- Schoppmann, S.F., Birner, P., Stöckl, J., Kalt, R., Ullrich, R., Caucig, C., Kriehuber, E., Nagy, K., Alitalo, K., Kerjaschki, D., 2002. Tumor-associated macrophages express lymphatic endothelial growth factors and are related to peritumoral lymphangiogenesis. *The American Journal of Pathology* 161, 947–956. doi:10.1016/S0002-9440(10)64255-1
- Schrama, D., Voigt, H., Eggert, A.O., Xiang, R., Zhou, H., Schumacher, T.N.M., Andersen, M.H., Straten, P., Reisfeld, R.A., Becker, J.C., 2007. Immunological tumor destruction in a murine melanoma model by targeted LT $\alpha$  independent of secondary lymphoid tissue. *Cancer Immunol Immunother* 57, 85–95. doi:10.1007/s00262-007-0352-x
- Schumacher, T.N., Kesmir, C., van Buuren, M.M., 2015. Biomarkers in Cancer Immunotherapy. *Cancer Cell* 27, 12–14. doi:10.1016/j.ccell.2014.12.004
- Schumacher, T.N., Schreiber, R.D., 2015. Neoantigens in cancer immunotherapy. *Science* 348, 69–74. doi:10.1126/science.aaa4971
- Sckisel, G.D., Bouchlaka, M.N., Monjazeb, A.M., Crittenden, M., Curti, B.D., Wilkins, D.E.C., Alderson, K.A., Sungur, C.M., Ames, E., Mirsoian, A., Reddy, A., Alexander, W., Soulika, A., Blazar, B.R., Longo, D.L., Wilttrout, R.H., Murphy, W.J., 2015. Out-of-Sequence Signal 3 Paralyzes Primary CD4<sup>+</sup> T-Cell-Dependent Immunity. *Immunity* 43, 240–250. doi:10.1016/j.immuni.2015.06.023

- Sharma, S., Stolina, M., Luo, J., Strieter, R.M., Burdick, M., Zhu, L.X., Batra, R.K., Dubinett, S.M., 2000. Secondary Lymphoid Tissue Chemokine Mediates T Cell-Dependent Antitumor Responses In Vivo. *The Journal of Immunology* 164, 4558–4563. doi:10.4049/jimmunol.164.9.4558
- Sharma, S., Stolina, M., Zhu, L., Lin, Y., Batra, R., Huang, M., Strieter, R., Dubinett, S.M., 2001. Secondary lymphoid organ chemokine reduces pulmonary tumor burden in spontaneous murine bronchoalveolar cell carcinoma. *Cancer Research* 61, 6406–6412.
- Shayan, R., Karnezis, T., Murali, R., Wilmott, J.S., Ashton, M.W., Taylor, G.I., Thompson, J.F., Hersey, P., Achen, M.G., Scolyer, R.A., Stacker, S.A., 2012. Lymphatic vessel density in primary melanomas predicts sentinel lymph node status and risk of metastasis. *Histopathology* 61, no–no. doi:10.1111/j.1365-2559.2012.04310.x
- Shields, J.D., Fleury, M.E., Yong, C., Tomei, A.A., Randolph, G.J., Swartz, M.A., 2007. Autologous chemotaxis as a mechanism of tumor cell homing to lymphatics via interstitial flow and autocrine CCR7 signaling. *Cancer Cell* 11, 526–538. doi:10.1016/j.ccr.2007.04.020
- Shields, J.D., Kourtis, I.C., Tomei, A.A., Roberts, J.M., Swartz, M.A., 2010. Induction of lymphoidlike stroma and immune escape by tumors that express the chemokine CCL21. *Science* 328, 749–752. doi:10.1126/science.1185837
- Snyder, A., Makarov, V., Merghoub, T., Yuan, J., Zaretsky, J.M., Desrichard, A., Walsh, L.A., Postow, M.A., Wong, P., Ho, T.S., Hollmann, T.J., Bruggeman, C., Kannan, K., Li, Y., Elipenahli, C., Liu, C., Harbison, C.T., Wang, L., Ribas, A., Wolchok, J.D., Chan, T.A., 2014. Genetic Basis for Clinical Response to CTLA-4 Blockade in Melanoma. *N Engl J Med* 371, 2189–2199. doi:10.1056/NEJMoa1406498
- Spranger, S., Bao, R., Gajewski, T.F., 2015. Melanoma-intrinsic  $\beta$ -catenin signalling prevents anti-tumour immunity. *Nature* 523, 231–235. doi:10.1038/nature14404
- Spranger, S., Koblisch, H.K., Horton, B., Scherle, P.A., Newton, R., Gajewski, T.F., 2014. Mechanism of tumor rejection with doublets of CTLA-4, PD-1/PD-L1, or IDO blockade involves restored IL-2 production and proliferation of CD8(+) T cells directly within the tumor microenvironment. *J Immunother Cancer* 2, 3. doi:10.1186/2051-1426-2-3
- Spranger, S., Spaapen, R.M., Zha, Y., Williams, J., Meng, Y., Ha, T.T., Gajewski, T.F., 2013. Up-Regulation of PD-L1, IDO, and T-reg in the Melanoma Tumor Microenvironment Is Driven by CD8(+) T Cells. *Sci Transl Med* 5, –200ra116. doi:10.1126/scitranslmed.3006504
- Stacker, S.A., Williams, S.P., Karnezis, T., Shayan, R., Fox, S.B., Achen, M.G., 2014. Lymphangiogenesis and lymphatic vessel remodelling in cancer. *Nature Publishing Group* 14, 159–172. doi:10.1038/nrc3677
- Swartz, M.A., 2014. Immunomodulatory roles of lymphatic vessels in cancer progression. *Cancer Immunology Research* 2, 701–707. doi:10.1158/2326-6066.CIR-14-0115
- Tammela, T., Alitalo, K., 2010. Lymphangiogenesis: Molecular Mechanisms and Future Promise. *Cell* 140, 460–476. doi:10.1016/j.cell.2010.01.045
- Thompson, E.D., Enriquez, H.L., Fu, Y.X., Engelhard, V.H., 2010. Tumor masses support naive T cell infiltration, activation, and differentiation into effectors. *Journal of Experimental Medicine* 207, 1791–1804. doi:10.1038/nrc1586

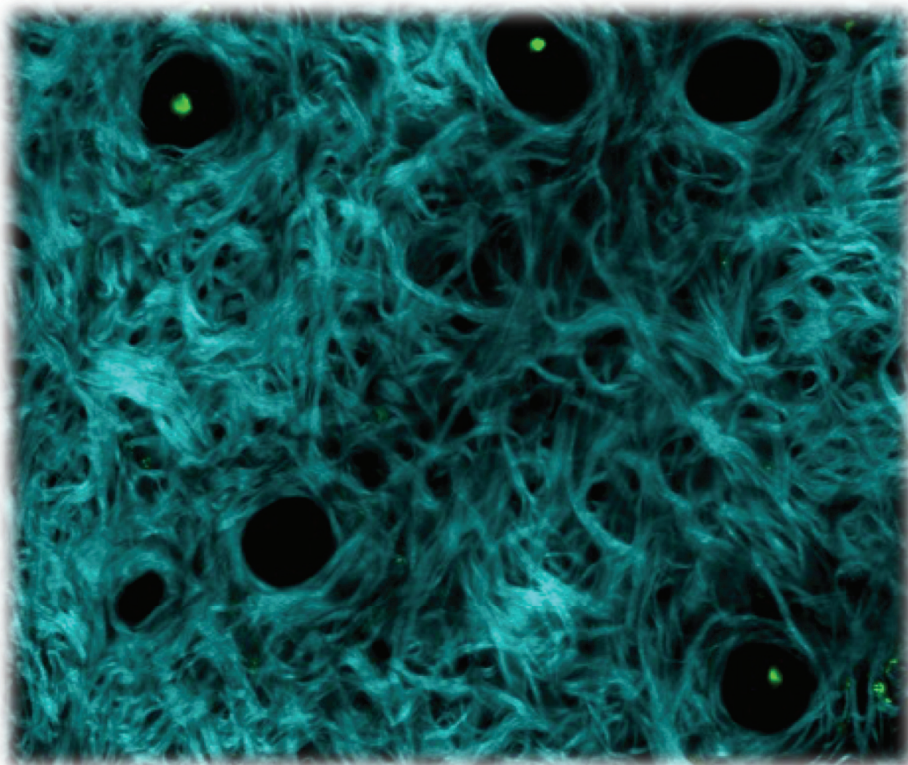
- Thurston, G., 2003. Role of Angiopoietins and Tie receptor tyrosine kinases in angiogenesis and lymphangiogenesis. *Cell and Tissue Research* 314, 61–68. doi:10.1007/s00441-003-0749-6
- Tumeh, P.C., Harview, C.L., Yearley, J.H., Shintaku, I.P., Taylor, E.J.M., Robert, L., Chmielowski, B., Spasic, M., Henry, G., Ciobanu, V., West, A.N., Carmona, M., Kivork, C., Seja, E., Cherry, G., Gutierrez, A.J., Grogan, T.R., Mateus, C., Tomasic, G., Glaspy, J.A., Emerson, R.O., Robins, H., Pierce, R.H., Elashoff, D.A., Robert, C., Ribas, A., 2014. PD-1 blockade induces responses by inhibiting adaptive immune resistance. *Nature* 515, 568–571. doi:10.1038/nature13954
- Van Allen, E.M., Miao, D., Schilling, B., Shukla, S.A., Blank, C., Zimmer, L., Sucker, A., Hillen, U., Foppen, M.H.G., Goldinger, S.M., Utikal, J., Hassel, J.C., Weide, B., Kaehler, K.C., Loquai, C., Mohr, P., Gutzmer, R., Dummer, R., Gabriel, S., Wu, C.J., Schadendorf, D., Garraway, L.A., 2015. Genomic correlates of response to CTLA-4 blockade in metastatic melanoma. *Science* 350, 207–211. doi:10.1126/science.aad0095
- Webster, R.M., Mentzer, S.E., 2014. The malignant melanoma landscape. *Nat Rev Drug Discov* 13, 491–492. doi:10.1038/nrd4326
- Wolchok, J.D., Hoos, A., O'Day, S., Weber, J.S., Hamid, O., Lebbé, C., Maio, M., Binder, M., Bohnsack, O., Nichol, G., Humphrey, R., Hodi, F.S., 2009. Guidelines for the evaluation of immune therapy activity in solid tumors: immune-related response criteria. *Clinical Cancer Research* 15, 7412–7420. doi:10.1158/1078-0432.CCR-09-1624
- Yu, P., Lee, Y., Liu, W., Chin, R.K., Wang, J., Wang, Y., Schietinger, A., Philip, M., Schreiber, H., Fu, Y.-X., 2004. Priming of naive T cells inside tumors leads to eradication of established tumors. *Nat Immunol* 5, 141–149. doi:10.1038/ni1029
- Zheng, W., Aspelund, A., Alitalo, K., 2014. Lymphangiogenic factors, mechanisms, and applications. *J. Clin. Invest.* 124, 878–887. doi:10.1172/JCI71603



## Chapter 4

# Engineered lymphangiogenesis promotes local expression of CCL21 and accumulation of T cell infiltrates

Manuel Fankhauser, Shann S Yu, Petra Aigner, Melody A Swartz



Fibrillar collagens (cyan) and hair follicles (green dots) of the mouse ear dermis.  
Two-photon microscopy.

## 4.1 Abstract

The lymphatic network is of vital importance to appropriate fluid homeostasis and immune regulation in steady-state and disease. Lymphatic vessels (LVs) form a one-way drainage system that transports cells, macromolecules, ions, and interstitial fluid from peripheral tissues to secondary lymphoid organs (SLOs). Within SLOs, information coming from the periphery is systematically scanned for abnormalities such as cancer and pathogens, and countermeasures in the form of adaptive immune responses are induced when needed. Although the role of lymphatic vessels in shaping immunity via passive transmission of peripheral information has been well established, the notion that lymphatic endothelial cells (LECs) can be actively involved in immune cell education and trafficking has only recently emerged. LEC-secreted chemokines such as CCL21 are essential for the orchestration of immune cell trafficking from peripheral tissues to SLOs, from the blood circulations to SLOs, within SLOs themselves, as well as for the egress from SLOs back into blood circulation. However, it is not well understood whether LECs secrete cytokines to regulate trafficking of immune cells in peripheral tissues themselves. We thus asked whether engineered lymphangiogenesis induces chemokine mediated immune cell recruitment into skin, and if so, whether this can be therapeutically exploited. We first show that an injectable hydrogel system for the sustained and highly localized delivery of the lymphatic growth factor VEGFC is able to induce local lymphangiogenesis with minimal induction of bystander inflammation in the mouse dermis. Furthermore, we found that lymphangiogenic sites resemble tertiary lymphoid organs (TLOs) in that they express higher levels of CCL21 and contain more CD4<sup>+</sup> and CD8<sup>+</sup> T cells infiltrates as compared to non-lymphangiogenic sites. Interestingly, delivery of the model antigen ovalbumin (OVA) into engineered lymphangiogenic sites led to increased numbers of IFN $\gamma$  secreting effector cells upon antigen re-challenge, indicating that this environment could be permissive for therapeutic modulation of immune responses. We thus propose that LECs might have an underappreciated role in driving the formation of tertiary lymphoid organs in peripheral tissues such as skin, and that engineered peripheral lymphangiogenesis might create therapeutic applications for the modulation of immune responses.

## 4.2 Introduction

Lymphatic vessels (LVs) are essential for fluid homeostasis and immune regulation in steady-state and disease (Lund et al., 2016). LVs form a one-way drainage system consisting of a hierarchical network of open-ended, permeable initial lymphatics that lead into collecting vessels characterized by a continuous basement membrane, pericyte coverage, and a system of valves that prevents retrograde fluid flow (Kerjaschki, 2014). By transporting cells, macromolecules, ions, and interstitial fluid through this network, LVs transfer information from peripheral tissues to secondary lymphoid organs (SLOs) and then relay it back into the blood circulation via efferent lymphatics that drain into the subclavian veins. The information that reaches the SLOs via lymphatics contains important cues essential to regulating adaptive immunity including soluble antigens (Clement et al., 2011), antigen-loaded dendritic cells (Randolph et al., 2005), danger signals and cytokines (Card et al., 2014). Depending on the tissue context such as homeostasis, inflammation, cancer, or infection, these cues lead to either tolerogenic adaptive immune mechanisms that maintain tolerance to self-antigens, or to the induction or resolution of effector mechanisms that try to battle tumor cells and invading pathogens (Lund et al., 2016). Although the role of lymphatic vessels in shaping immunity as passive conduits has been well established, the concept that LVs can also be actively involved in immune cell education and trafficking has only recently emerged (Card et al., 2014). However, as long as there is no better understanding of how lymphatic vessels actively regulate immunity, no rational approaches can be designed to exploit this biology for therapeutic interventions.

Lymphatic endothelial cells (LECs) actively participate in regulating immunity by influencing immune cell trafficking (Johnson and Jackson, 2013). LECs orchestrate immune cell trafficking via differential expression of chemokines and cell adhesion molecules (Card et al., 2014). CC-chemokine ligand 21 (CCL21) is the most thoroughly studied chemokine secreted by LECs (Gunn et al., 1998; Kriehuber et al., 2001; Vigl et al., 2011). In peripheral tissues, initial lymphatics secrete CCL21 to create a peri-lymphatic gradient, which attracts activated, antigen-loaded DCs via their expression of the CCL21 receptor, CCR7 (Teijeira et al., 2014). Once in contact with the LVs, dendritic cells transmigrate into lymphatic capillaries with the help of cell-cell interactions between integrins such as Mac-1 and LFA-1, and LEC-expressed adhesion molecules such as ICAM-1 and VCAM-1 which are upregulated by pro-inflammatory cytokines (Johnson et al., 2006). Inside initial lymphatics, DCs first actively crawl along the luminal vessel wall, before they reach collecting lymphatics from where they are passively transported to the draining lymph node by flow (Tal et al., 2011). When they arrive in the lymph node, DCs are further guided to the T cells zones via CCL21 gradients established by lymph node stromal cells including LECs. This is where DCs encounter naïve T cells, which are similarly guided to these areas by CCL21 gradients. In contrast to DCs, naïve CCR7<sup>+</sup> T cells arrive from the blood circulation via extravasation along CCL21 chemokine gradients present on high endothelial venules (HEVs), specialized blood endothelial cells that are present in SLOs (Andrian and Mempel, 2003), tertiary lymphoid organs (Ruddle, 2014) and tumors (Martinet et al., 2012). Interestingly, HEVs can translocate perivascular chemokine to their luminal surface, suggesting that extravasation can be influenced by chemokine producing stromal cells adjacent to HEVs (Baekkevold et al., 2001; Carlsen

et al., 2005). In the absence of their cognate antigen, typically lymphocytes are thought to spend 24h in a single lymph node, although the transit time may increase to 3-4 days if the cognate antigen is present (Bousso, 2008). Naïve and activated lymphocytes then both upregulate sphingosine-1-phosphate receptors (S1PRs), which allows them to egress into efferent lymphatics by sensing a gradient of sphingosine-1-phosphate (S1P) - itself a LEC-secreted sphingolipid with chemokine-like function (Cyster and Schwab, 2012). In contrast, dendritic cells have a short half-life (1.5-3 days) once activated and undergo apoptosis within the lymph node (Kushwah and Hu, 2010). Taken together, chemokine secretion by LECs is crucial for immune cell trafficking from peripheral tissue or the blood circulation to SLOs, within SLOs themselves, as well as for the egress from SLOs back into blood circulation. However, to our knowledge, it has not been explored whether initial lymphatics might regulate extravasation of immune cells from the circulation into peripheral tissues by means of chemokine secretion. Uncovering LEC mediated mechanisms that govern immune cell extravasation in peripheral tissues could enable the development of novel therapeutic strategies to regulate immune responses.

The purpose of this study was to determine whether engineered tissue lymphangiogenesis induces chemokine mediated immune cell recruitment into peripheral tissues and if so, whether this could be therapeutically exploited. To this end, we designed an injectable hydrogel system for the sustained and highly localized delivery of the lymphatic growth factor VEGFC into the mouse dermis. We used either the natural polymer fibrinogen, or functionalized poly(ethylene glycol) (PEG), a synthetic polymer with very low protein adsorption and complement activation levels *in vivo*, to form the hydrogel matrices. To increase retention of VEGFC and other proteins of interest within the hydrogels, they were engineered as a fusion protein with a transglutaminase (TG) targeting tag, which enables it to be covalently cross-linked into the fibrinogen or functionalized PEG matrix. Because we observed that fibrinogen based matrices induce inflammation in the draining lymph node, we did not further pursue this system. However, following intradermal injection into healthy wild-type mice, local delivery of VEGFC-TG from PEG gels led to increased local lymphangiogenesis, while delivery of soluble VEGFC did so in the draining lymph nodes. At the gel site, this was accompanied by increased local expression of CCL21, similar to observations in lymphangiogenic tumors, and associated with increased recruitment of CD4<sup>+</sup> and CD8<sup>+</sup> T cells. In the draining lymph node, even though no notable changes in cytokine expression could be detected following lymphangiogenesis, we found increased numbers of CCR7<sup>+</sup> immune cells including CD4<sup>+</sup> T cells, CD8<sup>+</sup> T cells, and CD11c<sup>+</sup> dendritic cells. To further examine the immunological relevance of these observations on antigen-specific T cell populations, mice were conditioned with hydrogels delivering both VEGFC-TG and the model antigen ovalbumin (OVA-TG). When mice were challenged with a local injection of OVA into the lymphangiogenic skin site, increased number of IFN $\gamma$  producing cells were detected as compared to the control groups. Our studies suggest a role for lymphangiogenesis in the extravasation of immune cells into peripheral tissues such as the skin, and that engineered lymphangiogenesis could potentially be exploited to modulate therapeutic immune responses.

## 4.3 Materials and methods

### 4.3.1 Hydrogel-binding protein variants

Cloning of VEGFC-TG: a matrix metalloproteinase (MMP)-cleavage site followed by the fibrin-binding domain (TG: NQEQVSPL) was added at the C-terminus of the mouse VEGFC sequence (accession NM\_009506.2, mature peptide, amino acid 108-223) by sequential polymerase chain reactions. Similarly, a poly-His tag followed by a thrombin-cleavage site was added at the N-terminus of VEGFC (VEGFC-TG final design: "polyHis-thrombin-VEGFC-MMP-TG"). The resulting sequence of VEGFC-TG was then inserted in pSeqTagA plasmid backbone. Cloning of aprotinin-TG: the fibrin-binding domain (TG: NQEQVSPL) was added at the C-terminus of the bovine aprotinin sequence (as described by Lorentz et al. 2011) by sequential polymerase chain reactions. Similarly, a poly-His tag followed by a thrombin-cleavage site was added at the N-terminus of aprotinin (aprotinin-TG final design: "polyHis-thrombin-aprotinin-TG"). The resulting sequence of aprotinin-TG was then inserted in pSeqTagA plasmid backbone. Cloning of OVA-TG: the fibrin-binding domain (TG: NQEQVSPL) was added at the C-terminus of the chicken ovalbumin (OVA) sequence (accession P01012, full length), and a poly-His tag followed by a thrombin-cleavage site was added at the N-terminus of OVA, by sequential polymerase chain reactions (OVA-TG final design: "polyHis-thrombin-OVA-TG"). The resulting sequence of OVA-TG was inserted into pSeqTagA plasmid backbone. Production of proteins: VEGFC-TG, aprotinin-TG, and OVA-TG have been produced as follows. The plasmid was transfected into HEK-293E using 25kDa polyethylenimine as a transfection agent and cells and cultured in FreeStyle medium (Invitrogen, Carlsbad, USA) supplemented with glutamine (4mM) and valproic acid (3.75mM). At 7 days post-transfection, the expressed protein was isolated from the cell culture supernatants using Ni<sup>2+</sup>-affinity chromatography (for the poly-His tag). The poly-His tag was then cleaved with a commercial agarose bead-bound thrombin cleavage kit (Sigma-Aldrich, St. Louis, USA), and purified using size-exclusion chromatography. The purified proteins were further dialyzed against Tris-buffer saline, sterilized through 0.22µm filtration and stored at -80°C.

### 4.3.2 Hydrogel synthesis, preparation, and injection

Fibrin hydrogels: human fibrinogen (10mg/ml, F3879; Sigma), aprotinin-TG, fluorescently labeled TG-factors, as well as human thrombin (2U/ml, T4394; Sigma), human factor XIII (2U/ml, 00671; CSL Behring), and CaCl<sub>2</sub> (2mM) were mixed and immediately injected intradermally using 0.3ml insulin syringes. PEG hydrogels: 8-arm, 40kDa poly(ethylene glycol) (PEG)-maleimide was reacted with 9.6x molar excess of either Ac-FKGGVPMSMRGGGERCG-Amide or NQEQVSPLERCG-Amide peptides in dimethylformamide, in the presence of 10x molar excess of triethylamine. The reaction was allowed to proceed for at least 4h at 37°C with agitation, after which the completed polymer-peptide conjugates (8APEG-FKGG & 8APEG-NQEQVSPL) were isolated using a size-exclusion chromatography and characterized by NMR and BCA assay to confirm peptide conjugation. 5%wt hydrogels were prepared by mixing 1mg of 8APEG-FKGG & 1mg of 8APEG-NQEQVSPL with desired bioactive TG-proteins, Factor XIII (0.2U), and thrombin (0.075U), adjusted to a final volume of 40µL in TBS with 50mM CaCl<sub>2</sub>. This mixture was pipetted to mix and injected into the interscapular region of isoflurane-anesthetized, healthy wild-type mice intradermally, where it polymerizes within 10-15 min of injection.

#### **4.3.3 VEGFR3 phosphorylation assay**

Bioactivity of VEGFC-TG was determined using a VEGFR3 phosphorylation assay. Human LECs (about 70-80% confluent) were starved for 16h in 10cm petri dishes containing starving media (EBM + 2% FBS + 1% penicillin/streptomycin + 50 $\mu$ M DBcAMP + 1 $\mu$ g/ml hydrocortisone acetate + 1% L-Glut). VEGFC-TG was added to the starving media for 10 minutes (100ng/ml and 500ng/ml respectively), before the media was replaced with 10ml ice cold PBS. Cells were washed twice in ice cold PBS and then lysed by the addition of 500 $\mu$ l RIPA protein extraction buffer (R0278; Sigma). Lysates were collected in 1.5ml microcentrifuge tubes, spun down at 12'000g for 10' to get rid of cell debris, and the supernatant transferred into new 1.5ml microcentrifuge tubes. BCA assay was performed to measure total protein concentration, and all samples normalized to the same concentration (0.2-1mg/ml depending on how much total protein was available) in a total volume of 1ml RIPA buffer. Next, immunoprecipitation of VEGFR3 was performed. 40 $\mu$ l Protein A/G plus agarose (sc-2003, Santa Cruz Biotechnology) was added and incubated for 4h with rotation at 4°C to remove unspecific binders. Beads were spun down at 2500g for 3', and the supernatant transferred into new 1.5ml microcentrifuge tubes. 2 $\mu$ l of anti-VEGFR3 antibody (sc-321; Santa Cruz Biotechnology) was added and incubated for 1h with rotation at 4°C. Next, 20 $\mu$ l of Protein A agarose was added and incubated O/N with rotation at 4°C. Beads were spun down at 2500g for 3', the supernatant discarded, and the beads washed 3x with 500 $\mu$ l RIPA buffer. After the last wash, all liquid was removed using a 0.3ml insulin syringe, before 20 $\mu$ l Laemmli sample buffer (161-0764; BioRad) was added. Samples were then loaded on a 7.5% acrylamide gel, and standard SDS-page followed by Western Blot analysis performed. Antibodies used or Western Blot: anti-pTyr (sc-7020, Santa Cruz Biotechnology), and anti-VEGFR3 (sc-321; Santa Cruz Biotechnology).

#### **4.3.4 Plasmin inhibition assay**

Bioactivity of aprotinin-TG was determined using a plasmin inhibition assay. 2.61 $\mu$ M of aprotinin-TG or WT aprotinin were incubated with 0.1U/mL human plasmin (10602361001; Roche) in the presence of 100 $\mu$ M fluorogenic plasmin substrate, N-Succinyl-Ala-Phe-Lys-7-amido-4-methylcoumarin acetate salt (s0763; Sigma-Aldrich) in phosphate-buffered saline (PBS) at pH 8.5. Fluorescence emission was measured at 438nm with a plate reader (Safire II, Tecan).

#### **4.3.5 OT-I proliferation assay**

Bioactivity of OVA-TG was determined using an OT-I proliferation assay. Briefly, bone marrow-derived DCs (BMDCs) were harvested from C57BL/6 mice, differentiated in GM-CSF as described (Lutz et al., 1999). 7 days later, 1x10<sup>4</sup> DCs were put in a coculture with naïve, CFSE-labeled CD8+ T cells from OT-I mice (1:10 ratio) in 96-well plates for 72 hours in 200 $\mu$ l coculture media (IMDM with 10% FBS and 1% penicillin/streptomycin). Cells were then processed and analyzed by flow cytometry. Cellular proliferation was monitored by CFSE dilution.

#### **4.3.6 *In vitro* VEGFC-TG release assay**

To assess the *in vitro* cross-linking efficiency of TG-factor into fibrin hydrogels, matrices with a total volume of 200 $\mu$ l containing VEGFC-TG (1 $\mu$ g/ml or 0.2 $\mu$ g/ml), as well as thrombin (2U/ml), factor XIII



(2U/ml), and  $\text{CaCl}_2$  (2mM) were mixed in ultralow protein-binding polystyrene 96 well plates (Costar #3474) and polymerized at 37°C for 45 minutes. Ultralow protein-binding polystyrene 24 well plates (Costar #3473) were blocked at 37°C with PBS + 2% BSA in the meantime. The preformed gels were then transferred into the blocked 24 well plates, where they were rinsed with 500µl release buffer (PBS + 0.1% BSA). The release buffer was collected and replaced every 12 hours. The concentration of VEGFC-TG in the release buffer was quantified using ELISA.

#### **4.3.7 Mice**

Gender-matched wild-type mice (Harlan), all on the C57BL/6 or BALB/c background, were used between 8-12 weeks of age. All experiments were performed with approval from the Veterinary Authority of the Canton de Vaud, Switzerland.

#### **4.3.8 Intravital imaging and analysis**

Mice were anesthetized using isoflurane and imaged with a fluorescent-mediated tomography (VisEn FMT1500, PerkinElmer) or Xenogen IVIS Spectrum (Caliper LifeSciences / Perkin-Elmer, Waltham, MA, United States) *in vivo* imaging system. For the VisEn system, AlexaFluor650-tagged fibrinogen was detected using the appropriate excitation and emission channel. 3D ROIs were set and the voxel density quantified using the manufacturer's software (Perkin-Elmer, TrueQuant 3.1). For the IVIS system, AlexaFluor750-tagged VEGFC-TG was detected via excitation and emission filters set at 745/800nm and exposure time at 0.5 seconds. To quantify protein release from the hydrogels, ROIs were defined for each gel injection site using images obtained at the time of gel implantation. For any given gel injection site, the same ROIs were kept for the duration of the experiment. Background-corrected total photon counts within ROIs were quantified using Perkin-Elmer Living Image software (version 4.0) and normalized against total photon counts within the ROI at the time of injection in order to obtain release profiles of the fluorescently-labeled proteins over time.

#### **4.3.9 Lymph node and gel site cell isolation**

Stromal cells ( $\text{CD45}^-$ ) and  $\text{CD45}^+$  immune cells were recovered from gel sites (skin), and draining and non-draining lymph nodes (LNs) according to the previously published "Broggi Style" protocol (Broggi et al., 2014). Lymph nodes were placed in a well of a 24 well plate containing 500µl digestion medium consisting of DMEM (41965-062; GIBCO, no pyruvate) + 1% Pen/Strep + 1.2mM  $\text{CaCl}_2$  + 2% FBS. To facilitate the digestion process, the lymph node capsules were then gently disrupted with syringe needles (26G) and transferred into 5ml round-bottom tubes (Falcon-BD Bioscience) containing 750µl digestion buffer I, which consisted of digestion medium supplemented with 1mg/ml Collagenase IV (CLS4 LS004188; Worthington) and 40µg/ml DNase I (11284932001; Roche). Digestion was done for 30' at 37°C in a beaker with water on a heating plate with magnetic stirring (~1turn/sec). The supernatant was then carefully collected into a 5ml round-bottom filter tube (Falcon-BD Bioscience), and 750µl digestion buffer II, which consisted of digestion medium supplemented with 3.3mg/ml Collagenase D (1108886600; Roche) and 40µg/ml DNase I, was added to the 5ml tube with the remaining tissue pieces. Digestion was then continued for 5 minutes, before the suspension was disrupted by repeated pipetting with an electronic pipette. Digestion was then continued for another



10 minutes, before further disruption of the remaining cell aggregates by repeated pipetting. To inactivate the enzymes, 7.5µl EDTA (500mM) was added to each tube to reach a final concentration of 5mM (pH 7.2), and this mixture was pipetted thoroughly to mix, strained, and collected into a 5ml round-bottom filter tube (Falcon-BD Bioscience), and spun down at 2000g for 5min. Cells were then resuspended in an appropriate volume of FACS buffer (PBS + 2% FBS) to proceed for FACS staining. For the gel sites (skin), aforementioned protocol was slightly adapted. Skin pieces were first placed in a 10cm petri dish containing 2ml of basal IMDM, and minced with scalpel blades. Skin pieces were then transferred into a 5ml round-bottom tube containing 750µl digestion buffer I (+0.05U plasmin per gel). Digestion was done for 30' at 37°C in a beaker with water on a heating plate with magnetic stirring (~1turn/sec). The supernatant was then carefully collected through a 70µm nylon filter into a 50ml conical tube and 750µl digestion buffer II (+0.05U plasmin per gel) was added to the 5ml tube with the remaining tissue pieces. Three cycles of 15' digestion, followed by 100 times pipetting were then done. After the last cycle, 7.5µl EDTA (500mM) was added to each tube to reach a final concentration of 5mM (pH 7.2), before pipetting again 100 times. The entire cell suspension was then collected through the 70µm into the 50ml conical tube. Remaining tissue pieces were smashed through the filter using the plunger of a 3ml syringe, and the filter subsequently washed with 10ml HBSS. The cell suspension was then spun down at 2000g for 5' and resuspended in an appropriate amount of FACS buffer to proceed for FACS staining.

#### **4.3.10 Flow cytometry**

Antibody stainings for surface targets were done in FACS buffer (PBS + 2% FCS), and intracellular stainings were done after fixation and permeabilization according to the manufacturers protocol. The following anti-mouse antibodies were used for flow cytometry: CD45-APC (17-0451-82; eBioscience) or biotinylated CD45 (13-0451-85; eBioscience), CD4-PacBlue (100531; Biolegend) or CD4-PE-Cy7 (100528; Biolegend), CD8α-PacOrange (MCD0830; Invitrogen), F4/80-PerCPCy5.5 (123128; Biolegend), CD25-FITC (101908; Biolegend), FoxP3-PerCPCy5.5 (45-5773-82; eBioscience), CD62L-PE (12-0621-82; eBioscience), CD44-APCeF780 (47-0441-82; eBioscience), CCR7-PE-Cy7 (25-1971-82; eBioscience) or CCR7-PerCPCy5.5 (45-1971-82; eBioscience), biotinylated CD11b (13-0112-82; eBioscience), MHCII-AF647 (107619; BioLegend), PD1-bio (13-9981-82, eBioscience), CD31-eFluor450 (48-0311-82; eBioscience), gp38-AF488 (127406; BioLegend). Cell viability was determined by staining with Fixable live/dead blue, aqua (L34957; Invitrogen) or red (L23102; Invitrogen) dyes according to manufacturer's specifications. Flow cytometry acquisition was performed on a Cyan (Beckman Coulter) LSR2 flow cytometer (BD Bioscience) and data analysis was performed with FlowJo (Version 9.7.7.).

#### **4.3.11 ELISA and Luminex**

Protein lysates were generated from gel sites (skin) and lymph node by homogenizing the tissues in 400µl (lymph nodes) or 700µl (skin) T-Per protein extraction buffer (78510; ThermoFisher) containing cOMplete protease inhibitor cocktail (1 tablet per 10ml, 11836145001; Roche). Tissue lysates were spun down at 2000g for 2min, and transferred into new 1.5ml microcentrifuge tubes. Tissue lysates were then spun at 12'000g for 10min to get rid of cell debris, and the supernatant was transferred into

new 1.5ml eppendorf tubes which were stored at -80°C. ELISAs were performed according to standard protocols. Custom chemokine/cytokine multiplexed Luminex assays were purchased from R&D Systems and performed according to manufacturer's specifications.

#### **4.3.12 ELISPOT assay**

IFN $\gamma$  Elispot 96 well filter plates (Millipore) were pre-wetted, coated, and blocked according to the manufacturer's protocol.  $1 \times 10^6$  lymph node cells or splenocytes, or  $1 \times 10^5$  skin cells were then plated per well. Cells were stimulated with 1mg/ml full-length OVA grade V (A5503; Sigma) in 200 $\mu$ l co-culture media (IMDM + 10% FBS + 1X PS + 1X Non-essential amino acids) per well for 36h at 37°C. Plates were then coated with secondary HRP-conjugated antibody, followed by the addition of AEC substrate. The reaction was stopped by washing the plate in MilliQ water and the plates dried overnight at 4°C. Membranes were then analyzed using an automated ELISpot reading system.

## 4.4 Results

### 4.4.1 Purification and characterization of recombinant VEGFC-TG, aprotinin-TG, and OVA-TG.

In chapter one of this thesis, we found that tumor-derived VEGFC can influence local immune infiltration by inducing the secretion of CCL21 by LECs. To better understand the role of VEGFC in shaping immune responses in peripheral tissues, we wanted to use an *in vivo* platform in which VEGFC is released from a more controlled environment as compared to the tumor microenvironment. A platform that allows controlled release of bioactive factors from hydrogels has been previously described (Schense and Hubbell, 1999; Zisch et al., 2001). Controlled release is achieved by the addition of a transglutaminase (TG) substrate tag (NQEQVSPL) to the proteins of interest, which allows their enzymatic incorporation into fibrin scaffolds by the action of factor XIIIa. The *in vivo* release rate of TG-proteins can be manipulated by the addition of matrix metalloproteinase (MMP) cleavage sites into the protein sequence (Patterson and Hubbell, 2010). At the same time, the persistence of fibrin gels can be increased by incorporating aprotinin, an inhibitor of the fibrin degrading enzyme plasmin (Lorentz et al., 2011). To assess the effect of peripheral lymphangiogenesis on immune responses, we first engineered VEGFC-TG, aprotinin-TG, and OVA-TG fusion proteins by cloning them into pSeqTagA vectors, and producing the recombinant TG-proteins in mammalian HEK293E cells (Figure 4.1A). TG-proteins were isolated from the cell culture supernatants using Ni<sup>2+</sup>-affinity chromatography, followed by cleavage of the poly-His tag and size-exclusion chromatography. The purity of TG-protein batches was assessed by SDS-PAGE with Coomassie staining (Figure 4.1B). VEGFC-TG batches contained monomers and dimers, which were pooled as both forms can potentially be bioactive (Joukov et al., 1997). Dose-dependent phosphorylation of the VEGFC receptor VEGFR3 in LECs indicated that the recombinant VEGFC-TG was bioactive (Figure 4.1C). Aprotinin-TG showed comparable activity to commercial wildtype aprotinin as assessed by the efficiency of plasmin inhibition (Figure 4.1D). OVA-TG was able to induce T cell proliferation, however, to a lesser extent than wildtype OVA (Figure 4.1E), indicating that the processing and loading on MHC I might be less efficient. To determine how well VEGFC-TG would be cross-linked into a fibrin scaffold, an *in vitro* release assay was performed, which showed that most of the loaded VEGFC-TG was still retained after 36h (Figure 4.1F). Even though the initial burst release of VEGFC-TG was increased at the high concentrations (1µg/ml), a plateau of about 4% was reached after 36h. Because collagenase D or plasmin, both used to digest fibrin scaffolds, also cleaved VEGFC-TG (Figure 4.1F), we were not able to determine the amount of VEGFC-TG remaining within fibrin gels. These data demonstrate that bioactive VEGFC-TG, aprotinin-TG, and OVA-TG can be engineered and purified from a mammalian expression system, and that VEGFC-TG is largely retained in fibrin hydrogels *in vitro*.

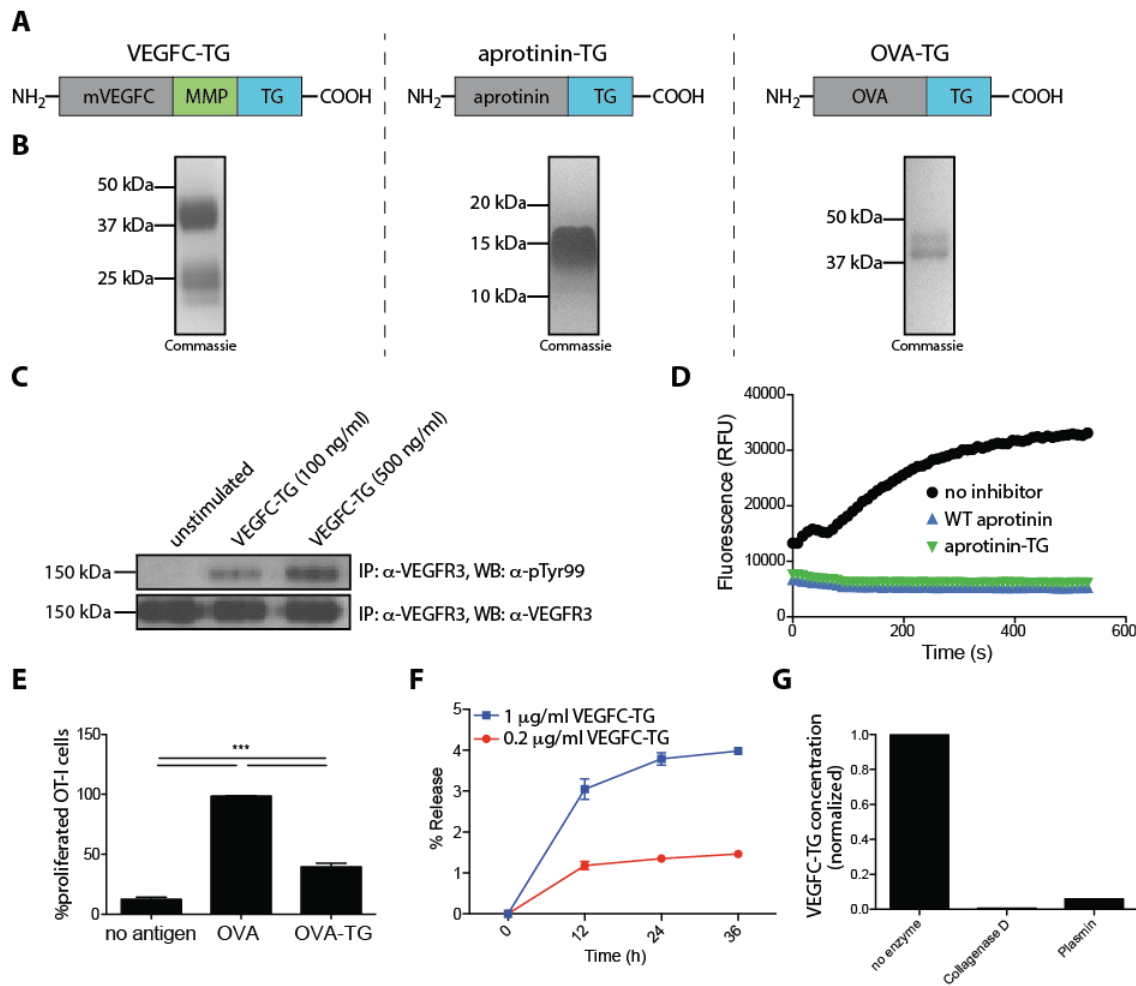


**Figure 4.1 Purification and characterization of recombinant TG-proteins.** (A) Schematic representation of recombinant VEGFC-TG, aprotinin-TG, and OVA-TG protein domains. (B) Coomassie-stained SDS-PAGE gels of the purified TG-proteins. (C) Bioactivity of VEGFC-TG was assessed by measuring its ability to induce VEGFR3 phosphorylation in human LECs. LECs were starved for 16h in media containing 2% FBS, before VEGFC-TG was added to the media for 10 minutes (100ng/ml and 500ng/ml respectively). VEGFR3 was then immunoprecipitated from the cell lysate, and a western blot for VEGFR3 and phosphorylated tyrosine (pTyr) performed. (D) Bioactivity of aprotinin-TG was assessed by measuring its ability to inhibit the cleavage of the model plasmin substrate N-succinyl-Ala-Phe-Lys-7-amido-4-methylcoumarin in the presence of 0.1 U/mL plasmin, and either 2.61μM wildtype aprotinin or aprotinin-TG. (E) Bioactivity of OVA-TG. Shown are percentages of proliferation of CFSE-labeled OT-I CD8<sup>+</sup> T cells after 3 days of coculture with DCs derived from wildtype mice in the presence of OVA or OVA-TG. Bar graphs show mean ± SEM (n=3, \*\*\*p< 0.001 using one-way ANOVA with Tukey's post-test). (F) To assess the *in vitro* cross-linking efficiency of VEGFC-TG into fibrin hydrogels, matrices with a total volume of 200μl containing 10mg/ml fibrinogen were polymerized in 96 well plates at 37°C for 45 minutes. Preformed gels were then transferred into 24 well plates and rinsed with 500μl release buffer (PBS + 0.1% BSA) every 12h. VEGFC concentrations were quantified by ELISA. (G) To determine whether VEGFC-TG was digested by enzymes used to digest fibrin hydrogels, VEGFC-TG (1μg/ml) was incubated with Collagenase D (0.2 mg/ml) or plasmin (0.02 U/ml) in a total volume of 70μl buffer (20mM HEPES + 150mM NaCl, pH 7.5) at 37°C for 3h. VEGFC concentration in the supernatant was then determined using ELISA.

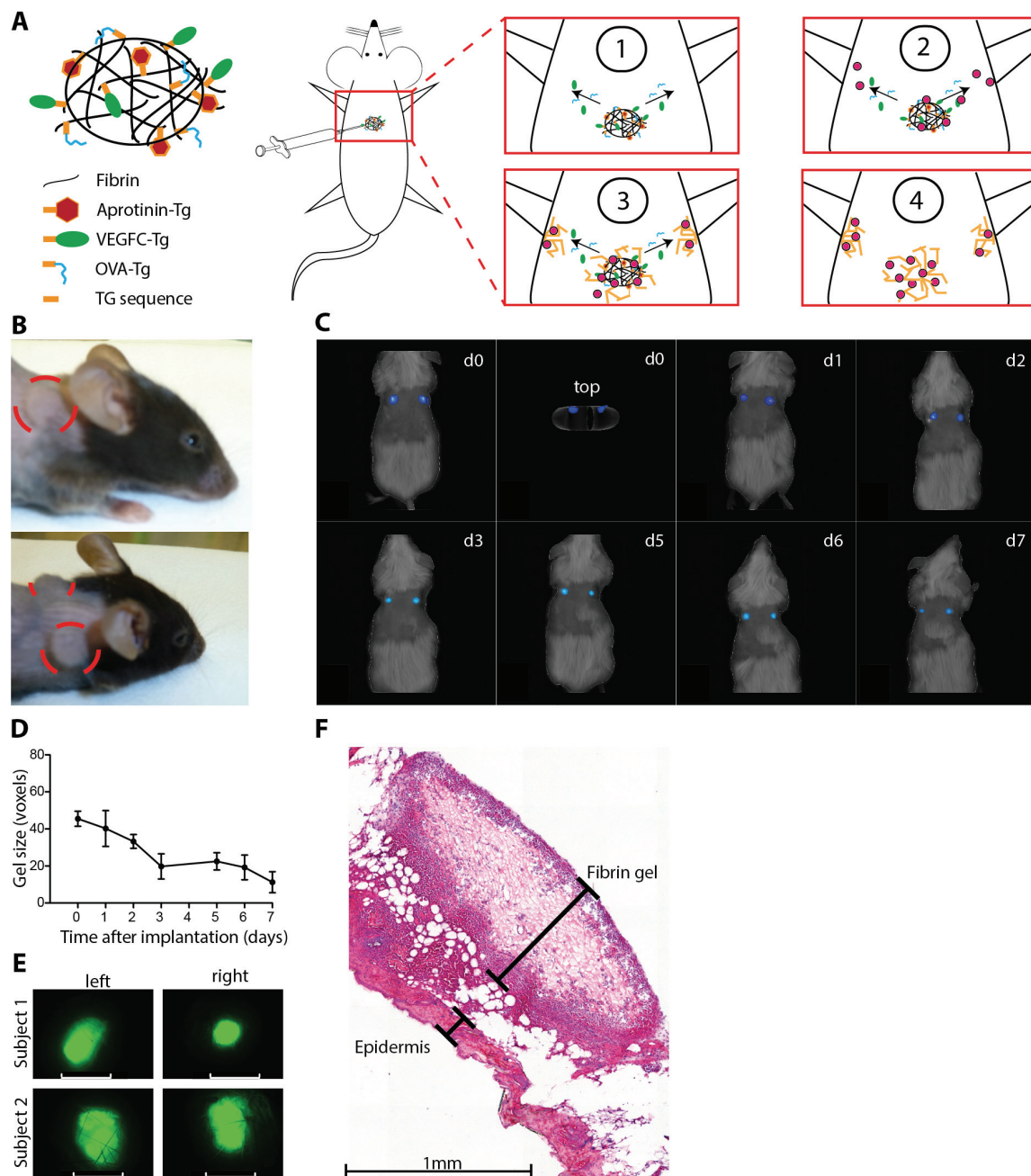


**Figure 4.2 Fibrin hydrogels containing aprotinin-TG can be injected intradermally to polymerize *in situ* and persist over extended periods of time *in vivo*.** (A) Schematic of controlled release of TG-proteins from fibrin hydrogels *in vivo*. (B-D) Two hydrogels with a total volume of 50µl each containing unlabeled fibrinogen (10mg/ml), fibrinogen-AF-680 (0.1mg/ml), and aprotinin-TG (20µM) were intradermally injected above the shoulders. (B) Representative images of fibrin hydrogel spheres after intradermal injection in the front shoulder region. (C) Representative 3D reconstruction of fibrin hydrogels containing fluorescently labeled fibrinogen degrading over time. Images were taken every day using fluorescence-mediated tomography (FMT). (D) Quantification of gel size over time as assessed by FMT. Data shown as mean ± SEM (n=4). (E) Fluorescent images of skin biopsies 15 days after hydrogel injection (10X, scale bar = 2mm). (F) H&E section of skin containing a fibrin hydrogel seven days after injection.

#### **4.4.2 Fibrin hydrogels containing aprotinin-TG can be injected intradermally to polymerize *in situ* and persist over extended periods of time *in vivo*.**

Fibrin hydrogels have previously been used for the controlled release of bioactive factors, for example for the *in vivo* delivery of anti-tumor vaccines (Julier et al., 2015). However, in order to avoid inflammation caused by surgery, we wanted to establish a platform that allowed the injection and *in situ* polymerization of TG-factor loaded hydrogels (Figure 4.2A). To do so, fibrinogen was prepared separately at room temperature, while a mix containing TG-factors, Factor XIII,  $\text{CaCl}_2$  and thrombin was kept on ice until shortly before the injection. Once mixed, the gels were immediately injected intradermally where they polymerized within 10-20 seconds and formed solid spheres (Figure 4.2B). To assess the persistence of fibrin hydrogels *in vivo*, 1% of Alexa Fluor 647 (AF647) labeled fibrinogen was added to the hydrogels containing 20 $\mu\text{M}$  aprotinin-TG, and the fluorescence measured daily using fluorescence-mediated tomography (Figure 4.2C). Even though the hydrogel size decreased about 4-fold within one week (Figure 4.2D), skin biopsies taken 15 days after hydrogel injection still possessed detectable fluorescent signal, although the size had shrunk to approximately 1-1.5mm in diameter (Figure 4.2E), indicating that hydrogel remnants can be stable in the tissue over extended periods of time. H&E stained cryosections of tissue biopsies retrieved 7 days after injection confirmed that hydrogels were localized just below the epidermal layer (Figure 4.2F). These results show that fibrin matrices containing aprotinin-TG can be injected intradermally to polymerize *in situ*, and that they persist more than a week *in vivo*.

#### **4.4.3 Empty fibrin hydrogels induce inflammation in the draining lymph node.**

Because we wanted to assess the effects of engineered lymphangiogenesis on local immune responses, we first had to determine whether fibrin hydrogels themselves might contribute to inflammation. To evaluate whether injection of fibrin hydrogels would change the local immune microenvironment, mice were injected intradermally with either empty or VEGFC-TG containing hydrogels. Mice that received intradermal injections of CpG or LPS adjuvant served as positive control groups for agents that induce inflammation in the draining lymph nodes. All groups were euthanized five days later, and the skin draining lymph nodes (brachial, axillary, inguinal) collected for flow cytometry analysis. We found that all treatment groups had increased numbers of  $\text{CD45}^+$  immune cells in their draining lymph nodes as compared to the naïve control group (Figure 4.3A). Similar to the CpG treated control group, both fibrin hydrogel groups showed increased fractions of B cells, and decreased fractions of  $\text{CD4}^+$  and  $\text{CD8}^+$  T cells, independently of the presence of VEGFC-TG (Figure 4.3B). In terms of phenotype, there was an increase in the fraction of naïve  $\text{CD8}^+$  T cells in both fibrin hydrogels groups (Figure 4.3C), while VEGFC-TG containing fibrin hydrogels also increased the fraction of effector  $\text{CD4}^+$  T cells (Figure 4.3D). PD1 expression, a sign of T cell activation (Parry et al., 2005), was upregulated on  $\text{CD4}^+$  and to a lesser extent on  $\text{CD8}^+$  T cells (Figure 4.3E). Finally, we assessed the number and maturation state of  $\text{CD11c}^+$  dendritic cells. Even though the number was constant across all groups, empty fibrin hydrogels induced upregulation of MHCII (Figure 4.3F), indicating enhanced maturation of DCs (Dalod et al., 2014). Taken together, these data indicate that empty fibrin hydrogels themselves induce changes in the draining lymph node similar to CpG-induced inflammation.



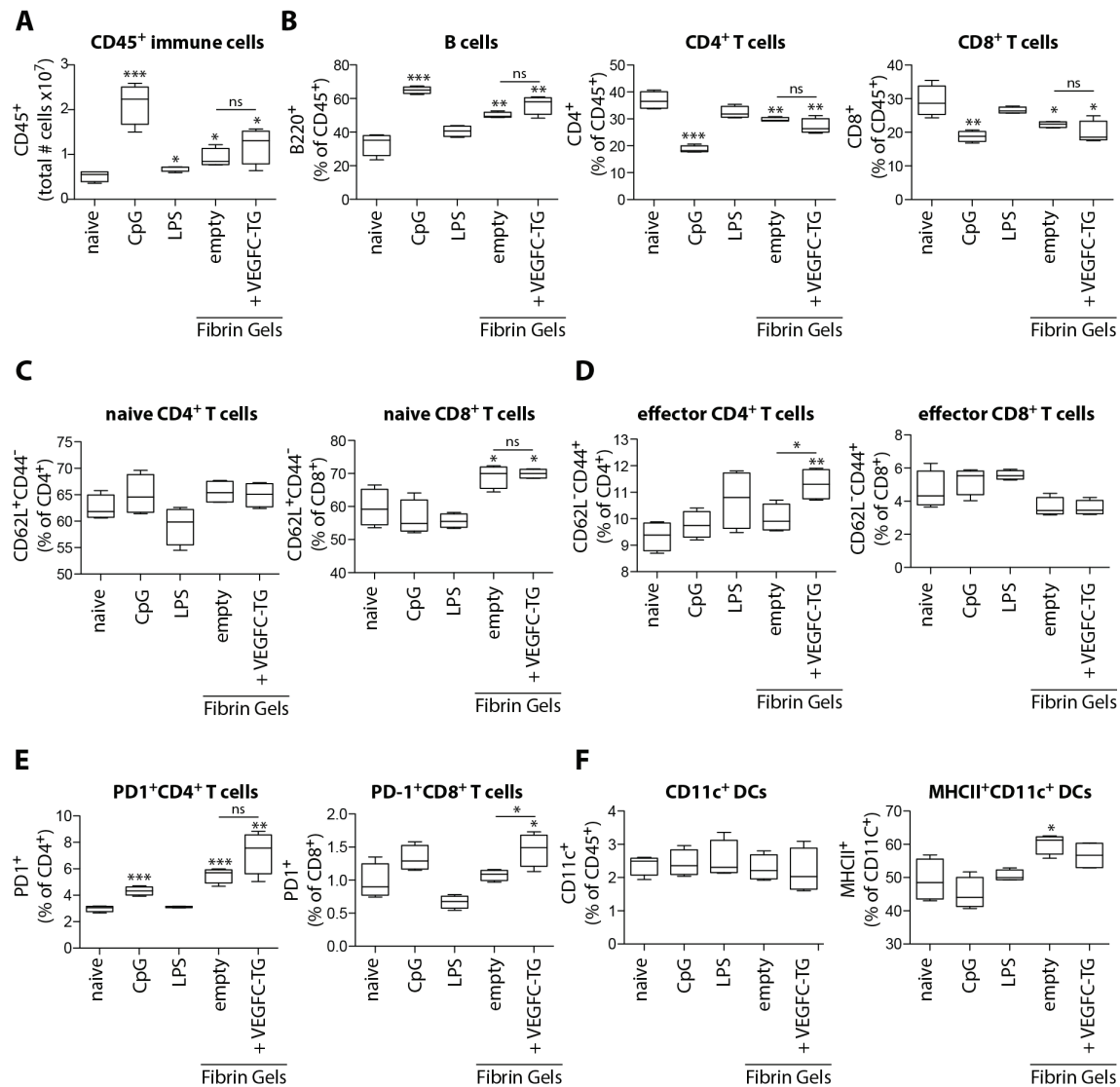


**Figure 4.3 Empty fibrin hydrogels induce inflammation in the draining lymph node.** (A-F) Two hydrogels with a total volume of 50 $\mu$ l each containing fibrinogen (10mg/ml), aprotinin-TG (20 $\mu$ M), and VEGFC-TG (5 $\mu$ g/ml) were intradermally injected in the anterior and posterior back skin of mice. Control groups received CpG (60 $\mu$ g total) or LPS (100ng total) intradermally injected into all four footpads. Five days later, the draining lymph nodes (brachial, axillary, inguinal) were collected, and single cell suspensions analyzed by flow cytometry. Quantification of (A) overall CD45<sup>+</sup> immune cells (gated on live cells), (B) B cells (B220<sup>+</sup>CD3<sup>+</sup>CD45<sup>+</sup>), CD4<sup>+</sup> (CD4<sup>+</sup>CD3<sup>+</sup>CD45<sup>+</sup>), and CD8<sup>+</sup> (CD8<sup>+</sup>CD3<sup>+</sup>CD45<sup>+</sup>) T cells. (C-D) Phenotype of CD4<sup>+</sup> and CD8<sup>+</sup> T cells with (C) showing naive T cells (CD62L<sup>+</sup>CD44<sup>-</sup>) and (D) showing effector T cells (CD62L<sup>-</sup>CD44<sup>+</sup>). (E) Status of programmed cell death (PD1) expression on CD4<sup>+</sup> and CD8<sup>+</sup> T cells. (F) Quantification and MHCII<sup>+</sup> status of CD11c<sup>+</sup> dendritic cells. Data shown as box (showing median and 25<sup>th</sup> to 75<sup>th</sup> percentile) and whiskers (showing min and max) (n=4, \*p<0.05, \*\*p<0.01, \*\*\*p<0.001 with Student's t-test as compared to the naive group except indicated differently with a bar).



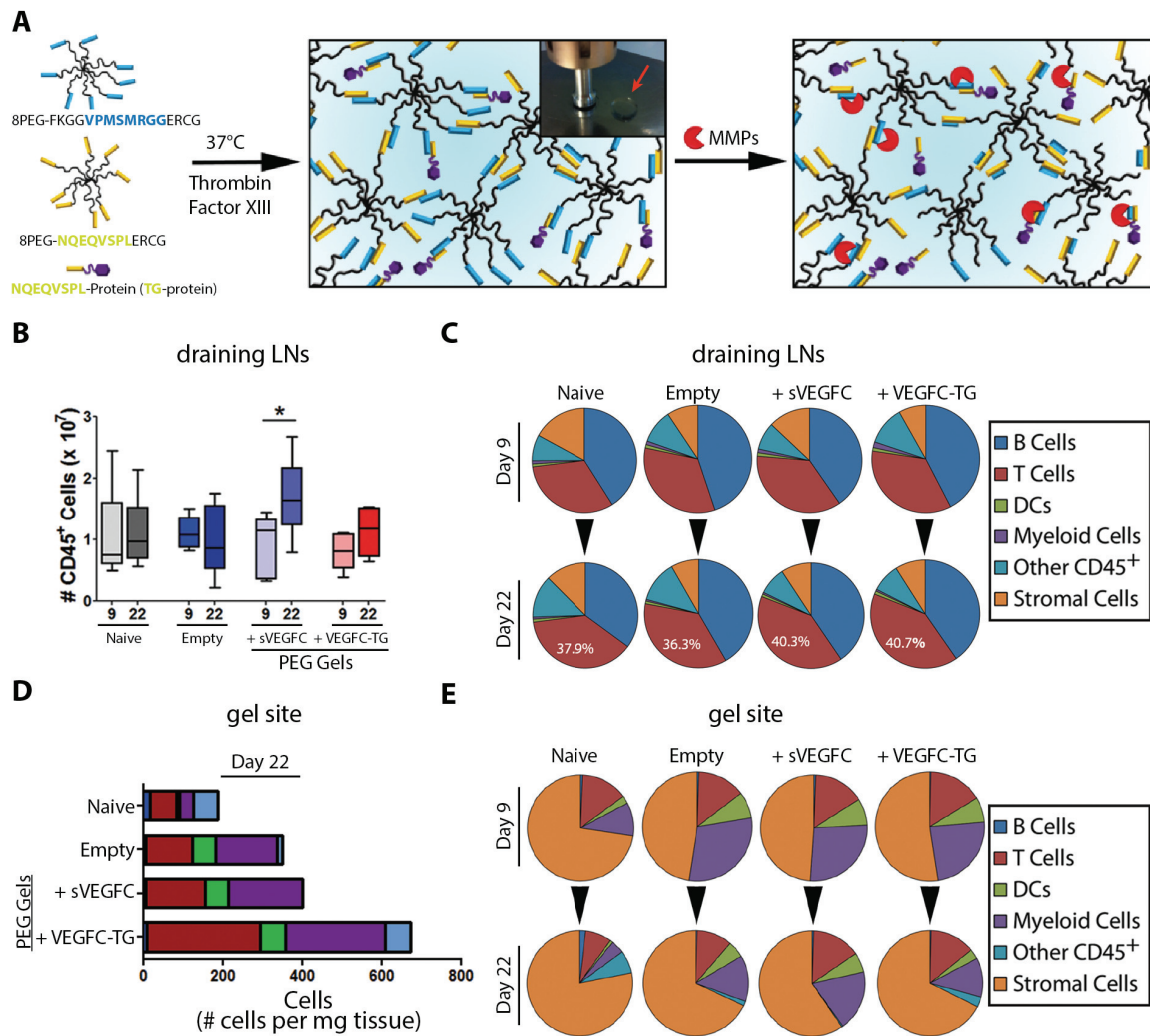


**Figure 4.4 PEG gels induce inflammation at the injection site but not in the dLNs.** (A) Functionalized PEG polymers and TG-proteins are mixed and crosslinked in the presence of thrombin and the clotting Factor XIII to create hydrogels. Inset photo showcases a hydrogel polymerized in vitro (red arrowhead). In the presence of MMPs, the hydrogel matrix is degraded, releasing the free protein. (B-E) Mice were injected intradermally in the anterior back skin with 40 $\mu$ l hydrogels containing sVEGFC (2 $\mu$ g) or VEGFC-TG (2 $\mu$ g). Mice injected with buffer only (naïve) or empty hydrogels (empty) are shown as negative control. Mice were euthanized 9 or 22 days later, and the gel site and draining lymph nodes (brachial) excised. Single cell suspensions of these tissues were used for flow cytometry analysis. (B) Quantification of overall CD45<sup>+</sup> immune cells in the draining lymph node on day 9 and 22. Data shown as box (showing median and 25<sup>th</sup> to 75<sup>th</sup> percentile) and whiskers (showing min and max) (n=5-8, \*p<0.05 with Student's t-test). (C) Distribution of immune cell subsets in the draining lymph node on day 9 and 22. (D) Overall immune cells at the gel site on day 22 and (E) distribution of immune cells subsets at the gel site on day 9 and 22. B cells: B220<sup>+</sup>CD3<sup>-</sup>CD45<sup>+</sup>, T cells: B220<sup>-</sup>CD3<sup>+</sup>CD45<sup>+</sup>, DCs: CD11c<sup>+</sup>B220<sup>-</sup>CD3<sup>+</sup>CD45<sup>+</sup>, myeloid cells: CD11b<sup>+</sup>B220<sup>-</sup>CD3<sup>+</sup>CD45<sup>+</sup>, stromal cells: CD45<sup>-</sup>.

#### 4.4.4 PEG gels induce inflammation at the injection site but not in the draining lymph nodes.

Because we found that fibrin hydrogels induce baseline inflammation in the local microenvironment, we predicted that subtle changes to local immune cell homing or education induced by VEGFC-TG could be masked by the effects of the fibrin hydrogel system alone. We thus switched from using the natural polymer fibrin to the inert synthetic polymer polyethylene glycol (PEG) as the scaffold of our hydrogels. Fibrin-mimic PEG hydrogels have previously been developed, enabling the incorporation of TG-fusion proteins via Factor XIIIa (Ehrbar et al., 2007). Briefly, functionalized PEG polymers and TG-proteins are mixed in the presence of thrombin and the clotting Factor XIII and immediately

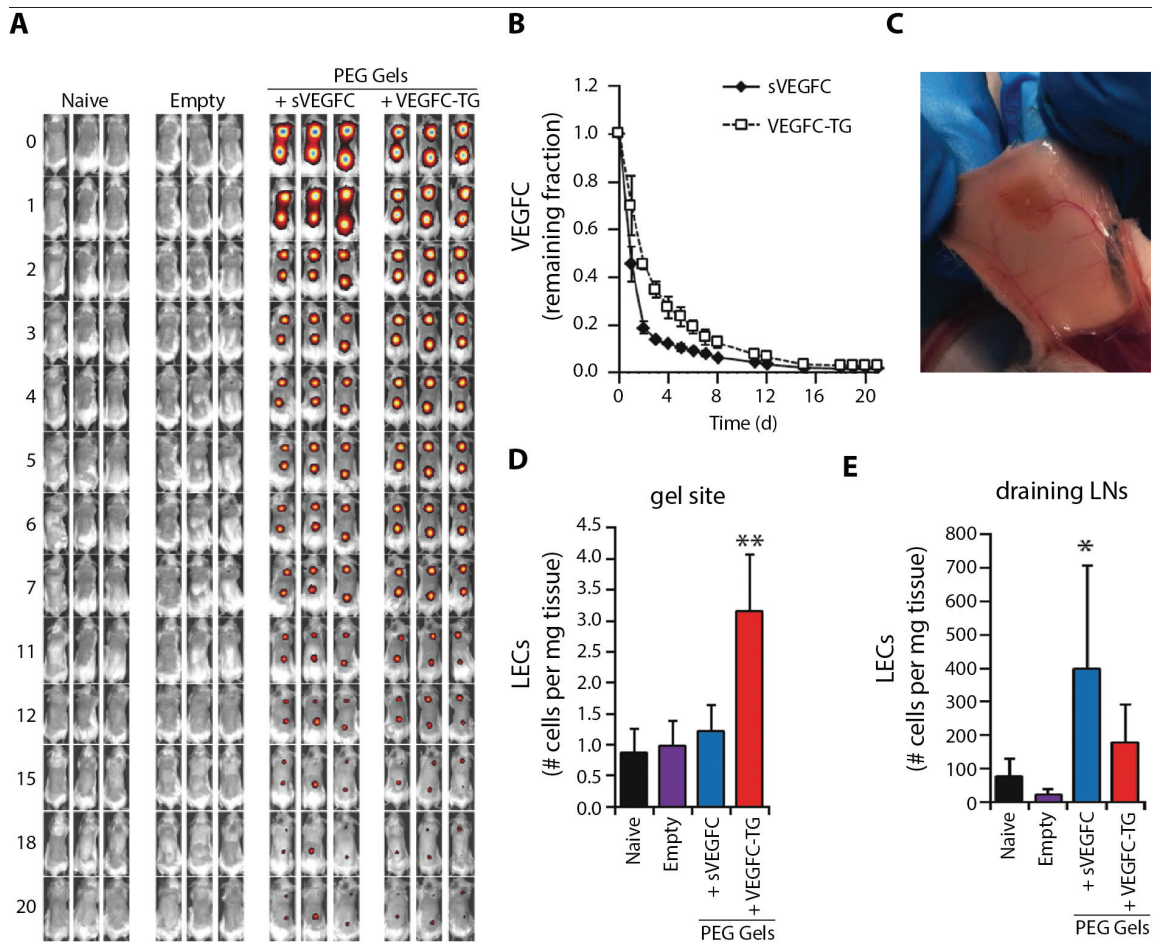


**Figure 4.5 The release rate of VEGFC from PEG hydrogels dictates the site of lymphangiogenesis.** (A-B) Mice were injected intradermally in the anterior back skin with 40 $\mu$ l hydrogels containing AF750-labeled VEGFC, either soluble (sVEGFC, 2 $\mu$ g) or cross-linkable (VEGFC-TG, 2 $\mu$ g) format. Mice injected with buffer only (naïve) or empty hydrogels (empty) are shown as negative control. (A) Intravital fluorescence imaging of the release of AF750-labeled VEGFC from hydrogels over 20 days. (B) Quantification of sVEGFC and VEGFC-TG release profiles over the study period. Data shown as mean  $\pm$  SD (n=3). (C-E) Characterization of lymphangiogenesis at the gel site and at the draining lymph nodes 22 days after hydrogel injection. (C) Representative image of a gel site from a VEGFC-TG releasing PEG hydrogel 22 days after injection. (D-E) Quantification of LECs by flow cytometry (CD45<sup>+</sup>gp38<sup>+</sup>CD31<sup>+</sup>) at the gel site (D) and in the draining brachial LNs (E). (Data points and error bars represent mean  $\pm$  SD of n = 3-4 measurements. \*p < 0.05 by Student's t-test vs. all other groups; \*\*p < 0.05 versus all other treatment groups by one-way ANOVA with Tukey's post-test.

injected intradermally where they polymerize to hydrogels within 10-15 minutes. TG-proteins are slowly released upon MMP mediated cleavage (Figure 4.4A). To assess whether PEG gels induce local inflammation that might obscure VEGFC induced changes, mice were injected intradermally with either empty or VEGFC containing hydrogels. As opposed to fibrin gels, empty PEG gels did not induce inflammation in the draining lymph node, neither on day 9 or 22 after injection (Figure 4.4B-C). Interestingly, addition of soluble VEGFC (sVEGFC) increased the numbers of CD45<sup>+</sup> immune cells (Figure 4.4B), while the distribution of immune cell subsets stayed relatively constant (Figure 4.4C). At the gel site, the presence PEG hydrogels led to an increase of overall CD45<sup>+</sup> immune cells including CD3<sup>+</sup> T cells, myeloid cells and dendritic cells (Figure 4.4D-E), indicating some degree of local inflammation. Interestingly, the addition of VEGFC-TG led to a higher increase of CD45<sup>+</sup> immune cell density as compared to empty or sVEGFC containing gels, suggesting that prolonged local presence of VEGFC can influence immune cell infiltration (Figure 4.4D). Altogether, these data suggest that PEG gels do not induce inflammation in the draining lymph node, but only at the injection site. Furthermore, it shows that release of soluble VEGFC mainly affects the immune composition in the draining lymph node, while release of VEGFC-TG induces changes at the injection site itself.

#### **4.4.5 The release rate of VEGFC from PEG hydrogels dictates the site of lymphangiogenesis.**

Having shown that PEG gels induce less bystander inflammation than fibrin hydrogels, we next assessed the potential of controlled release of VEGFC from PEG gels to induce local lymphangiogenesis. Mice were injected with PEG hydrogels containing fluorescently labeled sVEGFC or VEGFC-TG and their release measured over 20 days using intravital fluorescent imaging (Figure 4.5A). Crosslinking of VEGFC to PEG hydrogels led to a slower *in vivo* release profile (Figure 4.5B). While sVEGFC levels dropped to 20% of administered amounts within 2 days post-injection, it took 3 times longer (6 days) for VEGFC-TG to reach this level. When gel sites were excised at the end of the experiment, VEGFC-TG releasing gels could be recognized by having remodeled the local tissue (Figure 4.5C). Interestingly, while VEGFC-TG induced an increased number of LECs at the gel site (Figure 4.5D), soluble VEGFC did so in the draining lymph node (Figure 4.5E). These results suggest that the rate by which VEGFC is released from PEG hydrogels determines whether lymphangiogenesis is induced in the local tissue or in the draining lymph nodes.

#### **4.4.6 VEGFC-TG induced lymphangiogenesis increases local CCL21 expression.**

Lymphatic endothelial cells can express an array of cytokines (Card et al., 2014), including the lymphocyte homing chemokine CCL21 (Förster et al., 2008; Gunn et al., 1998; Kriehuber et al., 2001; Kuroshima et al., 2004; Shields et al., 2007), which we found to be upregulated in lymphangiogenic melanoma tumors (chapter 3). To evaluate whether lymphangiogenesis induces changes in the local cytokine milieu in the context of a steady-state environment, we screened protein concentrations of protein lysates from gel sites and draining lymph nodes excised on day 7, day 15 and day 22 after injection of PEG hydrogels. Protein concentration analysis using a multiplex assay revealed several clusters of cytokines that were differentially expressed across the different groups within the gel sites (Figure 4.6A-D). On day 7, most clusters differentiated naïve tissues from PEG hydrogel sites independent of the presence of VEGFC-TG, indicating a degree of baseline inflammation following

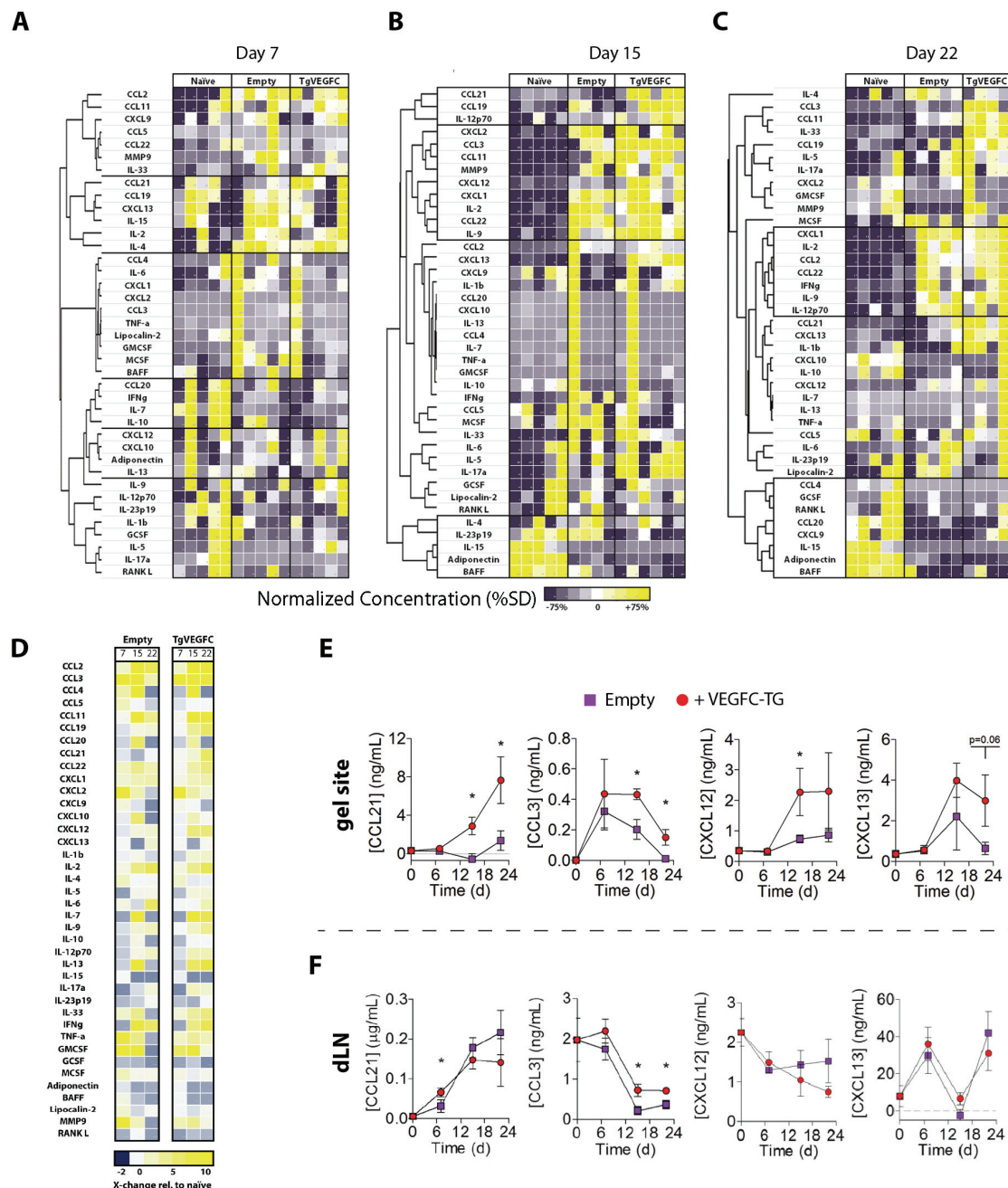


**Figure 4.6 VEGFC-TG induced lymphangiogenesis increases local CCL21 expression.** (A-F) Mice were injected intradermally in the anterior back skin with 40 $\mu$ l hydrogels containing VEGFC-TG (2 $\mu$ g). Mice injected with buffer only (naïve) or empty hydrogels (empty) are shown as negative control. (A-D) Protein lysates from gel sites retrieved on day 7 (A), 15 (B), and 22 (C) were analyzed for the concentration of cytokines using Luminex or ELISA (CCL21, CCL19, CXCL3, IL-15) assays. (A-C) Concentrations were normalized by subtracting the mean protein concentration determined across all mice from the protein concentration determined for an individual mouse, and dividing this by the SD protein concentration determined across all mice. Unsupervised hierarchical clustering of the protein data was performed based on Pearson correlations via GENE-E. (D) The same data from (A-C) normalized to protein concentrations in naïve skin. (E-F) The tissue concentrations of selected immunologic markers assayed in (A-D) are plotted over time with (E) showing the gel site and (F) the draining lymph nodes. Data shown as mean  $\pm$  SD (n=4-6, \*p<0.05 with Student's t-test).



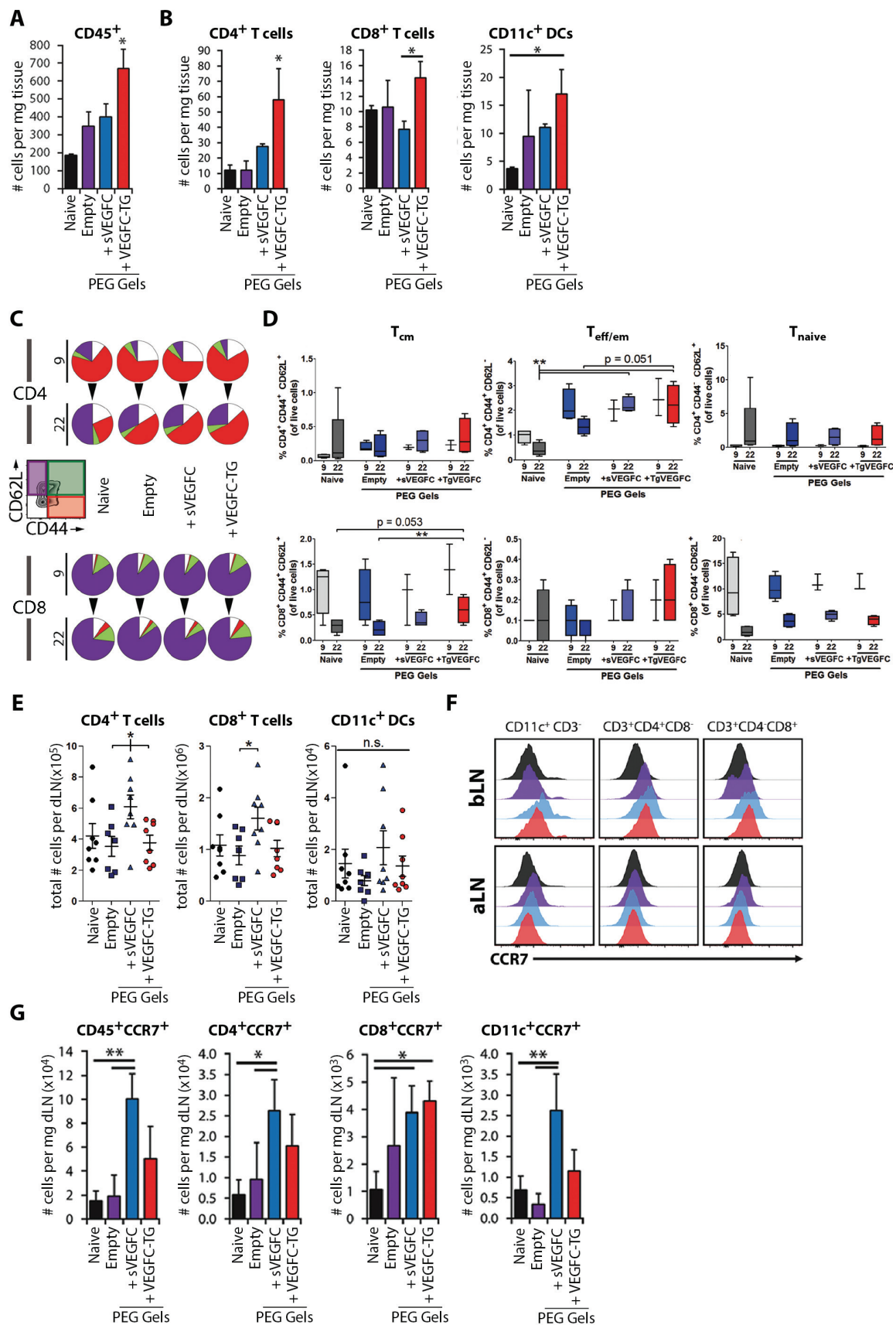


Figure 4.7 Lymphangiogenesis increases the local infiltration of CD4<sup>+</sup> and CD8<sup>+</sup> T cells.

(A-G) Mice were injected intradermally in the anterior back skin with 40µl hydrogels containing sVEGFC (2µg) or VEGFC-TG (2µg). Mice injected with buffer only (naïve) or empty hydrogels (empty) are shown as negative control. Mice were euthanized 9 or 22 days later, and the gel site and draining lymph nodes (brachial) excised. Single cell suspensions of these tissues were used for flow cytometry analysis. The gel site (A-D) and the draining lymph node (E-G) were analyzed. (A) Quantification of CD45<sup>+</sup> immune cells, (B) CD4<sup>+</sup> T cells (CD45<sup>+</sup>CD3e<sup>+</sup>CD11c<sup>-</sup>CD4<sup>+</sup>CD8<sup>-</sup>), CD8<sup>+</sup> T cells (CD45<sup>+</sup>CD3e<sup>+</sup>CD11c<sup>-</sup>CD4<sup>-</sup>CD8<sup>+</sup>), and conventional DCs (CD45<sup>+</sup>CD3e<sup>-</sup>B220<sup>-</sup>CD11b<sup>+</sup>CD11c<sup>+</sup>) normalized to tissue weight at 22 days post injection. (C) Phenotype of infiltrated immune cells based on CD44 and CD62L expression. Percent of central memory T cells (T<sub>cm</sub>, CD62L<sup>+</sup>CD44<sup>+</sup>), effector / effector-memory T cells (T<sub>eff/em</sub>, CD62L<sup>-</sup>CD44<sup>+</sup>), and naïve T cells (T<sub>naïve</sub>, CD62L<sup>+</sup>CD44<sup>-</sup>) of CD4<sup>+</sup> T cells or CD8<sup>+</sup> T cells. (D) Quantification of CD4 and CD8 T cell phenotype as a percentage of total live cells. Data shown as box (showing median and 25<sup>th</sup> to 75<sup>th</sup> percentile) and whiskers (showing min and max) (n=7-8, \*p<0.05 with Student's t-test). (E) Quantification of CD4<sup>+</sup> T cells, CD8<sup>+</sup> T cells, and conventional DCs per brachial LN at 22 days post injection. (F-G) Analysis of CCR7 expression on CD4<sup>+</sup> T cells, CD8<sup>+</sup> T cells, and DCs in regional LNs at 22 days post injection. (F) At the selected implant site, the bLN and not the axillary LN (aLN) is typically the major draining lymph node. Histograms show CCR7 expression of the different immune cell subsets. (G) Quantification of CCR7 expression on CD4<sup>+</sup> T cells, CD8<sup>+</sup> T cells, and conventional DCs at 22 days post injection normalized to weight. Bar graphs or dot plots shown as mean ± SD (n=3-10, pooled from up to 3 independent experiments. \*p<0.05 by Student's t-test. \*\*p<0.05 by one-way ANOVA with Tukey's post-test).

injection (Figure 4.6A). However, on day 15 and day 22, we found clusters specific to the presence of VEGFC-TG (Figure 4.6B-C). Similar patterns were observed when the data was normalized to protein concentrations in naïve tissue (Figure 4.6D). The most notable difference within the gel sites was detected for CCL21, which steadily increased from day 15 (~5.6 fold increase) to day 22 (~6.8 fold increase) when gels were draining VEGFC-TG (Figure 4.6E). Others cytokines including CCL3, CXCL13, CCL5, and IL-33 showed differences. However, their expression was more variable or even decreasing over time, suggesting that their expression is induced due to inflammation in the presence of the hydrogel. In the draining lymph node, we did not find a cytokine that consistently changed over time except for CCL3 (Figure 4.6F), indicating that VEGFC-TG induced lymphangiogenesis leads to local changes in the cytokine environment. These data demonstrate that CCL21 might be one of the most differentially expressed cytokines induced by engineered lymphangiogenesis in peripheral tissues.

#### 4.4.7 Lymphangiogenesis increases local infiltration of CD4<sup>+</sup> and CD8<sup>+</sup> T cells.

CCL21 is a ligand for CCR7, a CC-chemokine receptor mainly expressed by naïve, regulatory and central memory T cells as well as dendritic cells. Classically, CCL21 is expressed in the lymph node by stromal cells, high endothelial venules (HEVs) and LECs to guide CCR7<sup>+</sup> immune cell subsets into the lymph node parenchyma, either from the blood stream (T cells) or from peripheral tissues (DCs) (Cyster, 1999; Förster et al., 2008). In addition, previous reports and the first chapter of this thesis have established the importance of CCL21 in recruiting immune cells into peripheral tissues, mostly in the context of tumors (Peske et al., 2015; Shields et al., 2010) and tertiary lymphoid organs induced during chronic inflammation (Ruddle, 2014). Given that engineered lymphangiogenesis induced changes to the peripheral tissue cytokine milieu, notably CCL21 expression, we asked the question of how this would affect local infiltration of immune cells. We found more CD45<sup>+</sup> immune cells (Figure 4.7A), including CD4<sup>+</sup> T cells, CD8<sup>+</sup> T cells and CD11c<sup>+</sup> dendritic cells (Figure 4.7B) infiltrating the tissue sites of VEGFC-TG but not sVEGFC draining PEG gels. Using CD44 and CD62L staining, we

determined that the majority of infiltrating CD4<sup>+</sup> T cells had an effector phenotype, while CD8<sup>+</sup> T cells were mostly naïve both on day 9 and 22 after gel injection (Figure 4.7C). Interestingly, the presence of VEGFC-TG skewed the infiltrating CD4<sup>+</sup> population towards an effector / effector-memory, and the CD8<sup>+</sup> populations towards a central-memory phenotype (Figure 4.7D). In the draining lymph nodes, we found that soluble VEGFC but not VEGFC-TG increased the number of CD4<sup>+</sup> and CD8<sup>+</sup> T cells, but not of dendritic cells (Figure 4.7C). In line with our hypothesis that lymphangiogenesis associated immune infiltration might be at least partially CCL21 driven, immune cells in the draining but not in the non-draining (axillary) LN had increased CCR7 levels on their surface (Figure 4.7F). In the sVEGFC group, CCR7 expression was not only higher in terms of surface density, but also in terms of absolute numbers of immune cells expressing this receptor (Figure 4.7G). Intriguingly, there was a large fraction of CCR7<sup>+</sup> immune cells that could not be further characterized by the available markers. Collectively, these data demonstrate that engineered lymphangiogenesis can induce the recruitment of T cells and dendritic cells into the local microenvironment, and that this mechanism might partially dependent on the CCL21/CCR7 axis.

#### 4.4.8 Engineered lymphangiogenic sites modulate local immune responses.

We showed in the third chapter of this thesis that lymphangiogenic tumors have increased immune infiltrates as compared to non-lymphangiogenic ones, and that these infiltrates can contribute to anti-tumor immunity when locally activated. Thus, we hypothesized that immune infiltrates attracted by

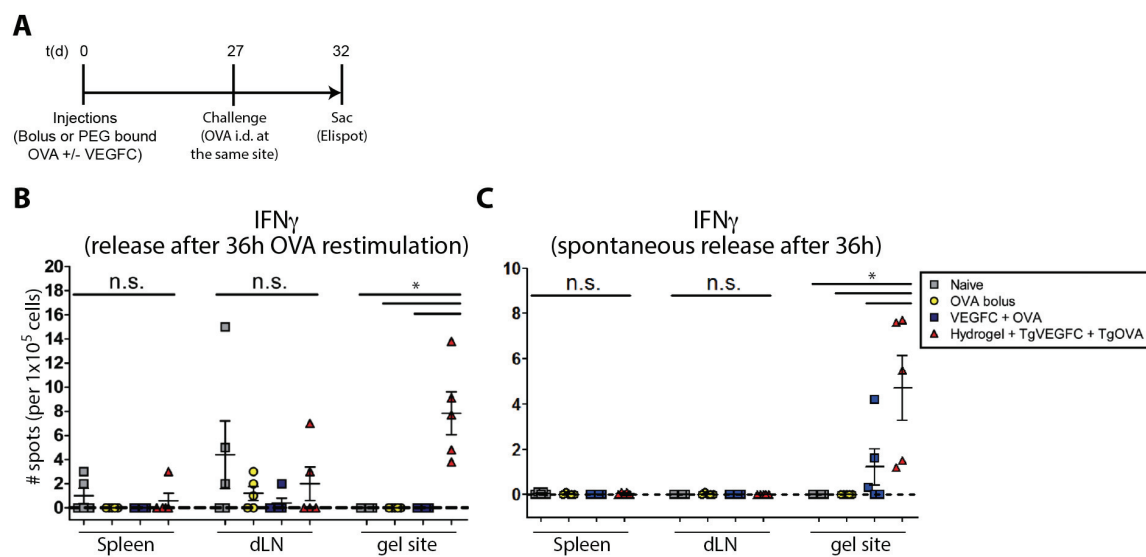


**Figure 4.8 Engineered lymphangiogenic sites modulate local immune responses.** (A-C) Mice were injected intradermally in the anterior back skin with four 40 $\mu$ l hydrogels containing VEGFC-TG (2 $\mu$ g) and OVA-TG (10 $\mu$ g). Mice injected with OVA (10 $\mu$ g) or VEGFC (2 $\mu$ g) + OVA (10 $\mu$ g) served as control. 27 days later, mice were re-challenged with an intradermal injection of OVA (10 $\mu$ g) into the lymphangiogenic site. Mice were euthanized 5 days later, and the gel site and draining lymph nodes (brachial), and spleens excised. (A) Experimental schedule. (B-C) ELISPOT assay showing the number of IFN $\gamma$  producing cells after antigen-specific restimulation (Figure 8B) or spontaneous release (Figure 8C). Data show as mean  $\pm$  SD (n=5, \*p<0.05 by one-way ANOVA with Tukey's post-test).



engineered lymphangiogenesis can be exploited to regulate local immune responses. To assess whether local immunity could indeed be modulated by engineered lymphangiogenesis, mice received intradermal injections either of soluble OVA or OVA + VEGFC, or PEG hydrogels containing the same dose of crosslinked OVA-TG and VEGFC-TG (Figure 4.8A). To establish a local lymphangiogenic environment, we then waited 27 days. Next, mice were challenged with OVA by injecting a bolus of soluble antigen at the same site where they received the first injection. Interestingly, groups that received PEG gels including OVA-TG and VEGFC-TG had increased number of cells secreting IFN $\gamma$  in the gel sites (Figure 4.8B). This was not the case for cells derived from the spleen or draining lymph node, suggesting that immunomodulation only happened locally at the engineered lymphangiogenic site. Interestingly, a similar but slightly decreased IFN $\gamma$  release pattern was observed when single cell suspensions were restimulation with control media that did not contain OVA (Figure 4.8B), indicating that a fraction of IFN $\gamma$  cells did not rely on antigen-specific restimulation. Taken together, these findings suggest that engineered lymphangiogenesis generates an environment which offers a point of intervention for the modulation of therapeutic immune responses.

## 4.5 Discussion

Here we show that engineered lymphangiogenesis can be achieved in mouse dermis by controlled release of VEGFC from PEG hydrogels. Furthermore, we found that these lymphangiogenic sites associated with increased concentrations of the chemokine CCL21, and with increased infiltration of CD4<sup>+</sup> and CD8<sup>+</sup> T cells, as compared to control PEG hydrogels. We thus propose that the orchestration of immune cell recruitment is a novel role of LEC-secreted chemokines in peripheral tissues. Finally, we observed that delivery of the model antigen ovalbumin into engineered lymphangiogenic sites led to increased numbers of IFN $\gamma$  secreting effector cells in response to antigen re-challenge, suggesting opportunities for the regulation of therapeutic immune responses.

In this study, we aimed at engineering of local tissue lymphangiogenesis to dissect mechanisms of LV-mediated peripheral immunoregulation without confounding effects such as tumor-associated inflammation. Approaches to engineering lymphangiogenesis have so far mainly focused on the local delivery of soluble VEGFC, either via simple intradermal injection of recombinant protein (Kajiya et al., 2009; Szuba et al., 2002) or local overexpression using gene therapy (Karkkainen et al., 2001; Saaristo et al., 2002; Tammela et al., 2007; Yoon et al., 2003). In the attempt to treat lymphedema, the accumulation of interstitial fluid due to lack of lymphatic drainage, several studies have even combined the local delivery of VEGFC with the transplantation of lymph nodes (Hartiala and Saaristo, 2010; Lähteenvuo et al., 2011). Even though some of these studies showed induction of functional lymphangiogenesis, these approaches have been facing several issues. For example, adenovirus-mediated VEGFC overexpression in the ear skin induces not only the formation of hyperplastic lymphatic vessels, but also of leaky blood vessel via VEGFR2 signaling (Saaristo et al., 2002). Furthermore, it was shown that high levels of VEGFC may enhance LEC proliferation and cause lymphatic hyperplasia, however, these effects were only transient and did not lead to increased functionality of the lymphatic network (Goldman et al., 2005). The observation that sustained but low-dose release of VEGFA from the extracellular matrix (ECM) induces more physiological blood vessel formation as compared to soluble growth factor (Ehrbar et al., 2004; Martino et al., 2014) led to our hypothesis that the same approach might be suitable for engineering lymphangiogenesis in peripheral tissues *in vivo*. In fact, our lab has previously established that there is a synergy between the controlled release of VEGFC and flow, establishing a morphogenic gradient that fosters lymphatic capillary formation *in vitro* (Helm et al., 2005). Here we show that the sustained release of VEGFC-TG from functionalized PEG hydrogels leads to increased density of LECs at the gel site (Figure 4.5). This study thus introduces a novel approach by which therapeutic lymphangiogenesis can be induced under minimally inflammatory conditions *in vivo*.

Lymphatic endothelial cells express an array of immunomodulatory cytokines that attract T cells, B cells, DCs as well as innate immune cells including monocytes, basophils, and neutrophils (Card et al., 2014). While it is well established that the secretion of CCL21 from LECs is crucial for the chemoattraction and transmigration of 1) tissue-resident DCs into afferent lymphatics during inflammation (Johnson and Jackson, 2010), and 2) circulating T cells into secondary lymphoid organs during steady-state and inflammation (Förster et al., 2008), it is less clear what the function of other

LEC secreted chemokines might be. We hypothesized that chemokines secreted by peripheral tissue LECs could potentially be involved in orchestrating extravasation of immune cells. This hypothesis is supported by recent observations that endothelial cells can translocate chemokines from the abluminal interstitium to their luminal surface, a process called transcytosis (Nibbs and Graham, 2013). This process allows chemokines to be transported intact across cells, so that immune cell extravasation can be influenced by chemokine producing stromal cells adjacent to endothelial cells (Baekkevold et al., 2001; Carlsen et al., 2005; Lee et al., 2003). In line with this hypothesis, we found that lymphangiogenic sites had increased levels of CCL21 (Figure 4.6), and increased density of CD4<sup>+</sup> and CD8<sup>+</sup> T cells (Figure 7). Interestingly, these findings are very similar to the ones presented in the previous chapter, where we showed that lymphangiogenic melanoma tumors had high levels of CCL21 and increased infiltration of naïve T cells. Even though the phenotype of infiltrating T cells was different in this model based on CD44 and CD62L staining, we previously discussed that extravasation of different immune cell subsets depends not only on chemokine gradients, but also on the phenotype of the vasculature, which varies between different tissue contexts (Lanitis et al., 2015). Taken together, our studies around both engineered and tumor-associated lymphangiogenesis establish that peripheral lymphatics might be involved in the chemoattraction of immune cells, possibly by supplying the blood endothelium with chemokines such as CCL21.

Inflammation and lymphangiogenesis in peripheral tissues often goes hand in hand, including during acute and chronic infections, autoimmune diseases such as Crohn's disease and Rheumatoid Arthritis, wound healing, cancer, and transplant rejection (Alitalo, 2011). Classically, it is thought that inflammation precedes lymphangiogenesis, and that the latter represents a crucial feedback mechanism that ensures tissue clearance and resolution of the inflammatory process. For example, pro-inflammatory signaling increases the responsiveness of LECs towards VEGFC and VEGFD (Flister et al., 2010) while promoting the secretion of these growth factors from infiltrating and tissue-resident cell types such as macrophages and DCs (Buckley et al., 2015). Furthermore, infiltrating lymphocytes secrete the lymphangiogenic factor lymphotoxin-alpha at the site of inflammation (Mounzer et al., 2010), further promoting local expansion of LECs. When an inflammation cannot be resolved and turns chronic, immune infiltrates and stroma are often restructured into well-defined lymphoid-like tissues, so called tertiary lymphoid organs (TLOs) (Aloisi and Pujol-Borrell, 2006). Interestingly, lymphatic vessels have been shown to be involved in the orchestration of immune infiltrates within TLOs. In the context of human kidney transplants, LVs within TLOs actively recruit lymphocytes via secretion of CCL21 in the absence of specialized HEVs, suggesting that the infiltrating lymphocytes were recruited locally and not from the circulation (Kerjaschki et al., 2004). In addition, together with the blood endothelium and other stroma cells, the lymphatic endothelium can influence chemokine gradients that lead to the accumulation of lymphocytes within the tissue during chronic inflammation (Burman et al., 2005). Taken together, it becomes clear that there is a close and complex interplay between lymphangiogenesis and the presence of immune cells in peripheral tissues. Even though we correlated engineered lymphangiogenesis with increased CCL21 levels and increased presence of CD4<sup>+</sup> and CD8<sup>+</sup> T cells, we were not able to demonstrate what the underlying mechanisms are. Further studies are needed to understand whether engineered lymphangiogenesis

leads to accumulation or recruitment of immune cells, and if it's the latter, whether it is from the adjacent tissue or from the circulation.

Co-delivery of antigen into lymphangiogenic sites led to enhanced effector immune responses upon antigen-restimulation as assessed by IFN $\gamma$  secretion (Figure 8). This was rather surprising, because lymphatic endothelial cells are usually associated with immunological tolerance (Fletcher et al., 2011; Lund et al., 2012). Even though LECs can present endogenous and exogenous antigens to adaptive immune cells on MHC I and MHC II molecules, they do not express co-stimulatory molecules such as CD40, CD80, and CD86, which are needed to induce effective immune responses (Hirosue and Dubrot, 2015). However, recent data from our lab suggests that LEC-educated T cells might not be terminally tolerized, but rather take on an antigen-primed memory-phenotype, preparing them for reactivation. It is thought that this might be analogous to the non-terminally tolerized phenotype induced in antigen-specific T cells stromal cell type, liver sinusoidal endothelial cell (LSECs). During non-inflammatory conditions, LSECs induce antigen-experienced T cells with a central memory-like phenotype in secondary lymphoid organs (Böttcher et al., 2013). These cells are not terminally committed to their nonresponsive state, but generate effector T cells when their TCR is re-engaged under inflammatory conditions. Notably, we showed in this study that peripheral lymphangiogenesis associated immune infiltrates seem to have a effector/effector-memory (for CD4<sup>+</sup> T cells) or central memory (for CD8<sup>+</sup> T cells) phenotype (Figure 4.7D). Whether these cells were recruited with this phenotype, or whether they were recruited as naïve cells and then locally educated needs to be investigated.

Our study has limitations. First of all, our goal was to understand immunoregulation mechanism of tumor-associated lymphatics by reducing the complexity of the tumor microenvironment into a sterile, engineered lymphangiogenic environment. One of the major drawbacks is that the amount of VEGFC released and the release profile from the two systems might be fundamentally different. In the B16 melanoma model studied in the previous chapter, the tumor cells overexpress VEGFC, presumably leading to an exponential increase of released growth factor as the tumor grows. When we tested the intratumoral concentration on day 9, it was roughly 0.5-1.0 $\mu$ g/ml (Chapter 3, Figure 3.2A, re-calculated as the actual concentration within the tumors) at a tumor volume of about 100 $\mu$ l, resulting in a total amount of 50-100ng of VEGFC at this point in time alone. To counterbalance the different release profiles, we included a high dose of VEGFC-TG (2 $\mu$ g) in the hydrogels, which then exponentially decreased over time (Figure 4.5B). 40ng of remaining VEGFC-TG was reached at day 6 after implantation. However, thanks to the high initial dose and increased retention time of VEGFC-TG in the tissue, one can assume that we were in the same order of magnitude in terms of VEGFC that was available for VEGFR3 signaling. Secondly, even though we were able to abolish inflammation in the draining lymph node by switching from a fibrinogen to a PEG based hydrogel system (Figure 4.3 and 4.4), we still found baseline infiltration of lymphocytes and myeloid cells at the PEG gel injection site (Figure 4.4D). We cannot exclude that these infiltrates themselves participated in inducing lymphangiogenesis, cytokine secretion, and immune cell recruitment (Flister et al., 2010). Engineering approaches that induce completely non-inflammatory lymphangiogenesis are needed to further decipher the role of LECs in immunoregulation. A protein

domain from the placenta growth factors 2 was recently described to binding ECM with super-affinity (Martino et al., 2014). Tagging VEGFC with this domain might allow controlled release *in vivo* without having to crosslink the growth factor into hydrogels. Thirdly, VEGFC itself can act as a chemo attractant, mainly on VEGFR3<sup>+</sup> macrophages (Kerjaschki, 2005). Interestingly, these cells can express VEGFC themselves, leading to a positive feedback loop that further drives lymphangiogenesis (Skobe et al., 2010). Absence of VEGFC-mediated chemoattraction of hematopoietic cells could potentially be achieved by bone marrow transplantation from tissue-specific VEGFR3 knockout into wildtype mice, because complete VEGFR3 knockout mice are embryonic lethality (Dumont et al., 1998). Fourthly, even though we correlated CCL21 and immune infiltration in engineered lymphangiogenic skin sites, we have not formally proven any mechanistic link as we did for lymphangiogenic B16 melanomas in the previous chapter. Further studies, including blocking of CCR7 signaling during engineered lymphangiogenesis will be needed to do so. Fifthly, we have not shown the functionality of engineered lymphangiogenesis in terms of drainage. Even though we observed increased LEC density following controlled release of VEGFC-TG (Figure 4.5D), we have not yet characterized whether these cells form functional vessels that connect to the existing lymphatic network. We assume that highly sensitive drainage assays need to be developed in order to tease out the potentially very small differences in drainage. Finally, there are technical difficulties inherent to studying lymphangiogenesis in peripheral tissue such as skin. Only very small numbers of cells (in the order of 100'000-500'000 per gel site) can be extracted as compared to several millions from lymph nodes and tumors. Thus, one can only do a limited number of meaningful analyses per extracted gel site, one of the reasons why we were not able to have the same readouts for all tissues. More sophisticated analysis methods such as multi-parametric CyTOF and single-cell omics might be needed to do further in depth characterization.

We conclude that controlled released of VEGFC from an injectable scaffold offers a platform for engineering peripheral lymphangiogenesis. Furthermore, we establish that VEGFC-mediated induction of LECs under minimally inflammatory conditions leads to an altered cytokine and immune cell environment, including high levels of CCL21 and increased infiltrating lymphocytes. We thus add more evidence to the previously formulated hypothesis that LECs might have an underappreciated role in driving the formation of TLOs in peripheral tissues (Kerjaschki, 2005). Although we have shown that such an environment can be exploited for the regulation of therapeutic immune responses *in vivo*, further studies will need to establish whether this concept might have applications in clinical settings.

## 4.6 References

- Alitalo, K., 2011. The lymphatic vasculature in disease. *Nature Medicine* 17, 1371–1380. doi:10.1038/nm.2545
- Aloisi, F., Pujol-Borrell, R., 2006. Lymphoid neogenesis in chronic inflammatory diseases. *Nat. Rev. Immunol.* 6, 205–217. doi:10.1038/nri1786
- Andrian, von, U.H., Mempel, T.R., 2003. Homing and cellular traffic in lymph nodes. *Nat. Rev. Immunol.* 3, 867–878. doi:10.1038/nri1222
- Baekkevold, E.S., Yamanaka, T., Palframan, R.T., Carlsen, H.S., Reinholt, F.P., Andrian, von, U.H., Brandtzaeg, P., Haraldsen, G., 2001. The CCR7 ligand elc (CCL19) is transcytosed in high endothelial venules and mediates T cell recruitment. *J. Exp. Med.* 193, 1105–1112. doi:10.1084/jem.193.9.1105
- Bousso, P., 2008. T-cell activation by dendritic cells in the lymph node: lessons from the movies. *Nat. Rev. Immunol.* 8, 675–684. doi:10.1038/nri2379
- Böttcher, J.P., Schanz, O., Wöhleber, D., Abdullah, Z., Debey-Pascher, S., Staratschek-Jox, A., Höchst, B., Hegenbarth, S., Grell, J., Limmer, A., Atreya, I., Neurath, M.F., Busch, D.H., Schmitt, E., van Endert, P., Kolanus, W., Kurts, C., Schultze, J.L., Diehl, L., Knolle, P.A., 2013. Liver-Primed Memory T Cells Generated under Noninflammatory Conditions Provide Anti-infectious Immunity. *Cell Rep* 3, 779–795. doi:10.1016/j.celrep.2013.02.008
- Broggi, M.A.S., Schmalzer, M., Lagarde, N., Rossi, S.W., 2014. Isolation of Murine Lymph Node Stromal Cells. *JoVE* 1–6. doi:10.3791/51803
- Buckley, C.D., Barone, F., Nayar, S., Bénézech, C., Caamaño, J., 2015. Stromal cells in chronic inflammation and tertiary lymphoid organ formation. *Annu. Rev. Immunol.* 33, 715–745. doi:10.1146/annurev-immunol-032713-120252
- Burman, A., Haworth, O., Hardie, D.L., Amft, E.N., Siewert, C., Jackson, D.G., Salmon, M., Buckley, C.D., 2005. A chemokine-dependent stromal induction mechanism for aberrant lymphocyte accumulation and compromised lymphatic return in rheumatoid arthritis. *The Journal of Immunology* 174, 1693–1700. doi:10.4049/jimmunol.174.3.1693
- Card, C.M., Yu, S.S., Swartz, M.A., 2014. Emerging roles of lymphatic endothelium in regulating adaptive immunity. *J. Clin. Invest.* 124, 943–952. doi:10.1172/JCI73316
- Carlsen, H.S., Haraldsen, G., Brandtzaeg, P., Baekkevold, E.S., 2005. Disparate lymphoid chemokine expression in mice and men: no evidence of CCL21 synthesis by human high endothelial venules. *Blood* 106, 444–446. doi:10.1182/blood-2004-11-4353
- Clement, C.C., Rotzschke, O., Santambrogio, L., 2011. The lymph as a pool of self-antigens. *Trends in Immunology* 32, 6–11. doi:10.1016/j.it.2010.10.004
- Cyster, J.G., 1999. Chemokines and the homing of dendritic cells to the T cell areas of lymphoid organs. *J. Exp. Med.* 189, 447–450.
- Cyster, J.G., Schwab, S.R., 2012. Sphingosine-1-Phosphate and Lymphocyte Egress from Lymphoid Organs. *Annu. Rev. Immunol.* 30, 69–94. doi:10.1146/annurev-immunol-020711-075011



- Dalod, M., Chelbi, R., Malissen, B., Lawrence, T., 2014. Dendritic cell maturation: functional specialization through signaling specificity and transcriptional programming. *The EMBO Journal* 33, 1104–1116. doi:10.1002/emboj.201488027
- Dumont, D.J., Jussila, L., Taipale, J., Lymboussaki, A., Mustonen, T., Pajusola, K., Breitman, M., Alitalo, K., 1998. Cardiovascular failure in mouse embryos deficient in VEGF receptor-3. *Science* 282, 946–949.
- Ehrbar, M., Djonov, V.G., Schnell, C., Tschanz, S.A., Martiny-Baron, G., Schenk, U., Wood, J., Burri, P.H., Hubbell, J.A., Zisch, A.H., 2004. Cell-demand liberation of VEGF121 from fibrin implants induces local and controlled blood vessel growth. *Circ. Res.* 94, 1124–1132. doi:10.1161/01.RES.0000126411.29641.08
- Ehrbar, M., Rizzi, S.C., Schoenmakers, R.G., Miguel, B.S., Hubbell, J.A., Weber, F.E., Lutolf, M.P., 2007. Biomolecular hydrogels formed and degraded via site-specific enzymatic reactions. *Biomacromolecules* 8, 3000–3007. doi:10.1021/bm070228f
- Fletcher, A.L., Malhotra, D., Turley, S.J., 2011. Lymph node stroma broaden the peripheral tolerance paradigm. *Trends in Immunology* 32, 12–18. doi:10.1016/j.it.2010.11.002
- Flister, M.J., Wilber, A., Hall, K.L., Iwata, C., Miyazono, K., Nisato, R.E., Pepper, M.S., Zawieja, D.C., Ran, S., 2010. Inflammation induces lymphangiogenesis through up-regulation of VEGFR-3 mediated by NF-kappaB and Prox1. *Blood* 115, 418–429. doi:10.1182/blood-2008-12-196840
- Förster, R., Davalos-Misilitz, A.C., Rot, A., 2008. CCR7 and its ligands: balancing immunity and tolerance. *Nat. Rev. Immunol.* 8, 362–371. doi:10.1038/nri2297
- Goldman, J., Le, T.X., Skobe, M., Swartz, M.A., 2005. Overexpression of VEGF-C causes transient lymphatic hyperplasia but not increased lymphangiogenesis in regenerating skin. *Circ. Res.* 96, 1193–1199. doi:10.1161/01.RES.0000168918.27576.78
- Gunn, M.D., Tangemann, K., Tam, C., Cyster, J.G., Rosen, S.D., Williams, L.T., 1998. A chemokine expressed in lymphoid high endothelial venules promotes the adhesion and chemotaxis of naive T lymphocytes. *Proc. Natl. Acad. Sci. U.S.A.* 95, 258–263.
- Hartiala, P., Saaristo, A.M., 2010. Growth factor therapy and autologous lymph node transfer in lymphedema. *Trends Cardiovasc. Med.* 20, 249–253. doi:10.1016/j.tcm.2011.11.008
- Helm, C.-L.E., Fleury, M.E., Zisch, A.H., Boschetti, F., Swartz, M.A., 2005. Synergy between interstitial flow and VEGF directs capillary morphogenesis in vitro through a gradient amplification mechanism. *Proc. Natl. Acad. Sci. U.S.A.* 102, 15779–15784. doi:10.1073/pnas.0503681102
- Hirosue, S., Dubrot, J., 2015. Modes of Antigen Presentation by Lymph Node Stromal Cells and Their Immunological Implications. *Front Immunol* 6, 446. doi:10.3389/fimmu.2015.00446
- Johnson, L.A., Clasper, S., Holt, A.P., Lalor, P.F., Baban, D., Jackson, D.G., 2006. An inflammation-induced mechanism for leukocyte transmigration across lymphatic vessel endothelium. *J. Exp. Med.* 203, 2763–2777. doi:10.1084/jem.20051759
- Johnson, L.A., Jackson, D.G., 2013. Control of dendritic cell trafficking in lymphatics by chemokines. *Angiogenesis* 17, 335–345. doi:10.1007/s10456-013-9407-0

- Johnson, L.A., Jackson, D.G., 2010. Inflammation-induced secretion of CCL21 in lymphatic endothelium is a key regulator of integrin-mediated dendritic cell transmigration. *Int. Immunol.* 22, 839–849. doi:10.1093/intimm/dxq435
- Joukov, V., Sorsa, T., Kumar, V., Jeltsch, M., Claesson-Welsh, L., Cao, Y., Saksela, O., Kalkkinen, N., Alitalo, K., 1997. Proteolytic processing regulates receptor specificity and activity of VEGF-C. *The EMBO Journal* 16, 3898–3911.
- Julier, Z., Martino, M.M., de Titta, A., Jeanbart, L., Hubbell, J.A., 2015. The TLR4 Agonist Fibronectin Extra Domain A is Cryptic, Exposed by Elastase-2; use in a fibrin matrix cancer vaccine. *Sci. Rep.* 5, 8569–10. doi:10.1038/srep08569
- Kajiya, K., Sawane, M., Huggenberger, R., Detmar, M., 2009. Activation of the VEGFR-3 pathway by VEGF-C attenuates UVB-induced edema formation and skin inflammation by promoting lymphangiogenesis. *Journal of Investigative Dermatology* 129, 1292–1298. doi:10.1038/jid.2008.351
- Karkkainen, M.J., Saaristo, A., Jussila, L., Karila, K.A., Lawrence, E.C., Pajusola, K., Bueler, H., Eichmann, A., Kauppinen, R., Kettunen, M.I., Yla-Herttuala, S., Finegold, D.N., Ferrell, R.E., Alitalo, K., 2001. A model for gene therapy of human hereditary lymphedema. *Proc. Natl. Acad. Sci. U.S.A.* 98, 12677–12682. doi:10.1073/pnas.221449198
- Kerjaschki, D., 2014. The lymphatic vasculature revisited. *J. Clin. Invest.* 124, 874–877. doi:10.1172/JCI74854
- Kerjaschki, D., 2005. The crucial role of macrophages in lymphangiogenesis. *Journal of Clinical Investigation* 115, 2316–2319. doi:10.1172/JCI26354
- Kerjaschki, D., Regele, H.M., Moosberger, I., Nagy-Bojarski, K., Watschinger, B., Soleiman, A., Birner, P., Krieger, S., Hovorka, A., Silberhumer, G., Laakkonen, P., Petrova, T., Langer, B., Raab, I., 2004. Lymphatic neoangiogenesis in human kidney transplants is associated with immunologically active lymphocytic infiltrates. *Journal of the American Society of Nephrology* 15, 603–612. doi:10.1097/01.ASN.0000113316.52371.2E
- Kriehuber, E., Breiteneder-Geleff, S., Groeger, M., Soleiman, A., Schoppmann, S.F., Stingl, G., Kerjaschki, D., Maurer, D., 2001. Isolation and characterization of dermal lymphatic and blood endothelial cells reveal stable and functionally specialized cell lineages. *J. Exp. Med.* 194, 797–808.
- Kuroshima, S.-I., Sawa, Y., Yamaoka, Y., Notani, K., Yoshida, S., Inoue, N., 2004. Expression of cys–cys chemokine ligand 21 on human gingival lymphatic vessels. *Tissue and Cell* 36, 121–127. doi:10.1016/j.tice.2003.10.004
- Kushwah, R., Hu, J., 2010. Dendritic cell apoptosis: regulation of tolerance versus immunity. *The Journal of Immunology* 185, 795–802. doi:10.4049/jimmunol.1000325
- Lanitis, E., Irving, M., Coukos, G., 2015. Targeting the tumor vasculature to enhance T cell activity. *Curr. Opin. Immunol.* 33, 55–63. doi:10.1016/j.coi.2015.01.011

- Lähteenvuo, M., Honkonen, K., Tervala, T., Tammela, T., Suominen, E., Lähteenvuo, J., Kholová, I., Alitalo, K., Ylä-Herttuala, S., Saaristo, A., 2011. Growth factor therapy and autologous lymph node transfer in lymphedema. *Circulation* 123, 613–620. doi:10.1161/CIRCULATIONAHA.110.965384
- Lee, J.S., Frevert, C.W., Wurfel, M.M., 2003. Duffy antigen facilitates movement of chemokine across the endothelium in vitro and promotes neutrophil transmigration in vitro and in vivo. *The Journal of ...* doi:10.4049/jimmunol.170.10.5244
- Lorentz, K.M., Kontos, S., Frey, P., Hubbell, J.A., 2011. Engineered aprotinin for improved stability of fibrin biomaterials. *Biomaterials* 32, 430–438. doi:10.1016/j.biomaterials.2010.08.109
- Lund, A.W., Duraes, F.V., Hirose, S., Raghavan, V.R., Nembrini, C., Thomas, S.N., Issa, A., Hugues, S., Swartz, M.A., 2012. VEGF-C promotes immune tolerance in B16 melanomas and cross-presentation of tumor antigen by lymph node lymphatics. *Cell Rep* 1, 191–199. doi:10.1016/j.celrep.2012.01.005
- Lund, A.W., Medler, T.R., Leachman, S.A., Coussens, L.M., 2016. Lymphatic Vessels, Inflammation, and Immunity in Skin Cancer. *Cancer Discovery* 6, 22–35. doi:10.1158/2159-8290.CD-15-0023
- Lutz, M.B., Kukulski, N., Ogilvie, A., Rossner, S., Koch, F., Romani, N., Schuler, G., 1999. An advanced culture method for generating large quantities of highly pure dendritic cells from mouse bone marrow. *J. Immunol. Methods* 223, 77–92. doi:10.1016/S0022-1759(98)00204-X
- Martinet, L., Le Guellec, S., Filleron, T., Lamant, L., Meyer, N., Rochaix, P., Garrido, I., Girard, J.-P., 2012. High endothelial venules (HEVs) in human melanoma lesions: Major gateways for tumor-infiltrating lymphocytes. *Oncoimmunology* 1, 829–839. doi:10.4161/onci.20492
- Martino, M.M., Briquez, P.S., Güç, E., Tortelli, F., Kilarski, W.W., Metzger, S., Rice, J.J., Kuhn, G.A., Muller, R., Swartz, M.A., Hubbell, J.A., 2014. Growth Factors Engineered for Super-Affinity to the Extracellular Matrix Enhance Tissue Healing. *Science* 343, 885–888. doi:10.1126/science.1247663
- Mounzer, R.H., Svendsen, O.S., Baluk, P., Bergman, C.M., Padera, T.P., Wiig, H., Jain, R.K., McDonald, D.M., Ruddle, N.H., 2010. Lymphotoxin- $\alpha$  contributes to lymphangiogenesis. *Blood* 116, 2173–2182. doi:10.1182/blood-2009-12-256065
- Nibbs, R., Graham, G.J., 2013. Immune regulation by atypical chemokine receptors. *Nat. Rev. Immunol.* doi:10.1038/nri3544
- Parry, R.V., Chemnitz, J.M., Frauwirth, K.A., Lanfranco, A.R., Braunstein, I., Kobayashi, S.V., Linsley, P.S., Thompson, C.B., Riley, J.L., 2005. CTLA-4 and PD-1 receptors inhibit T-cell activation by distinct mechanisms. *Molecular and Cellular Biology* 25, 9543–9553. doi:10.1128/MCB.25.21.9543-9553.2005
- Patterson, J., Hubbell, J.A., 2010. Enhanced proteolytic degradation of molecularly engineered PEG hydrogels in response to MMP-1 and MMP-2. *Biomaterials* 31, 7836–7845. doi:10.1016/j.biomaterials.2010.06.061
- Peske, J.D., Thompson, E.D., Gemta, L., Baylis, R.A., Fu, Y.-X., Engelhard, V.H., 2015. Effector lymphocyte-induced lymph node-like vasculature enables naive T-cell entry into tumours and enhanced anti-tumour immunity. *Nature Communications* 6, 7114. doi:10.1038/ncomms8114

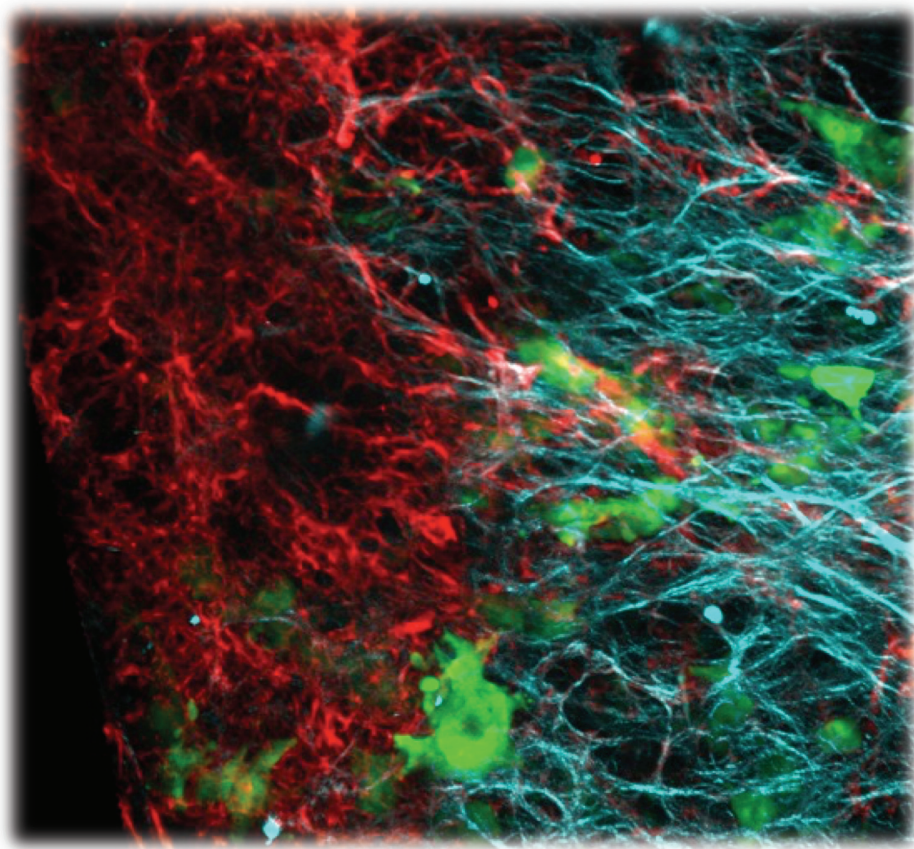
- Randolph, G.J., Angeli, V., Swartz, M.A., 2005. Dendritic-cell trafficking to lymph nodes through lymphatic vessels. *Nat. Rev. Immunol.* 5, 617–628. doi:10.1038/nri1670
- Ruddle, N.H., 2014. Lymphatic vessels and tertiary lymphoid organs. *J. Clin. Invest.* 124, 953–959. doi:10.1172/JCI71611
- Saaristo, A., Veikkola, T., Enholm, B., Hytönen, M., Arola, J., Pajusola, K., Turunen, P., Jeltsch, M., Karkkainen, M.J., Kerjaschki, D., Bueler, H., Ylä-Herttuala, S., Alitalo, K., 2002. Adenoviral VEGF-C overexpression induces blood vessel enlargement, tortuosity, and leakiness but no sprouting angiogenesis in the skin or mucous membranes. *FASEB J.* 16, 1041–1049. doi:10.1096/fj.01-1042com
- Schense, J.C., Hubbell, J.A., 1999. Cross-linking exogenous bifunctional peptides into fibrin gels with factor XIIIa. *Bioconjug. Chem.* 10, 75–81. doi:10.1021/bc9800769
- Shields, J.D., Fleury, M.E., Yong, C., Tomei, A.A., Randolph, G.J., Swartz, M.A., 2007. Autologous chemotaxis as a mechanism of tumor cell homing to lymphatics via interstitial flow and autocrine CCR7 signaling. *Cancer Cell* 11, 526–538. doi:10.1016/j.ccr.2007.04.020
- Shields, J.D., Kourtis, I.C., Tomei, A.A., Roberts, J.M., Swartz, M.A., 2010. Induction of lymphoidlike stroma and immune escape by tumors that express the chemokine CCL21. *Science* 328, 749–752. doi:10.1126/science.1185837
- Skobe, M., Hamberg, L.M., Hawighorst, T., Schirner, M., Wolf, G.L., Alitalo, K., Detmar, M., 2010. Concurrent Induction of Lymphangiogenesis, Angiogenesis, and Macrophage Recruitment by Vascular Endothelial Growth Factor-C in Melanoma. *The American Journal of Pathology* 159, 893–903. doi:10.1016/S0002-9440(10)61765-8
- Szuba, A., Skobe, M., Karkkainen, M.J., Shin, W.S., Beynet, D.P., Rockson, N.B., Dakhil, N., Spilman, S., Goris, M.L., Strauss, H.W., Quertermous, T., Alitalo, K., Rockson, S.G., 2002. Therapeutic lymphangiogenesis with human recombinant VEGF-C. *FASEB J.* 16, 1985–1987. doi:10.1096/fj.02-0401fje
- Tal, O., Lim, H.Y., Gurevich, I., Milo, I., Shipony, Z., Ng, L.G., Angeli, V., Shakhar, G., 2011. DC mobilization from the skin requires docking to immobilized CCL21 on lymphatic endothelium and intralymphatic crawling. *Journal of Experimental Medicine* 208, 2141–2153. doi:10.1084/jem.20102392
- Tammela, T., Saaristo, A., Holopainen, T., Lyytikä, J., Kotronen, A., Pitkonen, M., Abo-Ramadan, U., Ylä-Herttuala, S., Petrova, T.V., Alitalo, K., 2007. Therapeutic differentiation and maturation of lymphatic vessels after lymph node dissection and transplantation. *Nat. Med.* 13, 1458–1466. doi:10.1038/nm1689
- Teijeira, A., Russo, E., Halin, C., 2014. Taking the lymphatic route: dendritic cell migration to draining lymph nodes. *Semin Immunopathol* 36, 261–274. doi:10.1007/s00281-013-0410-8
- Vigl, B., Aebischer, D., Nitschké, M., Iolyeva, M., Röthlin, T., Antsiferova, O., Halin, C., 2011. Tissue inflammation modulates gene expression of lymphatic endothelial cells and dendritic cell migration in a stimulus-dependent manner. *Blood* 118, 205–215. doi:10.1182/blood-2010-12-326447

- Yoon, Y.-S., Murayama, T., Gravereaux, E., Tkebuchava, T., Silver, M., Curry, C., Wecker, A., Kirchmair, R., Hu, C.S., Kearney, M., Ashare, A., Jackson, D.G., Kubo, H., Isner, J.M., Losordo, D.W., 2003. VEGF-C gene therapy augments postnatal lymphangiogenesis and ameliorates secondary lymphedema. *J. Clin. Invest.* 111, 717–725. doi:10.1172/JCI15830
- Zisch, A.H., Schenk, U., Schense, J.C., Sakiyama-Elbert, S.E., Hubbell, J.A., 2001. Covalently conjugated VEGF--fibrin matrices for endothelialization. *J Control Release* 72, 101–113.

## Chapter 5

# Intravital Immunofluorescence Imaging of the Dynamic Tumor Microenvironment

Manuel Fankhauser, Esra Güç, Witold W Kilarski, Amanda W Lund, and Melody A Swartz  
(adapted from Esra Güç\* and Manuel Fankhauser\* et al., JoVE, 2014)



Tumor cells (green) within the fibrillar (cyan) and mesh-like (red) tumor extracellular matrix.  
Two-photon microscopy.



## 5.1 Abstract

Tumors not only consist of tumor cells, but also of a surrounding tumor microenvironment (TME). The TME includes the extracellular matrix (ECM) and non-malignant cells such as fibroblasts, blood and lymphatic endothelial cells, and immune cells. Besides offering a physical scaffold to maintain tissue morphology, the ECM is actively involved in regulating cell and tissue function. It does so by acting via biochemical, biomechanical, and biophysical signaling pathways, such as through the release of bioactive ECM protein fragments, regulating tissue tension, and providing pathways for cell migration. The ECM of the tumor microenvironment undergoes substantial remodeling during tumor initiation and progression, characterized by the degradation, deposition and organization of fibrillar and non-fibrillar scaffolds. However, it is currently unclear how reorganization of ECM within the tumor microenvironment influences processes such as tumor cell migration towards blood and lymphatic vessels or the outcome of cancer immunotherapy. Dynamic imaging of these processes is currently limited to observation within the context of fibrillar collagens that can be detected by second harmonic generation using multi-photon microscopy, leaving the majority of matrix components largely invisible. Here we describe an adapted intravital microscopy method that allows simultaneous, high resolution and dynamic visualization of different components of the tumor microenvironment, including immune cells and fibrillar as well as mesh-like matrix proteins. The protocol includes procedures for tumor inoculation in the thin dorsal ear skin, immunolabeling of TME components, and intravital imaging of the exposed tissue in live mice using fluorescence stereomicroscopy or two-photon microscopy. We found that this intravital immunofluorescence protocol is suitable for imaging interactions between tumor cells and their microenvironment, without inducing noticeable immunotoxicity or photobleaching. For example, this allowed us to observe tumor cell migration along collagen IV structures, and T-cell mediated tumor cell killing over a period of 12 hours. Furthermore, we found that fibrillar matrix of the TME detected with second harmonic generation is spatially distinct from non-fibrillar matrix components such as tenascin C. Taken together, this method allows the dynamic observation of tumor cells in a more holistic microenvironment, which may provide important insights into the mechanisms underlying tumor progression and ultimate success or resistance to cancer immunotherapy.

## 5.2 Introduction

The tumor microenvironment surrounding tumors is defined as the extracellular matrix as well as non-malignant cells including blood and lymphatic endothelial cells, fibroblasts, mesenchymal stem cells, and immune cells (Turley et al., 2015). The tumor microenvironment is actively involved in regulating tumor growth, metastatic spread, as well as access and responsiveness to therapeutics (Joyce and Pollard, 2009; Nakasone et al., 2012; Polyak et al., 2009). Understanding the interactions between tumor cells and the TME is thus crucial for the development of novel prognostic biomarkers and anti cancer therapies (Sund and Kalluri, 2009). The ECM undergoes substantial remodeling during tumor development, tissue inflammation and wound healing (Bonnans et al., 2014). The remodeling of tumor-associated ECM is characterized by the degradation, deposition and organization of fibrillar and non-fibrillar matrix proteins (Lu et al., 2012). One consequence of ECM remodeling is stromal stiffening, which promotes tumor growth and invasion due to stress-induced signaling mechanisms (Pickup et al., 2014) and causes reorganization of blood and lymphatic vessels (Kilarski et al., 2009). However, mechanistic insight into how the ECM contributes to tumor cell migration towards either lymphatic or blood vessels for metastatic dissemination is lacking (Mueller and Fusenig, 2004). In addition, if and how ECM remodeling influences tumor infiltration by lymphocytes such as after cancer immunotherapy is largely unknown (Boissonnas et al., 2007). This is partially due to the fact that intravital imaging of matrix proteins has classically been limited to large, heavily polymerized fibers or fibrillar collagens (I and II, III, V, VI) that can be detected by second harmonic generation using multi-photon microscopy (Chen et al., 2012; Perentes et al., 2009). Therefore, the majority of matrix components including collagen type IV, tenascin C, fibronectin, hyaluronic acid, and perlecan have been largely invisible to intravital imaging approaches (Chen et al., 2012).

Intravital imaging of processes associated with tumor initiation and progression, such as inflammation, metastasis, and matrix remodeling has added tremendously to our understanding on how these complex biologic phenomena unravel in the context of their native tissue (Ellenbroek and van Rheenen, 2014; Munn and Padera, 2014; Pittet and Weissleder, 2011). Intravital imaging is usually done using confocal or multi-photon scanning microscopy, because out-of-focus fluorescent signals detected by more conventional imaging modalities such as fluorescence stereomicroscopy reduce image quality and limit light penetration into the tissue (Halin et al., 2005). Using faster, less expensive epifluorescence stereomicroscopy is only possible with nearly two-dimensional tissues such as the chicken chorio-allantoic membrane or the mouse ear dermis (Kilarski et al., 2012; Kilarski et al., 2013). Most imaging systems take advantage of transgenic mice expressing various fluorescent proteins in a cell type-specific fashion (Martínez-Corral et al., 2012; Snippert et al., 2010). However, these approaches have several disadvantages. Firstly, even though these proteins offer weak phototoxicity, they can induce immune responses against the cells expressing them, thereby disturbing the native tissue context (Steinbauer et al., 2003). Secondly, it is difficult and time-consuming to switch between the observation of specific cell subtypes or phenotypes, as this usually requires the engineering of a new genetic model. Thirdly, fluorescent protein expression is generally restricted to intracellular compartments, and it is thus usually not feasible to image extracellular

structures like basement membrane proteins or chemokine deposits in the tissue (Ohashi et al., 1999). Instead, indirect labeling with antibodies targeting extracellular antigens offers flexibility for virtually any cell-type or matrix specific component (Egeblad et al., 2008; Tal et al., 2011). The major disadvantage of this labeling approach is associated with immunotoxicity mediated by antigen-antibody immune complexes that can trigger complement system dependent cell toxicity and phagocytosis of cells and extracellular structures (Roos et al., 2005). Thus, despite substantial advances within the field of intravital imaging, simpler and more widely accessible methods are needed to image cell behaviors in the context of living tissue physiology.

Our lab recently published a novel intravital imaging method that allows visualization of various extracellular matrix components of the normal skin using a fluorescence stereomicroscope (Kilarski et al., 2013). Intravital immunofluorescence (IF) is based on the innovative concept of using immunostaining for live cells and tissue matrix elements on surgically exposed mouse dermis with causing minimal immuno- and phototoxic side effects. Immunotoxicity of antibody stainings is avoided by saturating Fc $\gamma$  receptors and complement with mouse polyclonal IgGs raised against and immunocomplexed with human IgGs, while phototoxicity is avoided using a special ascorbate buffer. The surgical procedure itself is safe to the dermis vasculature as it relies only on the separation of two skin layers in the ear that are independently innervated, autonomously fed by blood and drained by separate lymphatic circulations. While established imaging techniques are generally limited to about 30 minutes to 6 hours of imaging (Giampieri et al., 2009; Heymann et al., 2015; Lämmermann et al., 2008; Padera et al., 2002; Pinner and Sahai, 2008; Sahai et al., 2005; Wyckoff et al., 2000), intravital IF allows continuous imaging of up to 12 hours. Thus, this experimental setup enables long-term observation of a range of important physiological or pathophysiological events within their native tissue context, including leukocyte trafficking between blood and lymphatic vessels, wound healing processes, and tumor progression.

Here we describe a modified intravital immunofluorescence method that besides allowing long term imaging of the tumor microenvironment using standard fluorescence stereomicroscopy, is also suitable for the visualization using two-photon microscopy. The protocol includes procedures for tumor inoculation in the thin dorsal ear skin, immunolabeling of different components of the tumor microenvironment, and intravital imaging of the exposed tissue in live mice using fluorescence stereomicroscopy and two-photon microscopy. We show that this protocol can be used for the long-term visualization of interactions between tumor cells and their microenvironment, without inducing major side effects such as immunotoxicity or photobleaching. We show examples of dynamic processes such as tumor cell migration along collagen IV structures, and T-cell mediated tumor cell killing over a period of 12 hours. Furthermore, we demonstrate that fibrillar matrix components of the TME detected with second harmonic generation can be deposited in spatially distinct niches from the non-fibrillar matrix protein tenascin C. In conclusion, this method allows the simultaneous, dynamic imaging of tumor cells and several components of the TME that have previously been mostly invisible to observation.

## 5.3 Protocol

All procedures performed on animals were in strict accordance with the Swiss Animal Protection Act, the ordinance on animal protection and the ordinance on animal experimentation. We confirm that our Institutional Animal Care and Use Committee (IACUC), named Commission de Surveillance de l'Etat de Vaud (Permit Number: 2687), approved this study.

### 5.3.1 Tumor inoculation of the ear

1. Culture B16F10-GFP melanoma cells in a 10cm petri dish using Dulbecco's modified Eagle's medium (DMEM) supplemented with 10% fetal bovine serum (FBS).
2. When the cells are 80-90% confluent, wash them with 1X phosphate buffered saline (PBS) and detach them by trypsinization. Spin down cells at 1,500g for 5min at 4°C, resuspend the pellet in 1ml Ringer's buffer and transfer it into a 1.5ml microcentrifuge tube. Spin again and remove all supernatant except a thin layer of medium that stays just above the pellet. Resuspend the cells to end up with a cell slurry.
3. Anesthetize the mouse with a mixture of ketamine/dorbene (75mg/kg-1mg/kg) and confirm that the animal is sufficiently anesthetized by performing a gentle toe pinch. Keep mouse on a rectal thermistor controlled heating pad (37°C) during the whole procedure and protect its eyes with an appropriate ophthalmic ointment.
4. Prepare a Hamilton syringe for the injection of the cells. Remove the tip cap with the needle and load 20µl of cell slurry on top of the tip chamber. Pull back the plunger until 5µl slurry is loaded inside the syringe. Remove the excess slurry from the tip chamber and close the tip cap.
5. Using adhesive tape, fix the proximal edge of the ear on the tip of an index finger. In a 45° angle, slowly insert the Hamilton syringe needle between dorsal dermis and the cartilage. Once inside, penetrate the ear proximal to distal for about 2-3mm. Note: a trained and certified technician should do the cell injection procedure. In addition, this process must be performed slowly and in sequence: first, the needle should be placed horizontally to the ear skin and inserted slowly into the ear dermis. Once the needle is in the skin, press the plunger carefully to inoculate the cells between the two dermal layers of the ear (Figure 5.1A).
6. Inject 3µl of cell slurry and slowly retract the needle from the ear. Let the tumor cells proliferate and form a solid tumor during the following 7-9 days. The tumor growth can be observed by fluorescence stereomicroscopy.

### 5.3.2 Interactions of activated splenocytes with tumor cells *in situ*

To visualize interactions between tumor-specific lymphocytes and tumor cells, this procedure can be performed prior to the immunofluorescence staining of the ear.

1. Collect the spleen of tumor-bearing mouse seven days after intradermal inoculation of GFP-B16F10 melanoma cells into the back skin. Isolate splenocytes with mechanical disruption of the spleen through a 70µm cell strainer.
2. Label splenocytes for 8min at 37°C with 1µM CMTPX CellTracker in PBS. Then, wash the

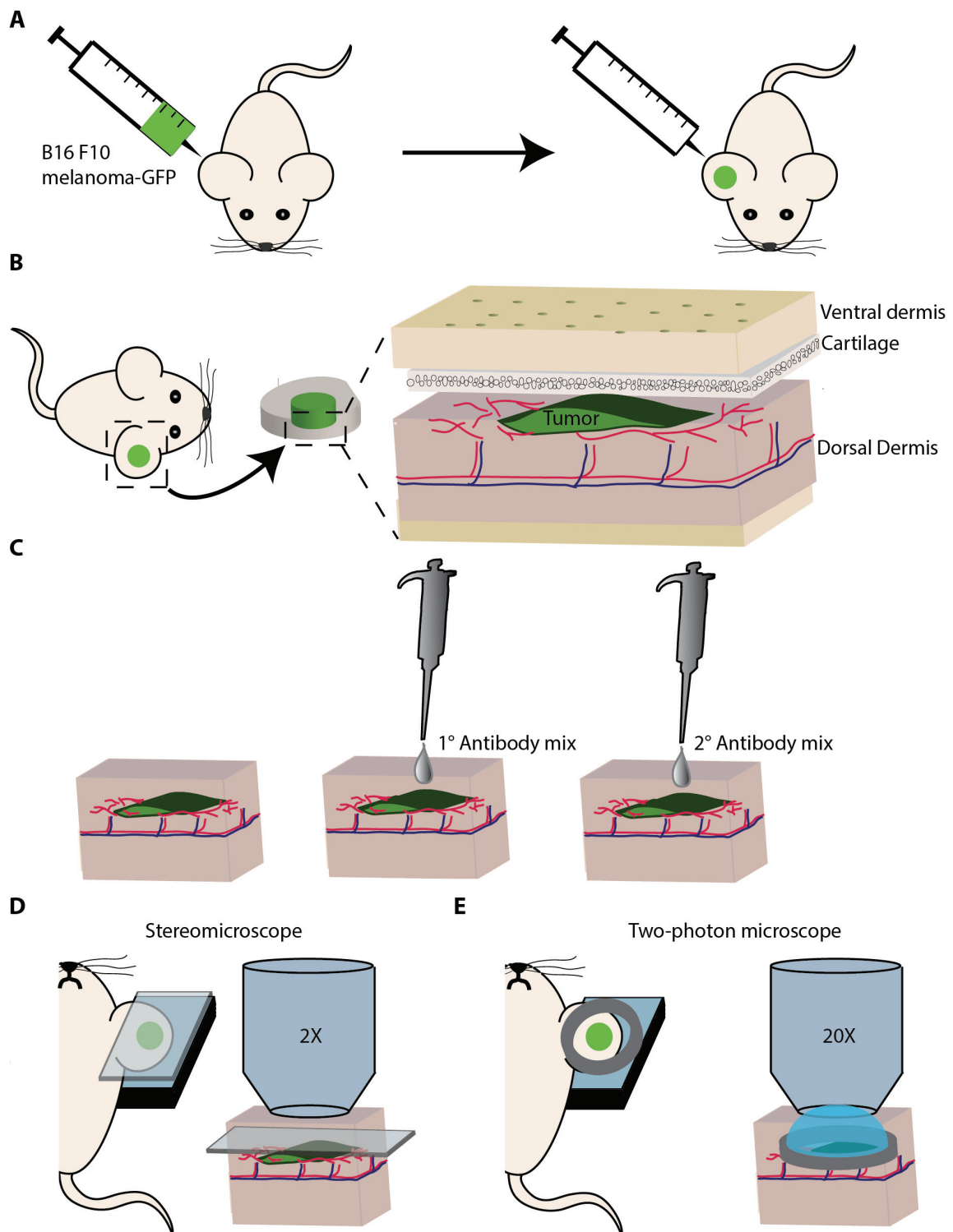


**Figure 5.1 Schematic of the intravital immunofluorescence imaging method.** (A) GFP labeled B16F10 melanoma cells are injected into the mouse ear dermis. (B) 7-9 days after injection, the ventral and dermal ear skin layers are surgically separated from each other. (C) The dorsal dermis containing the tumor mass is immunostained with primary and secondary antibodies against the targets of interest. (D) Imaging setup for acquisition using a fluorescent stereomicroscope. (E) Imaging setup for acquisition using a multiphoton microscope.

cells 4 times in 15ml PBS at 4°C. Finally, inject the cells in 200µl serum free medium into the tail vein of mouse whose ears were inoculated with B16F10-GFP 7 days earlier.

### **5.3.3 Ear surgery**

1. Three days before the experiment, shave the mouse head, and depilate the hairs around the head and ear (for example using hair depilation cream for 10-15 seconds) and thoroughly rinse the area with water.
2. Anesthetize the mouse with a mixture of humidified oxygen and isoflurane (3-4% induction, 1-2% maintenance) and confirm that the animal is sufficiently anesthetized by performing a gentle toe pinch. Increase the isoflurane concentration in steps of 0.1% in case movements are observed (e.g. withdrawal of the paw). Keep mouse on a rectal thermistor controlled heating pad (37°C) during the whole procedure and protect its eyes with an appropriate ophthalmic ointment.
3. Build a platform made out of 8 glued glass histology slides. Turn the mouse on its back and gently place the tumor-bearing ear on the stack of glass slides. Use small stripes of adhesive tape to fixate the anterior and posterior edges of the ear to the stack.
4. Cut the ventral skin of the ear along the antihelix of the mouse pinna using a scalpel. With the help of curved tweezers, gently peel off the ventral dermis and the cartilage from the dorsal dermis where the tumor was inoculated (Figure 5.1B). Pull off the ventral skin and cartilage with curved forceps, exposing the dorsal dermis. NOTE: If a major vessel of the ear is cut or the blood circulation does not return to normal flow within 15 minutes after surgery, the ear cannot be used for imaging. Always keep the opened ear skin wet by using Ringer's buffer and protect the humidity by using a coverslip.
5. In case there is a persistent bleeding from a capillary, stop the bleeding by adding 100µl thrombin (5U/ml) in Ringer's buffer on top of the ear for 5 minutes.
6. Wash the ear twice with approximately 5ml of Ringer's buffer and remove extra liquid with sterile wipes. Immediately proceed to the next step (do not let the open ear dry at any point!).

### **5.3.4 Immunofluorescence staining**

Use Ringer's buffer supplemented with human serum (1:10), mouse polyclonal secondary antibody to human IgG (1:50), and 125IU/ml (2.5mg/ml) aprotinin (AP92; Elastin) (=blocking buffer) for all staining steps. Aprotinin inhibits plasmin, thereby promoting coagulation to limit initial bleeding that may occur after surgery.

1. Fold the part of the ear with the open dermis into the eminentia conchae and dry the outer unopened ear dermis with sterile wipes. Immobilize the ear on the stack of glass slide by applying 0.5µl of surgical glue to the anterior and posterior dorsal edges. Then, gently flatten the dorsal ear dermis onto the glass.
2. Apply primary antibodies targeting extracellular matrix molecules at a concentration of 10µg/ml in a total volume of 100µl blocking buffer to the exposed ear (Figure 5.1C). Cover the ear with a cover slip in order to prevent the staining solution to dry on the ear edges. Incubate for 15min. Wash the ear twice with approximately 5ml of Ringer's buffer.



3. Apply appropriate secondary antibodies or streptavidin conjugates at a concentration of 10 $\mu$ g/ml in a total volume of 100 $\mu$ l blocking buffer to the exposed ear. Cover the ear with a cover slip and incubate for 15min. Wash the ear twice with approximately 5ml of Ringer's buffer.

#### **5.3.5 Intravital imaging using fluorescence stereomicroscopy**

1. For short-term imaging (up to 2 hours), add freshly prepared sterile ascorbate-Ringer's buffer containing 140mM sodium ascorbate, 10mM HEPES, 4mM KCl and 5mM CaCl<sub>2</sub>, at a pH of 7.5 (ascorbate-Ringer's buffer final osmolarity is 320mOsm) on top of the immobilized ear. Cover the ear with a coverslip (Figure 5.1D).
2. For long-term imaging (more than 2 hours), place the outlet of a needle (connected to a reservoir containing ascorbate-Ringer's buffer) under the coverslip, about 0.5cm away from the ear. Use a peristaltic pump at a speed of 1 $\mu$ l/min to constantly deliver ascorbate-Ringer's buffer to the chamber under the coverslip.
3. Change the 1X lens (Leica Microsystems CMS GmbH, working distance 6cm) to a 2X lens (Leica Microsystems CMS GmbH, working distance 2cm). Open the acquisition software (Leica LAS AF) and configure the settings of the fluorescent stereomicroscope. In the camera settings, choose 12bit as the image color depth and adjust the camera range of grey-scale values from 0% (minimum) to 5.1% (maximum) and set gamma correction to 2. Set acquisition gain to 1 (minimum), fluorescence intensity to 1,000 (maximum), magnification set to 280X-320X, and adjust the exposure time avoiding over- or under- exposure (should be less than 1sec). Depending on the number of imaging fields (usually 10 to 20), the time interval for the acquisition cycles should be set between 1 to 2min. Shorter times may cause photobleaching and -toxicity.
4. Choose several fields that contain tumor cells as well as stained ECM proteins (such as in Figure 5.4). Using the motorized stage, acquire images of the appropriate fluorescent channels (such as GFP and AlexaFluor-647 in Figure 5.4) over time (e.g. every 2min).
5. After the experiment, euthanize the mouse according to institutional animal guidelines. In our case, anesthetized mice were euthanized by cervical dislocation followed by exsanguination (intracardiac perfusion).

#### **5.3.6 Intravital imaging using two-photon microscopy**

1. Using silicon grease, build a circular wall of about 2cm diameter and 2-3mm height around the ear, starting at the base of the ear (Figure 5.1E). Make sure there are no leaking points. Fill the circle with ascorbate-Ringer's buffer.
2. Place the mouse on a (motorized) microscope stage and connect the heating pad (37 °C).
3. Open acquisition software (Leica LAS AF) and configure the settings of the multiphoton microscope (LEICA SP5, Leica Microsystems CMS GmbH).
4. Choose several fields that contain tumor cells and stained ECM proteins (such as in Figure 5.5). Acquire images of the appropriate fluorescent channels (such as GFP and AlexaFluor-594 in Figure 5.5) and second harmonic generation over time, e.g. every 2min, with an 20X

immersion lens (HCX APO, 1.00 NA, 2mm working distance).

5. After the experiment, euthanize the mouse according to institutional animal guidelines. In our case, anesthetized mice were euthanized by cervical dislocation followed by exsanguination (intracardiac perfusion).

### **5.3.7 Reagents**

- Hamilton syringe (barrel: 84853; Hamilton, syringe: 7803-05; Hamilton)
- Ringer's buffer (445968; B. Braun Medical AG)
- Aprotinin (AP92; Elastin)
- Thrombin (T7326; Sigma-Aldrich)
- Sodium ascorbate (11140; Sigma-Aldrich)
- Mouse serum raised against human IgG (AB 34834; Abcam)
- Rabbit anti-collagen IV (AB 6581; Abcam)
- Rat anti-perlecan (AB79465; Abcam)
- Goat anti-tenascin C (AF3358; RnD)
- Goat anti-podoplanin (AF3244; RnD)
- Rabbit anti-lyve1 (103-PA50; Reliatech)
- Streptavidin Alexa Fluor 647 (S11222; Invitrogen)
- Streptavidin Alexa Fluor 488 (S11223; Invitrogen)
- Donkey anti-goat 594 (A21113; Invitrogen)
- Donkey anti-rabbit 594 (A21207; Invitrogen)
- Donkey anti-rat 594 (A21209; Invitrogen)
- CMTPX CellTracker (C34552; Lifetechnologies)

## 5.4 Results

### 5.4.1 Immersion of the exposed ear tissue in a large volume of ascorbate buffer inhibits photobleaching during image acquisition.

Immunostaining is not typically done in live tissue, mainly because staining antibodies can form immune complexes that lead to a high staining background and immunotoxicity. Our lab previously published an intravital immunostaining protocol that circumvents these issues in large part (Kilarski et al., 2013). To avoid immunotoxicity, Fc $\gamma$  receptors and complement were saturated with mouse polyclonal IgGs raised against and immunocomplexed with human IgGs, thus blinding phagocytes and the complement system to the subsequent immunostaining. Immersing the exposed ear tissue in anti-oxidant ascorbate-Ringer's buffer ensured that photobleaching was inhibited. However, because we wanted to adapt intravital IF to high-energy two-photon microscopy, we wanted to further optimize the protection from photobleaching, ensuring that the fluorescent probes would be stable for long-term imaging. Thus, we changed two parameters about the use of ascorbate-Ringer's: 1) We noticed that ascorbate-Ringer's oxidized during storage, thereby losing its anti-oxidant activity. We thus started to prepare fresh ascorbate-Ringer's for each experiment. 2) Rather than using a small volume of buffer, we now immersed the tissues in a large volume of ascorbate-Ringer's (100 $\mu$ l) within the chamber where the ears were immobilized, ensuring that the antioxidant capacity would not immediately exhaust. Indeed, we found that adapting the protocol led to increased resistance to photobleaching (Figure 5.2A-B). To assess bleaching of a fluorescent probe that binds abundantly to the ECM, we stained the basal membrane matrix protein collagen IV with AlexaFluor-647 and imaged it continuously for 300 seconds. Images taken at either t=0 or t=300s show that while the fluorescence decreases when the tissue is immersed in normal Ringer's, the signal is stable when it is immersed in ascorbate-Ringer's (Figure 5.2A). Note that 300 seconds of constant imaging time corresponds to 10 hours of imaging when pictures are collected for 500ms every one minute (the average imaging settings). We further confirmed that adaptation of the ascorbate-Ringer's protocol was an improvement from the initial description (Kilarski et al., 2013), as photobleaching could now be completely prevented during 17.5 minutes of continuous imaging (Figure 5.2B). This data suggests that long-term intravital imaging with a fluorescence stereomicroscope can be achieved without inducing photobleaching when a large volume of freshly prepared ascorbate-based buffer is used to protect the exposed tissue.

### 5.4.2 Intravital immunofluorescence can be used to visualize ECM components such as perlecan and CCL21 in the normal mouse ear.

We next asked whether our adapted intravital immunofluorescence method was suitable for the visualization of components of the tumor microenvironment, such as lymphatic vessels, ECM proteins and ECM-bound chemokines. To validate the protocol, we performed intravital IF for perlecan (basement membrane), Lyve-1 (lymphatics), podoplanin (lymphatics), and the chemokine CCL21 (Figure 5.3A-D). Structures such as blood vessels and collecting lymphatics can be distinguished based on their morphology after immunostaining for perlecan (Figure 5.3A). Direct staining for specific

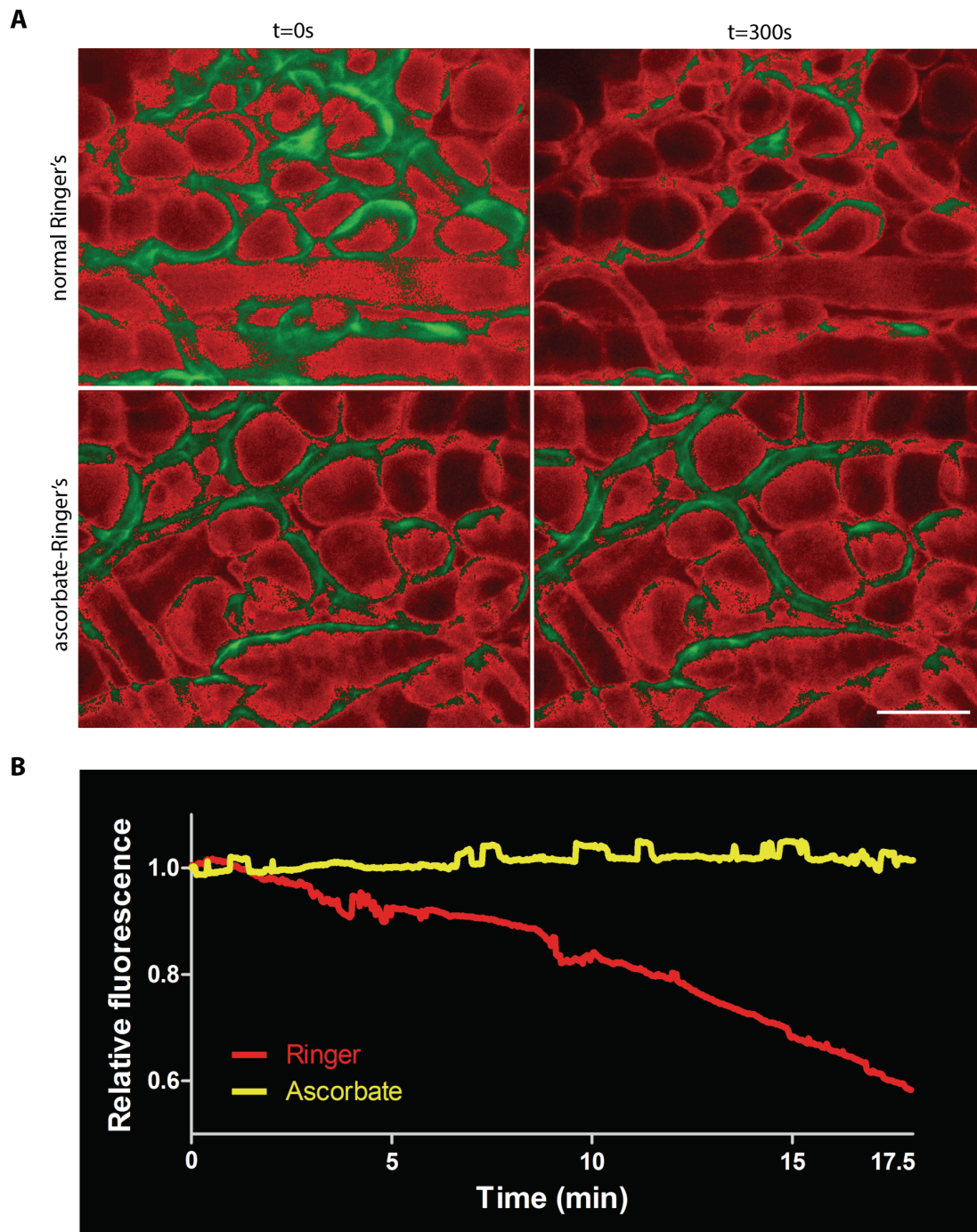


**Figure 5.2 Placing the exposed ear tissue in a large volume of ascorbate buffer inhibits photobleaching during image acquisition.** (A) Tissue was stained first with a biotinylated antibody against collagen IV, a basement membrane matrix protein. The staining was detected with streptavidin-AF647 (red), and then constantly imaged for 300 seconds in either normal Ringer's buffer (upper panel) or ascorbate-Ringer's (lower panel). The brightest 25% of pixel intensity values are colored in green. (B) Quantification of immunofluorescence decay over 17.5m during continuous image acquisition (50% decay in Ringer's vs. 0% in ascorbate-Ringer's). Values were normalized to the initial fluorescence. Image acquisition was done using an immunofluorescence stereomicroscope. Scale bar in (A): 100 $\mu$ m.

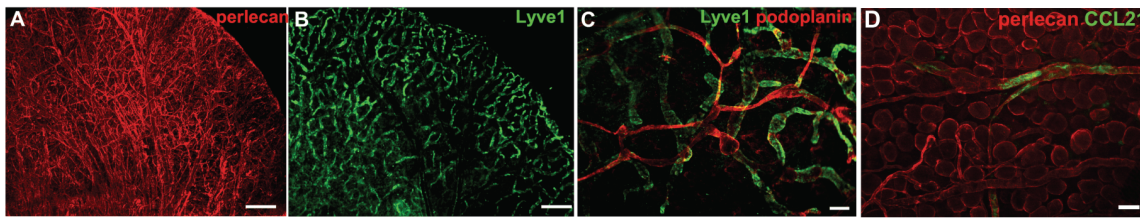


**Figure 5.3 Intravital immunofluorescence can be used to visualize ECM components such as perlecan and CCL21 in the normal mouse ear.** (A) Staining for perlecan, a basement membrane component, depicts all blood and lymphatic vessels, nerves, muscle fibers and adipocytes. (B) Lyve1 staining marks the initial lymphatic capillary network. (C) Co-staining for Lyve1 (green) and podoplanin (red), a pan-lymphatic marker, depicts networks of initial (Lyve1<sup>+</sup>podoplanin<sup>low</sup>) and collecting lymphatics (Lyve1<sup>+</sup>podoplanin<sup>high</sup>). The dorsal ear dermis can be imaged using classic fluorescence stereomicroscopy (without optical sectioning) as the ear dermis has low number of adipocytes that would otherwise cover the imaging field. (D) CCL21 staining (green) on lymphatic basement membrane stained for perlecan (red). Images collected with an immunofluorescence stereomicroscope. Scale bars in (A) and (B): 1mm; in (C): 100μm; and in (D): 50μm.

cell surface markers such as Lyve1 (Figure 5.3B) and podoplanin (Figure 5.3C) further allows distinguishing initial, capillary lymphatics (Lyve1<sup>+</sup>podoplanin<sup>low</sup>) from lymphatic collectors (Lyve1<sup>+</sup>podoplanin<sup>high</sup>). Staining for matrix-bound CCL21 revealed chemokine deposits on the basement membrane of lymphatic collectors identified with the staining for perlecan (Figure 5.3D). Taken together, this data shows that intravital immunofluorescence is suitable for the visualization of components of the ECM that are often part of the tumor microenvironment.

#### **5.4.3 Intravital immunofluorescence is suitable for the long-term visualization of interactions between tumor cells and their microenvironment including anti-tumor immune responses.**

Having demonstrated that intravital IF can be used to visualize components of the extracellular environment over prolonged periods of time in the normal mouse ear, we next explored whether this approach would be suitable for imaging of an actual tumor microenvironment. We first assessed whether B16F10-GFP melanoma cells would be viable and interacting with the microenvironment when placed directly on the exposed and immunostained ear dermis. We thus freshly isolated B16F10-GFP tumor cells and added 100'000 cells directly on the exposed ear dermis that was already immunostained for collagen IV (Figure 5.4A). We observed that after adhering to the tissue, some groups of cells started to migrate along the basement membrane of blood vessels and adipocytes (Figure 5.4A, white arrows), indicating that even though they were simply placed on the exposed naïve tissue, tumor cells were viable and could start interacting with the local microenvironment. To mimic a more natural situation, we next assessed how tumor cells interact with the microenvironment after they established themselves within the tissue. To do so, mice ears were inoculated with B16F10-GFP cells, and the cells given time to organize *in situ* for a few days before imaging. As we were specifically interested in visualizing anti-tumor immune responses, we adoptively transferred tumor-educated splenocytes into these mice seven days after inoculation of the ear tumors. Five hours later, enough time for the adoptively transferred cells to reach the tumor site, the dorsal ear dermis was exposed and immunostained for collagen IV. Because imaging of entire tumor



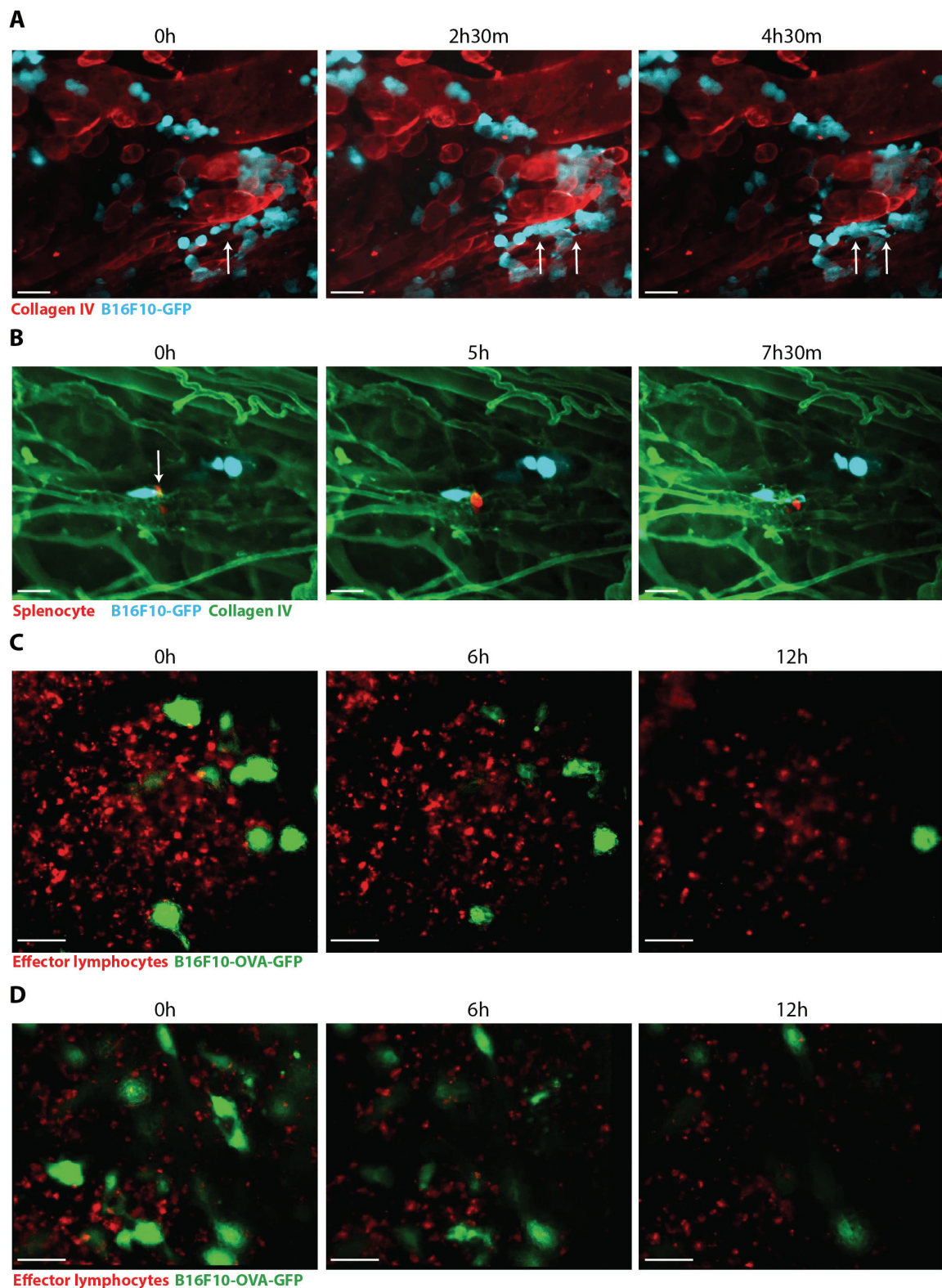


**Figure 5.4** Intravital immunofluorescence is suitable for the long-term visualization of interactions between tumor cells and their microenvironment including anti-tumor immune responses. (A) The exposed ear dermis of a non-tumor bearing mouse was immunostained for collagen IV, and freshly isolated B16F10-GFP tumor cells were directly added (100'000 cells in 50 $\mu$ l Ringer's buffer) on top of the exposed ear. Images were then collected every 1.5 minutes with an



immunofluorescence stereomicroscope over 5 hours. Migration of tumor cells along the basement membrane of blood vessels and adipocytes was observed (white arrows). (B) Seven days after inoculation, a B16F10-GFP tumor-bearing mouse received adoptive transfer of tumor-educated CMPTX-labeled splenocytes. Five hours later, the tumor microenvironment in the dorsal ear dermis was exposed and immunostained for collagen IV. Images were then collected over 8 hours every 47 seconds with an immunofluorescence stereomicroscope. Rare interactions (white arrow) of splenocytes (red) with tumor cells (cyan) within the context of the collagen IV matrix (green) could be observed, even if they did not seem to result in tumor cell killing. (C-D) One day after inoculation, a B16F10-OVA-GFP tumor-bearing mouse received an OVA-specific vaccination (40 $\mu$ g OVA + 20 $\mu$ g CpG) to raise an endogenous anti-tumor immune response. Eight days later, the tumor microenvironment in the dorsal ear dermis was exposed and immunostained for CD69, a marker of T cell activation. Images were then collected over 12 hours every 2 minutes with an immunofluorescence stereomicroscope. In two different imaging fields, (C) and (D). Abundant interactions of activated immune cells (red) with tumor cells (green) could be observed, most of which resulted in tumor cell killing within the observed time. Scale bar in all images: 50 $\mu$ m.

---

masses generally caused out-of-focus images, we chose to image fields that only showed single tumor cells dispersed within the tissue (Figure 5.4B). We found that a splenocytes arrived from the circulation (Figure 5.4B, left panel, white arrow) and interacted with a tumor cell for almost 8 hours (Figure 5.4B, center and right panel) before leaving again (Figure 5.4B, right panel). Interestingly, the interaction between the tumor cell and the splenocyte did not seem to induce tumor cell killing in this case, indicating that it might have been a non-antigen specific interaction. Finally, to induce a potent endogenous anti-tumor immune response, a B16F10-OVA-GFP tumor-bearing mouse received an OVA-specific vaccination (40 $\mu$ g OVA + 20 $\mu$ g CpG) one day after tumor inoculation into the ear. Eight days later, the tumor microenvironment in the dorsal ear dermis was exposed and immunostained for CD69, a marker of T cell activation. Images were then collected over 12 hours every 2 minutes with an immunofluorescence stereomicroscope (Figure 5.4C and D). Strikingly, we were able to visualize two different fields with extensive infiltration of activated immune cells that were swarming around tumor cells. These interactions induced tumor cell death, as most of the tumor cells underwent apoptosis and disappeared within the 12 hours of imaging. This was not an artifact due to photobleaching or out-of-focus imaging, as residual tumor cells and activated immune cells were still clearly visible at the end of the experiment (Figure 5.4C and D, right panels). These results demonstrate that intravital immunofluorescence is suitable for the observation of tumor cell behavior in their complex microenvironment over prolonged periods of time, allowing one to study processes such as tumor cell migration along ECM and interactions between tumor cells and anti-tumor immunity.

#### **5.4.4 Intravital two-photon microscopy can be used to visualize B16F10 melanoma cells in the context of fibrillar and non-fibrillar extracellular matrix proteins.**

Because we found that intravital IF was suitable for long-term imaging using fluorescent stereomicroscopy, we next asked whether the same staining technique is suitable for intravital imaging using high-energy two-photon microscopy. Amongst other applications, combining second harmonic generation and fluorescence would allow us to simultaneously visualize fibrillar and non-fibrillar ECM networks, which to our knowledge has not previously been achieved *in vivo* (Brown et al., 2003). The B16-F10 tumor stroma of an exposed dorsal mouse ear was exposed 9 days after

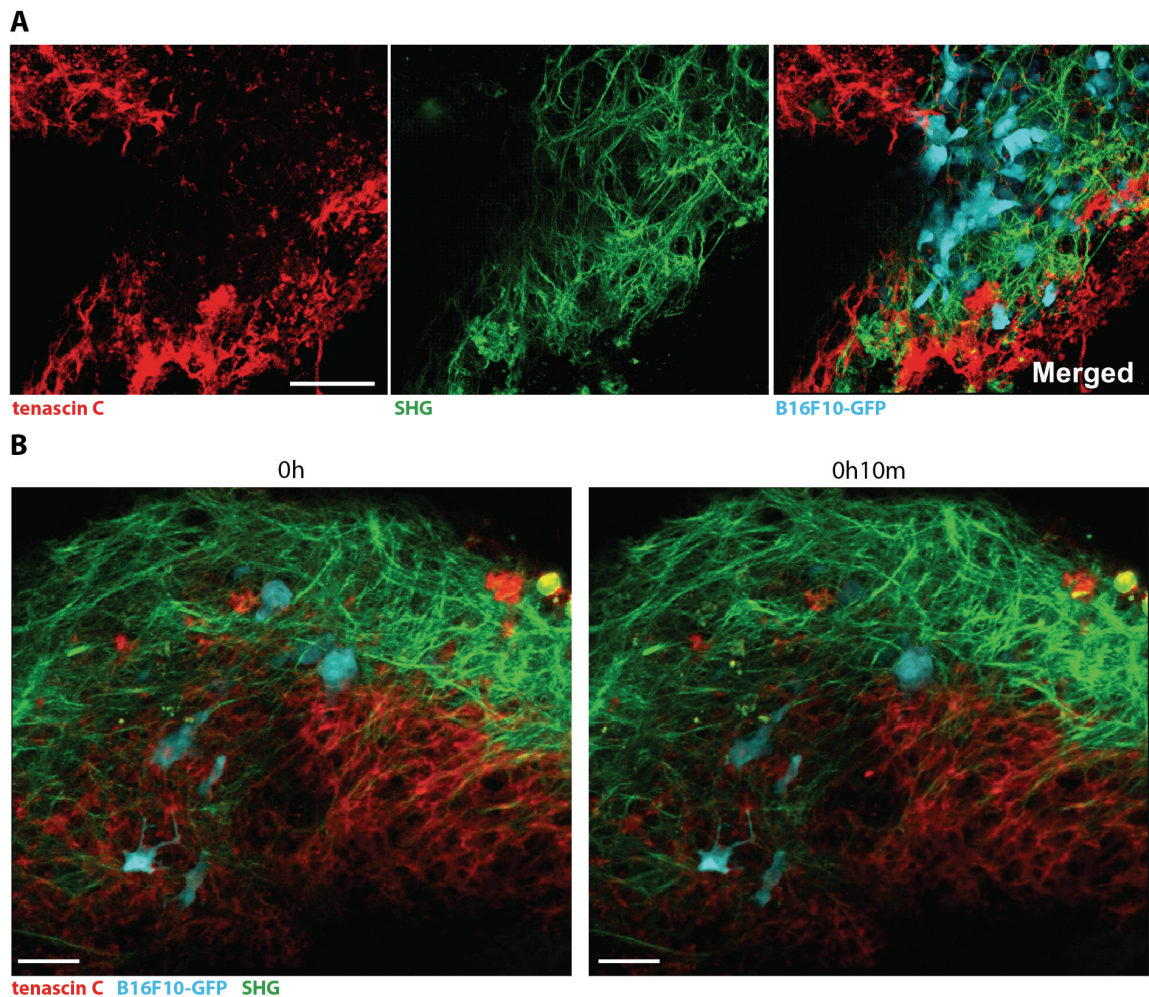


**Figure 5.5 Intravital two-photon microscopy can be used to visualize B16F10 melanoma cells in the context of fibrillar and non-fibrillar extracellular matrix proteins.** The B16-F10 tumor stroma of an exposed dorsal mouse ear was imaged 9 days after inoculation. The fluorescent signal was protected by application of ascorbate-Ringer's buffer onto the tissue, and images collected with a two-photon microscope. (A) Fluorescence of the tenascin C (red) network (left panel) and second harmonic generation (SHG, green) (center panel) of fibrillar collagens were detected. These two networks are superimposed with B16F10-GFP tumor cells (cyan) (right panel). Non-fibrillar ECM represented by tenascin C does not seem to overlap with fibrillar collagens detected with SHG. Images were acquired over 44, 4x averaged z-sections with z-step 1.0 $\mu$ m. The maximum intensity projection is shown. Scale bar: 100 $\mu$ m. (B) Field of the tumor microenvironment showing tenascin C (red), fibrillar collagens (green) and B16F10-GFP tumor cells (cyan). Images were acquired over 11, 4x averaged z-sections with z-step 1.9 $\mu$ m. Images were taken every minute over 10 minutes. The maximum intensity projection at a given time point is shown. Scale bar: 50 $\mu$ m.

inoculation, and an immunostaining for tenascin C performed. Next, GFP labeled tumor cells and tenascin C were imaged *in vivo* using fluorescence stereomicroscopy, and fibrillar ECM using SHG capabilities of a two-photon microscope. Interestingly, we found that tenascin C, a matrix protein that is expressed during tumorigenesis, wound healing and inflammation (Midwood and Orend, 2009) is deposited in different locations of the tumor microenvironment than fibrillar collagens (Figure 4A). Using two-photon microscopy with immunostaining is problematic the high photon flux used in these

experiments can quickly bleach fluorescent dyes that are not protected from oxidation (Patterson and Piston, 2000). To assess whether our adapted protocol using ascorbate-Ringer's might protect the immunostaining, we performed a time-lapse experiment where we imaged the same field containing tenascin C, fibrillar collagens, and tumor cells every minute over 10 minutes (Figure 5.5B). Indeed, the signal of immuno-labeled tenascin C did not noticeably decrease over the course of the experiment (Figure 5.5B, left vs. right panel). Collectively, these data show that our intravital immunofluorescence protocol allows the dynamic observation of tumor cells in the context of fibrillar and non-fibrillar extracellular matrix proteins using intravital two-photon microscopy.

## 5.5 Discussion

Here we present a novel intravital microscopy method that allows simultaneous, high resolution and dynamic visualization of different components of the tumor microenvironment, including immune cells and fibrillar as well as mesh-like matrix proteins. This method addresses several shortcomings of current intravital imaging techniques: (i) Even though intravital immunostaining offers a high variety of potential target stainings, existing protocols are not able to achieve homogenous distribution of primary and secondary antibodies in the tissue except in the rare cases where the targets are within the blood or lymphatic network (Egawa et al., 2013; Kilarski et al., 2013; Woodruff et al., 2014). (ii) Concerns about immunotoxicity and photobleaching have limited the applications for intravital immunofluorescence, especially in the context of high energy two-photon microscopy (Patterson and Piston, 2000; Roos et al., 2005). (iii) The use of genetically modified reporter mice allows for specific cell types to be imaged, but requires their availability (or substantial effort to create new ones) and limits the number of interacting cell types that can be studied. (iii) Extracellular matrix can be imaged *in vivo* using second harmonic generation, but this technique can only detect fibrillar collagens, leaving a large number of important extracellular components such as basement membranes, fibronectins, tenascins, growth factors, chemokines and tissue glycosaminoglycans out of reach for current research. Our method overcomes some of these limitations. By performing intravital IF in a controlled environment in the exposed ear dermis, we show that multiple cell types, tissue structures, deposits of heparin sulfate binding growth factors (e.g. VEGF (Jakobsson et al., 2006)) and chemokines (e.g. CCL21 (Kilarski et al., 2013; Weber et al., 2013) and Figure 5.3D), or extracellular matrix proteins can be visualized over prolonged periods of time without inducing major side effects. Thus, this method allows one to look at live processes within the tissue microenvironment in a more holistic manner while simultaneously tracking blood and/or lymphatic flows. Applications of intravital IF include but are not limited to the investigation of skin immunity during inflammation, mechanisms of transplant rejection, blood and lymphatic vessel growth during tumorigenesis, and of anti-tumor immune responses. To this end, we were able to observe lymphocyte mediated tumor killing in real time using standard fluorescence stereomicroscopy (Figure 5.3C-D), achieving similar results as other studies that used more elaborate imaging approaches (Boissonnas et al., 2007; Breart et al., 2008; Deguine et al., 2010). Interestingly, our preliminary observation that B16F10 tumor cells are killed approximately within 6-12 hours is in line with a study by Breart et al. that showed that killing of one target tumor cell occupied an individual cytotoxic T cell (CTL) for an average of 6 hours (Breart et al., 2008). The ability to stain and observe the lymphocyte activation marker CD69 indicates that intravital IF could be used to detect dynamic phenotype changes of tumor infiltrating immune cells, thereby shedding light on processes such as T cell exhaustion within the tumor microenvironment (Baitsch et al., 2011; Jiang et al., 2015).

Because we found that intravital IF is suitable for visualization using two-photon microscopy, we were able to image non-fibrillar components of the tumor microenvironment in combination with SHG-detected fibrillar and matured collagens (Figure 5.5). Tenascin C is heterogeneously expressed in tumors, and often accumulates at the invasive front (Lowy and Oskarsson, 2015). In line with this,

we found that tenascin C occupies different areas in the TME as compared to fibrillar collagens. Future work will have to establish whether matrix heterogeneity is relevant for tumor cell migration towards lymphatic and blood vessels. Apart from the ability to do SHG, another advantage of using two-photon microscopy over standard fluorescence stereomicroscopy is the possibility to do z-stacks. This enables one to observe spatial co-localization of events occurring within the extracellular matrix, such as tumor cell intravasation into lymphatic or blood vessel. In the case of standard fluorescence stereomicroscopy, conclusions can be only inferred from morphological changes of the invading cell, as it is impossible to determine whether a cell is above, inside, or behind a vessel.

Our method has several limitations. First, fluorescence stereomicroscopy based imaging of intravital IF is limited to thin skin flaps that are deprived of thick hypodermis (adipose tissue). To extend the use of intravital IF to other body areas, one could consider using this approach in the context of an *in vivo* observation chamber. Different models such as the dorsal skin fold chamber (DSFC) (Koehl et al., 2009) or the chronic lymph node window (CLNW) (Jeong et al., 2015) have been established to study primary tumor growth or lymph node metastasis, respectively, over several days to weeks. We propose that intravital IF could especially be interesting in settings where the removal of the chamber's cover slip directly exposes the tissue to be stained. Second, rapid antibody staining (in the order of 15 minutes) in intravital IF is only achieved thanks to functional lymphatic drainage and interstitial fluid flow. Therefore, no staining can be observed if lymphatic vessels are occluded (Kilarski et al., 2014). In line with that, lymphatic vessels stain stronger than leaky blood vasculature (injured vessels, arterioles) (Kilarski et al., 2013). Third, even though the separation of the dorsal and ventral ear skin flaps is a mild surgical procedure, it still causes injury to some capillaries and cell death to various tissue cells. This might be a problem when one needs to investigate completely intact tissue, for example to assess effects of drugs on cell survival. Fourth, the need for ascorbate-Ringer's for the protection from phototoxicity and photobleaching excludes certain metabolic studies, such as on oxidative stress or nitric oxide biology, from the use of this protocol. In order to study such phenomena, ascorbate has to be replaced with other tissue compatible media that does not interfere with the experimental output. Finally, saturating tissue resident phagocytes and the complement system with immune complexes might modulate both innate and adaptive immunity, and thus influence the study of local tissue immune responses (Kolev et al., 2014; Nimmerjahn and Ravetch, 2008). Using secondary antibodies with cleaved Fc fragments (F(ab)<sub>2</sub> antibody fragments) or the use of biotinylated antibodies and fluorescent streptavidin as detection reagents could reduce this effect. In either case, local immunity will most likely be modulated to a certain extent, and interpretation of the interactions such as between tumor cells and anti-tumor immunity thus needs to be done with caution.

In summary, we present an adapted intravital IF protocol that bridges real-time, local measurements of physiological function with molecular imaging of complex cellular events in the context of the native microenvironment. With its flexibility and high-throughput potential, we propose that this intravital technique could be specifically interesting to elucidate mechanisms of anti-tumor immune responses, such as in the context of cancer immunotherapy.



## 5.6 References

- Baitsch, L., Baumgaertner, P., Devèvre, E., Raghav, S.K., Legat, A., Barba, L., Wieckowski, S., Bouzourene, H., Deplancke, B., Romero, P., Rufer, N., Speiser, D.E., 2011. Exhaustion of tumor-specific CD8<sup>+</sup> T cells in metastases from melanoma patients. *J. Clin. Invest.* 121, 2350–2360. doi:10.1172/JCI46102
- Boissonnas, A., Fetler, L., Zeelenberg, I.S., Hugues, S., Amigorena, S., 2007. In vivo imaging of cytotoxic T cell infiltration and elimination of a solid tumor. *Journal of Experimental Medicine* 204, 345–356. doi:10.1084/jem.20061890
- Bonnans, C., Chou, J., Werb, Z., 2014. Remodelling the extracellular matrix in development and disease. *Nat Rev Mol Cell Biol* 15, 786–801. doi:10.1038/nrm3904
- Breart, B., Lemaître, F., Celli, S., Bousso, P., 2008. Two-photon imaging of intratumoral CD8<sup>+</sup> T cell cytotoxic activity during adoptive T cell therapy in mice. *J. Clin. Invest.* 118, 1390–1397. doi:10.1172/JCI34388
- Brown, E., McKee, T., diTomaso, E., Pluen, A., Seed, B., Boucher, Y., Jain, R.K., 2003. Dynamic imaging of collagen and its modulation in tumors in vivo using second-harmonic generation. *Nat. Med.* 9, 796–800. doi:10.1038/nm879
- Chen, X., Nadiarynkh, O., Plotnikov, S., Campagnola, P.J., 2012. Second harmonic generation microscopy for quantitative analysis of collagen fibrillar structure. *Nat Protoc* 7, 654–669. doi:10.1038/nprot.2012.009
- Deguine, J., Breart, B., Lemaître, F., Di Santo, J.P., Bousso, P., 2010. Intravital Imaging Reveals Distinct Dynamics for Natural Killer and CD8<sup>+</sup> T Cells during Tumor Regression. *Immunity* 33, 632–644. doi:10.1016/j.immuni.2010.09.016
- Egawa, G., Nakamizo, S., Natsuaki, Y., Doi, H., Miyachi, Y., Kabashima, K., 2013. Intravital analysis of vascular permeability in mice using two-photon microscopy. *Sci. Rep.* 3, 1–6. doi:10.1038/srep01932
- Egeblad, M., Ewald, A.J., Askautrud, H.A., Truitt, M.L., Welm, B.E., Bainbridge, E., Peeters, G., Krummel, M.F., Werb, Z., 2008. Visualizing stromal cell dynamics in different tumor microenvironments by spinning disk confocal microscopy. *Disease Models and Mechanisms* 1, 155–67– discussion 165. doi:10.1242/dmm.000596
- Ellenbroek, S.I.J., van Rheenen, J., 2014. Imaging hallmarks of cancer in living mice. *Nature Publishing Group* 14, 406–418. doi:10.1038/nrc3742
- Giampieri, S., Manning, C., Hooper, S., Jones, L., Hill, C.S., Sahai, E., 2009. Localized and reversible TGFbeta signalling switches breast cancer cells from cohesive to single cell motility. *Nat Cell Biol* 11, 1287–1296. doi:10.1038/ncb1973
- Halin, C., Mora, J.R., Sumen, C., Andrian, von, U.H., 2005. In vivo imaging of lymphocyte trafficking. *Annu. Rev. Cell Dev. Biol.* 21, 581–603. doi:10.1146/annurev.cellbio.21.122303.133159



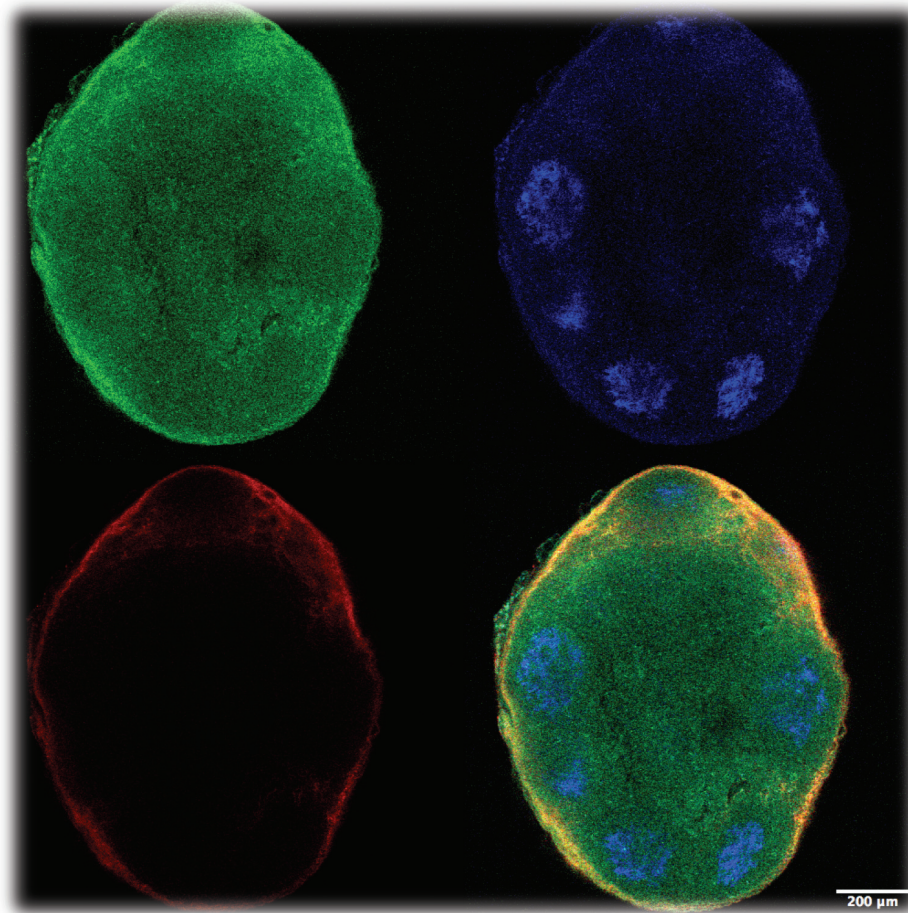
- Heymann, F., Niemietz, P.M., Peusquens, J., Ergen, C., Kohlhepp, M., Mossanen, J.C., Schneider, C., Vogt, M., Tolba, R.H., Trautwein, C., Martin, C., Tacke, F., 2015. Long term intravital multiphoton microscopy imaging of immune cells in healthy and diseased liver using CXCR6.Gfp reporter mice. *JoVE*. doi:10.3791/52607
- Jakobsson, L., Kreuger, J., Holmborn, K., Lundin, L., Eriksson, I., Kjellén, L., Claesson-Welsh, L., 2006. Heparan sulfate in trans potentiates VEGFR-mediated angiogenesis. *Dev. Cell* 10, 625–634. doi:10.1016/j.devcel.2006.03.009
- Jeong, H.-S., Jones, D., Liao, S., Wattson, D.A., Cui, C.H., Duda, D.G., Willett, C.G., Jain, R.K., Padera, T.P., 2015. Investigation of the Lack of Angiogenesis in the Formation of Lymph Node Metastases. *JNCI Journal of the National Cancer Institute* 107. doi:10.1093/jnci/djv155
- Jiang, Y., Li, Y., Zhu, B., 2015. T-cell exhaustion in the tumor microenvironment. *Cell Death Dis* 6, e1792. doi:10.1038/cddis.2015.162
- Joyce, J.A., Pollard, J.W., 2009. Microenvironmental regulation of metastasis. *Nature Reviews Cancer*. doi:10.1038/nrc2618
- Kilarski, W.W., Güç, E., Teo, J.C.M., Oliver, S.R., Lund, A.W., Swartz, M.A., 2013. Intravital Immunofluorescence for Visualizing the Microcirculatory and Immune Microenvironments in the Mouse Ear Dermis. *PLoS ONE* 8, e57135. doi:10.1371/journal.pone.0057135.s018
- Kilarski, W.W., Muchowicz, A., Wachowska, M., Mężyk-Kopeć, R., Golab, J., Swartz, M.A., Nowak-Sliwinska, P., 2014. Optimization and regeneration kinetics of lymphatic-specific photodynamic therapy in the mouse dermis. *Angiogenesis* 17, 347–357. doi:10.1007/s10456-013-9365-6
- Kilarski, W.W., Petersson, L., Fuchs, P.F., Zielinski, M.S., Gerwins, P., 2012. An in vivo neovascularization assay for screening regulators of angiogenesis and assessing their effects on pre-existing vessels. *Angiogenesis* 15, 1–13. doi:10.1007/s10456-012-9287-8
- Kilarski, W.W., Samolov, B., Petersson, L., Kvanta, A., Gerwins, P., 2009. Biomechanical regulation of blood vessel growth during tissue vascularization. *Nat. Med.* 15, 657–664. doi:10.1038/nm.1985
- Koehl, G.E., Gaumann, A., Geissler, E.K., 2009. Intravital microscopy of tumor angiogenesis and regression in the dorsal skin fold chamber: mechanistic insights and preclinical testing of therapeutic strategies. *Clin. Exp. Metastasis* 26, 329–344. doi:10.1007/s10585-008-9234-7
- Kolev, M., Le Friec, G., Kemper, C., 2014. Complement — tapping into new sites and effector systems. *Nat. Rev. Immunol.* 14, 811–820. doi:10.1038/nri3761
- Lämmermann, T., Bader, B.L., Monkley, S.J., Worbs, T., Wedlich-Söldner, R., Hirsch, K., Keller, M., Förster, R., Critchley, D.R., Fässler, R., Sixt, M., 2008. Rapid leukocyte migration by integrin-independent flowing and squeezing. *Nature* 453, 51–55. doi:10.1038/nature06887
- Lowy, C.M., Oskarsson, T., 2015. Tenascin C in metastasis: A view from the invasive front. *Cell Adhesion & Migration* 9, 112–124. doi:10.1080/19336918.2015.1008331
- Lu, P., Weaver, V.M., Werb, Z., 2012. The extracellular matrix: A dynamic niche in cancer progression. *The Journal of Cell Biology* 196, 395–406. doi:10.1084/jem.186.12.1985

- Martínez-Corral, I., Olmeda, D., Diéguez-Hurtado, R., Tammela, T., Alitalo, K., Ortega, S., 2012. In vivo imaging of lymphatic vessels in development, wound healing, inflammation, and tumor metastasis. *Proc. Natl. Acad. Sci. U.S.A.* 109, 6223–6228. doi:10.1073/pnas.1115542109
- Midwood, K.S., Orend, G., 2009. The role of tenascin-C in tissue injury and tumorigenesis. *J Cell Commun Signal* 3, 287–310. doi:10.1007/s12079-009-0075-1
- Mueller, M.M., Fusenig, N.E., 2004. Friends or foes — bipolar effects of the tumour stroma in cancer. *Nat Rev Cancer* 4, 839–849. doi:10.1038/nrc1477
- Munn, L.L., Padera, T.P., 2014. Imaging the lymphatic system. *Microvasc. Res.* 96, 55–63. doi:10.1016/j.mvr.2014.06.006
- Nakasone, E.S., Askautrud, H.A., Kees, T., Park, J.-H., Plaks, V., Ewald, A.J., Fein, M., Rasch, M.G., Tan, Y.-X., Qiu, J., Park, J., Sinha, P., Bissell, M.J., Frengen, E., Werb, Z., Egeblad, M., 2012. Imaging Tumor-Stroma Interactions during Chemotherapy Reveals Contributions of the Microenvironment to Resistance. *Cancer Cell* 21, 488–503. doi:10.1016/j.ccr.2012.02.017
- Nimmerjahn, F., Ravetch, J.V., 2008. Fcγ receptors as regulators of immune responses. *Nat. Rev. Immunol.* 8, 34–47. doi:10.1038/nri2206
- Ohashi, T., Kiehart, D.P., Erickson, H.P., 1999. Dynamics and elasticity of the fibronectin matrix in living cell culture visualized by fibronectin-green fluorescent protein. *Proc. Natl. Acad. Sci. U.S.A.* 96, 2153–2158.
- Padera, T.P., Stoll, B.R., So, P.T., Jain, R.K., 2002. Conventional and high-speed intravital multiphoton laser scanning microscopy of microvasculature, lymphatics, and leukocyte-endothelial interactions. *Mol Imaging* 1, 9–15.
- Patterson, G.H., Piston, D.W., 2000. Photobleaching in two-photon excitation microscopy. *Biophys. J.* doi:10.1016/S0006-3495(00)76762-2
- Perentes, J.Y., McKee, T.D., Ley, C.D., Mathiew, H., Dawson, M., Padera, T.P., Munn, L.L., Jain, R.K., Boucher, Y., 2009. In vivo imaging of extracellular matrix remodeling by tumor-associated fibroblasts. *Nat Meth* 6, 143–145. doi:10.1038/nmeth.1295
- Pickup, M.W., Mouw, J.K., Weaver, V.M., 2014. The extracellular matrix modulates the hallmarks of cancer. *EMBO Rep.* 15, 1243–1253. doi:10.15252/embr.201439246
- Pinner, S., Sahai, E., 2008. Imaging amoeboid cancer cell motility in vivo. *Journal of Microscopy* 231, 441–445. doi:10.1111/j.1365-2818.2008.02056.x
- Pittet, M.J., Weissleder, R., 2011. Intravital Imaging. *Cell* 147, 983–991. doi:10.1016/j.cell.2011.11.004
- Polyak, K., Haviv, I., Campbell, I.G., 2009. Co-evolution of tumor cells and their microenvironment. *Trends in Genetics* 25, 30–38. doi:10.1016/j.tig.2008.10.012
- Roos, A., Trouw, L.A., Ioan-Facsinay, A., Daha, M.R., Verbeek, J.S., 2005. Complement System and Fc Receptors: Genetics. John Wiley & Sons, Ltd, Chichester, UK. doi:10.1038/npg.els.0005992
- Sahai, E., Wyckoff, J., Philippar, U., Segall, J.E., Gertler, F., Condeelis, J., 2005. Simultaneous imaging of GFP, CFP and collagen in tumors in vivo using multiphoton microscopy. *BMC Biotechnol.* 5, 14. doi:10.1186/1472-6750-5-14

- Snippert, H.J., van der Flier, L.G., Sato, T., van Es, J.H., van den Born, M., Kroon-Veenboer, C., Barker, N., Klein, A.M., van Rheenen, J., Simons, B.D., Clevers, H., 2010. Intestinal Crypt Homeostasis Results from Neutral Competition between Symmetrically Dividing Lgr5 Stem Cells. *Cell* 143, 134–144. doi:10.1016/j.cell.2010.09.016
- Steinbauer, M., Guba, M., Cernaianu, G., Kohl, G., Cetto, M., Kunz-Schughart, L.A., Geissler, E.K., Falk, W., Jauch, K.W., 2003. GFP-transfected tumor cells are useful in examining early metastasis in vivo, but immune reaction precludes long-term tumor development studies in immunocompetent mice. *Clin. Exp. Metastasis* 20, 135–141.
- Sund, M., Kalluri, R., 2009. Tumor stroma derived biomarkers in cancer. *Cancer Metastasis Rev* 28, 177–183. doi:10.1007/s10555-008-9175-2
- Tal, O., Lim, H.Y., Gurevich, I., Milo, I., Shipony, Z., Ng, L.G., Angeli, V., Shakhar, G., 2011. DC mobilization from the skin requires docking to immobilized CCL21 on lymphatic endothelium and intralymphatic crawling. *Journal of Experimental Medicine* 208, 2141–2153. doi:10.1084/jem.20102392
- Turley, S.J., Cremasco, V., Astarita, J.L., 2015. Immunological hallmarks of stromal cells in the tumour microenvironment. *Nat. Rev. Immunol.* 15, 669–682. doi:10.1038/nri3902
- Weber, M., Hauschild, R., Schwarz, J., Moussion, C., de Vries, I., Legler, D.F., Luther, S.A., Bollenbach, T., Sixt, M., 2013. Interstitial dendritic cell guidance by haptotactic chemokine gradients. *Science* 339, 328–332. doi:10.1126/science.1228456
- Woodruff, M.C., Heesters, B.A., Herndon, C.N., Groom, J.R., Thomas, P.G., Luster, A.D., Turley, S.J., Carroll, M.C., 2014. Trans-nodal migration of resident dendritic cells into medullary interfollicular regions initiates immunity to influenza vaccine. *Journal of Experimental Medicine* 211, 1611–1621. doi:10.1084/jem.20132327
- Wyckoff, J.B., Jones, J.G., Condeelis, J.S., Segall, J.E., 2000. A critical step in metastasis: In vivo analysis of intravasation at the primary tumor. *Cancer Research* 60, 2504–2511.

## Chapter 6

### Conclusions, Implications and Future Directions



Lymph node showing follicular dendritic cells (FDCs, blue), after injection of free antigen (green) versus nanoparticle bound antigen (red). Confocal microscopy.

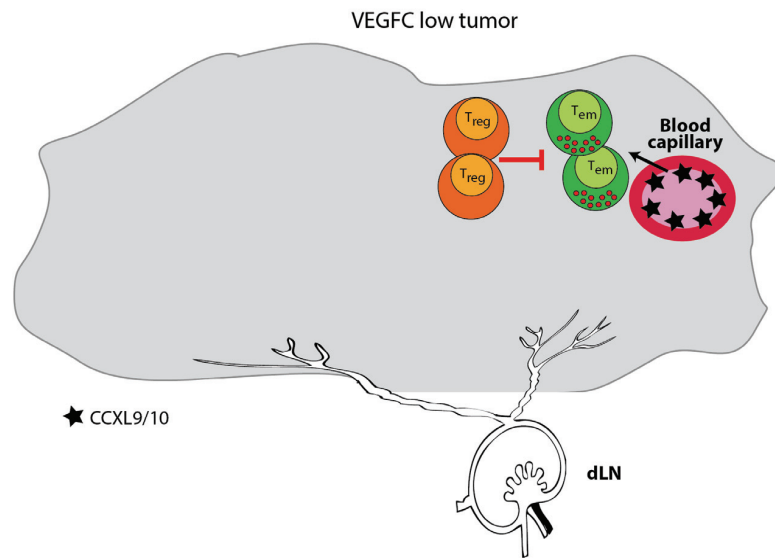
## 6.1 LEC-mediated chemokine secretion as a driving force of immune cell trafficking into peripheral tissues

Lymphatic endothelial cells are passive and active modulators of adaptive immune responses (Card et al., 2014; Hirose and Dubrot, 2015). In this context, three main modes of actions have been ascribed to LECs: 1) Acting as an information highway by offering a physical connection between the periphery and the draining lymph nodes. 2) Influencing immune cell trafficking by secretion of chemokines, most notably CCL21. 3) Influencing immune cell education by mediating cell-cell interactions through molecules such as MHCI and MCHII, or secreting immunomodulatory molecules such as IDO and TGF $\beta$ . Even though a considerable amount of work has been done towards understanding the role of LECs in active immunomodulation, one question has been very difficult to address experimentally: where in terms of anatomical location do these mechanisms take place in a complex human body? Because the lymphatic network is spread throughout the entire organism, ranging from the very periphery, to the lymph nodes, back into the blood circulation, it is very difficult if not impossible to conclude physiological function from pure *in vitro* systems. For example, even though it has been well established that LECs can present exogenous and endogenous antigens on MHC class I and class II molecules, it is still unclear where this happens in the physiological context. Do initial lymphatics present antigen to influence immunity in peripheral organs? Do pre-collecting or collecting lymphatics do it to re-educate effector cells egressing through lymphatics from peripheral tissues? Does it only happen in the lymph node, and if yes, in which particular zone? Or is it needed to fine-tune immune responses when activated T cells egress from the lymph node into the circulation?

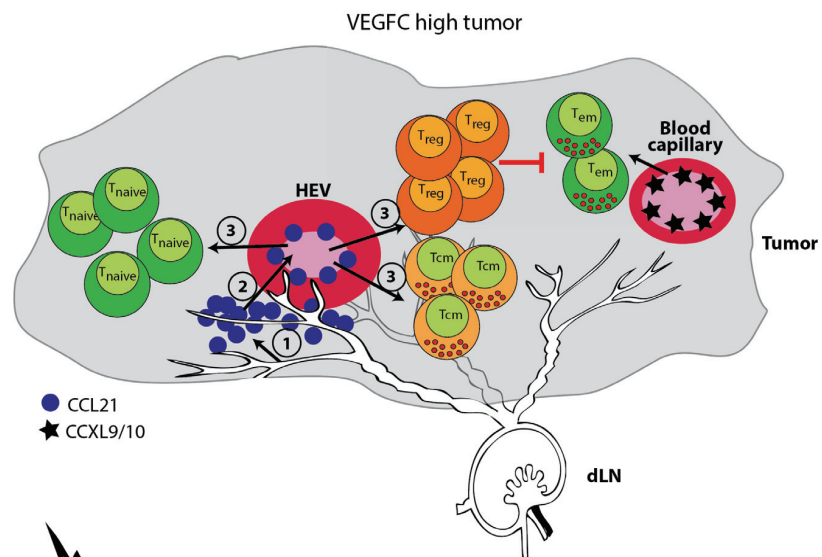
We specifically aimed at better understanding the role of the second mode of action, LEC-mediated immunomodulation by secretion of chemokines, in peripheral tissues. CCL21 has been the most widely studied LEC-secreted chemokine (Gunn et al., 1998; Kriehuber et al., 2001; Vigl et al., 2011). In peripheral tissues, initial lymphatics produce CCL21 to generate a chemokine gradient that attracts activated, antigen-loaded CCR7<sup>+</sup> DCs (Teijeira et al., 2014). DCs then transmigrate into lymphatic capillaries from where they first actively crawl along the luminal vessel wall, before they are passively transported through collecting vessels to reach the draining lymph node (Tal et al., 2011). In the lymph node, CCL21 gradients established by lymph node stromal cells including LECs orchestrate the encounter antigen-loaded DCs from the periphery with naïve CCR7<sup>+</sup> T cells arriving from the blood circulation via high endothelial venules (HEVs) (Andrian and Mempel, 2003). Interestingly, HEVs can translocate perivascular chemokine to their luminal surface by a process called transcytosis, suggesting that extravasation can be influenced by chemokine producing stromal cells adjacent to HEVs (Baekkevold et al., 2001; Carlsen et al., 2005). Thus, chemokine secretion by LECs has so far shown to be crucial for immune cell trafficking from peripheral tissue or the blood circulation to secondary lymphoid organs (SLOs), within SLOs themselves, as well as for the egress from SLOs back into blood circulation. However, it has not yet been explored whether initial lymphatics might employ similar mechanisms to regulate trafficking of immune cells from the circulation into peripheral tissues. Because our lab has previously shown that tumor-derived CCL21 attracts immune cells that



A



B



C

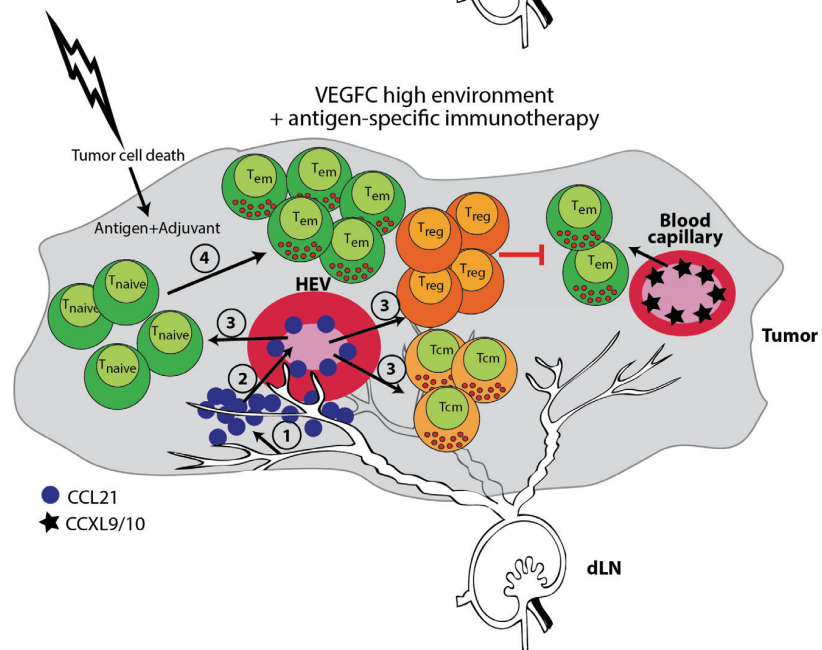




**Figure 6.1 Lymphangiogenic potentiation of antigen-specific cancer immunotherapy.** (A) VEGFC low tumors show low lymphatic density, and baseline immune infiltrations including effector T cells (Tem) and regulatory T cells (Treg) that keep each other in check. Tem cells are classically infiltrated via the blood vasculature, which is decorated with effector chemokines such as CXCL9/10. (B) VEGFC high tumors have high levels of CCL21 (blue). We hypothesize that CCL21 is transcytosed on the luminal side of HEVs, leading to the chemoattraction and extravasation of CCR7<sup>+</sup> immune cells, including naïve (Tnaive), central memory (Tcm) and more regulatory T cells. Overall, the microenvironment in these tumors shows hallmarks of immunosuppression, and no spontaneous regression induced by an endogenous effector anti-tumor immune response is observed. (C) However, in the context of antigen-specific cancer immunotherapy, massive cell death is induced, releasing antigen and danger signal from the dying cancer cells. These signals are most likely activating local antigen presenting cells, which in turn activate the tissue resident naïve T cells. This broadens the endogenous anti-tumor immune response to novel antigens, and immunological memory protects the host from tumor re-challenge.

---

establish a lymphoid-like structure in primary melanoma tumors (Shields et al., 2010), we hypothesized that LEC-derived CCL21 might have a similar role in local immunoregulation, especially in the context of lymphangiogenic melanoma tumors.

Throughout this thesis research, we used three different approaches to address questions relevant to our overall hypothesis: first, we used melanoma mouse models to study the effect of tumor-associated lymphangiogenesis on the local immune environment. Second, we used an engineering approach with the goal to induce and study lymphangiogenesis in mouse dermis, representing a more controlled environment as compared to the tumor microenvironment. Third, we developed a novel intravital imaging modality that allows observation of immune responses in the context of the dynamic tumor microenvironment. Our findings suggest a relatively simple mechanism of peripheral LEC-mediated immunoregulation, which seems to be common amongst both the tumor and the steady-state peripheral tissue microenvironment: VEGFC induced lymphangiogenesis upregulates the local secretion of CCL21, which in turn leads to the infiltration of CCR7<sup>+</sup> immune cells (Figure 6.1, step 1 to 3). We found that different CCR7<sup>+</sup> immune cell subsets were attracted in different settings, indicating that the specificity most likely depends on multiple factors, such as the presence of other cytokines or adhesion molecules on the tissue vasculature. Because we found similar mechanisms occurring both in lymphangiogenic melanoma and the engineered lymphangiogenic dermis, we propose that chemoattraction by LECs might happen as a bystander effect: the more LECs there are, the more CCL21 is constitutively secreted into the microenvironment. This might certainly be further exaggerated in settings of enhanced flow and presence of inflammatory cytokines, as both of these stimuli can further upregulate CCL21 expression by LECs (Martín-Fontecha et al., 2003; Miteva et al., 2010). An important question remains: once CCL21 is deposited in the interstitium by LECs, how exactly does it influence immune cell trafficking into the tissue? Does it reach the luminal sides of high endothelial venules by transcytosis to influence immune cell extravasation? Or does it simply attract cells from the adjacent tissue by creating chemokine gradients? Considering that we observed the infiltration of naïve T cells into lymphangiogenic tumors, and that these cells are usually in the circulation rather than in the periphery, a model where CCL21 is transcytosed to influence immune cell extravasation seems more plausible. However, these novel hypotheses are based on our observations and will need further experimental validation.

## **6.2 Exploiting lymphangiogenic sites to induce tolerance or immunity: a question of context?**

An increasing body of literature has been describing the immunosuppressive capacity of lymphatic endothelial cells (Lund et al., 2016). The general concept has been that even though LECs can present antigen on MHC class I and II molecules to T cells, they lack costimulatory molecules necessary to induce effector immune responses. Surprisingly, this thesis research suggests that even though LEC-secreted chemokines establish a local immune microenvironment that shows hallmarks of immunosuppression, including regulatory T cells, this environment can be exploited to generate highly potent effector responses. This was especially striking in our experiments where we performed antigen-specific immunotherapy in lymphangiogenic melanoma tumors. We found that the release of danger signal and antigen following immunotherapy-induced cancer cell death was able to activate naïve T cells that previously infiltrated the tumor in a CCL21-dependent manner (Figure 6.1, step 4). Not only led this to a broader anti-tumor response by antigen-spreading, it also conferred immunological memory and thus protected mice from tumor re-challenge. Interestingly, similar mechanisms might be relevant in non-inflamed lymphangiogenic sites as we found that delivering the model antigen ovalbumin to lymphangiogenic tissue sites increased the effectors response upon antigen re-challenge. Our data suggest that the role of lymphangiogenic sites in immunoregulation might not be as black and white as previously assumed, and that they might be useful for therapeutic exploitation in settings of both tolerance and immunity.

## **6.3 Implications for the translation into clinics**

This thesis research has generated novel concepts that - after further pre-clinical validation - could be applicable for the translation into clinics:

- 1) Intratumoral lymphatic density, VEGFC and/or CCL21 expression as biomarkers to stratify cancer patients eligible for cancer immunotherapy.
- 2) Engineering lymphangiogenesis in non T-cell inflamed tumors could to render tumors more sensitive to cancer immunotherapy. One major concern of such an approach would be that increasing lymphangiogenesis in the primary tumor could increase the metastatic potential. However, as patients eligible for immunotherapy are usually already metastatic, this might not be of concern for this specific patient population.
- 3) Engineering lymphangiogenic skin sites could potentially be used to guide therapeutic immune responses. Our data suggested that using this approach might be suitable to increase the efficacy of vaccinations as we found increased effector responses upon antigen re-challenge.

## 6.4 Future directions

In this thesis, we introduced novel concepts and tools relevant to the field of lymphatic biology, cancer immunology, and bioengineering. Yet, by answering one scientific question, multiple follow up questions are generated. The ones I think are most interesting and pressing are summarized below.

### 6.4.1 The role of lymphangiogenesis in cancer immunotherapy

- What cells ultimately secrete CCL21 within lymphangiogenic tumors? Is it indeed LECs or does it come from other sources?
- Does VEGFC increase CCL21 production simply by increasing the number of cells that produce chemokine, or does VEGFR3 signaling itself upregulate CCL21 expression per cell?
- How does CCL21 finally attract immune cells into the tissue? Is it transcytosed to the luminal side of HEVs? Or could it be that CCL21 in the tissue signals to other molecular pathways that ultimately induce extravasation?
- What other cytokines and chemokines could be relevant to the observed effects?
- Are intratumoral lymphatics indeed non-functional in terms of drainage? We often observed vessels with a wide-open lumen, suggesting that they might still be able to transport cells and interstitial fluid.
- What cells are presenting tumor antigen in lymphangiogenic tumors in response to cancer immunotherapy? Is it dendritic cells, macrophages, or stromal cells? Are these cells also attracted by lymphangiogenesis, or are they already present within the tumor microenvironment?
- What are the growth factors driving lymphangiogenesis in the iBIP2 model of melanoma apart from VEGFR3 ligands? VEGFR3 blocking only reduced, but not completely abrogated the development of LVs.
- Is “lymphangiogenic potentiation of cancer immunotherapy” a generally applicable mechanism for any kind of lymphangiogenic tumor, or does it depend on other factors such as from what tissue the tumor arises?
- Could activation of naïve T cells within inflamed tissues be a more broadly relevant mechanism, taking place in a different set of diseases?
- Is there evidence for tertiary lymphoid organ formation specifically within lymphangiogenic tumors?
- Could it potentially be more efficient to generate “a local lymph node” / tertiary lymphoid organ because the immune response is directly generated at the place where it needs to act?
- Does this mechanism only work when cancer immunotherapy is targeting a neoantigen, or could it be equally efficient when targeting a cancer-testis, differentiation, or overexpressed antigen?
- Could other therapeutic interventions that lead to immunogenic cell death be used instead of cancer immunotherapy? Radiation?
- Do B16 melanoma cells overexpressing CCL21 react in the same way to immunotherapy as the VEGFC ones?

- Can non T cell-inflamed tumors be turned into inflamed ones by intratumoral injections of VEGFC? If yes, will they respond better to immunotherapy?
- Do VEGFC or CCL21 serum levels of patients undergoing cancer immunotherapy correlate with outcome?

#### **6.4.2 Engineering lymphangiogenic sites for therapeutic immunomodulation**

- Are engineered lymphangiogenic sites functional in terms of drainage? If yes, could the same system be used to re-connect the lymphatic network after damage that induces lymphedema?
- How can engineered lymphangiogenic sites be therapeutically exploited? Can they be used for therapeutic tolerance, or rather for increasing vaccine responses?
- Do LECs in lymphangiogenic sites contribute to immunoregulation only by chemokine secretion only, or also via immune cell education by actively engaging in cell-cell interactions? If both, what is the relevance of each of those as compared to the other mechanism?
- What is the functional consequence of inducing lymphangiogenesis in the downstream lymph node instead of in the periphery?
- Could other growth factors, or a combination of growth factors, be more efficient in inducing local lymphangiogenesis?
- Could the hydrogel system be avoided by designing growth factors that stick to the extracellular matrix?

#### **6.4.3 Intravital immunofluorescence to observe anti-tumor immune responses**

- Can intravital IF be used in other settings, such as in combination with intravital imaging windows to reach other organs than the ear dermis?
- Can intravital IF be used to quantify interactions between tumor cells and immune cells? How many cells can be killed by one immune cells and how long does it take?
- What are the actual mechanisms of tumor invasion and rejection by T cells?
- What is the relative contribution of direct tumor cell killing by cytotoxic T cells compared with killing by other effectors of innate immunity?
- How do the dynamics of anti-tumor immunity differ from a non-lymphangiogenic to a lymphangiogenic tumor microenvironment?
- Do tumor cells actively crawl along matrix proteins, and if so, which ones? Can we observe extravasation of tumor cells into lymphatic or blood vessels?
- Do interactions take place between LECs and infiltrating immune cells, indicating that LECs might be re-educating these cells?
- What is the phenotype of tumor killing cells, and does it change during tumor rejection?
- What are the dynamics of adaptive resistance mechanisms to cancer immunotherapy? E.g. can upregulation of PD-L1 during an ongoing anti-tumor immune response be observed?

## 6.5 References

- Andrian, von, U.H., Mempel, T.R., 2003. Homing and cellular traffic in lymph nodes. *Nat. Rev. Immunol.* 3, 867–878. doi:10.1038/nri1222
- Baekkevold, E.S., Yamanaka, T., Palframan, R.T., Carlsen, H.S., Reinholt, F.P., Andrian, von, U.H., Brandtzaeg, P., Haraldsen, G., 2001. The CCR7 ligand elc (CCL19) is transcytosed in high endothelial venules and mediates T cell recruitment. *J. Exp. Med.* 193, 1105–1112. doi:10.1084/jem.193.9.1105
- Card, C.M., Yu, S.S., Swartz, M.A., 2014. Emerging roles of lymphatic endothelium in regulating adaptive immunity. *J. Clin. Invest.* 124, 943–952. doi:10.1172/JCI73316
- Carlsen, H.S., Haraldsen, G., Brandtzaeg, P., Baekkevold, E.S., 2005. Disparate lymphoid chemokine expression in mice and men: no evidence of CCL21 synthesis by human high endothelial venules. *Blood* 106, 444–446. doi:10.1182/blood-2004-11-4353
- Gunn, M.D., Tangemann, K., Tam, C., Cyster, J.G., Rosen, S.D., Williams, L.T., 1998. A chemokine expressed in lymphoid high endothelial venules promotes the adhesion and chemotaxis of naive T lymphocytes. *Proc. Natl. Acad. Sci. U.S.A.* 95, 258–263.
- Hirosue, S., Dubrot, J., 2015. Modes of Antigen Presentation by Lymph Node Stromal Cells and Their Immunological Implications. *Front Immunol* 6, 446. doi:10.3389/fimmu.2015.00446
- Kriehuber, E., Breiteneder-Geleff, S., Groeger, M., Soleiman, A., Schoppmann, S.F., Stingl, G., Kerjaschki, D., Maurer, D., 2001. Isolation and characterization of dermal lymphatic and blood endothelial cells reveal stable and functionally specialized cell lineages. *J. Exp. Med.* 194, 797–808.
- Lund, A.W., Medler, T.R., Leachman, S.A., Coussens, L.M., 2016. Lymphatic Vessels, Inflammation, and Immunity in Skin Cancer. *Cancer Discovery* 6, 22–35. doi:10.1158/2159-8290.CD-15-0023
- Martín-Fontecha, A., Sebastiani, S., Höpken, U.E., Uguccioni, M., Lipp, M., Lanzavecchia, A., Sallusto, F., 2003. Regulation of dendritic cell migration to the draining lymph node: impact on T lymphocyte traffic and priming. *J. Exp. Med.* 198, 615–621. doi:10.1084/jem.20030448
- Miteva, D.O., Rutkowski, J.M., Dixon, J.B., Kilarski, W., Shields, J.D., Swartz, M.A., 2010. Transmural flow modulates cell and fluid transport functions of lymphatic endothelium. *Circ. Res.* 106, 920–931. doi:10.1161/CIRCRESAHA.109.207274
- Shields, J.D., Kourtis, I.C., Tomei, A.A., Roberts, J.M., Swartz, M.A., 2010. Induction of lymphoidlike stroma and immune escape by tumors that express the chemokine CCL21. *Science* 328, 749–752. doi:10.1126/science.1185837
- Tal, O., Lim, H.Y., Gurevich, I., Milo, I., Shipony, Z., Ng, L.G., Angeli, V., Shakhhar, G., 2011. DC mobilization from the skin requires docking to immobilized CCL21 on lymphatic endothelium and intralymphatic crawling. *Journal of Experimental Medicine* 208, 2141–2153. doi:10.1084/jem.20102392
- Teijreira, A., Russo, E., Halin, C., 2014. Taking the lymphatic route: dendritic cell migration to draining lymph nodes. *Semin Immunopathol* 36, 261–274. doi:10.1007/s00281-013-0410-8

Vigl, B., Aebischer, D., Nitschké, M., Iolyeva, M., Röthlin, T., Antsiferova, O., Halin, C., 2011. Tissue inflammation modulates gene expression of lymphatic endothelial cells and dendritic cell migration in a stimulus-dependent manner. *Blood* 118, 205–215. doi:10.1182/blood-2010-12-326447



Für Grossmama Erika Levi, am 20. März 2016

dene was guet geit  
giengs besser  
giengs dene besser  
was weniger guet geit  
was aber nid geit  
ohni dass's dene  
weniger guet geit  
was guet geit

drum geit weni  
für dass es dene  
besser geit  
was weniger guet geit  
und drum geits o  
dene nid besser  
was guet geit

Mani Matter

# Curriculum Vitae

## Personal Information

Name	Fankhauser
First Name	Manuel
Address	Schanzeneckstrasse 9 3012 Bern, Switzerland
Mobile Phone CH	+41'78'610'00'94
Email	manuel.fankhauser@me.com
Date of Birth	October 28 <sup>th</sup> 1986
Nationality	Swiss

## Languages

German	excellent written and spoken knowledge ( <i>mother tongue</i> )
English	excellent written and spoken knowledge ( <i>CPE</i> )
French	good written and spoken knowledge

## Education

2011 – spring 2016 (Expected)	Doctoral School in Biotechnology & Bioengineering (EDBB) Swiss Institute of Technology (EPFL), Lausanne, Switzerland
2009 - 2011	MSc in Biomedical Sciences University of Amsterdam, The Netherlands
2006 - 2009	BSc in Biomedical Sciences University of Fribourg, Switzerland
2001 - 2003 & 2004 - 2006	Matura (High School Degree) with focus Physics & Mathematics Gymnasium Neufeld, Berne, Switzerland
2003 - 2004	International High School Exchange Year Westerville North High School, Ohio, USA

## Work experience

2015 (Sept-Dec)	VentureLabs Fellow <b>Flagship Ventures</b> , Cambridge (MA), USA <ul style="list-style-type: none"> <li>Exploring the Flagship Venture's approach to new company generation and entrepreneurship in the area of clean and sustainable energy and therapeutics.</li> </ul>
2011 - spring 2016 (Expected)	Doctoral Research in Cancer Immunology and Lymphatic Biology Laboratory of Lymphatic and Cancer Bioengineering (LLCB) Under the supervision of Prof. Dr. Melody Swartz <b>Swiss Institute of Technology (EPFL)</b> , Lausanne, Switzerland <ul style="list-style-type: none"> <li>Doctoral thesis research in cancer immunology and lymphatic biology with the aim of enhancing therapeutic cancer vaccines. Methods include in vivo experiments, confocal and intravital multiphoton imaging, flow cytometry (Cyan, LSR2), in vitro experiments (immortalized and primary cells), immunohistochemistry, protein engineering, DNA Cloning</li> </ul>

- 2010 - 2011 MSc Traineeship II (9 months, full-time)  
Group Prof. Dr. Hidde Ploegh  
**Whitehead Institute for Biomedical Research, MIT, Cambridge US**
- *Master thesis research in molecular biology with the aim of identifying the in vivo function of a newly discovered protein. Methods included mouse tissue isolation, tissue culture (immortalized and primary cells), pulse-chase radiolabeling experiments, metabolic labelling, immunoprecipitation, western- and northern-blot, DNA cloning, bacterial culture, lipotransfection, viral transduction, in vivo glucose tolerance test*
- 2009 - 2010 MSc Traineeship I (9 months, full-time)  
Group Prof. Dr. Ton Schumacher, Division of Immunology  
**Netherlands Cancer Institute (NKI), Amsterdam, The Netherlands**
- *Master thesis research in immunology with the aim of identifying the specificity of tumor infiltrating lymphocytes in melanoma patient biopsies. Methods included human T cell tissue culture, tetramer staining, combinatorial coding flow cytometry analysis (LSR2 and Calibur), recombinant protein synthesis & purification, HPLC*
- 2008 - 2009 BSc Traineeship (9 months, part-time)  
Group Dr. Giovanni Solinas, Laboratory of Metabolic Stress Biology  
University of Fribourg, Switzerland
- *Northern-blot, gel-electrophoresis, genotyping of transgenic mice*

#### Peer-reviewed Publications

- 2016 **“Lymphatic vessels regulate immune microenvironments in human and murine melanoma.”** (2016) Amanda W. Lund, Marek Wagner, Manuel Fankhauser, Stefani Spranger, Thomas F. Gajewski, Kari Alitalo, Hans P. Eikesdal, Helge Wiig, and Melody A. Swartz – **Journal of Clinical Investigation (under review)**
- 2014 **“Long-term intravital immunofluorescence imaging of tissue matrix components with epifluorescence and two-photon microscopy.”** (2014) Güç E\*, Fankhauser M\*, Lund AW, Swartz MA, and Kilarski WW (\* these authors contributed equally) – **Journal of Visualized Experiments (JOVE)**
- 2013 **“A catalytically inactive mutant of the deubiquitylase YOD-1 enhances antigen cross-presentation.”** (2013) Sehwat S, Koenig PA, Kirak O, Schlieker C, Fankhauser M, Ploegh HL – **Blood**
- 2012 **„TIL therapy broadens the tumor-reactive CD8<sup>+</sup> T cell compartment in melanoma patients.”** (2012) Kvistborg P, Shu CJ, Heemskerk B, Fankhauser M, Thru CA, Toebes M, van Rooij N, Linnemann C, van Buuren M, Urbanus JHM, Beltman J, Straten PT, Li Y, Robbins P, Besser M, Schachter J, Kenter G, Dudley ME, Rosenberg SA, Haanen J, Hadrup SR and Schumacher TNM – **Onc Immunology**

#### Conference Presentations

- 2015 **Keystone Tumor Immunology, Banff, Alberta, Canada**  
Poster: *“Targeting tumor-associated lymphatics increases the efficacy of anti-tumor immunotherapies in melanoma mouse models”* Manuel Fankhauser, Maria Broggi, Amanda Lund, Stephan Wullschleger, Krisztian Homicsko, Douglas Hanahan, and Melody Swartz
- 2015 **Immunology 2015, New Orleans, Louisiana, USA**  
Poster: *“Localized, sustained presentation of VEGF-C in mouse dermis alters the local immune microenvironment”* SS Yu, M Fankhauser, P Aigner, J Kocher, & MA Swartz.

2014 **GRS/GRC Molecular Mechanisms in Lymphatic Function & Disease, Italy**  
Short talk and poster: *"Lymphangiogenic melanoma tumors establish an immuno suppressive microenviroment to dampen CD8 T cell infiltration and functionality in situ."*

2010 **Dutch Tumor Immunology Meeting, Breukelen, The Netherlands**  
Short talk: *"Dissecting Cancer-reactive T-cell Responses in Tumor Infiltrating Lymphocyte (TIL) Therapy of Human Melanoma."*

### Teaching experience

2015 (Feb-Aug) **Supervisor for Elodie Da Costa's Master Thesis Project**  
*"The effects of lymphangiogenesis on immunotherapies in mouse melanoma"*

2014 (Jul-Sept) **Supervisor for Christopher Tremblay's Summer Research Project**  
*"Non-invasive live cell imaging of lymphatic endothelial cells"*

2013 (Fall semester) **Teaching Assistant for "Introduction into Life Sciences" course**  
1<sup>st</sup> year Bachelor students at EPFL (School of Life Sciences)

2012 - 2013 **Teaching Assistant for "Practical Physiology" laboratory course**  
3<sup>rd</sup> year Bachelor students at EPFL (School of Life Sciences)

2012 (Spring semester) **Teaching Assistant for "Molecular and Cellular Biology III" course**  
2<sup>nd</sup> year Bachelor students at EPFL (School of Life Sciences)

### Grants

2015 - 2016 **InnoPactt 100k spin-off grant**  
Awarded by the University of Lausanne to explore a potential spin-off project in the field of microbiome health. Our team member Sandra Sulser has been performing the research under this grant during one year with the supervision of Prof. Van der Meer.

### Awards / Scholarships

2014 **Winner Team Novartis BioCamp 2014**  
Awarded by Novartis for winning the business case competition.

2013 **Winner Team Merck Serono Innovation Cup 2013**  
Awarded by Merck Serono for working out a convincing business plan for a new approach to increase the effectiveness of cancer vaccines. The potential of the idea is now evaluated and tested by internal R&D experts.

2009 - 2011 **HSP Huygens Excellence Scholarship**  
Awarded by The Dutch Minister of Education, Culture and Science to follow MSc in Biomedical Sciences at the University of Amsterdam.

### Extracurricular Activities / Voluntary Work

Since 2014 **President**  
**Innovation Forum Lausanne** ([www.inno-forum.org](http://www.inno-forum.org))

- *Leading a student-led, non-profit association that aims to bridge the gap between academia and industry by providing a platform where innovative minds across the fields of science, business, education, policy and art can connect, get trained, and think outside the box in order to come up with the innovations of tomorrow.*

Since 2013	<p>Member of Advisory Board  <b>Nanolive SA</b>, Lausanne, Switzerland (<a href="http://www.nanolive.ch">www.nanolive.ch</a>)</p> <ul style="list-style-type: none"> <li>• <i>Advising the technology startup Nanolive SA on how to plan and perform biological experiments with their disruptive proprietary holographic microscopy technology that allows for the very first time to explore a living cell in 3D without damaging it.</i></li> </ul>
2013 (spring semester)	<p>Participant in the “Venture Challenge” programme</p> <ul style="list-style-type: none"> <li>• <i>Start-up and entrepreneur training programme of the Commission for Technology and Innovation (CTI) sponsored by the Swiss Confederation.</i></li> <li>• <i>My idea of a “solar balloon” was chosen by the entire group to be forwarded and was to be pursued as a business case by our team.</i></li> </ul>
2008 - 2011	<p>Member of the Board  <b>EX-IT Event Management</b>, Berne, Switzerland</p> <ul style="list-style-type: none"> <li>• <i>Responsible for the organization and execution of major cultural events addressing several hundred participants</i></li> </ul>
2004 - 2009	<p>Regional Director  <b>YFU</b> (Youth for Understanding), Berne, Switzerland</p> <ul style="list-style-type: none"> <li>• <i>Supervision of host families and exchange students</i></li> <li>• <i>Volunteer management</i></li> </ul>

### Interests

---

Entrepreneurship, Technology Innovation, Science, Crowdsourcing, Knowledge Exchange (TED conferences), Travelling, Outdoors, Snow sports, Tennis, Hiking

